Special Technical Report 35

FULL-SCALE PATTERN MEASUREMENTS OF SIMPLE HF FIELD ANTENNAS IN A TROPICAL FOREST IN THAILAND

By: GARY E. BARKER GLENN D. KOEHRSEN

Prepared for:

U.S. ARMY ELECTRONICS COMMAND
FORT MONMOUTH, NEW JERSEY 07703

CONTRACT DA-36-039 AMC-00040(E)
ORDER NO. 5384-PM-63-91

STANFORD RESEARCH INSTITUTE
MENLO PARK CALIFORNIA

*SRI

421

February 1968

Special Technical Report 35

FULL-SCALE PATTERN MEASUREMENTS OF SIMPLE HF FIELD ANTENNAS IN A TROPICAL FOREST IN THAILAND

By: GARY E. BARKER GLENN D. KOEHRSEN

Prepared for:

U.S. ARMY ELECTRONICS COMMAND
FORT MONMOUTH, NEW JERSEY 07703

CONTRACT DA-36-039 AMC-00040(E)
ORDER NO. 5384-PM-63-91

SRI Project 4240

Approved: W. R. VINCENT, MANAGER
COMMUNICATION LABORATORY

D. R. SCHEUCH, EXECUTIVE DIRECTOR
ELECTRONICS AND RADIO SCIENCES

Sponsored by
ADVANCED RESEARCH PROJECTS AGENCY
ARPA ORDER 371

Copy No. 83

PREFACE

The work described in this report was performed with the support, and using the facilities, of the Military Research and Development Center (MRDC) in Bangkok, Thailand. The MRDC is a joint Thai-U.S. organization established to conduct research and development work in the tropical environment. The over-all direction of the U.S. portion of the MRDC has been assigned to the Advanced Research Projects Agency (ARPA) of the U.S. Department of Defense who, in 1962, asked the U.S. Army Electronics Command (USAFCOM) and Stanford Research Institute (SRI) to establish an electronics laboratory in Thailand to facilitate the study of radio communications in the tropics and related topics. The MRDC-Electronics Laboratory (MRDC-EL) began operation in 1963 [under Contract DA 36-039 AMC-00040(E)] and since that time ARPA has actively monitored and directed the efforts of USAECOM and SRI. In Bangkok, this function is carried out by the ARPA Research and Development Field Unit (RDFU-T). The cooperation of the Thai Ministry of Defense and the Thailand and CONUS representatives of ARPA and USAECOM made possible the work presented in this report, which is part of a continuing effort to better understand the effect of vegetation on antenna performance.

ABSTRACT

During June and July 1966, measurements of the radiation patterns and impedances of selected HF field-expedient antennas were made in a tropical forest in Thailand on frequencies in the range 2 to 15 Mc/s. These tests--part of the Advanced Research Projects Agency's SEACORE Program--completed a sequence of measurements on the same and similar antennas (including dipoles, inverted L's, slant wires, and monopoles) in an open, level field, in a U.S. conifer forest, and in a dry-evergreen forest in Southeast Asia.

The pattern measurements were made by towing a small, battery-powered transmitter driving a short Hertzian dipole on a long dielectric cable behind an aircraft whose position was electronically tracked. The results are presented as contour maps showing the response for orthogonal polarizations ("vertical," E_θ and "horizontal," E_ϕ) as functions of azimuth and elevation for the elevation range from about 5° to about 55° from the horizon. The power response (normalized Poynting vector) is presented in the same format for the elevation range from 5° to the zenith. Relative gain values are presented for the maximum observed response of the various antennas on a given frequency and for the polarization response E_θ/E_ϕ for a given antenna and frequency. The data indicate that vertical polarization is attenuated more than horizontal polarization, and that scattering of the vertically polarized signal begins at about 12 Mc/s.

Impedance data are presented on Smith charts for each antenna over the range of frequencies for which pattern data were obtained. They show that the environment tends to become part of the antenna.

CONTENTS

ILLUSTRATIONS

CONTOUR PLOTS

ILLUSTRATIONS (Concluded)

TABLES

I INTRODUCTION

The performance of conventional field-expedient antennas used under ideal conditions (e.g., perfectly conducting ground) are reasonably well known or can be calculated without major difficulty. Changes in the performance of these antennas can be expected, however, when they are used under typical field conditions, which are not ideal (e.g., unbalanced feed lines or installed over poor ground or in vegetation). The importance of measuring similar antennas in various situations also has been stressed in the previous reports on this contract. The first full-scale pattern measurements of field-expedient antennas were conducted under relatively ideal conditions--over open, flat terrain--near Lodi, California.[1] * A second set of measurements was conducted in a conifer forest near Lake Almanor, California.[2] This report discusses the third set of measurements conducted in a dry evergreen (tropical) forest in Thailand.

Radiation patterns of dipole, slant-wire, inverted-L, loop and monopole antennas were measured on several frequencies between 2 and 15 Mc/s; pattern data for both the E_ϕ (horizontal polarization) and the E_θ (vertical polarization) response for elevation angles from approximately 5 to 55° are presented in the form of contour plots. Relative power gain patterns (normalized Poynting vector plots) are presented for the portion of a hemisphere from 5° to the zenith.

A description of the field site and the tropical forest used for these measurements is presented in Sec. II, and a description of the antennas measured is presented in Sec. III. The measurement system and data-processing techniques are briefly described in Sec. IV.* Comparisons of the observed relative gain of the antennas are presented in Sec. V. This section also includes a discussion of the contour plots which are presented in the Appendix. Section VI describes the measurement of the antenna impedances and presents the measured impedance data for each antenna. A brief discussion of the results is given in Sec. VII.

*References are listed at the end of this report.

*A more complete description of the data acquisition and processing has been presented previously under this contract in Refs. 1 and 2.

II SITE DESCRIPTION

Measurements of HF field-expedient antennas were conducted during June and July 1966 in a dry-evergreen tropical forest near the village of Ban Mun Chit, Thailand (approximately 10 miles from Chon Buri). The measurement site was located on the edge of a tapioca plantation, as shown in Fig. 1. The antennas were erected in the forest adjoining the tapioca field and in clearings made in the tapioca. The characteristics of the vegetation and site are described briefly in the following paragraphs, and a more comprehensive description can be found in Ref. 3, which describes the site--documentation measurements conducted by the Environmental Sciences Division of the MRDC, Bangkok, Thailand. Electrical constants for the site were measured as discussed in Ref. 4.

The forest used for these measurements was mainly second growth. Scattered trees in the upper and middle story, remains of fallen trees, and decomposed stumps indicated that the forest has gone through a heavy exploitation in the past. A great number of large-sized trees of commercial value in the upper and middle stories had been removed; therefore, the remaining trees were either species of negligible value, or small trees associated with a dense undergrowth layer. Trees in the upper story were of an uneven height of over 75 feet, and the crown canopy was a discontinuous layer. There was relatively no separation in the lower stories. The greater part of the trees were in the lowest story and undergrowth layer. The densest vegetation was present from the ground up to 46 feet, and 88.7 percent of the trees were under 50 feet tall. The lowest story of the forest was about 20 to 46 feet high. Since some individual trees were lower than the undergrowth, there was no distinct line separating these these two layers. In parts of the area, shrubs and trees in the lowest story were totally covered by a common climber which made the ground appear to be covered with a green sheet. Because of the dense undergrowth, visibility was poor both vertically and horizontally. The average horizontal visibility was limited to approximately 33 feet.

The vegetation was removed from this site only where necessary for trails, coaxial transmission lines, and passage of equipment and personnel, and to provide a couple of feet of clearance between the vegetation and radiating elements of the antennas. Because the vegetation found in this forest consisted of undergrowth and trees intermixed, the terms foliage and forest are used interchangeably in this report.

FIG. 1 AERIAL PHOTOGRAPH OF ANTENNA MEASUREMENT SITE

III DESCRIPTION OF ANTENNAS

The antennas measured duplicated those measured over open, flat terrain[1] and in the conifer forest[2] in the United States. The antennas were scaled to be resonant at the same frequencies as were used previously. In addition, antennas of the same type were scaled to be resonant at 6 Mc/s so that the relative gains of antennas of different physical characteristics could be compared more readily. Because the number of antennas measured exceeded the number of available receiving and recording channels, it was necessary to erect the antennas in three sets. The antenna locations for these measurement sets are shown in Figs. 2 through 4.

These antennas, with the exception of the monopoles and the balanced dipoles over ground screens, were designed to conform as closely as possible to those commonly employed in tactical situations. This was easy in the case of the dipoles, since they are normally fed through a coaxial line. However, the slant wires and inverted L's are normally used with the radio set (and the operator) located at the feed point. This was not possible here, because the receivers and recorders were located at a distance from the antennas. For the inverted L's, the coaxial line was was led in at right angles, and the shield was simply connected to a 2-foot grounding rod at the feed point. In all cases, the shields of the coaxial lines were continuous from the antenna feed point to the equipment van. Contrary to tactical communication practice, grounding rods were used at various places to control currents on the coaxial lines--particularly to help define the limits of the coaxial-line counterpoise (see Figs. 5 through 15). It should be noted that these rods changed the current distributions in the ground systems to some extent, principally affecting the antenna impedances.

The radiating elements of all antennas were made of No. 12 solid copper wire, unless otherwise noted.

A. DIPOLE ANTENNAS

Balanced and unbalanced dipole antennas were located in and out of the forest to gain a better understanding of how the radiation patterns of the antennas were affected by the vegetation.

1. 6-Mc/s Dipole Antennas

Eight 6-Mc/s dipole antennas were measured. These antennas were scaled for a length of 95 percent of $\lambda/2$ at 6 Mc/s or 77.8 feet. The eight antennas measured were:

a. Balanced Dipole with Ground Screen in Clearing

The antenna was supported 41 feet above a ground screen by a dielectric rope and wooden poles (see Fig. 5). The ground screen consisted of poultry netting laced together with No. 12 copper wire (with approximately 6 inches of overlap) to form a square ground plane 100 feet on each side. A North Hills Model 0700-BB balun (balanced-to-unbalanced transformer) was used with the antenna. This device is a true ferrite-core transformer, nominally matching 50 ohms unbalanced to 300 ohms balanced. This high effective turns ratio was chosen to minimize the VSWR over the entire band of measurement frequencies, rather than match the resonant (6 Mc/s) impedance value to the 50-ohm receiver van input. The feed line consisted of 100 feet of RG-58 coaxial cable from the feed point of the dipole to the edge of the ground screen. At this point, the RG-58 was connected to RG-8 coaxial cable through an adapter, and the RG-8 cable led to the instrumentation van.

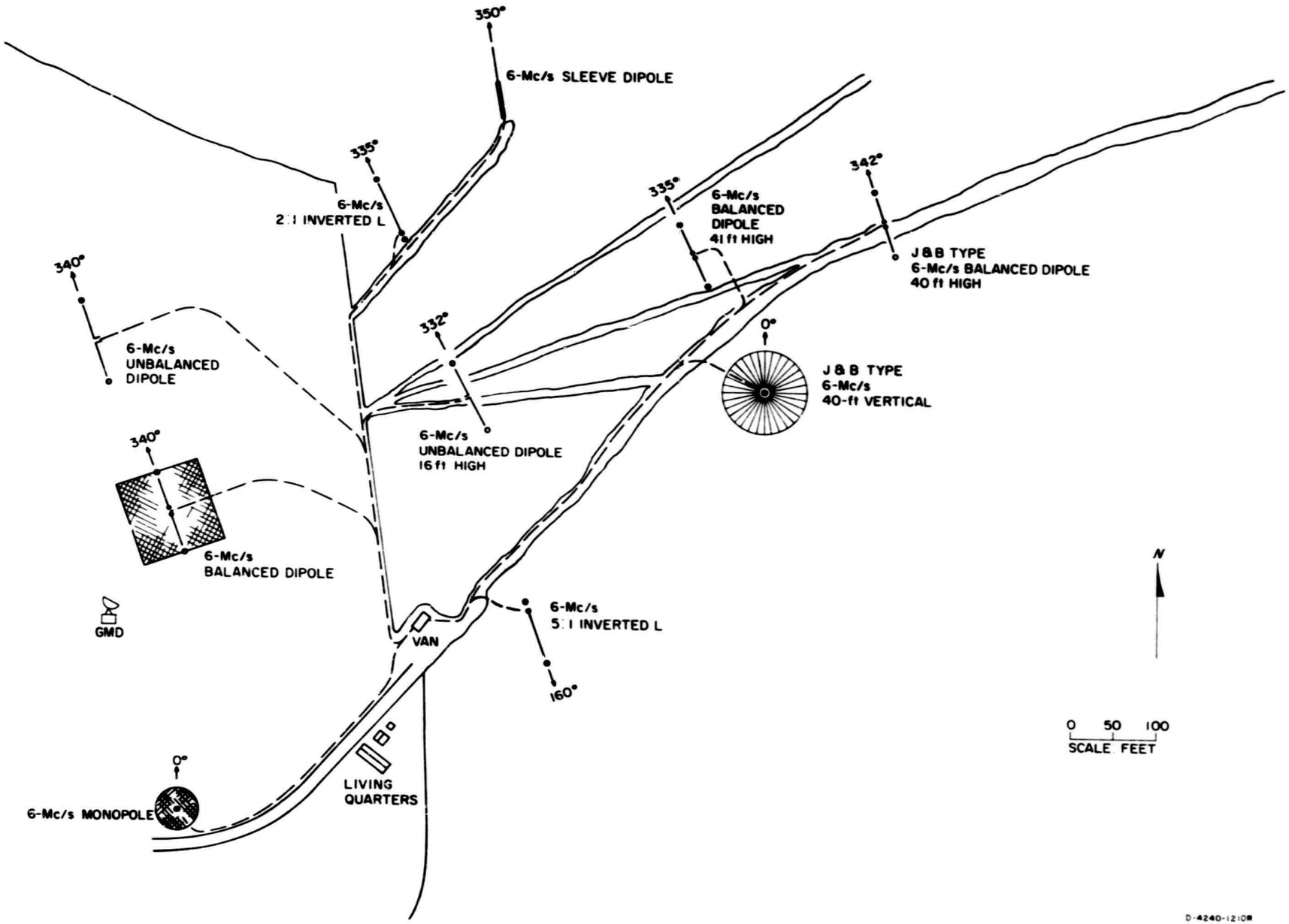

FIG. 2 SITE MAP SHOWING LOCATION OF ANTENNA SET 1

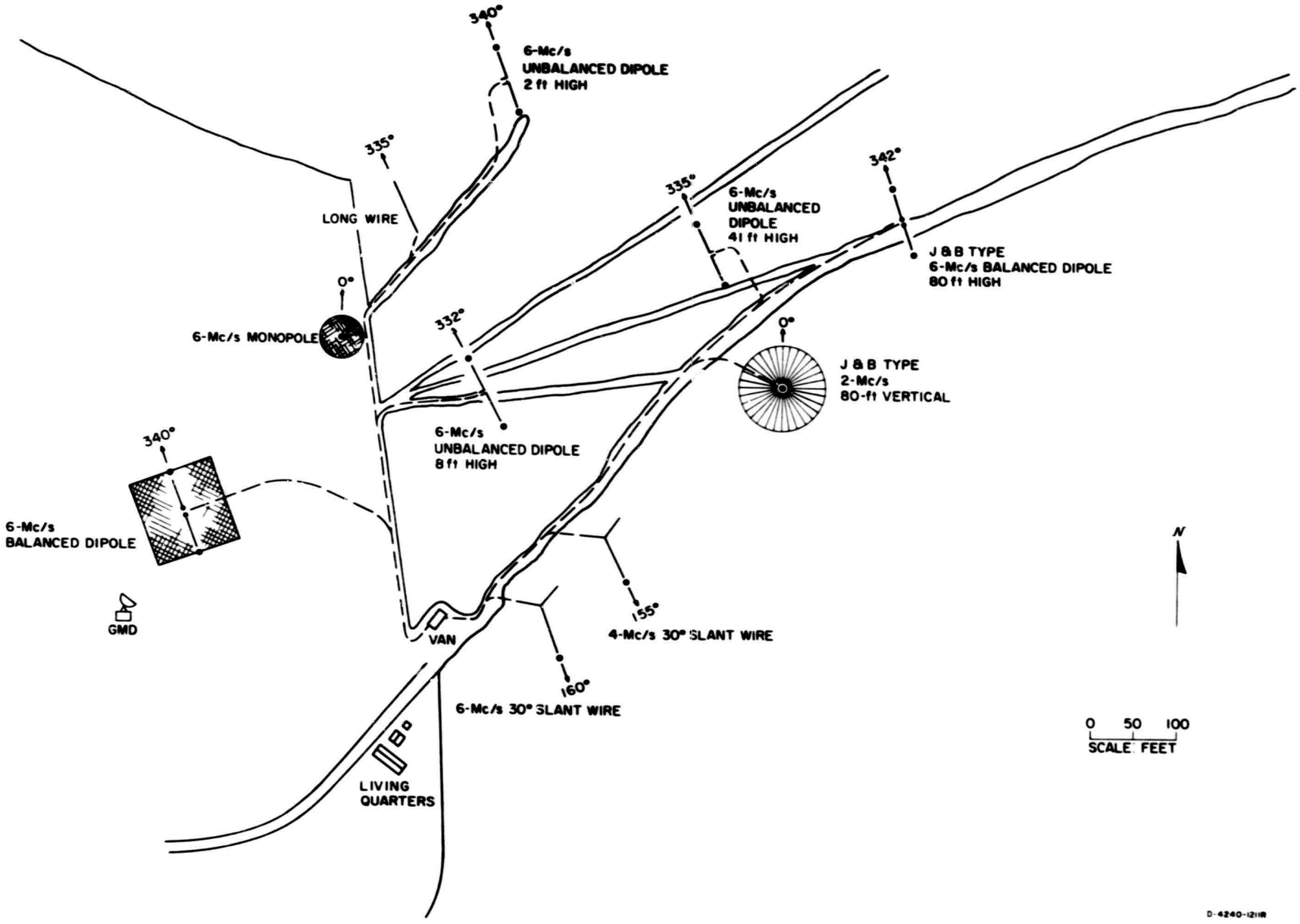

FIG. 3 SITE MAP SHOWING LOCATION OF ANTENNA SET 2

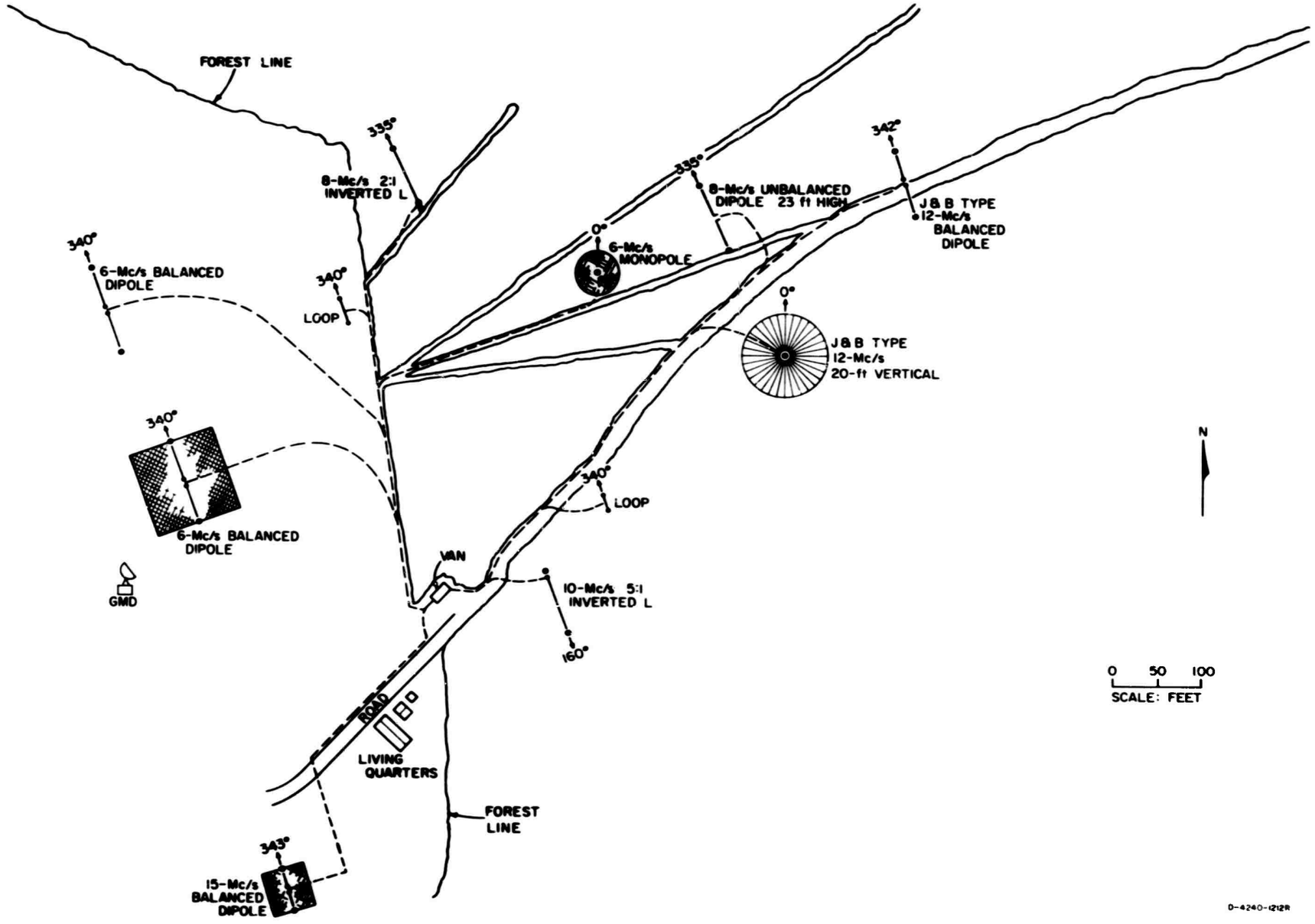

FIG. 4 SITE MAP SHOWING LOCATION OF ANTENNA SET 3

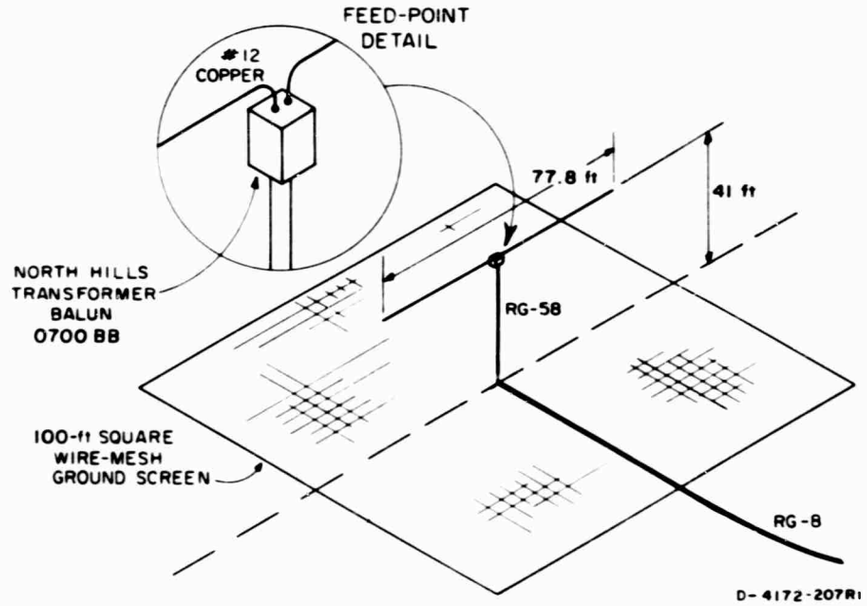

FIG. 5 6-Mc/s BALANCED DIPOLE ANTENNA

b. Balanced Dipole in Clearing

This antenna was constructed exactly as the 6-Mc/s balanced dipole over a ground screen described above, except no ground screen was used for this antenna. The coaxial feed line consisted of 100 feet of RG-58 coaxial cable and RG-8 coaxial cable leading to the instrumentation van. A North Hills 0700-BB balun also was used with this antenna.

c. Unbalanced Dipole in Clearing

This antenna was identical to the 6-Mc/s balanced dipole in the clearing, except that no balun was used.

d. Balanced Dipole in Forest

This antenna was identical to the 6-Mc/s balanced dipole in the clearing, but it was situated in the forest.

e. Unbalanced Dipole in Forest

The construction of this antenna was the same as that of the 6-Mc/s unbalanced dipole in the clearing, but it was located in the forest.

f. 16-ft-High, Unbalanced Dipole in Forest

This antenna was similar to the 6-Mc/s unbalanced dipole in the forest, but it was supported 16 feet from the ground instead of the 41 feet used for the previous antennas. Again, 100 feet of RG-58 coaxial cable was used in the feed line for this antenna.

g. 8-ft-High, Unbalanced Dipole in Forest

This antenna was similar to the 16-ft-high unbalanced dipole in the forest, except that it was supported 8 feet from the ground.

h. 2-ft-High, Unbalanced Dipole in Forest

This antenna was supported along its length by four wooden stakes driven into the ground at approximately 20-ft intervals. The transmission line consisted of a 2-ft piece of RG-58 coaxial line with the braid connected to a copper grounding rod where it was adapted to RG-8 coaxial line leading to the instrumentation van as indicated in Fig. 6.

2. 8-Mc/s, 23-ft-High Unbalanced Dipole Antenna

The elements of the 8-Mc/s, 23-ft-high unbalanced dipole were 29.2 feet long and were suspended by dielectric rope from tree trunks, approximately 18 feet from the ends of the radiators. The 23 feet of RG-58 coaxial line were perpendicular to the antenna and the ground with the braid connected to a copper grounding rod as indicated in Fig. 7. RG-8 coaxial line was used from the ground to the receiver van.

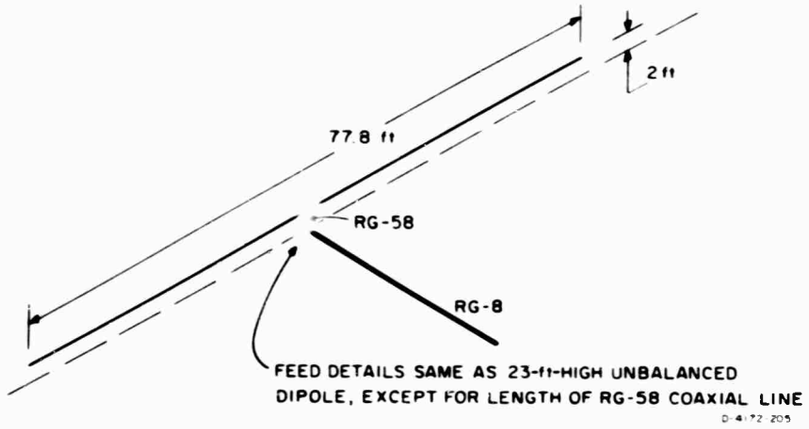

FIG. 6 2-ft-HIGH UNBALANCED DIPOLE ANTENNA

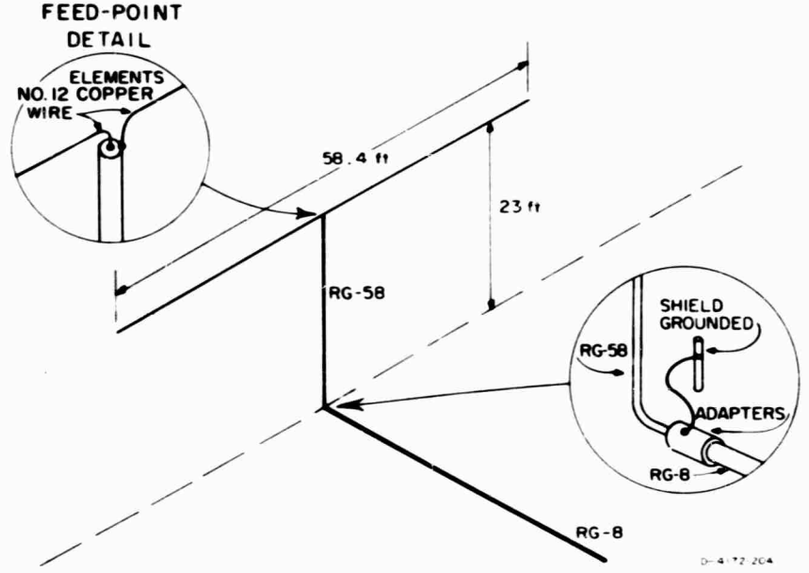

FIG. 7 23-ft-HIGH UNBALANCED DIPOLE ANTENNA

3. 15-Mc/s Balanced Dipole Antenna

The 15-Mc/s balanced dipole antenna consisted of two 15.6-ft elements, 16.4 feet from the ground. The antenna was supported by dielectric rope from two wooden poles at the edge of the ground screen in the clearing. The ground screen was constructed from poultry netting similar to that used with the 6 Mc/s balanced dipole in the clearing, described above; but in this case, the ground screen was only 50 feet on each side. A North Hills Model 0700-BB balun (300 ohm to 50 ohm) was used with the antenna. RG-58 coaxial line was used for the elevated portion of the feed line, while RG-8 coaxial line was used for the portion leading to the instrumentation van.

4. 6-Mc/s Sleeve Dipole Antenna

The 6-Mc/s sleeve dipole antenna consisted of 38.9 feet of tinned copper tubular braid over the insulation of RG-8 coaxial line and soldered to the shield of the coaxial line at the feed point. The center conductor of the coaxial line was soldered to 38.9 feet of solid copper wire, as shown in Fig. 8. This antenna was laid, in a straight line, directly on the ground in the forest with no direct connections made to the ground.

B. 6-Mc/s MONOPOLE ANTENNAS

Three 6-Mc/s monopole antennas were situated in three locations:

(1) In a clearing
(2) On the edge of the forest
(3) In the forest.

The radiating elements of the monopoles were constructed from one-inch-diameter copper tubing, 15.6 feet long and capped at both ends. The ground screens for these antennas were constructed

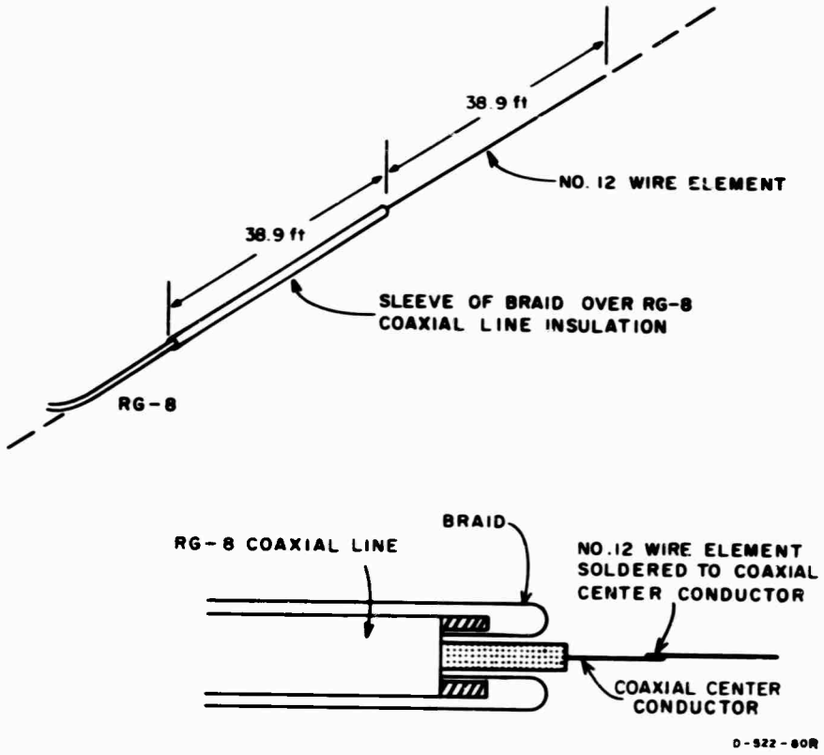

FIG. 8 SLEEVE DIPOLE ANTENNA

from poultry netting, laced together (with approximately 6 inches of overlap) with No. 12 copper wire and then soldered at one-foot intervals. This screen was cut to form a 50-foot-diameter circle.

The antenna impedances were matched to the 50-ohm RG-8 coaxial cable at 6-Mc/s using a passive matching circuit consisting of a (300 ohm to 50 ohm) North Hills balun in parallel with the coaxial cable, and a slug-tuned inductor in series with the radiating element, as indicated in Fig. 9.

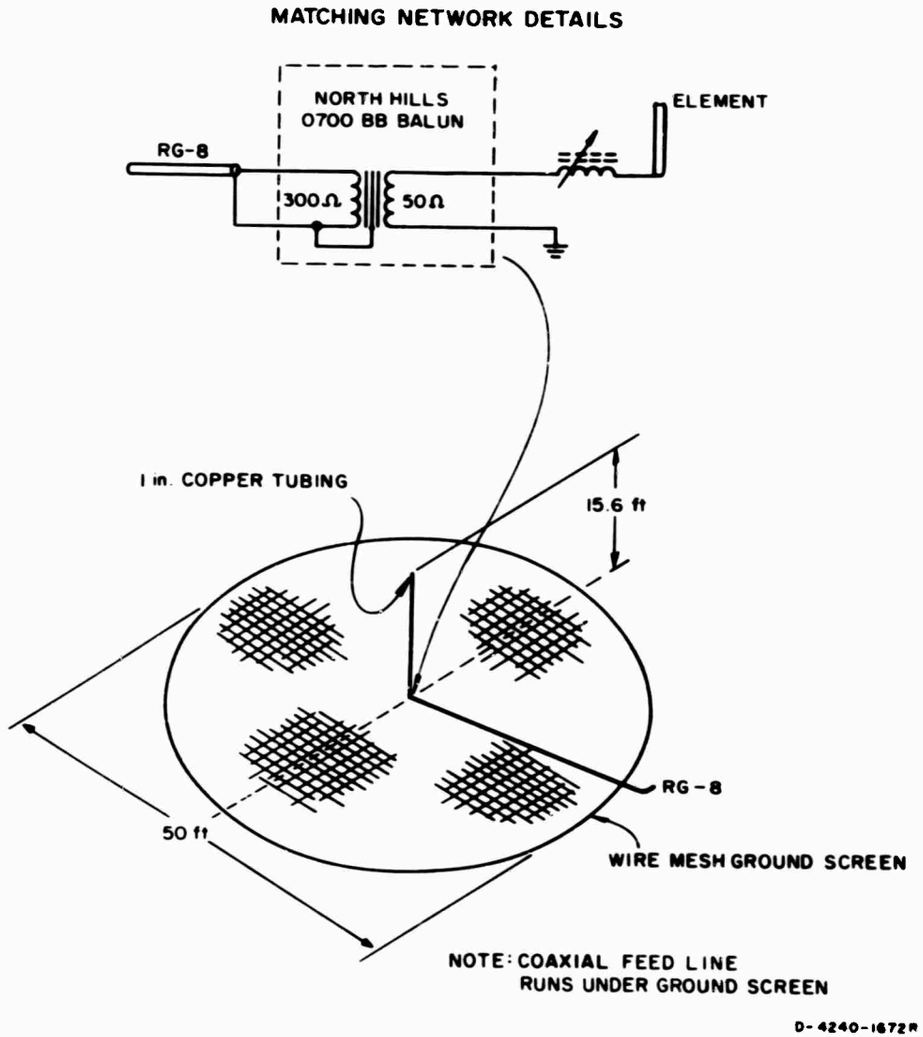

FIG. 9 MONOPOLE ANTENNAS

C. 2:1 INVERTED-L ANTENNAS

Two 2:1 inverted-L antennas were measured. One was resonant at 6 Mc s, and the other was resonant at 8 Mc s. The total length of the elevated wire for these antennas was 95 percent of three-quarters of a wavelength. The ratio of the horizontal wire length to the vertical wire length was 2:1, as the name implies. The horizontal elements were suspended by wooden poles. The vertical elements of these antennas were suspended between their connection with the horizontal elements and their feed points on the ground, thus determining the height above ground of the horizontal elements. The antenna transmission lines were RG-8 coaxial lines, with the braid connected to copper grounding rods at the feed points. The dimensions of these antennas are given in Fig. 10.

D. 5:1 INVERTED-L ANTENNAS

Two 5:1 inverted-L antennas were measured. One was resonant at 6 Mc s, and the other was resonant at 10 Mc s. The construction of these antennas was the same as that of the 2:1 inverted-L antennas, except the ratio of the wire length was 5:1 in this case. The dimensions of these antennas are given in Fig. 10.

E. 30° SLANT-WIRE ANTENNAS

The two 30° slant-wire antennas were scaled for 6 Mc s and 10 Mc s. These antennas consisted of elevated radiators scaled for 95 percent of one-quarter wavelength. The counterpoises were located 135 degrees in azimuth from the horizontal projection of the elevated radiators and were laid directly on the ground. The remote ends of the counterpoise wires were clamped to copper grounding rods. The transmission lines consisted of RG-8 coaxial cable, with the shield grounded at a distance equal to the length of the wire of the counterpoise in order to define the other leg of the counterpoise as indicated in Fig. 11.

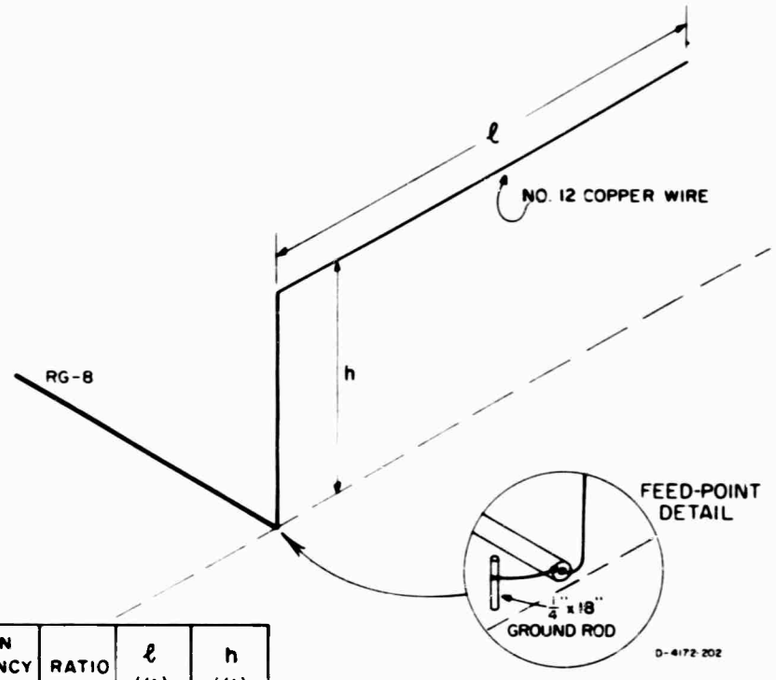

DESIGN FREQUENCY Mc/s	RATIO	ℓ (ft)	h (ft)
6	2:1	77.6	38.8
8	2:1	58.4	29.2
6	5:1	97.0	19.4
10	5:1	58.4	11.7

FIG. 10 INVERTED-L ANTENNAS

F. LOOP ANTENNAS

The two 60-foot loop antennas were measured both in the clearing and in the forest. These square loops consisted of a single turn of copper wire, 15 feet on a side, supported by wooden poles. The feed lines consisted of 50 feet of RG-58 coaxial cable connected to the loops through North Hills Model BB-1100 baluns (75 ohm to 75 ohm), as indicated in Fig. 12.

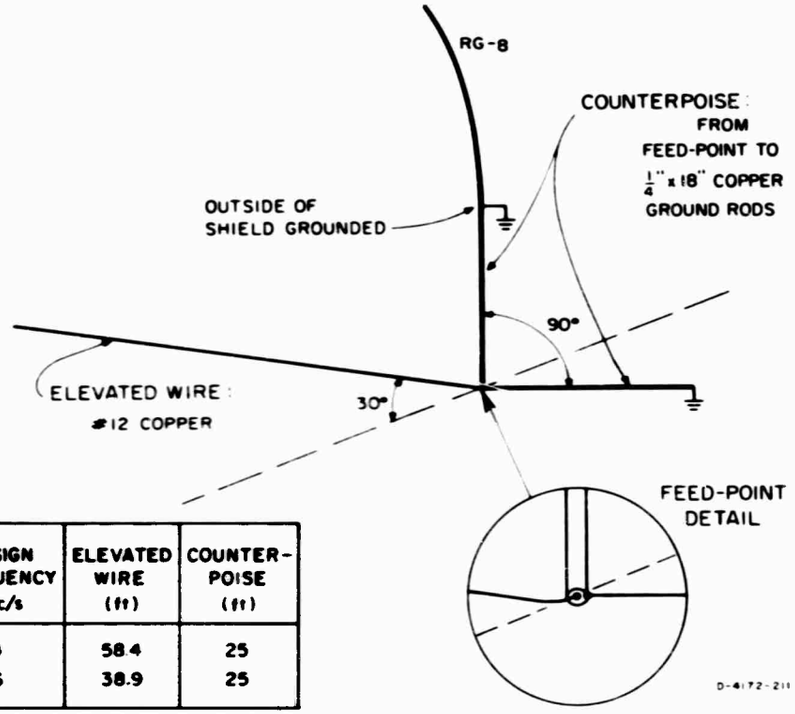

DESIGN FREQUENCY Mc/s	ELEVATED WIRE (ft)	COUNTER-POISE (ft)
4	58.4	25
6	38.9	25

FIG. 11 30° SLANT-WIRE ANTENNAS

G. 6-Mc/s LONG-WIRE ANTENNA

The long-wire antenna consisted of 38.9 feet of No. 12 copper wire soldered to the center conductor of 75 feet of RG-174 coaxial cable, with the braid of the coaxial cable left open-circuited at this point. The center of the antenna was supported over a tree branch, as indicated in Fig. 13.

H. JANSKY-AND-BAILEY-TYPE ANTENNAS

The Jansky-and-Bailey (J&B)-type antennas were constructed to duplicate, as much as possible, the transmitting antennas used

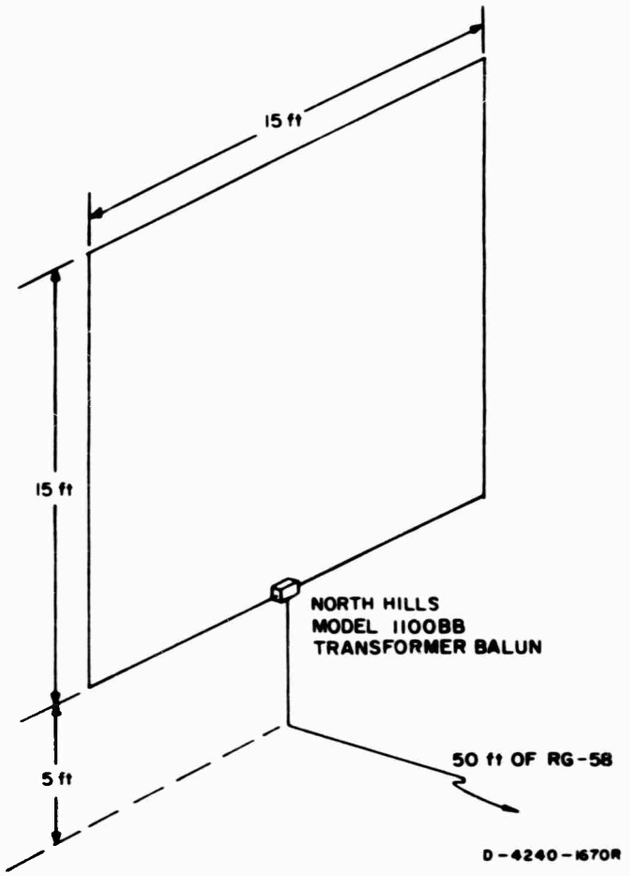

FIG. 12 LOOP ANTENNAS

by J&B for tropical-forest path-loss measurements near Pak Chong, Thailand.[5] These antennas were erected and adjusted at Ban Mun Chit by J&B personnel.

1. J&B-Type Balanced Dipole Antenna

A drawing of the J&B-type balanced dipole is shown in Fig. 14. The antenna was supported by two telescoping aluminum

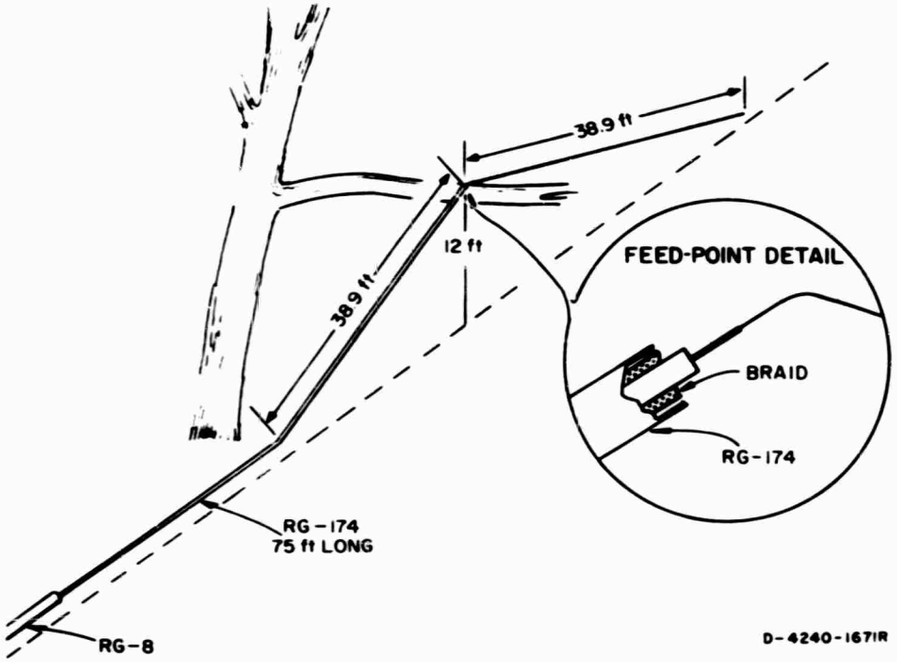

FIG. 13 LONG-WIRE ANTENNA

towers. The tower sections were 5 feet long; the base section was 8 inches in diameter, and the uppermost section was 2 inches in diameter. The height of the dipole antenna was determined by the number of tower sections extended. The radiating elements consisted of two 19.5-ft elements with porcelain insulators at the ends. Another 19.5 feet of copper wire was connected to the insulators, as shown in Fig. 14. When the antenna was measured as a 6-Mc/s dipole, jumpers were connecting the two wires together to form a 39-ft element; and when it was measured as a 12-Mc/s dipole, the jumpers were removed so that the elements were only 19.5-ft long. This procedure was similar to that used at the J&B

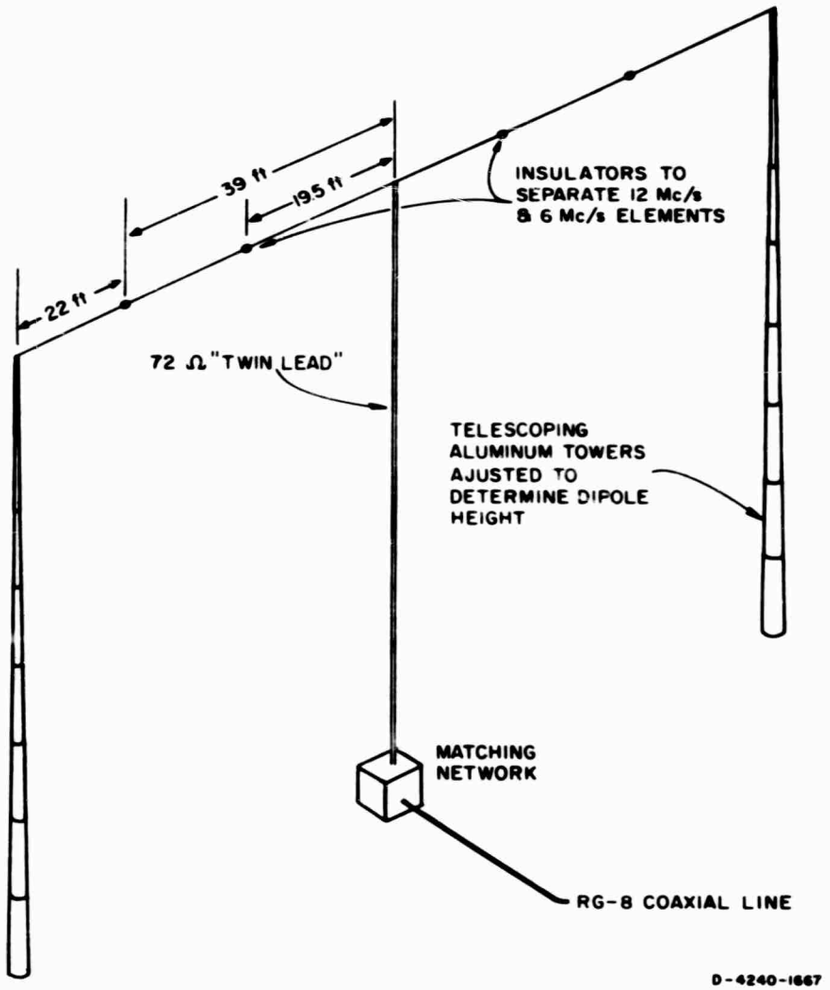

FIG. 14 J&B-TYPE BALANCED DIPOLE ANTENNAS

Pak Chong site, except that at Pak Chong, the towers were approximately 290 feet apart, so that they also could support a 2-Mc/s dipole.

The antenna feed line consisted of 72-ohm twin-lead transmission line from the antenna to a tunable balun on the ground and RG-8 coaxial transmission line from the balun to the instrumentation van. This antenna was measured when tuned for 6 Mc/s at heights of 40 feet and 80 feet, and when tuned for 12 Mc/s at a height of 40 feet.

2. J&B-Type Vertical Antennas

A drawing of the J&B-type vertical antenna is shown in Fig. 15. The vertical element of this antenna was a telescoping

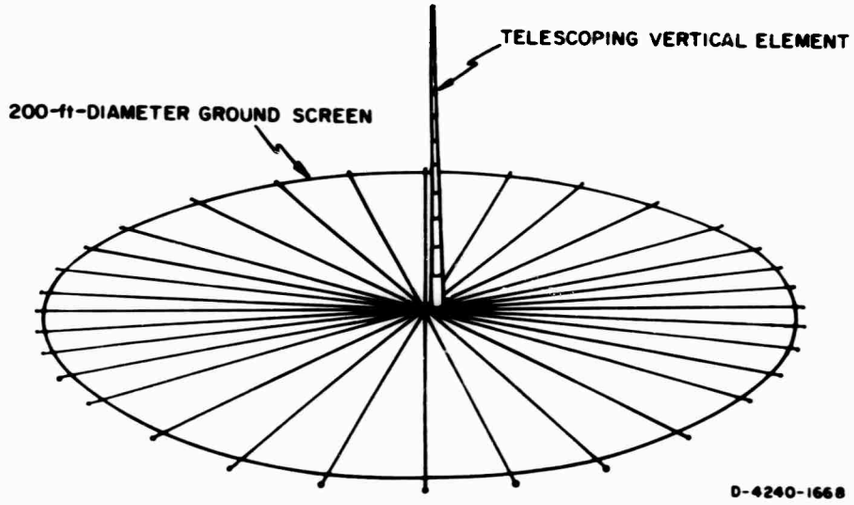

FIG. 15 J&B-TYPE VERTICAL ANTENNAS

aluminum tower of the same construction as the towers used to support the dipole antennas. The element was elevated from the ground with a "Premax" insulator. The ground screen consisted of thirty-two 100-ft copper wire radials connected to a copper grounding rod at the center. Every fourth radial was No. 12 copper wire, and the remainder were No. 18 copper wire; the circumference of the circle was formed with No. 18 copper wire. Every other radial was terminated with 3-ft-long, 1/4-inch-diameter bronze welding rod, and the remaining radials were tied to wooden stakes. A tunable balun transformer was located at the feed point of the vertical element to match the impedance of the antenna to the 50-ohm RG-8 coaxial transmission line. The antenna was tuned for 2 and 6 Mc/s by tuning the balun transformer for minimum VSWR with 80- and 40-ft vertical elements, respectively. The length of the vertical element was adjusted to approximately 20 feet to minimize the VSWR at 12 Mc/s without using the balun transformer.

IV PATTERN MEASUREMENT TECHNIQUES

The antenna patterns were measured by towing a special transmitter (Xeledop*) on specified courses (circles and linear passes) around the antennas with an aircraft modified especially for this purpose. The signals received by the test antennas on the ground were recorded on strip-charts, together with the position of the aircraft. Later, these analog data were scaled and punched onto IBM cards and plotted as contour maps, each of which shows one antenna's response to one frequency and polarization. The operation of the pattern-measuring system has been described in previous reports,[1,2] and the details of the basic system are described only briefly in this report.

A. THE XELEDOP

The Xeledop transmitter is towed behind the aircraft on a long dielectric rope. All the electronics and batteries are contained in a central sphere. Arms extending out from the sphere are fed as a balanced dipole antenna, whose total length is always less than one-half wavelength. Thus, the directivity pattern of the Xeledop is approximately that of a Hertzian dipole for all the measurement frequencies. The Xeledop can be towed to transmit either horizontally (E_ϕ) or vertically (E_θ when corrected for transmitting dipole pattern) polarized waves. The electrical symmetry of the Xeledop is such that the radiated polarization depends only upon its physical orientation.

On a cycle of about 1.5 seconds, the Xeledop pulses through eight selected frequencies between 2 and 30 Mc/s. For these tests, the frequencies were 2, 3, 4, 6, 8, 10, 12, and 15 Mc/s. Two separate checks were conducted daily during the measurement period to ensure that the radiated power of the Xeledop remained constant. The first check consisted of repeating one orbit that had been flown the previous day so that the data could be compared for two successive days. The second check consisted of assessing the radiated power with a wavemeter mounted on a special measuring stand, constructed so that the same physical relationship always existed between Xeledop and wavemeter. Measurements were taken each morning and evening when pattern measurements were conducted; thus, the readings could be compared from day to day, and before and after use to ensure that the radiated power of the Xeledop had remained constant during the period of use.

B. AIRCRAFT TRACKING

In addition to towing the Xeledop transmitter, the aircraft carried a low-power radio beacon transmitter and a modified AN/APX-6 (IFF) transponder unit. Both are used for position information: the beacon is tracked by ground equipment, which provides azimuth and elevation information for data processing; the airborne transponder works with a similar unit on the ground to indicate slant range for the pilot's information. The latter, displayed on a meter, is called the Pilot's Deviation Indicator, or PDI.

The ground-tracking unit is a Rawin AN/GMD-1 Weather Balloon Tracker (referred to as the GMD). A steerable parabolic dish antenna (with rotating dipole feed) tracks the aircraft beacon transmitter through the use of a servomechanism. Azimuth, elevation, and a sequence number (called the GMD time) are printed on adding-machine paper every 6 seconds. The position data (azimuth

*An acronym denoting Transmitting Elementary Dipole with Optional Polarization.

and elevation) are printed out to hundredths of a degree, but this information is precise only to tenths of a degree, with a stated accuracy of ±0.1 degree. We believe the equipment as used to be accurate to at least ±0.3 degree for this application.

Although the operating frequency of the GMD is approximately 1.6 Gc/s it has been found that metal and wooden towers--such as those normally found on an antenna farm--do not attenuate the signal enough to cause erratic operation of the tracking unit. However, previous experience has shown that the dish will start to "hunt" for the beacon, if the signal is attenuated (and/or scattered) by a large object such as a building or trees. For the measurements in Thailand, the GMD was elevated on a tower situated in a clearing. This was necessary to minimize the effect of the attenuation and scattering of the GMD signal due to the trees.

It was found that the GMD could track fairly well above 15 degrees elevation (breaking point between trees and sky); below this angle, manual assistance was required. As the elevation angle decreased and thus the amount of foliage between the beacon and the dish increased, the amount of manual slewing required also increased. For elevation angles below about 5 degrees, it was necessary to rely on the pilot to fly a circular orbit at constant altitude, aided by a barometric altimeter and the Pilot's Deviation Indicator (PDI) and simultaneously check against a circle drawn on an aerial photograph of the site area.

V RESULTS OF PATTERN MEASUREMENTS

A. CONTOUR PLOTS

The measured antenna patterns are presented in the form of contour maps in the Appendix. The display may appear at first glance to be unnecessarily complicated, but it has several advantages. The method of reading these maps is explained below, along with the advantages of using this type of display.

Each contour map shows all of the amplitude data taken on one antenna for one polarization at one frequency. The plot can be visualized in several ways. For example, one may picture placing a large hemisphere over the antenna being measured, then drawing the field strength contours on its surface. The contour plots are two-dimensional maps of this hemisphere regarded from above (see Fig. 16). Hence, the zenith angle is at the center of the plot; azimuth angles appear as radials; and elevation angles are concentric circles. The outer rim of the plot is the horizon, or 0° elevation. The azimuth angles numbered around the rim of the plot are in degrees relative to some principal axis of the antenna. These angles are indicate on the site maps (Figs. 2, 3, and 4) by arrows labeled in degrees magnetic. The relationship of the contour plot azimuth to each antenna is shown by the diagram in the center of the plot.

The contour interval is 3 dB, with the highest amplitude recorded for each plot taken as 0 dB. The 0-dB point is not shown, because its exact position is misleading without detailed knowledge regarding the aircraft orbits, but its true location can easily be inferred from the other contours.

The contour plot has merits both intrinsically, as a data display, and extrinsically--through its adaptability to the Xeledop measurement technique. As a data display, it has the advantage of showing the complete characteristics of the antenna in one diagram much more clearly than any possible series of polar cuts. It also emphasizes the energy distribution as a function of solid angle, a better measure of the usefulness of any antenna for communications than azimuthal beamwidth. Indeed, for HF tactical antennas, the concept of beamwidth is ambiguous and virtually useless.

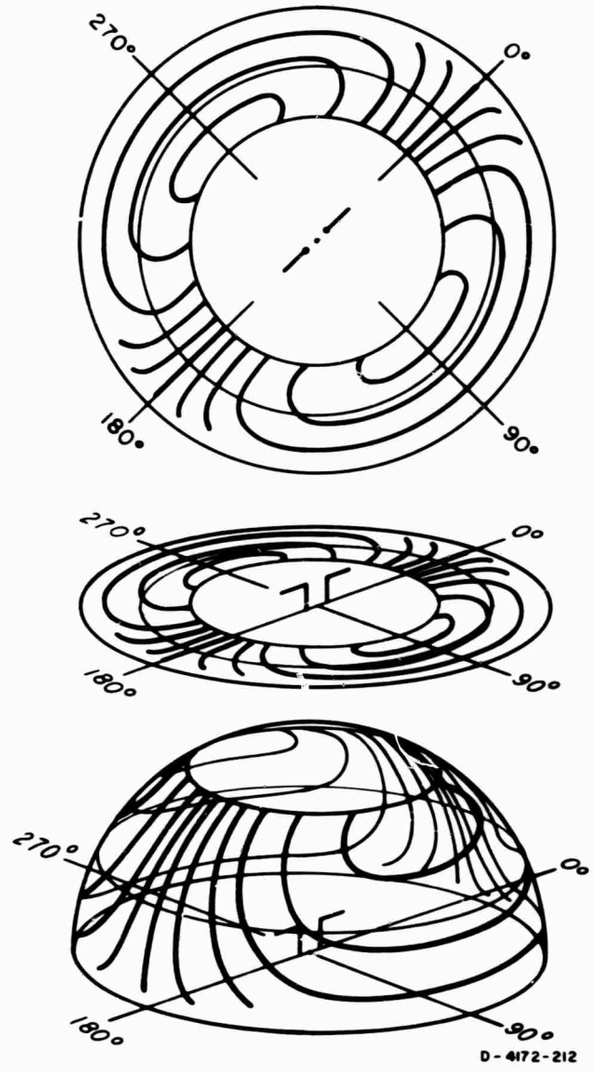

FIG. 16 A CONTOUR PLOT AS A MAP OF A THREE-DIMENSIONAL PATTERN

In addition to having these advantages as a display, the contour plots are very well adapted to the way in which the data are taken. Since the aircraft does not fly perfect orbits about each antenna, the elevation angles actually measured vary considerably during any given orbit and vary from one set of antennas to another. Thus it is neither accurate nor adequate simply to plot the measured amplitude as a function of azimuth on a polar chart. Some means of interpolating between the data taken at the various elevation angles is required, because the angles actually measured change from one set of orbits to the next. The contour plot program does this by finding the surface indicated by the available amplitude data.

The system's pattern accuracy is principally limited by the stability of the field equipment and that of the Xeledop (both of which appear to be very good) and the precision of the scaling of the strip charts. Evidence from overlaps, rereading, and the general correlation of the data indicates that systematic and predictable errors have been effectively eliminated, leaving a random scattering of the data of about 1.5 dB, or one-half contour interval. This offers the best test for the significance of features in a pattern: If the deviation is smaller than one-half the distance between the contour lines, it can be ignored; otherwise, it is significant. This is not strictly true for the lowest frequencies--and even 12 Mc/s in some cases--since many data points were lost because of overriding noise. These plots are distorted not by inaccurate readings but by randomly missing data points.

The angles are measured and plotted to better than 1°; however, with the relatively coarse sampling used, a figure of ±3° in azimuth and elevation would be a better test of significance.

An accurate scaling of the shape and depth of sharp nulls was not attempted, and the analysis above does not strictly apply to them. The angular position of a null is accurately determined, and the value shown on the contour plot is an upper bound for its signal strength. Hence, if -18 dB is shown, this means the null was as low as (or very likely lower than) -18 dB.

B. RELATIVE GAIN

1. Relative Gain for Different Antennas Measured on the Same Frequency

The term "relative" gain is used to distinguish it from "absolute" gain, which is usually derived theoretically and referenced to some absolute gain standard such as an isotropic radiator. By relative gain, we mean the maximum voltage observed across the (nominally) 50-ohm receiver input (expressed in dB)* while obtaining the data for a given contour plot (antenna, frequency, and polarization). The term relative gain here thus means the relative voltages to be expected across (or relative power delivered to) 50-ohm loads at each antenna's feed-point terminals for a constant-power source located at a constant distance in the far field at the azimuth and elevation and with the polarization corresponding to the maximum value measured for each pattern. Relative voltage measurements have been corrected for the loss of the coaxial feed-lines from the antenna to the equipment van but not for the VSWR (1.2:1 maximum) at the input to the receiving system. The circular flight patterns employed to generate these plots provided data only for the elevation range from about 4° to about 55°. Therefore, the dB contours are not necessarily directly related to the actual maximum gain of the antenna, as is

*The dB are relative to an arbitrary reference level chosen for convenience in computer programming. These relative voltage levels are the normalizing constants for the contour plots (i.e., zero decibel for each plot).

usually the convention in antenna measurements. Consequently the reader must be careful when interpreting the relative gain of a short vertical monopole (whose true maximum probably was observed) over that of a short horizontal dipole (whose maximum gain is toward the zenith,[6] and hence was not observed).

2. Relative Gain for Orthogonal Polarizations of the Same Antenna Measured on the Same Frequency

From the values of relative gain derived in Sec. IV-B-1, it is a simple matter to compare the relative response for the two polarizations on a given antenna at a given frequency as shown in Table I. The last column in Table I, E_θ/E_ϕ, tabulates the difference in the maximum response observed for the E_θ (vertical) and E_ϕ (horizontal) polarization, with a plus sign indicating that the E_θ response was higher. For example, for the 6-Mc/s unbalanced dipole in the clearing, the E_θ maximum (0 dB on the contour plot) was 9.2 dB higher than the E_ϕ maximum at 3.0 Mc/s, while at 6 Mc/s the E_ϕ maximum was 5.4 dB higher than the E_θ response. Note that for this example as for most cases, the E_θ maximum and E_ϕ maximum do not necessarily occur at the same azimuth and elevation angles for the same frequency.*

The accuracy of the data in Table I is determined by the contour interval (3 dB) of the contour plots, since they are tabulations of the maximum data-point value for each plot. Thus, the E_θ/E_ϕ values are accurate to within about 1.5 dB. Comparisons between antennas--relative voltage gains--include an additional 0.5-dB error due to the difference between the actual van input and 50 ohms.

*See Appendix Figs. A-25, A-26, A-31, and A-32 for locations of the maxima sited in the above examples.

3. Relative Maximum Power to Matched Loads

Table II presents relative power gains into matched loads, which were derived from the values from Table I through the following procedure:

(1) The mismatch loss from each antenna into 50 ohms at each measured frequency was estimated from the impedance data presented in Chapter VI.

(2) The estimated losses were added to each of the maximum received signal values to estimate the relative power that would have been delivered to a matched load.

(3) To simplify comparisons, the maximum for each frequency was arbitrarily set as the 0-dB reference, and all of the relative-gain values for that frequency were normalized to this maximum.

The resulting values include the 2-dB errors from Table I voltages, plus an error in the mismatch loss estimates. These losses are determined from antenna impedance, which is measured by a technique that finds the magnitude and angle of the reflection coefficient, with an accuracy of about ±5 percent in the magnitude $|\rho|$. Since the mismatch losses required to correct the gains become a more sensitive function of $|\rho|$ as it increases from 0 to 1 (or the VSWR as it increases from 1 to infinity), the relative gain estimates suffer a small error at low antenna VSWR and a large error for high antenna VSWR, all due to a constant 5-percent error in $|\rho|$. Although the effect of this error is minimized by the technique outlined in Sec. VI-A it should still be noted that an error is present. In Table II, those values for which the sum of the errors, including the voltage-gain errors, is potentially

Table I

RELATIVE VOLTAGE GAINS ACROSS 50-OHM LOADS AT PATTERN MAXIMA

Antenna and Design Frequency	Measurement: Frequency (Mc s)	Measurement: Polarization	Relative Voltage (dB)	E_θ E_ϕ (dB)
6 Mc s balanced dipole over ground screen in clearing	3.0	H	-44.2	+6.5
		V	-50.7	
	4.0	H	-39.9	-0.6
		V	-39.3	
	6.0	H	-26.3	-2.9
		V	-23.4	
	8.0	H	-25.5	-5.3
		V	-20.2	
6 Mc s balanced dipole in clearing	3.0	H	-53.5	-2.4
		V	-51.1	
	4.0	H	-41.4	+0.2
		V	-41.6	
	6.0	H	-26.9	-2.8
		V	-24.1	
	8.0	H	-26.5	-5.8
		V	-20.7	
6 Mc s unbalanced dipole in clearing	3.0	H	-49.2	+9.2
		V	-58.1	
	4.0	H	-47.5	-2.6
		V	-50.1	
	6.0	H	-26.2	-5.4
		V	-20.8	
	8.0	H	-33.5	-5.1
		V	-28.4	
6 Mc s balanced dipole in foliage	6.0	H	-57.5	-3.0
		V	-54.5	
6 Mc s unbalanced dipole in foliage	3.0	H	-56.1	-5.5
		V	-61.6	
	4.0	H	-47.1	-2.8
		V	-49.9	
	6.0	H	-20.3	-3.5
		V	-23.8	
	8.0	H	-34.6	-6.3
		V	-28.3	
6-Mc s, 16-ft-high, unbalanced dipole in foliage	6.0	H	-26.7	-3.6
		V	-23.1	
6-Mc s, 8-ft-high, unbalanced dipole in foliage	6.0	H	-26.5	-1.0
		V	-27.5	
6-Mc/s, 2-ft-high, unbalanced dipole	1.0	H	-55.1	0.0
		V	-55.1	
	6.0	H	-34.4	+2.8
		V	-37.2	
	8.0	H	-39.6	+1.4
		V	-41.0	

Table 1 (Continued)

RELATIVE VOLTAGE GAINS ACROSS 50-OHM LOADS AT PATTERN MAXIMA

Antenna and Design Frequency	Measurement: Frequency (Mc/s)	Measurement: Polarization	Relative Voltage (dB)	E_θ/E_θ (dB)
8-Mc s, 23-ft-high, unbalanced dipole	8.0	H	-22.8	-2.9
		V	-19.9	
15-Mc s balanced dipole over ground screen in clearing	4.0	H	-63.0	-0.7
		V	-62.3	
	6.0	H	-50.3	-1.8
		V	-48.5	
	8.0	H	-41.3	-2.6
		V	-38.7	
	12.0	H	-29.0	-4.2
		V	-24.8	
	15.0	H	-20.1	-4.0
		V	-16.1	
6-Mc s sleeve dipole	6.0	H	-41.9	+2.7
		V	-44.6	
6-Mc s monopole in clearing	6.0	H	-27.5	--
5-Mc s monopole on edge of clearing	4.0	H	-63.9	--
	6.0	H	-29.6	--
	8.0	H	-47.2	--
6-Mc s monopole in foliage	4.0	H	-61.0	--
	6.0	H	-37.0	--
	8.0	H	-43.8	--
6-Mc s 2:1 inverted L	3.0	H	-46.5	+0.7
		V	-47.2	
	4.0	H	-44.7	-0.1
		V	-44.6	
	6.0	H	-29.2	-3.0
		V	-26.2	
	8.0	H	-31.1	-1.5
		V	-32.6	
8 Mc/s 2:1 inverted L	8.0	H	-34.3	-1.0
		V	-33.3	
6-Mc s 5:1 inverted L	4.0	H	-43.2	+1.3
		V	-44.5	
	6.0	H	-32.4	-4.3
		V	-28.1	
	8.0	H	-31.0	+2.8
		V	-33.8	
10-Mc s 5:1 inverted L	10.0	H	-32.4	-3.5
		V	-28.9	
4-Mc s 30 slant wire	4.0	H	-38.6	+4.6
		V	-43.2	

Table 1 (Concluded)

RELATIVE VOLTAGE GAINS ACROSS 50-OHM LOADS AT PATTERN MAXIMA

Antenna and Design Frequency	Measurement Frequency (Mc/s)	Measurement Polarization	Relative Voltage (dB)	E_θ E_ϕ (dB)
6-Mc/s 30° slant wire	3.0	θ	-57.8	-9.2
		ϕ	-67.0	
	4.0	θ	-51.4	-7.3
		ϕ	-58.7	
	6.0	θ	-39.4	-5.8
		ϕ	-45.2	
	8.0	θ	-35.5	-5.4
		ϕ	-40.9	
6-Mc/s loop in clearing	6.0	θ	-51.0	-1.4
		ϕ	-52.4	
6-Mc/s loop in foliage	6.0	θ	-52.9	-0.7
		ϕ	-53.6	
6-Mc/s longwire	3.0	θ	-62.5	-2.5
		ϕ	-65.0	
	4.0	θ	-55.8	-1.3
		ϕ	-54.5	
	6.0	θ	-42.3	-3.0
		ϕ	-45.3	
	8.0	θ	-42.1	-1.5
		ϕ	-43.6	
J&B-type 40-ft-high, 6-Mc/s balanced dipole	6.0	θ	-21.1	-4.5
		ϕ	-16.6	
J&B-type 80-ft-high, 6-Mc/s balanced dipole	6.0	θ	-24.6	-3.5
		ϕ	-21.1	
J&B-type 40-ft-high, 12-Mc/s balanced dipole	12.0	ϕ	-16.1	--
J&B-type 6-Mc/s 40-ft vertical	6.0	θ	-28.9	--
J&B-type 2-Mc/s 80-ft vertical	2.0	θ	-42.3	--
J&B-type 12-Mc/s 20-ft vertical	12.0	θ	-17.5	--

Table II

RELATIVE POWER GAINS INTO MATCHED LOADS AT PATTERN MAXIMA

Measurement Frequency (Mc/s)	Antenna	Potential Error*	E_θ (dB)	E_ϕ (dB)
3.0	6-Mc/s balanced dipole over ground screen in clearing	x	0.0	-6.5
	6-Mc/s 2:1 inverted L		-4.1	-4.8
	6-Mc/s unbalanced dipole in clearing		-5.8	-15.0
	6-Mc/s balanced dipole in clearing	x	-10.5	-8.1
	6-Mc/s long wire	x	-11.6	-14.1
	6-Mc/s unbalanced dipole in foliage		-14.7	-20.2
	6-Mc/s 30° slant wire	x	-15.8	-25.0
4.0	6-Mc/s balanced dipole over ground screen in clearing		-0.6	0.0
	6-Mc/s 5:1 inverted L		-2.8	-4.1
	4-Mc/s 30° slant wire		-2.9	-7.5
	6-Mc/s balanced dipole in clearing		-3.9	-4.1
	6-Mc/s unbalanced dipole in foliage	x	-5.5	-8.3
	6-Mc/s 2:1 inverted L	x	-5.9	-5.8
	6-Mc/s unbalanced dipole in clearing	x	-7.6	-10.2
	6-Mc/s long wire	x	-8.4	-8.1
	6-Mc/s 30° slant wire	x	-12.8	-20.1
	6-Mc/s 2-ft-high dipole	x	-16.4	-16.4
	15-Mc/s balanced dipole	x	-22.6	-21.9

*Potential amplitude errors greater than ±3 dB because of VSWR measurement errors.

†All gains on one frequency normalized to set highest equal to 0.0 dB.

Table II (Continued)

RELATIVE POWER GAINS INTO MATCHED LOADS AT PATTERN MAXIMA

Measurement Frequency (Mc/s)	Antenna	Potential Error*	Gain† E_θ (dB)	Gain† E_ϕ (dB)
4.0 (continued)	6-Mc/s monopole on edge of clearing	x	-23.5	--
	6-Mc/s monopole in foliage	x	-24.8	--
6.0	6-Mc/s J&B type, 40-ft-high balanced dipole		-4.5	0.0
	6-Mc/s unbalanced dipole in foliage		-3.6	-7.1
	6-Mc/s unbalanced dipole in clearing		-9.7	-4.3
	6-Mc/s J&B-type, 80-ft-high balanced dipole		-8.4	-4.9
	6-Mc/s balanced dipole over ground screen in clearing		-8.6	-5.7
	6-Mc/s, 16-ft-high unbalanced dipole in foliage		-10.4	-6.8
	6-Mc/s balanced dipole in clearing		-10.2	-7.8
	6-Mc/s 2:1 inverted L		-11.5	-8.5
	6-Mc/s J&B-type 40-ft vertical	x	-8.8	--
	6-Mc/s 5:1 inverted L		-13.4	-9.1
	6-Mc/s, 8-ft-high unbalanced dipole in foliage		-10.2	-11.2
	6-Mc/s monopole in clearing		-11.3	--
	6-Mc/s monopole on edge of clearing		-13.4	--
	6-Mc/s long wire	x	-14.9	-17.9
	6-Mc/s sleeve dipole	x	-15.5	-18.2
	6-Mc/s 2-ft-high unbalanced dipole		-17.7	-20.5
	6-Mc/s monopole in foliage		-19.6	--

Table II (Continued)

RELATIVE POWER GAINS INTO MATCHED LOADS AT PATTERN MAXIMA

Measurement Frequency (Mc/s)	Antenna	Potential Error*	Gain† E_θ (dB)	Gain† E_ϕ (dB)
6.0 (continued)	6-Mc/s 30° slant wire		-20.5	-26.3
	6-Mc/s loop in clearing	x	-23.6	-25.0
	6-Mc/s loop in foliage	x	-25.6	-26.3
	15-Mc/s balanced dipole over ground screen in clearing	x	-28.3	-26.5
	6-Mc/s balanced dipole in foliage		-39.5	-35.0
8.0	6-Mc/s balanced dipole over ground screen in clearing	x	-5.3	0.0
	6-Mc/s balanced dipole in clearing		-11.9	--5.1
	8-Mc/s 23 ft-high dipole		-8.7	-5.8
	6-Mc/s unbalanced dipole in foliage	x	-16.6	-10.3
	6-Mc/s unbalanced dipole in clearing		-18.1	-13.0
	6-Mc/s 5:1 inverted L	x	-13.3	-16.1
	6-Mc/s long wire	x	-17.8	-19.3
	8-Mc/s 2:1 inverted L		-19.2	-18.2
	6-Mc/s 30° slant wire	x	-19.0	-24.4
	6-Mc/s 2:1 inverted L		-20.8	-19.3
	15-Mc/s balanced dipole over ground screen in clearing	x	-23.7	-21.1
	6-Mc/s 2-ft-high unbalanced dipole		-24.8	-26.2
	6-Mc/s monopole on edge of clearing	x	-26.6	--
	6-Mc/s monopole in foliage		-29.4	--

*Potential amplitude errors greater than ±3 dB because of VSWR measurement errors.

†All gains on one frequency normalized to set highest equal to 0.0 dB.

Table 11 (Concluded)

RELATIVE POWER GAINS INTO MATCHED LOADS AT PATTERN MAXIMA

Measurement Frequency (Mc/s)	Antenna	Potential Error*	Gains† E_θ (dB)	Gains† E_ϕ (dB)
12.0	12-Mc/s J&B-type 40-ft-high balanced dipole		-29.4	--
	12-Mc/s J&B-type 40-ft vertical		-0.8	--
	15-Mc/s balanced dipole over ground screen in clearing	x	-8.6	-4.4

*Potential amplitude errors greater than 3 dB because of VSWR measurement errors.

†All gains on one frequency normalized to set highest equal to 0.0 dB.

in excess of 3 dB and have been indicated by a cross. Potential errors of the unmarked values are less than 3 dB.

4. Comments on Absolute Gain and Comparison of Relative Gain Between Frequencies

Absolute gains cannot be derived from the measured data without assuming (or calculating) the gain of one receiving antenna relative to an isotropic radiator because the effective radiated power of the Xeledop is unknown.[7] This assumption or calculation of gain would have to be made at each measurement frequency. Comparison of the relative gain between frequencies would require knowledge of the difference in the effective radiated power of the Xeledop on the frequencies for which the comparison is desired, but this is also unknown. Therefore, comparison of relative gain between frequencies again requires an assumed gain characteristic for one antenna. In practice, comparison of relative gain between frequencies is most easily accomplished by comparing after conversion to absolute gain, which is beyond the scope of this report.

C. POWER PLOTS

The technique described in detail in Ref. 2 offers a practical method of measuring Poynting vector patterns (power plots) over the entire hemisphere above the antennas, especially providing an estimate of the effective directivity near the zenith--the direction of most interest for HF skywave applications on short ionospheric paths. Although not strictly reciprocal, as are individual polarization patterns, these power plots do apply to both ends of the communications system.

Consider briefly the derivation of a power plot from orthogonal-polarization pattern samples, such as the usual E_ϕ and E_θ plots. The latter are maps of many samples, each

effectively taken in a plane tangential to a hemisphere over the antennas; the plane defined by the ϕ and θ vectors is shown in Fig. 17. The plane containing these vectors will be called the

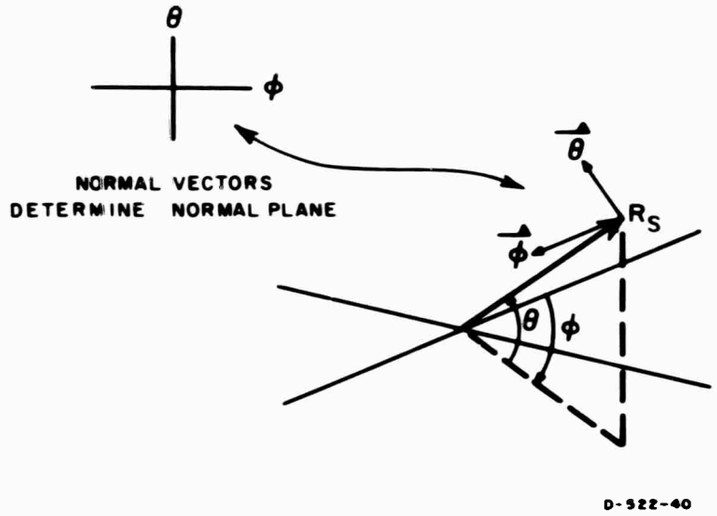

FIG. 17 DEFINITION OF NORMAL PLANE

normal plane because of its relationship to R_s, the vector from the antenna location to the measurement point. To find the power passing through such a sample point (transmitting case), one would take, by Poynting's theorem:

$$P = |E_\phi|^2 + |E_\theta|^2 \quad .$$

For the receiving case,* the time-average response to random polarization (imagine a rotating, constant-amplitude field vector) is proportional to the magnitude of the receiving antenna's maximum response vector, regardless of the latter's orientation. To find this vector, consider the situation in Fig. 18, showing the

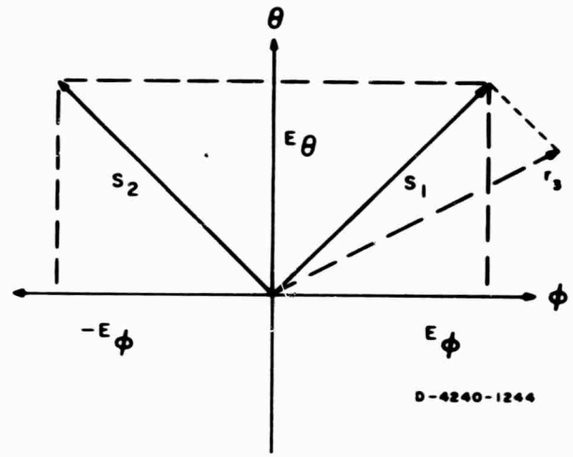

FIG. 18 DERIVATION OF S FROM E_ϕ AND E_θ SAMPLES

E_ϕ and E_θ vectors lying in the normal plane at a given azimuth-elevation sample point. If we assume for the moment that the antenna's actual response is linearly polarized, then it must be

*For the receiving case, the power plots can be thought of as approximating the time-average response of the antenna to randomly polarized incident waves arriving at the receiving antenna after reflection from the ionosphere. Note, however, that the received signal level at any given instant depends upon the resultant incident field strength and the actual polarization of both receiving antenna and incident field (i.e., ionospheric absorption and fading effects). For near-vertical incidence paths--the intended use of these field-expedient antennas--the randomization is not quite complete in equatorial areas.[8,9,10]

one of two vectors: S_1 or S_2. Which S cannot be determined without a third measured response, such as the r_3 vector, shown dotted. However, for our purposes, the polarization is immaterial; only the magnitudes $|S_1|$ and $|S_2|$ are of interest. Since the two magnitudes are equal, we can assign the value $S = |S_1| = |S_2|$ to this sample point, which represents the antenna's response to an optimally polarized incident wave.

Note that P given by power summation and S given by field vector summation are identical. Therefore, a single contour map can fill both needs described above: transmitting power pattern and time-average response pattern to randomly polarized incoming waves.

The measured power plots for each antenna are presented in the Appendix, following the E_θ and E_ϕ plots for the same antenna. For various practical reasons discussed in Ref. 2, the measurement of individual polarization was limited to comparing the response along orthogonal lines directly overhead. The passes were so oriented that they were within 10° of being collinear and parallel to (or orthogonal to) the axis of the antenna. Thus, there was usually a 20-dB difference between the two passes; therefore, their relative amplitude is not indicated in the center of the contour plots, as was done in Ref. 2.

VI IMPEDANCE MEASUREMENTS

Impedance measurements were made on all antennas as an aid to pattern analysis and derivation of relative gain figures. Such measurements also imply that the environment acts as part of the antenna, as do the counterpoise wires and grounding system of the antennas.

A. MEASUREMENT TECHNIQUE

These measurements were taken with an Alford automatic impedance plotter, which provides a rapid and continuous display of impedance at the antenna feed point over a wide frequency band. This capability makes it economically feasible to take a large number of measurements without missing any significant characteristics [which might be lost if a discrete-point technique (RX meter) were used]. The price of this convenience and continuity is the accuracy of any given data point. The plotter measured impedances indirectly by finding the load's reflection coefficient (compared to 50 ohms) and displaying that value on an oscilloscope face with a Smith-chart bezel. The equipment accuracy stated by the manufacturer is expressed as a percentage of the load reflection coefficient ($\pm 5\%$, $\pm 5^\circ$); hence, the resistance and reactance numbers near the rim of the chart are not precise. For this reason, the data are presented on Smith charts, rather than as tables of resistance and reactance as a function of frequency.

The inaccuracies of the impedance plotter have been discussed in previous reports in this series. As a reminder, these inaccuracies occur at the ends of the frequency bands of the phase splitters used with the plotter and at the "critical frequencies" of the coaxial cable between the antenna and the impedance plotter. To minimize these inaccuracies, the same techniques were used as were used for the measurements in a confier forest.[2] This procedure consisted of calibrating more often than is recommended by the manufacturer. The manufacturer advises that the instrument be calibrated once for the frequency band of the phase splitter in use. It was found that if the instrument were calibrated at the center frequency and at both ends of the frequency bands of these phase splitters, there would be less discrepancy when comparing measurements from the upper frequency and lower frequency of two consecutive phase splitters. The impedance plotter was also calibrated at each frequency transmitter by the Xeledop, to minimize antenna VSWR measurement errors at the frequencies at which data were taken for the radiation patterns and relative gain figures (see Sec. V).

B. MEASURED IMPEDANCE RESULTS

The impedance of each antenna was measured over the same frequency range through which the pattern measurements were conducted. These data are presented on Smith charts in Figs. 19 through 46. Data samples representing the impedance on fixed frequencies for which the values were accurately scaled from the bezel display are indicated by dots on the Smith charts. The adjacent number is the measurement frequency in megacycles. The solid curves through the points were sketched directly from the bezel display as frequency was swept through the band of interest. They should be considered to represent the general trend of feed-point impedance with frequency. Even though the impedance plotter was calibrated quite often, some of the measurements indicated the effect of the coaxial feed cable from the antenna to the impedance plotter were not completely compensated for. In these cases, the values are indicated on the Smith chart plots as a dashed curve. In some cases it is only possible to show the measured data points themselves and not the impedance function because of erratic operation of the impedance bridge and coaxial feed-line interaction.

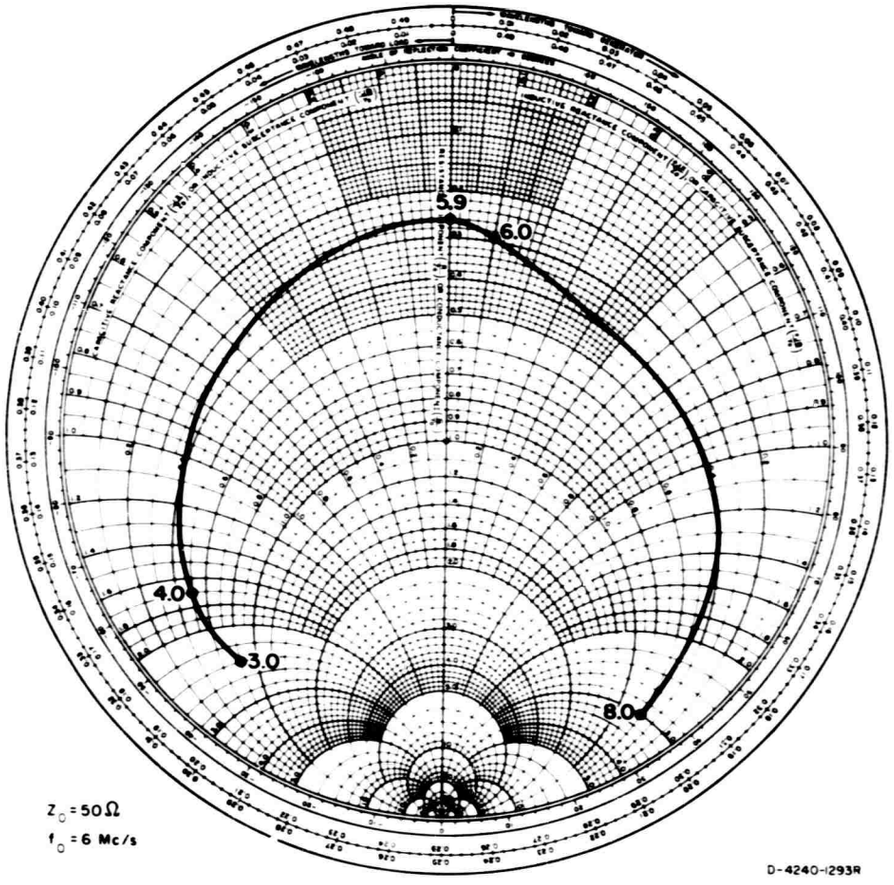

FIG. 19

SMITH CHART REPRESENTATION OF ANTENNA IMPEDANCE FOR 6-Mc s BALANCED DIPOLE WITH GROUND SCREEN IN CLEARING (3.0 To 8.0 Mc s)

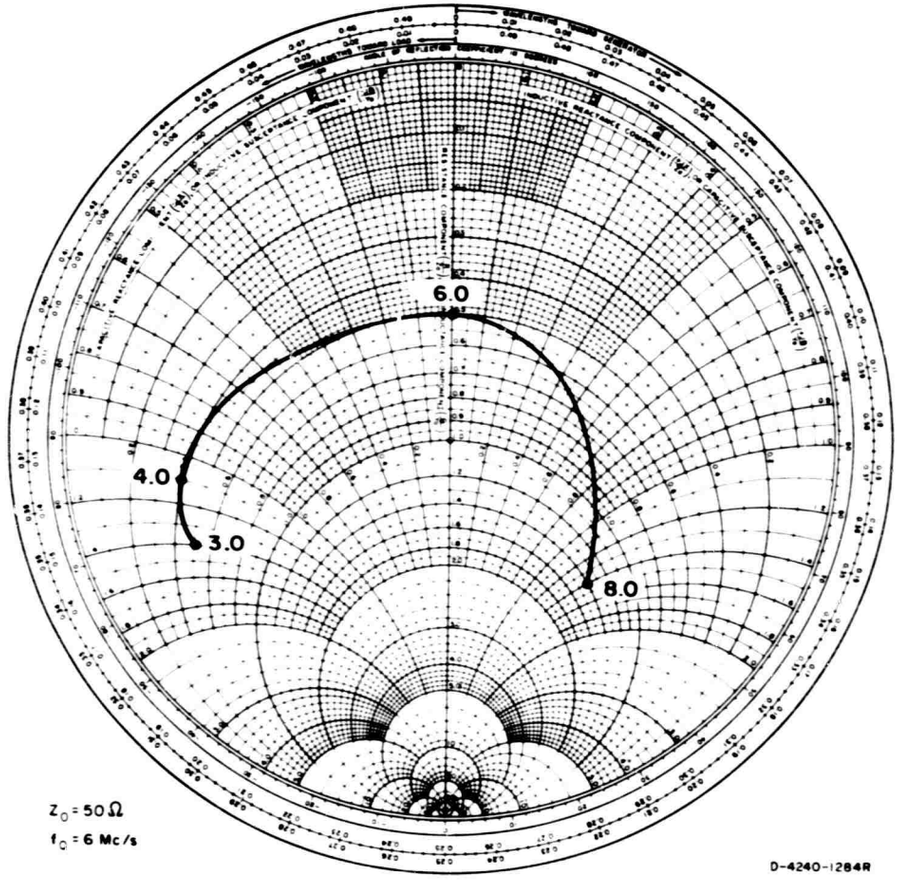

FIG. 20

SMITH CHART REPRESENTATION OF ANTENNA IMPEDANCE FOR 6-Mc s BALANCED DIPOLE IN CLEARING (3.0 To 8.0 Mc s)

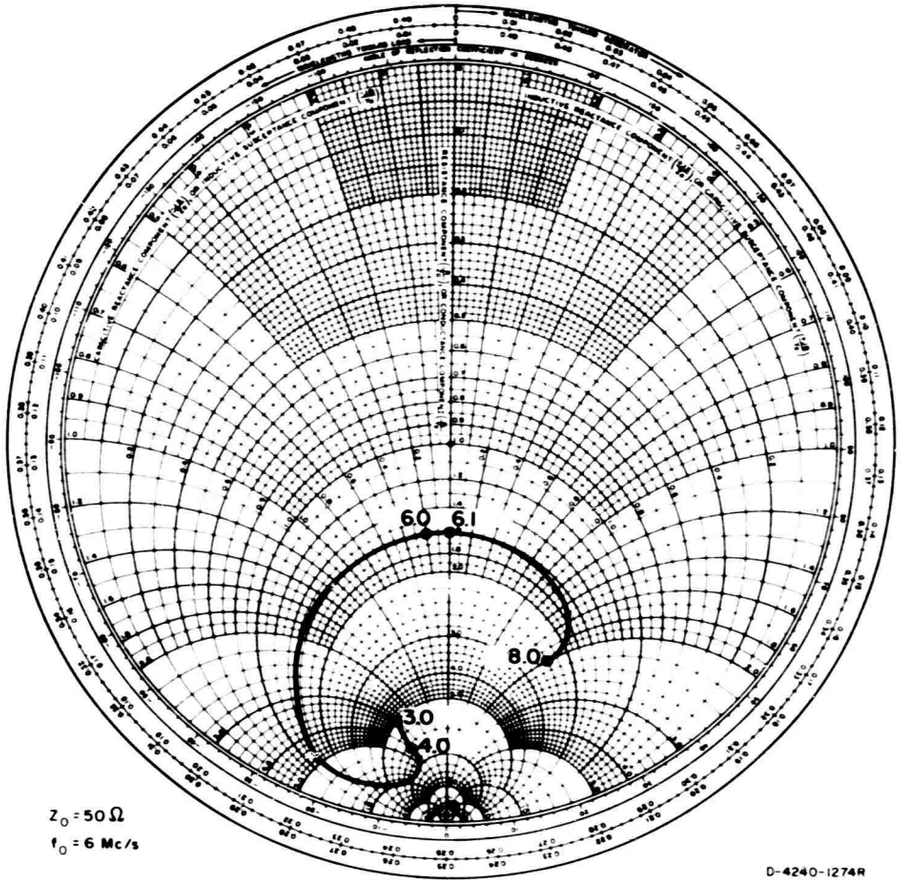

FIG. 21

SMITH CHART REPRESENTATION OF ANTENNA IMPEDANCE FOR 6-Mc s UNBALANCED DIPOLE IN CLEARING (3.0 To 8.0 Mc s)

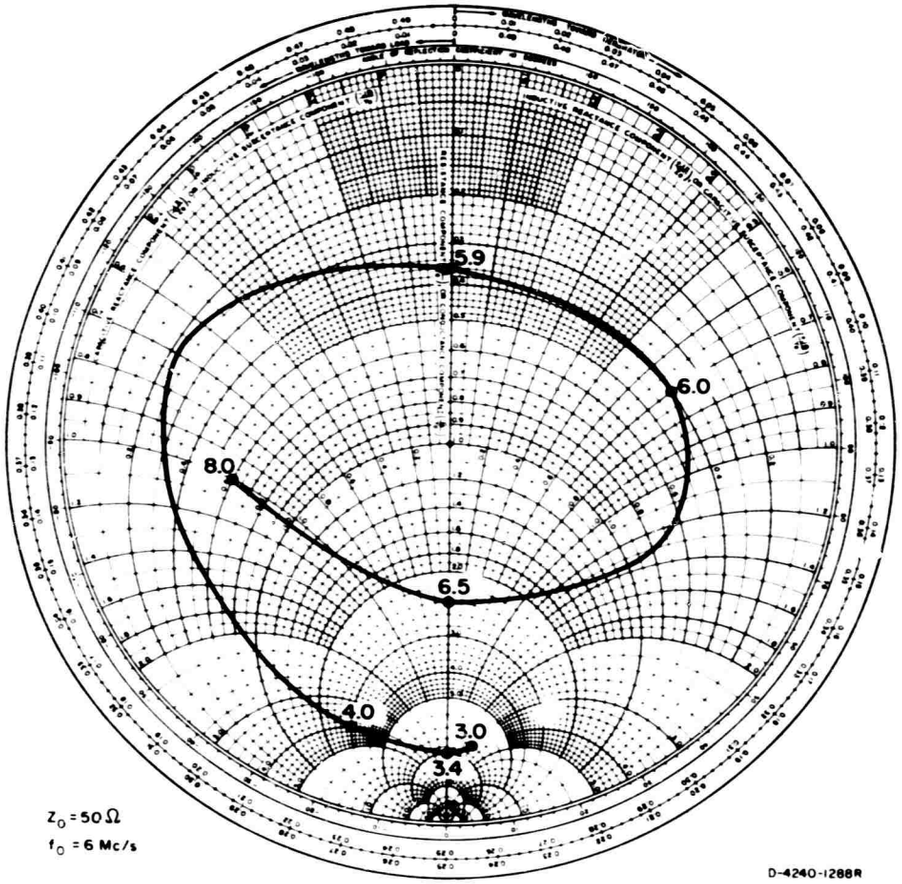

FIG. 22

SMITH CHART REPRESENTATION OF ANTENNA IMPEDANCE FOR 6-Mc s BALANCED DIPOLE IN FOLIAGE (3.0 To 8.0 Mc s)

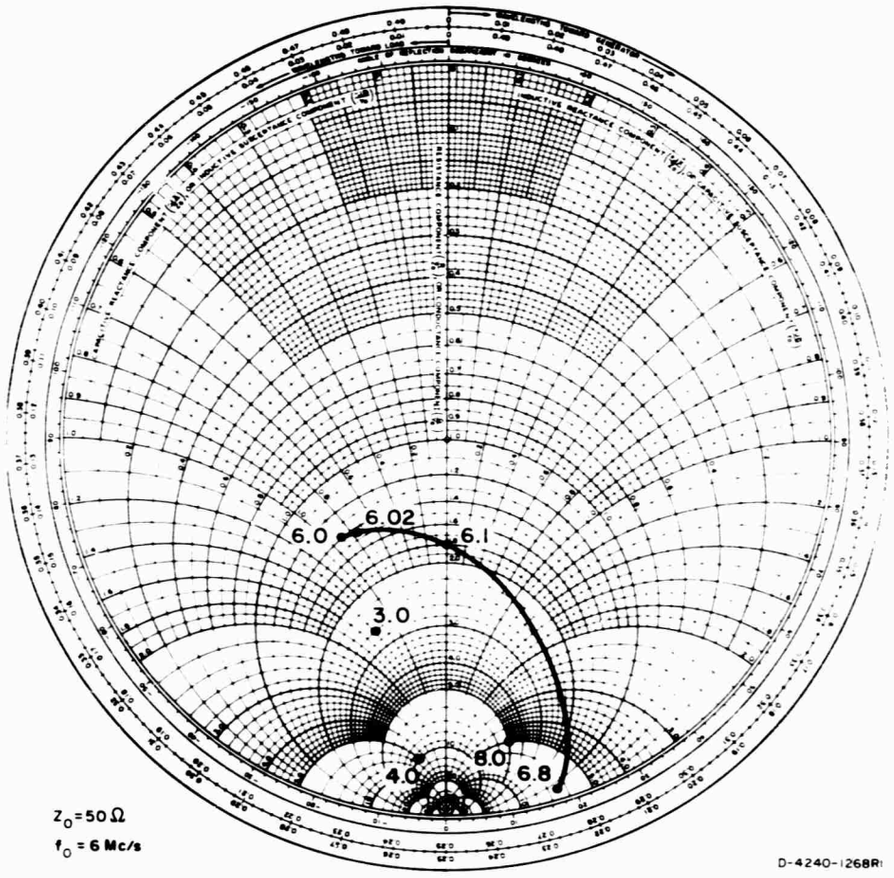

FIG. 23

SMITH CHART REPRESENTATION OF ANTENNA IMPEDANCE FOR 6-Mc s UNBALANCED DIPOLE IN FOLIAGE (3.0 To 8.0 Mc s)

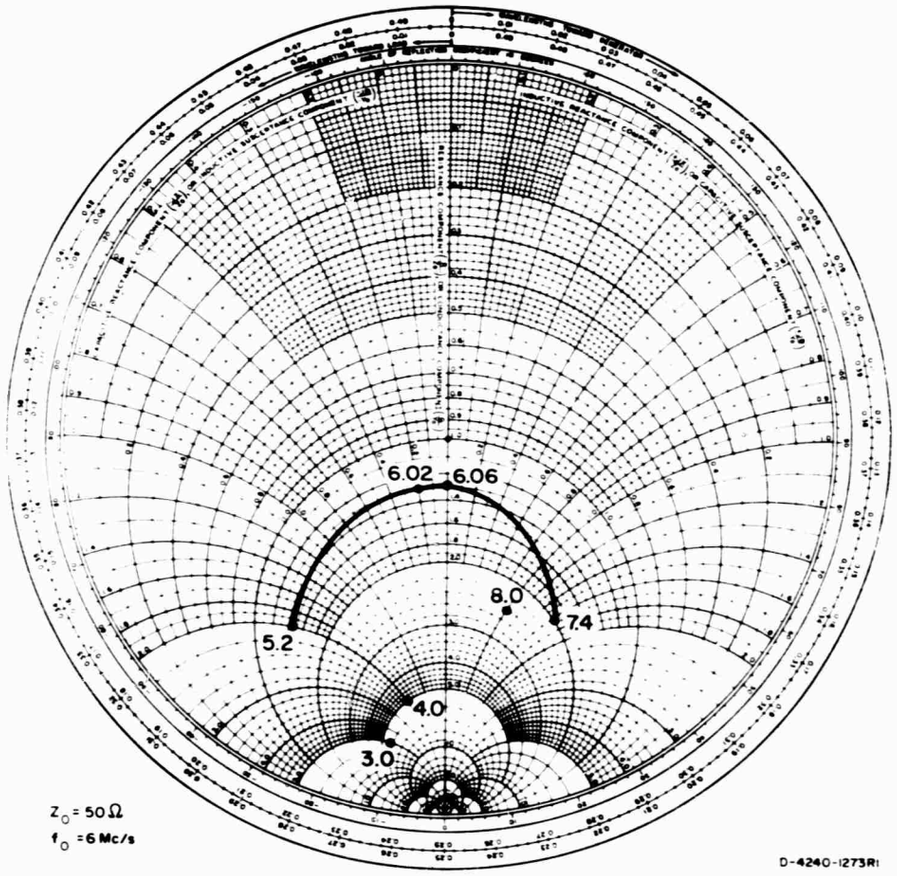

FIG. 24

SMITH CHART REPRESENTATION OF ANTENNA IMPEDANCE FOR 6-Mc s, 16-ft-HIGH UNBALANCED DIPOLE IN FOLIAGE (3.0 To 8.0 Mc s)

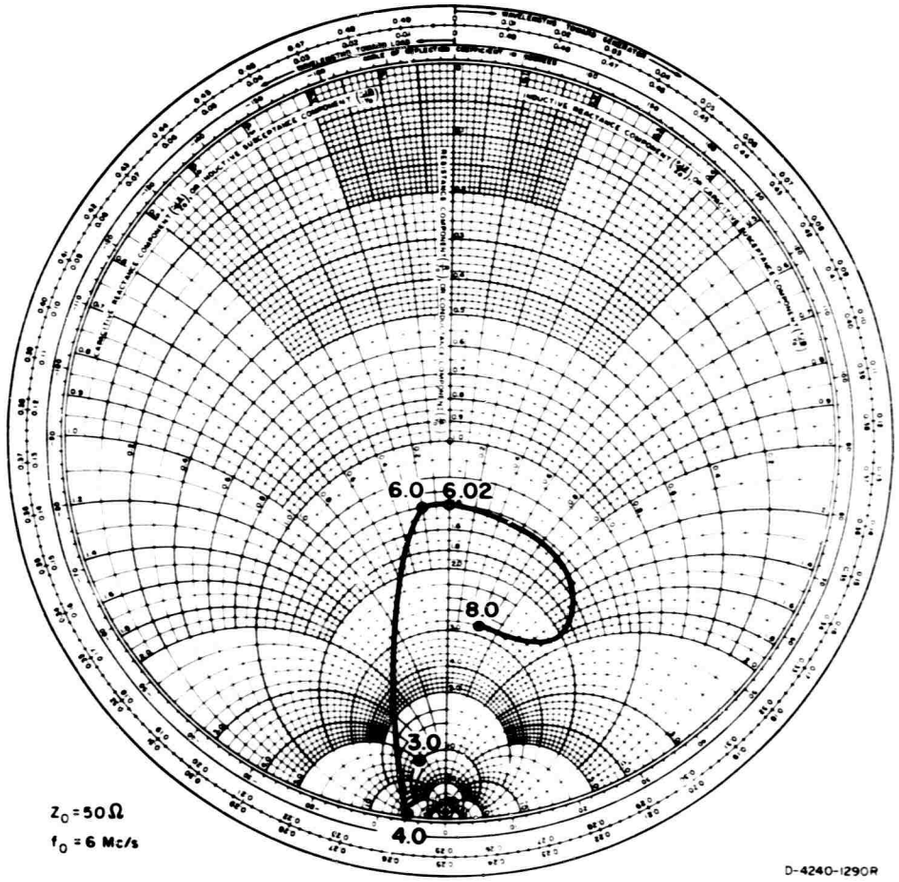

FIG. 25

SMITH CHART REPRESENTATION OF ANTENNA IMPEDANCE FOR 6-Mc s, 8-ft-HIGH UNBALANCED DIPOLE IN FOLIAGE (3.0 To 8.0 Mc s)

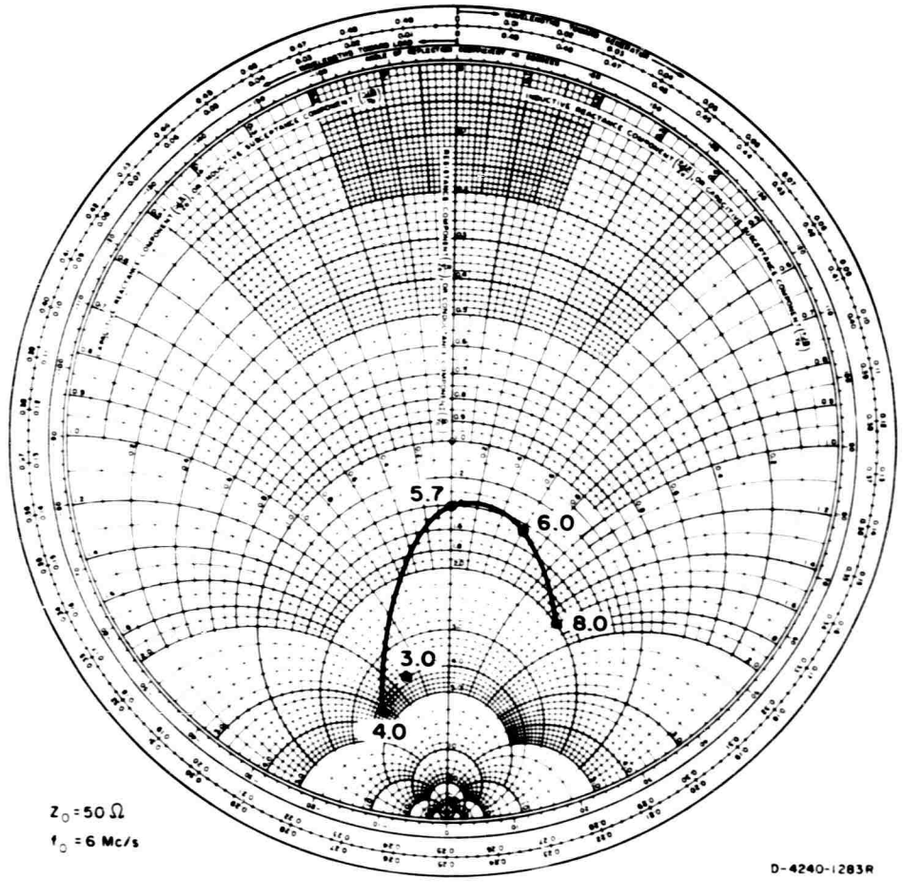

FIG. 26

SMITH CHART REPRESENTATION OF ANTENNA IMPEDANCE FOR 6-Mc s, 2-ft-HIGH UNBALANCED DIPOLE (3.0 To 8.0 Mc s)

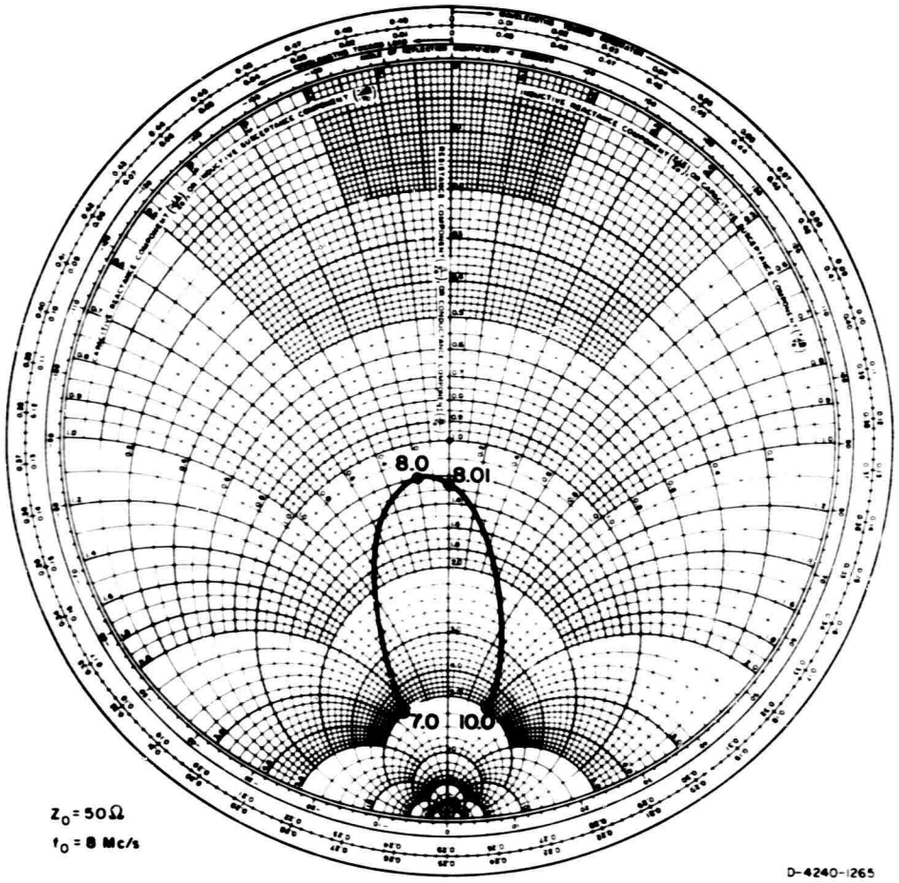

FIG. 27

SMITH CHART REPRESENTATION OF ANTENNA IMPEDANCE FOR 8-Mc s, 23-ft-HIGH UNBALANCED DIPOLE (7.0 To 10.0 Mc s)

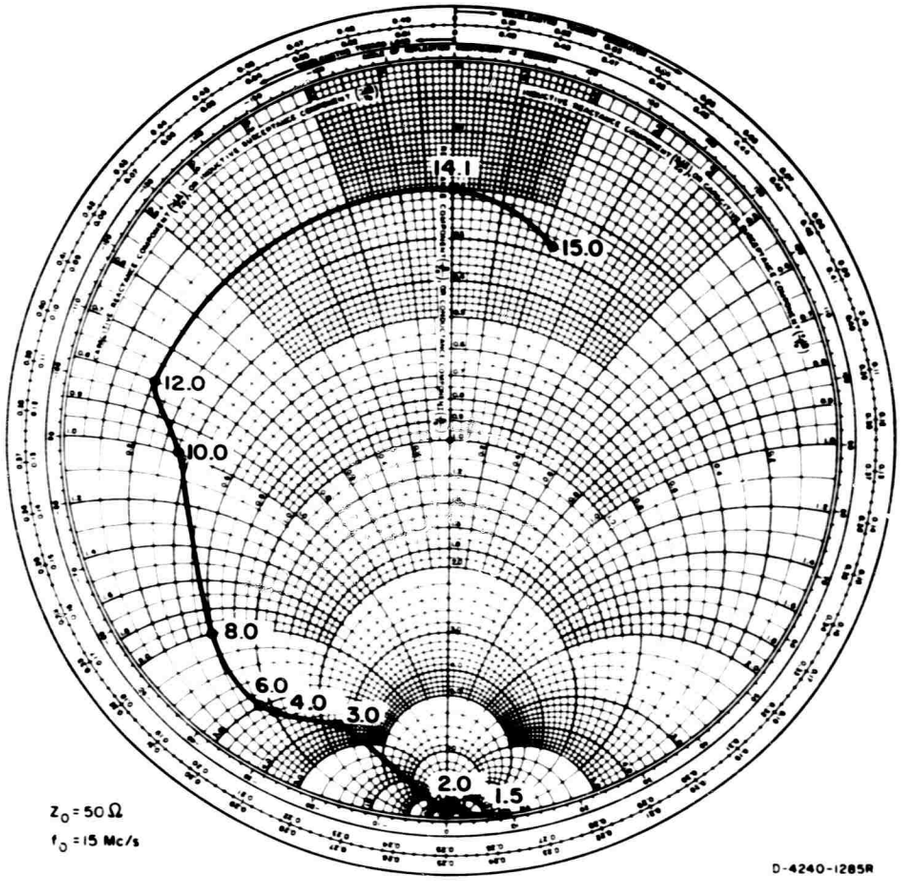

FIG. 28

SMITH CHART REPRESENTATION OF ANTENNA IMPEDANCE FOR 15-Mc s, BALANCED DIPOLE WITH GROUND SCREEN IN CLEARING (1.5 To 15.0 Mc s)

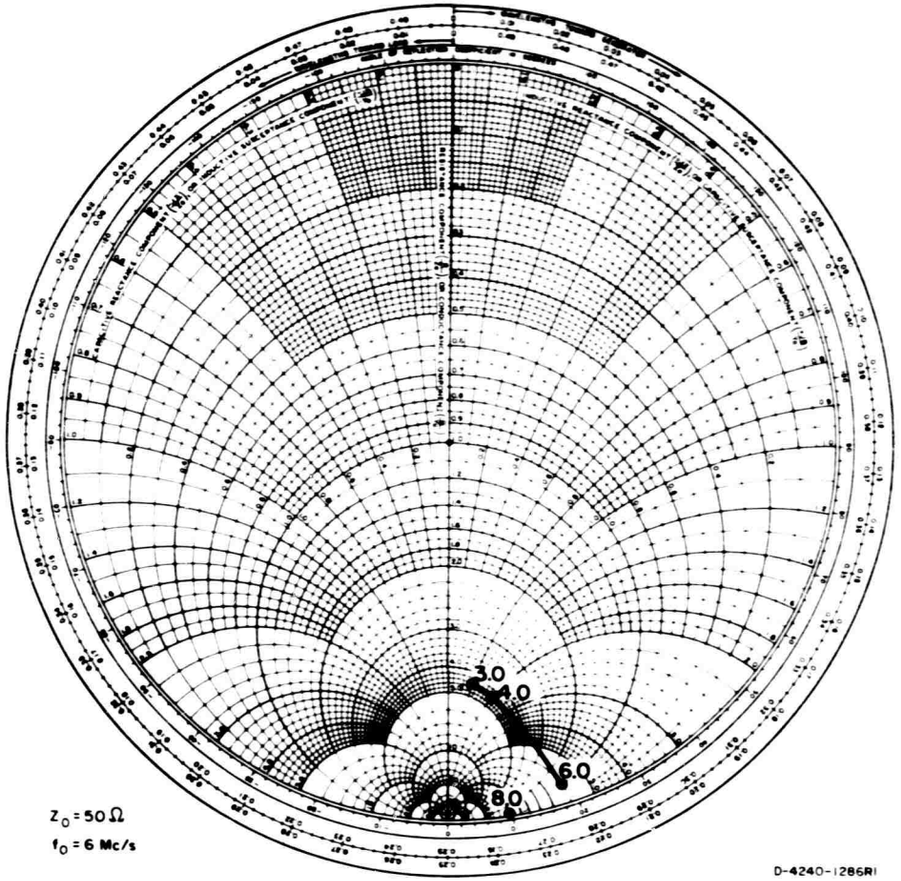

FIG. 29

SMITH CHART REPRESENTATION OF ANTENNA IMPEDANCE FOR 6-Mc s SLEEVE DIPOLE IN FOLIAGE (3.0 To 8.0 Mc s)

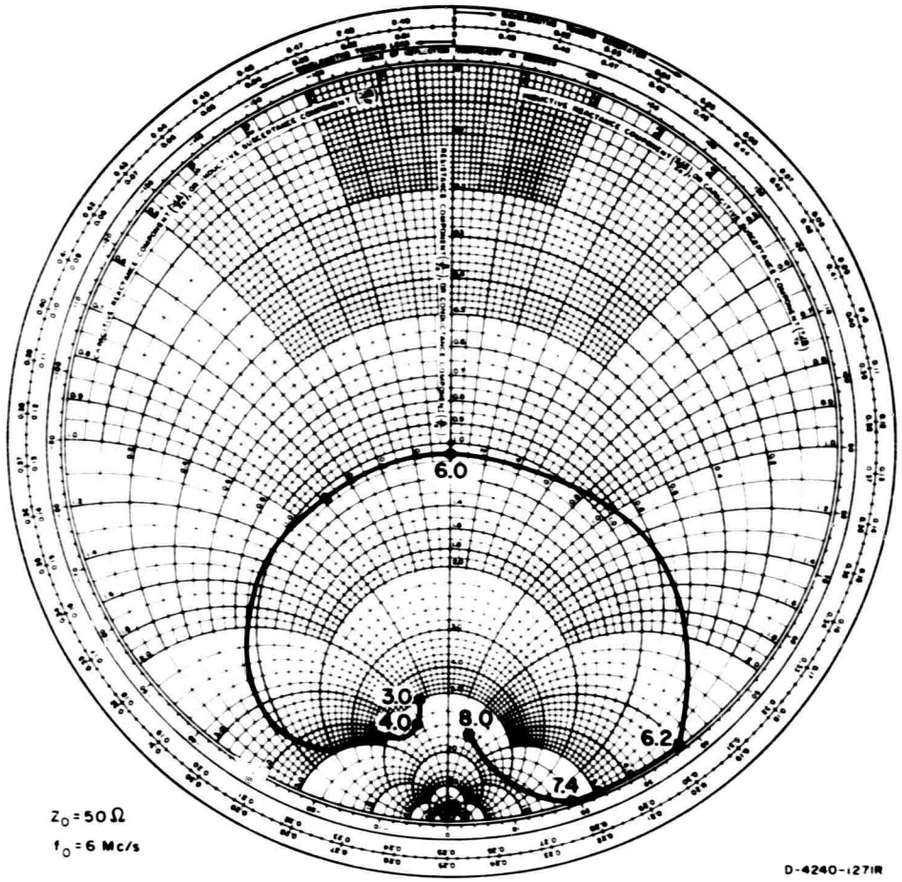

FIG. 30

SMITH CHART REPRESENTATION OF ANTENNA IMPEDANCE FOR 6-Mc s MONOPOLE IN CLEARING (3.0 To 8.0 Mc s)

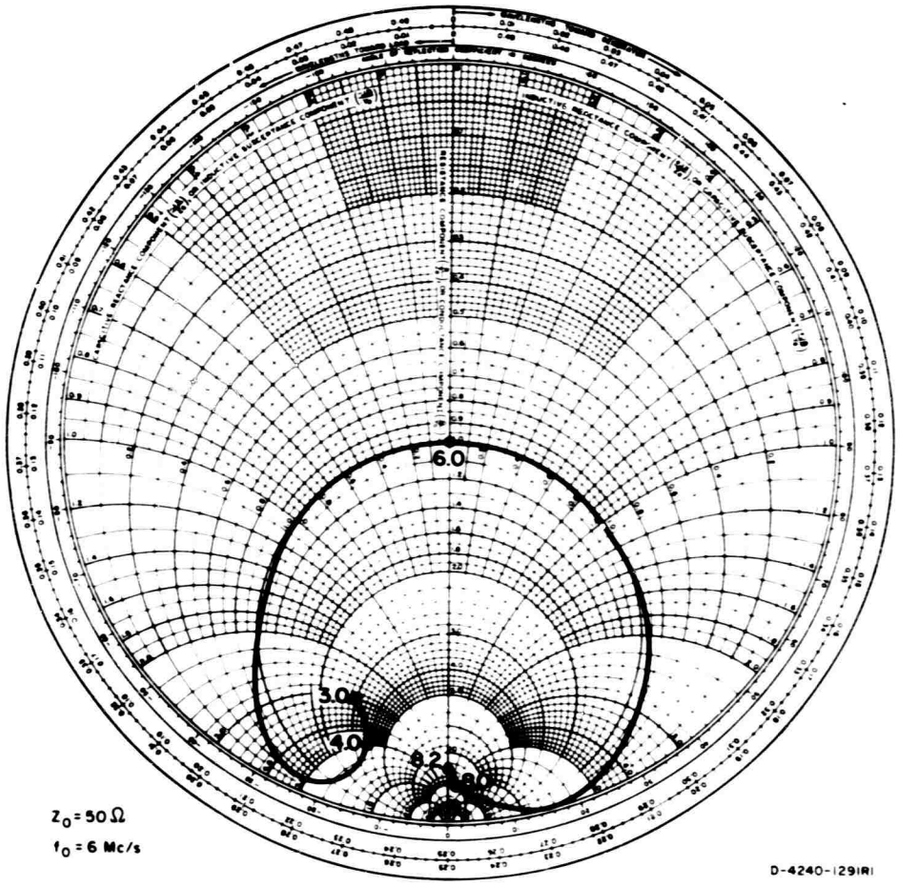

FIG. 31

SMITH CHART REPRESENTATION OF ANTENNA IMPEDANCE FOR 6-Mc s MONOPOLE ON EDGE OF CLEARING (3.0 To 8.2 Mc s)

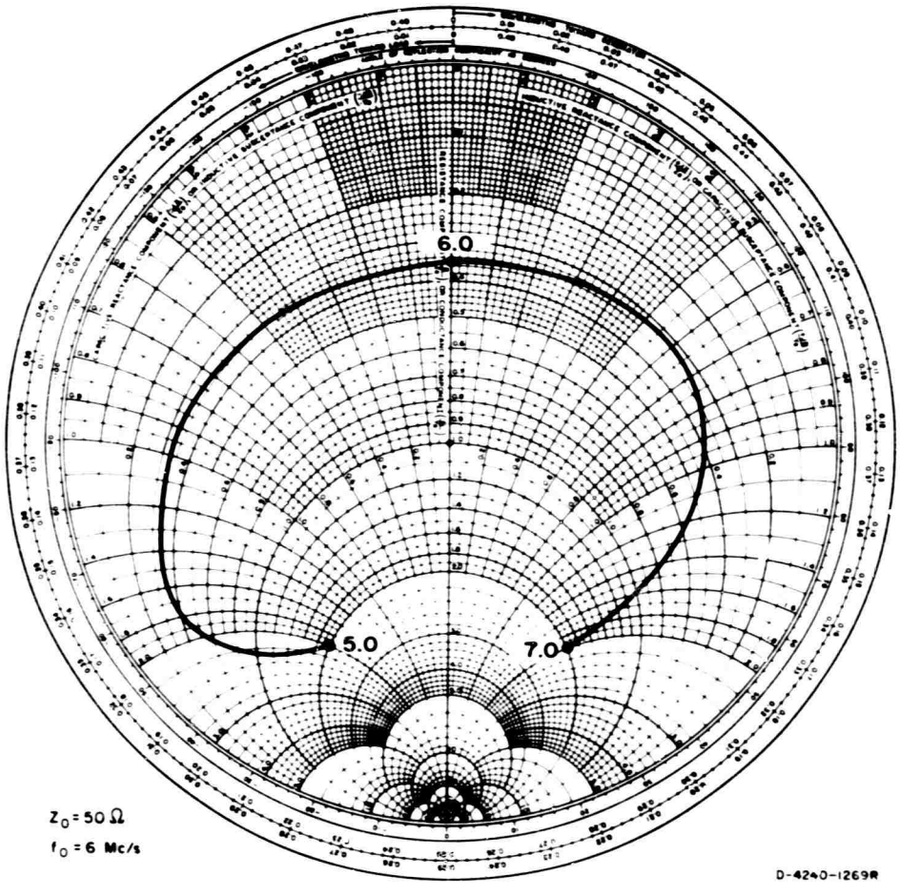

FIG. 32

SMITH CHART REPRESENTATION OF ANTENNA IMPEDANCE FOR 6-Mc s MONOPOLE IN FOLIAGE (5.0 To 7.0 Mc s)

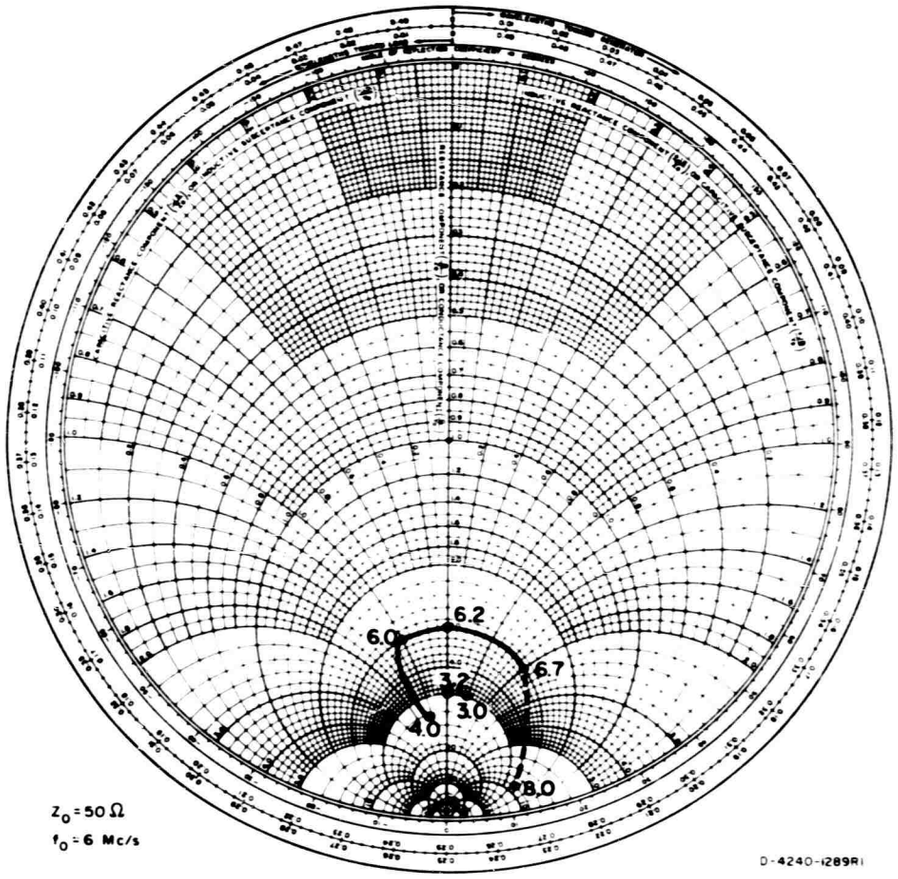

FIG. 33

SMITH CHART REPRESENTATION OF ANTENNA IMPEDANCE FOR 6-Mc s, 2:1 INVERTED L IN FOLIAGE (3.0 To 8.0 Mc s)

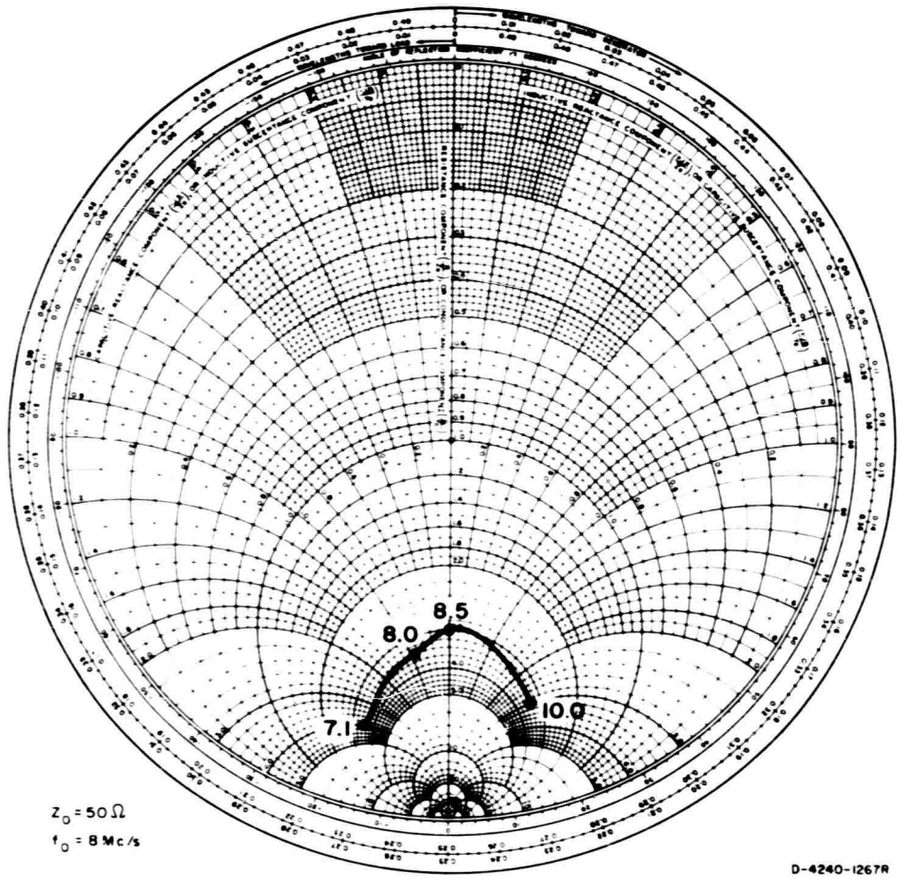

FIG. 34

SMITH CHART REPRESENTATION OF ANTENNA IMPEDANCE FOR 8-Mc s 2:1 INVERTED L IN FOLIAGE (7.1 To 10.0 Mc s)

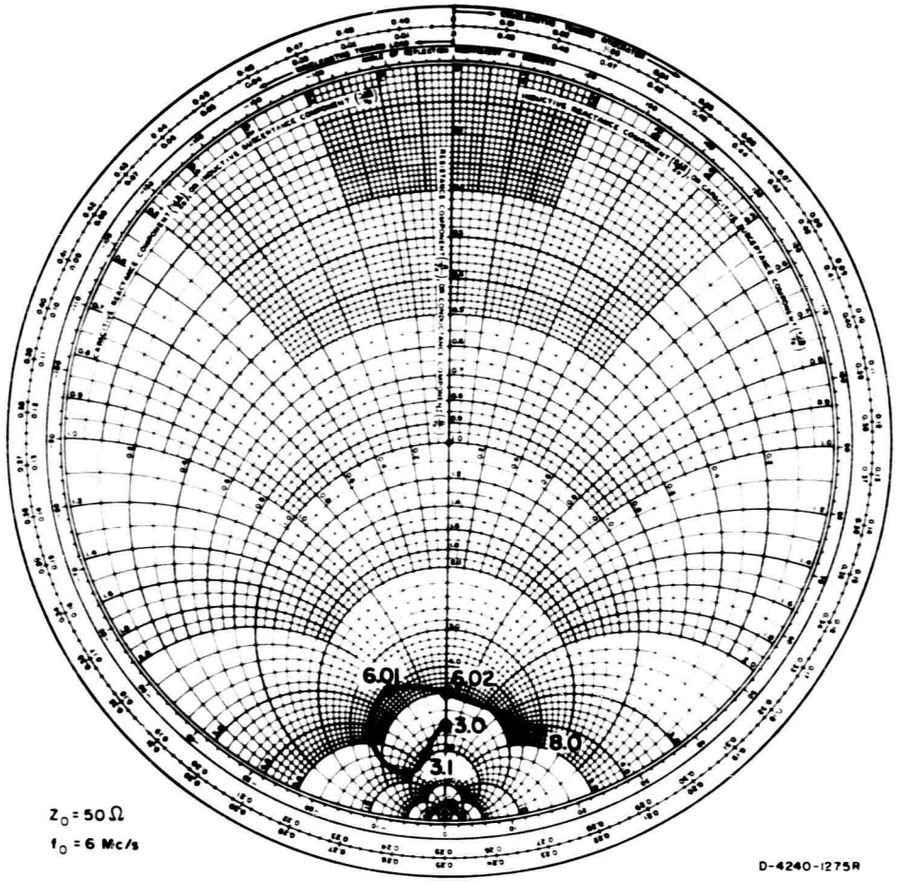

FIG. 35

SMITH CHART REPRESENTATION OF ANTENNA IMPEDANCE FOR 6-Mc s 5:1 INVERTED L IN FOLIAGE (3.0 To 8.0 Mc s)

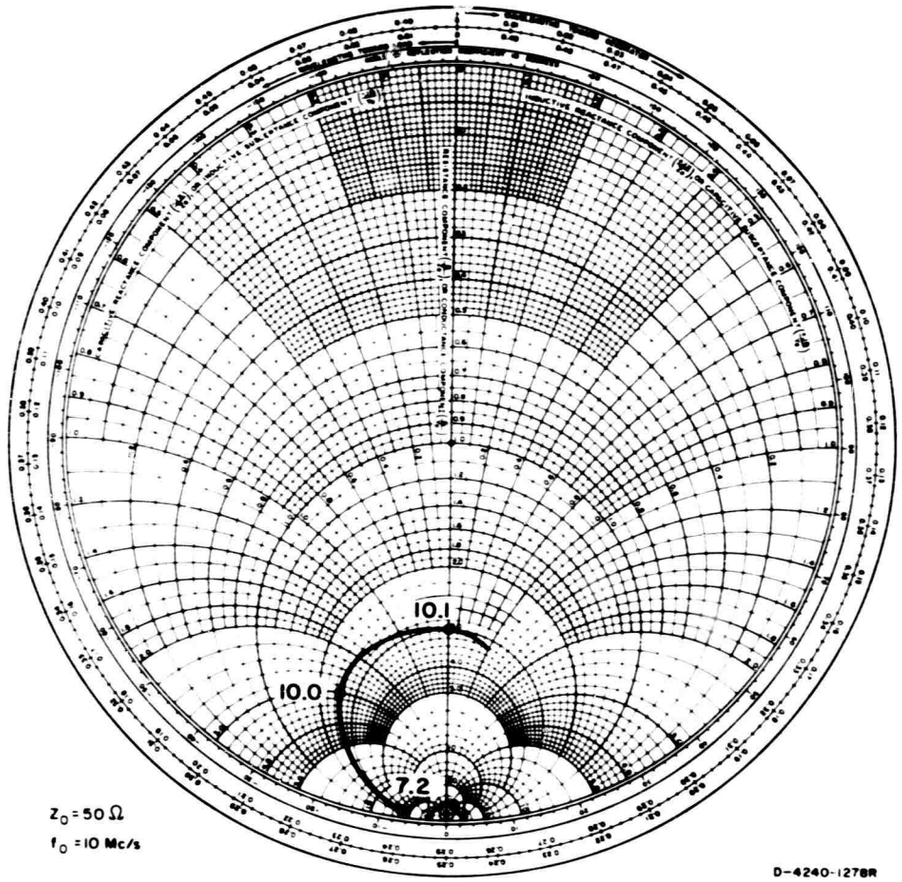

FIG. 36

SMITH CHART REPRESENTATION OF ANTENNA IMPEDANCE FOR 10-Mc s 5:1 INVERTED L IN FOLIAGE (7.2 To 10.1 Mc s)

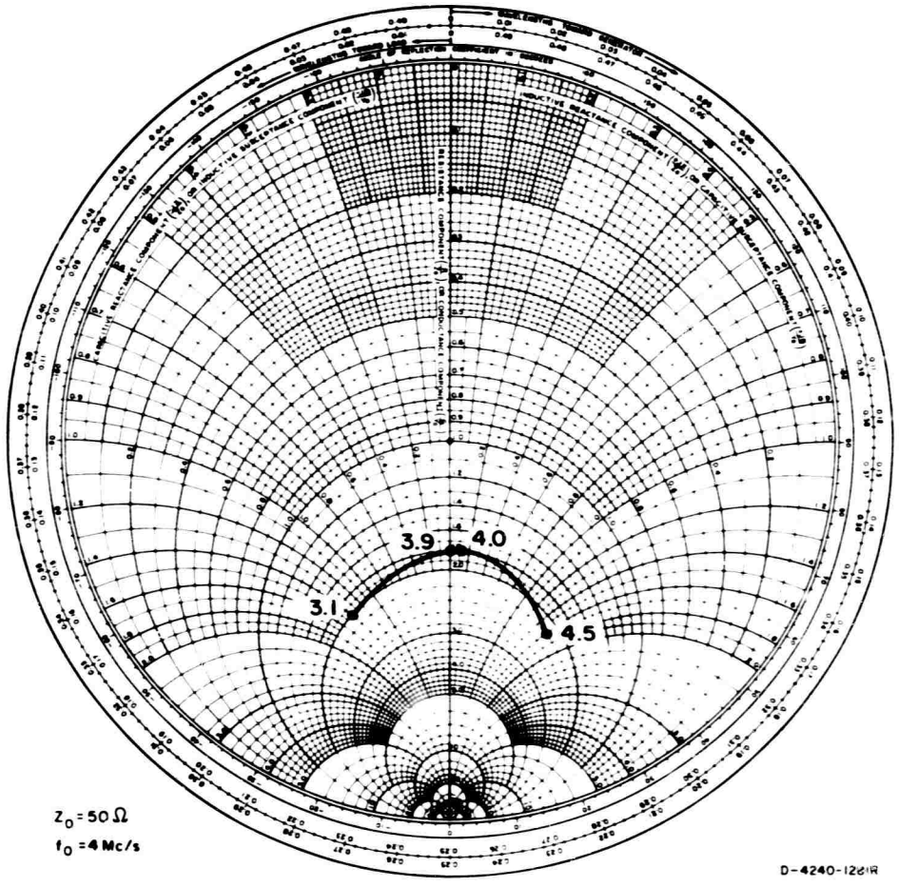

FIG. 37

SMITH CHART REPRESENTATION OF ANTENNA IMPEDANCE FOR 4-Mc s 30° SLANT WIRE IN FOLIAGE (3.1 To 4.5 Mc s)

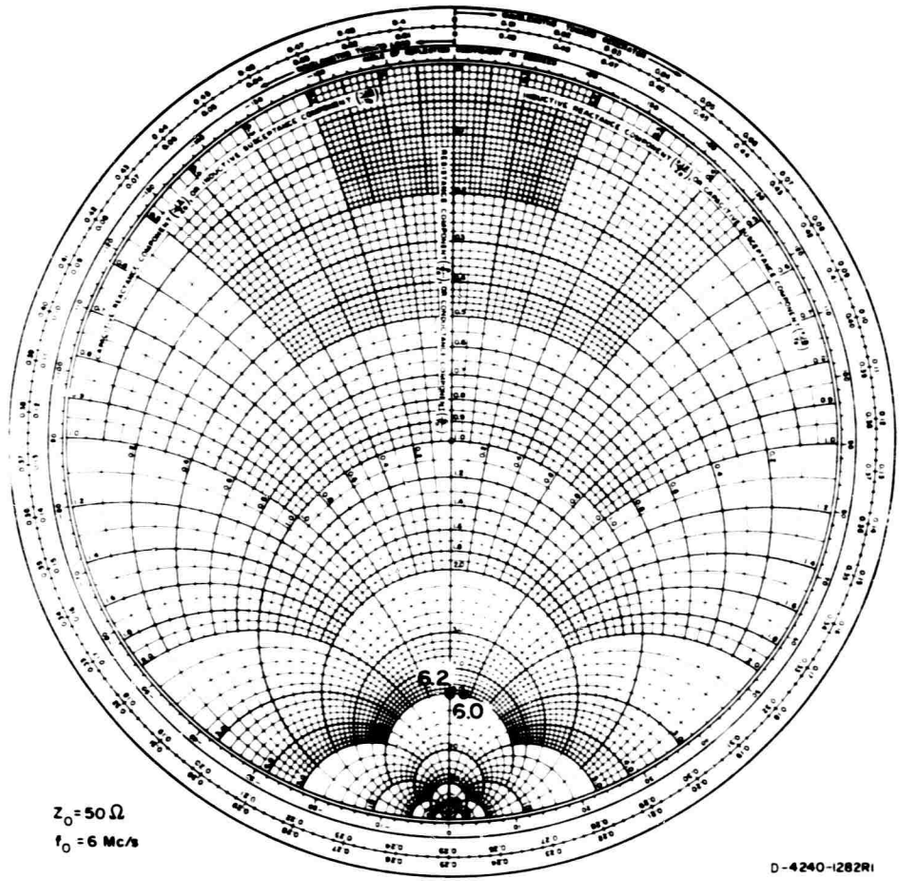

FIG. 38

SMITH CHART REPRESENTATION OF ANTENNA IMPEDANCE FOR 6-Mc s 30° SLANT WIRE IN FOLIAGE (6.0 To 6.2 Mc s)

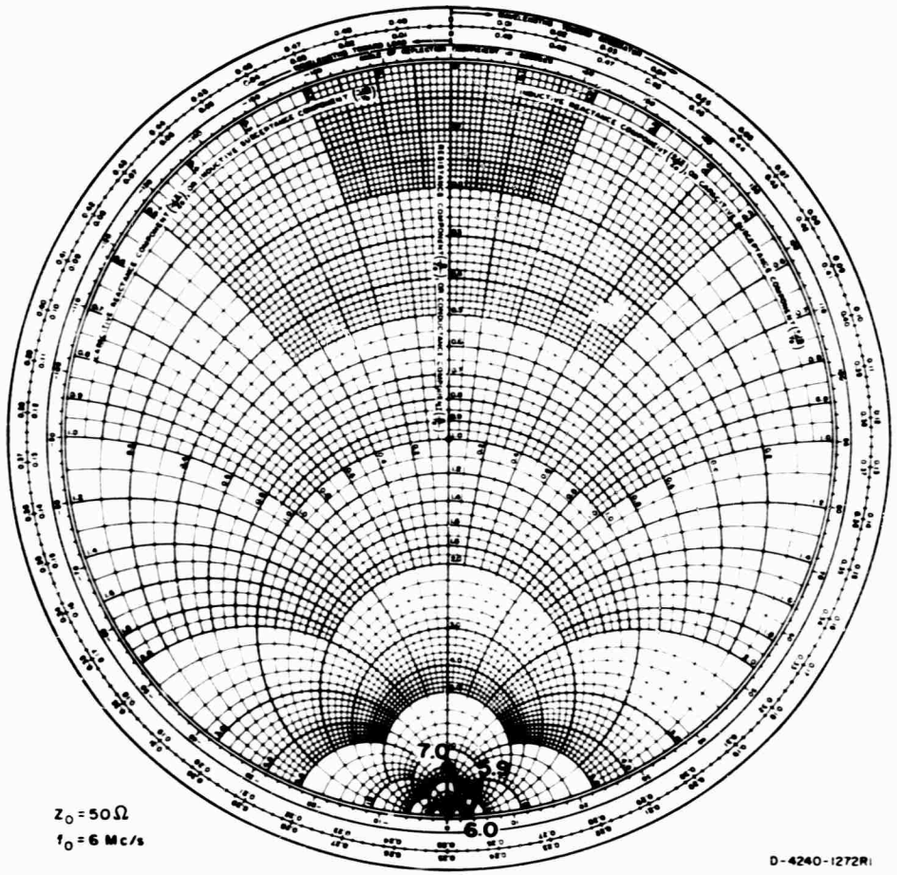

FIG. 39

SMITH CHART REPRESENTATION OF ANTENNA IMPEDANCE FOR LOOP IN CLEARING (5.9 To 7.0 Mc s)

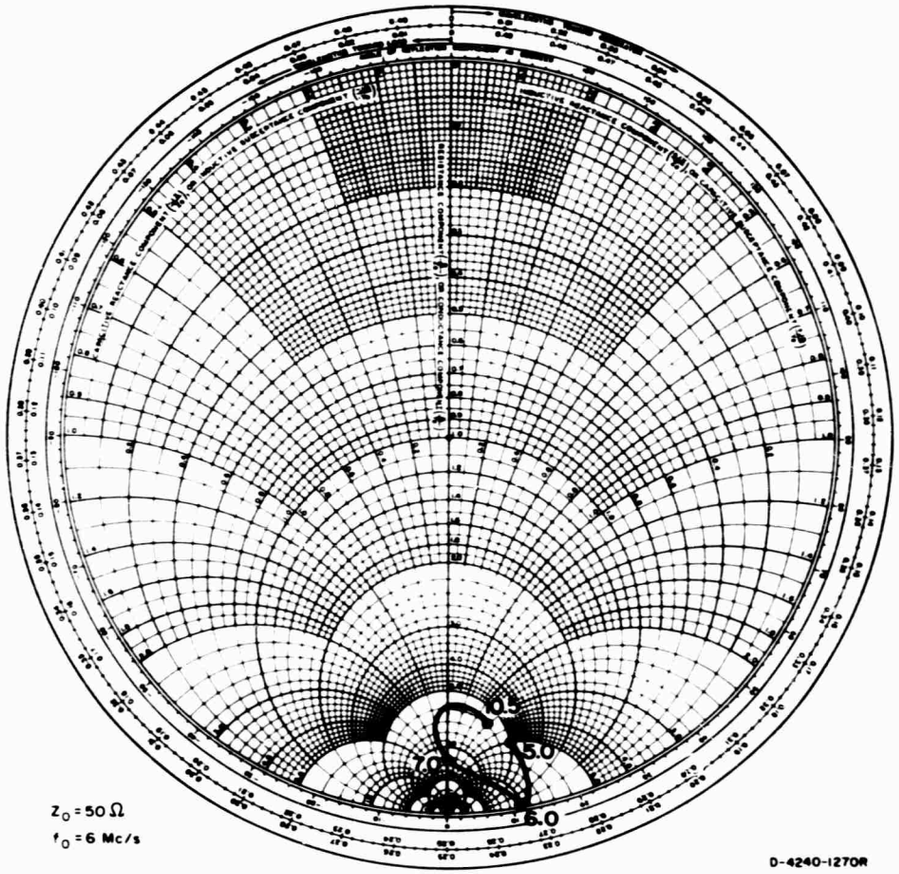

FIG. 40

SMITH CHART REPRESENTATION OF ANTENNA IMPEDANCE FOR LOOP IN FOLIAGE (5.0 To 10.5 Mc s)

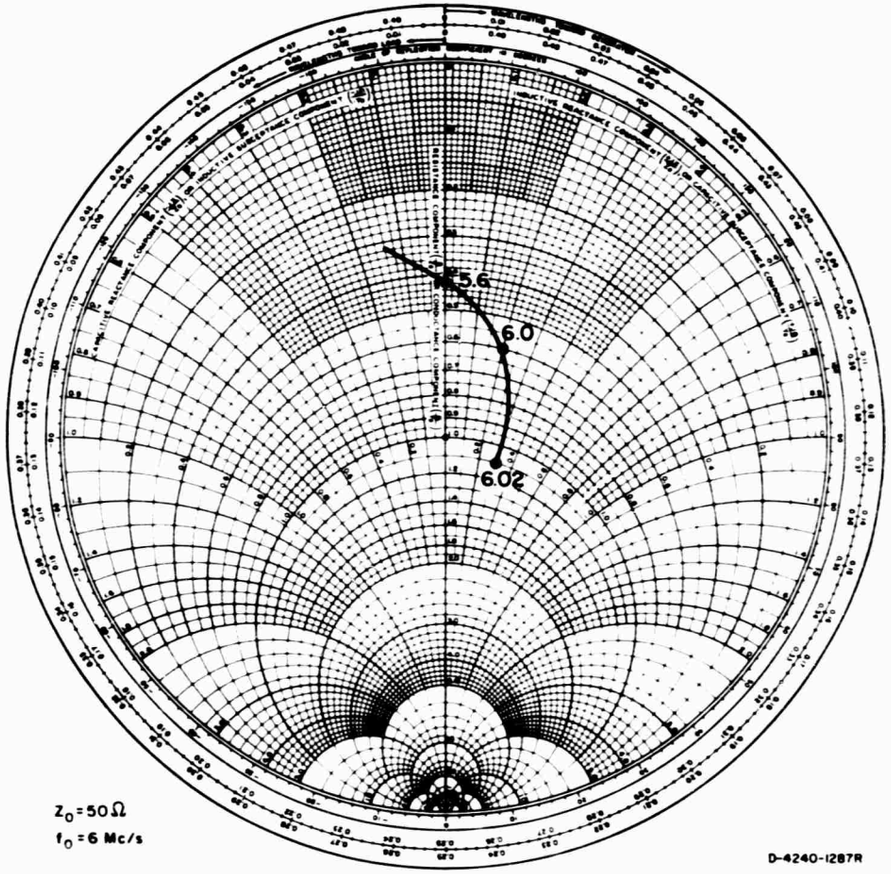

FIG. 41

SMITH CHART REPRESENTATION OF ANTENNA IMPEDANCE FOR 6-Mc s J&B-TYPE BALANCED DIPOLE — 40-ft-HIGH (5.6 To 6.02 Mc s)

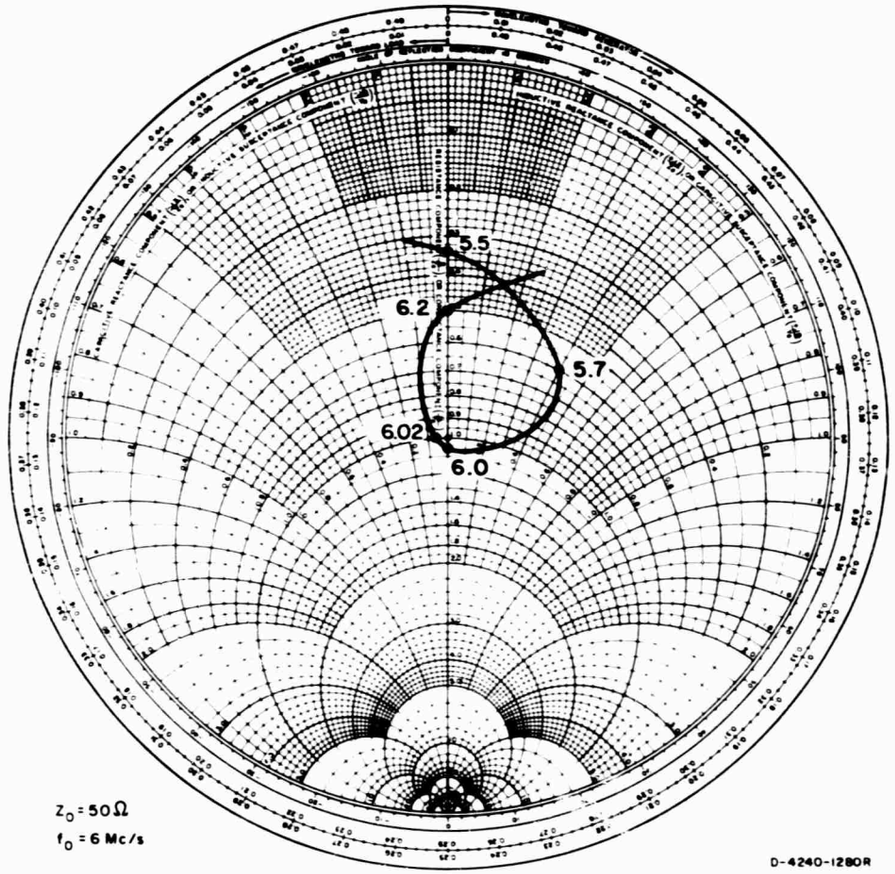

FIG. 42

SMITH CHART REPRESENTATION OF ANTENNA IMPEDANCE FOR 6-Mc s J&B-TYPE BALANCED DIPOLE —80-ft-HIGH (5.5 To 6.2 Mc s)

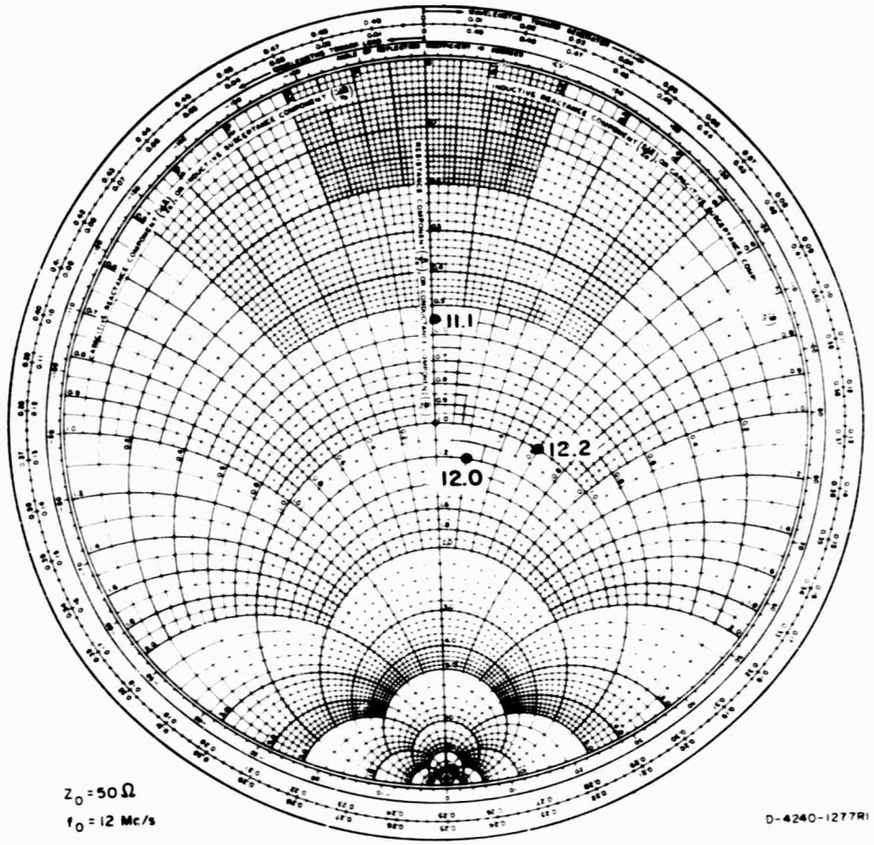

FIG. 43

SMITH CHART REPRESENTATION OF ANTENNA IMPEDANCE FOR 12–Mc s J&B–TYPE BALANCED DIPOLE (11.1 To 12.2 Mc s)

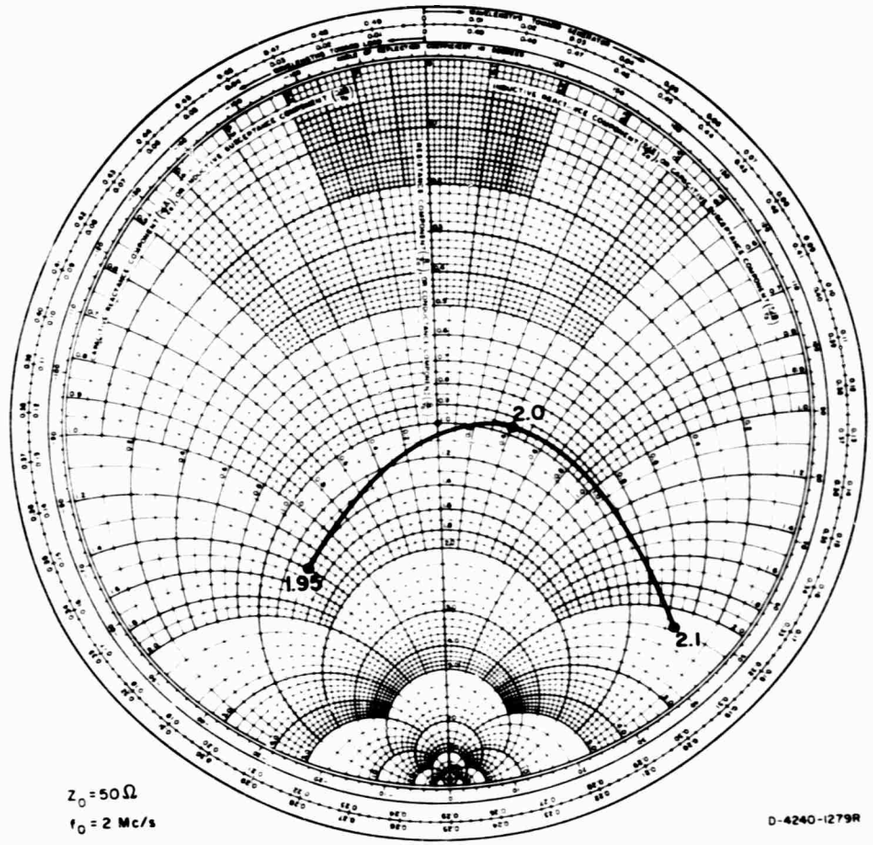

FIG. 44

SMITH CHART REPRESENTATION OF ANTENNA IMPEDANCE FOR 2–Mc s J&B–TYPE 80–ft VERTICAL (1.95 To 2.1 Mc s)

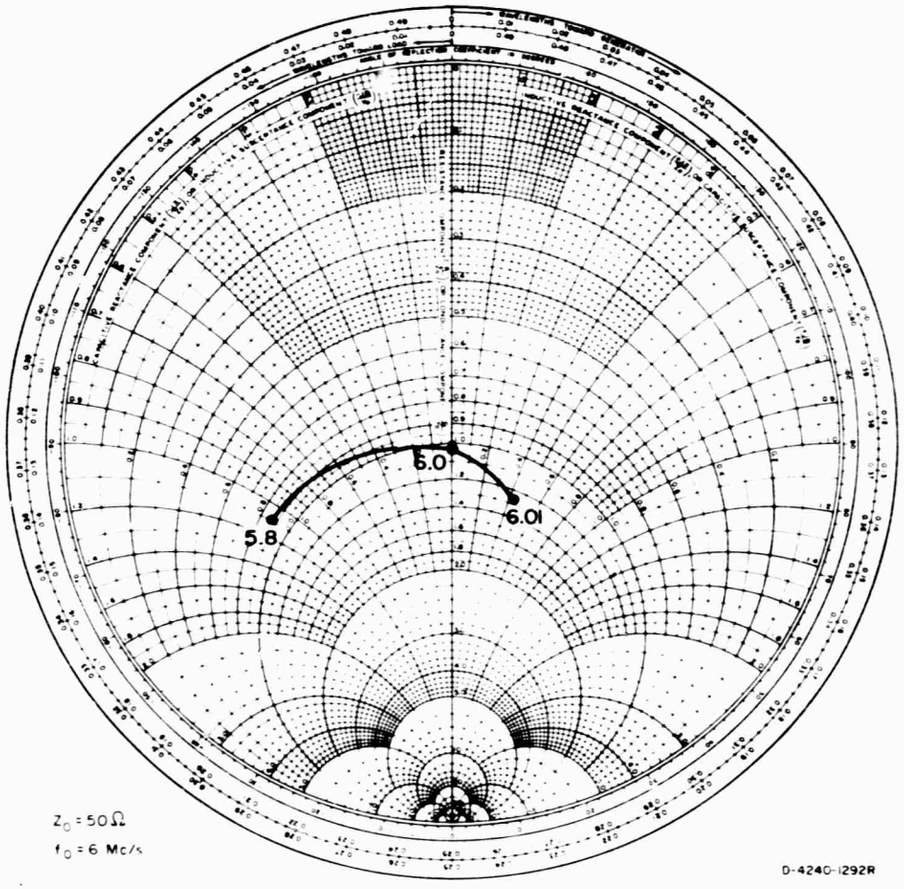

FIG. 45

SMITH CHART REPRESENTATION OF ANTENNA IMPEDANCE FOR 6-Mc s J&B-TYPE 40-ft VERTICAL (5.8 To 6.01 Mc s)

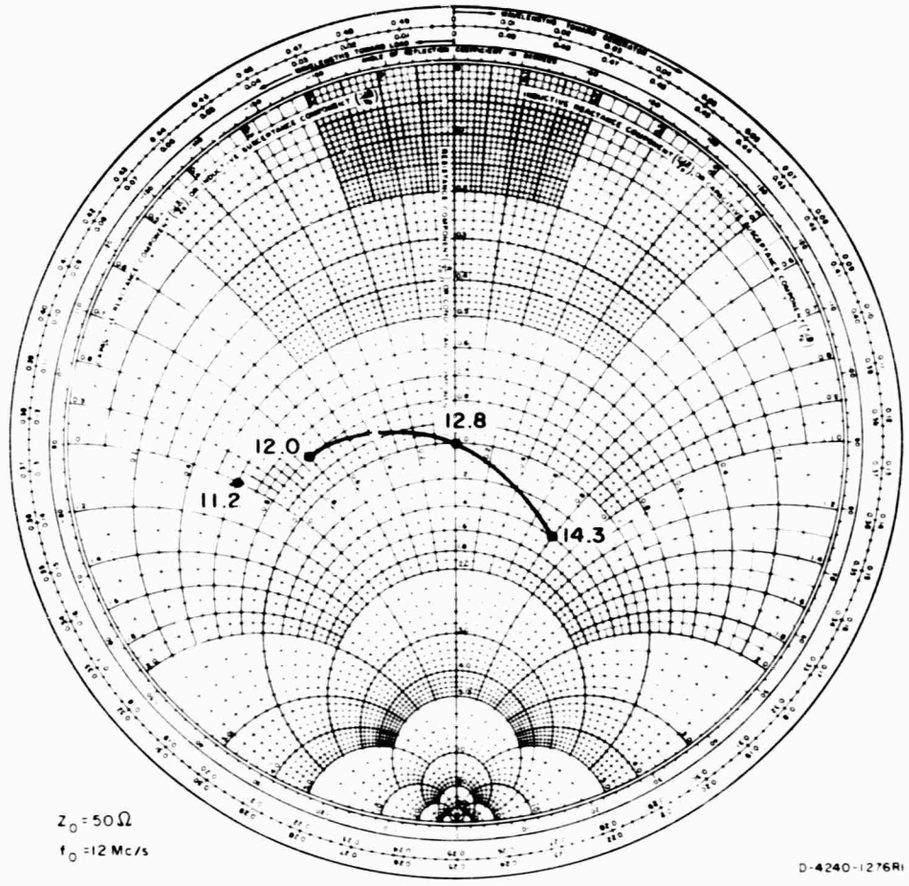

FIG. 46

SMITH CHART REPRESENTATION OF ANTENNA IMPEDANCE FOR 12-Mc s J&B-TYPE 20-ft Vertical (11.2 To 14.3 Mc s)

VII DISCUSSION OF RESULTS

This report investigated the effect of a surrounding tropical forest on the performance of selected types of HF field antennas. While not examined in detail, the report also provides a basis for the comparisons of the performance of antennas in a variety of environmental conditions by comparing the results contained in this report with previously published measurements.[1,2,6]

A number of examples of alterations in radiation pattern were observed between antennas with similar physical construction which were erected in the tropical forest and in a nearby clearing. These differences are quite evident from an examination of the measurements taken at 6 Mc/s (the principal design frequency used at the Ban Mun Chit Tropical Forest Site).

Comparing the patterns of the E_θ response of the 6 Mc/s unbalanced dipole in the clearing with those of the 6 Mc/s unbalanced dipole in the foliage, it can be seen that the maximum response of the dipole in the foliage occurs at a considerably higher elevation angle for the case of the dipole in the foliage (compare 3-dB contours of Figs. A-31 and A-46). But checking further it can be seen that the same amount of shift in elevation does not occur in the E_ϕ response patterns of these two antennas (Figs. A-32 and A-47).

The patterns of the monopole antennas provide an indication of the effect of the foliage on the response of a predominantely vertically polarized antenna receiving a vertically polarized wave. Comparing the E_ϕ response of the 6 Mc/s monopoles in the clearing and in the foliage (Figs. A-88 and A-93) one can observe that the patterns of both antennas are omni-directional but the response of the monopole in the clearing tends to decrease more rapidly with decreasing elevation. This "pattern roll-off" is possibly due to ground-screen-to-earth and the ground-screen-to-earth-and-foliage interface. The pattern of the monopole on the edge of the clearing indicates that the antenna receives more signal in the direction of the clearing (270°), as anticipated. In Table II it can be seen that there is a difference of -2.1 dB between the -3-dB contour of the monopole on the edge of the clearing and the monopole in the clearing and a difference of -8.3 dB between the -3-dB contour for the monopole in the clearing and the monopole in the foliage. It can also be seen that the maximum response (-3-dB contour) of the monopole in the clearing is generally at higher elevation angles than that of the monopole on the edge of the clearing or the monopole in the forest. Comparing the relative gain values, the data indicate possible reflection from the foliage causing the increased signal strength toward 270° azimuth at lower elevation angles for the monopole on the edge of the clearing, and attenuation of the signal by foliage in the azimuth sector near 90°.

The maximum of the E_θ response of the J&B 6-Mc/s balanced dipoles--40 feet and 80 feet high--occurs at a higher elevation angle than expected, but this is again apparently caused by the antenna being in the forest, as was previously indicated in the comparison of the unbalanced dipole in the clearing with that in the foliage.

The data from the J&B-type vertical antennas indicated the E_θ patterns of the 6-Mc/s and 2-Mc/s antennas to be omnidirectional as expected, with patterns comparable to those of the 15.6-foot monopole in the forest (note that relative gain is not considered here). But the E_θ pattern of the 12-Mc/s J&B-type vertical antenna (Fig. A-164) shows a slight scattering of the signal.

In conclusion, the data indicate that vertical polarization is attenuated more than horizontal polarization, and that scattering of the vertical polarization begins to occur at about 12 Mc/s.

REFERENCES

1. William A. Ray, "Full-Scale Pattern Measurement of Simple HF Field Antennas," Special Technical Report 10, Contract DA 36-039 AMC-00040(E), SRI Project 4240, Stanford Research Institute, Menlo Park, California (May 1966).

2. William A. Ray, Gary E. Barker, and Sandra S. Martensen, "Full-Scale Pattern Measurements of Simple HF Field Antennas in a U.S. Conifer Forest," Special Technical Report 25, Contract DA 36-039 AMC-00040(E), SRI Project 4240, Stanford Research Institute, Menlo Park, California (February 1967).

3. Somchit Pongpangan and D. V. Vanek, "Environmental Description of Stanford Research Institute Test Site at Ban Mun Chit, Thailand," Joint Thai-U.S. Military Research and Development Center, Bangkok, Thailand (in preparation).

4. H. W. Parker and Withan Makarabhiromya, "Electric Constants Measured in Vegetation and in Earth at Five Sites in Thailand," Special Technical Report 43, Contract DA 36-039 AMC-00040(E), SRI Project 4240, Stanford Research Institute, Menlo Park, California (December 1967).

5. "Tropical Propagation Research," Semiannual Report No. 3, for the period July-December 1963, Contract DA 36-039 SC-90889, Jansky & Bailey, Alexandria, Virginia.

6. John Taylor, "A Note on the Computed Radiation Patterns of Dipole Antennas in Dense Vegetation," Special Technical Report 16, Contract DA 36-039 AMC-00040(E), SRI Project 4240, Stanford Research Institute, Menlo Park, California (February 1966).

7. G. H. Hagn, D. J. Barnes, J. W. Chapman, J. E. van der Laan, D. J. Lyons, and J. P. Muro, "Field Test of AN/GRA-93( ) HF Antenna Kit for Short-Path Skywave Communication in Thailand Forest Environment," Final Report II, Contract DA 28-043 AMC-02201(E), SRI Project 6183, Stanford Research Institute, Menlo Park, California (August 1967).

8. George H. Hagn, "Orientation of Linearly Polarized HF Antennas for Short-Path Communication via the Ionosphere near the Geomagnetic Equator," Research Memorandum 5 (Revised), Contract DA 36-039 AMC-00040(E), SRI Project 4240, Stanford Research Institute, Menlo Park, California (June 1964).

9. George H. Hagn, "Absorption of Ionospherically Propagated HF Radio Waves under Conditions where the Quasi-Transverse (QT) Approximation Is Valid," Special Technical Report 9, Contract DA 36-039 AMC-00040(E), SRI Project 4240, Stanford Research Institute, Menlo Park, California (September 1964).

10. Lt. Cdr. Paibul Nacaskul, R.T.N., "Orientation Measurements in Thailand with HF Dipole Antennas for Tactical Communications," Special Technical Report 31, Contract DA 36-039 AMC-00040(E), SRI Project 4240, Stanford Research Institute, Menlo Park, California (June 1967).

Appendix

ANTENNA CONTOUR PLOTS

This appendix contains all of the antenna pattern contour plots grouped by antenna in this order: dipo monopoles, inverted L's, slant wires, loops, long wire, and J&B type antennas. For each antenna, the two individual polarization plots and the power plots are given for each measured frequency in order of increasing frequency. The title block in the upper right corner of each plot gives the antenna type; the antenna location; the antenna height, h_a (for dipoles); the antenna design frequency, f_0; the measurement frequency, f_m; and the measurement polarization. The polarizations are defined as in Sec. IV-A; as a reminder, E_ϕ is horizontal and E_θ is vertical.

Each contour map shows all the amplitude data taken on one antenna, for one polarization, at one frequency (see Sec. V-A). The contour plots are two-dimensional maps of a hemisphere covering the antenna, as it appears from above. Hence, the zenith angle is at the center of the plot, azimuth angles appear as radials, and elevation angles are concentric circles. The outer rim of the plot is the horizon, or 0-degree elevation. The azimuth angles numbered around the rim of the plot are in degrees relative to some principal axis of the antenna. As an example, for the 8 Mc/s, 23-ft-high unbalanced dipole antenna patterns, 0° azimuth on the plot is actually 335° from magnetic north. These angles are indicated on the three site maps (Figs. 2, 3, and 4) by arrows labeled in degrees magnetic. The relationship of contour plot azimuth to each antenna is also shown by the schematic diagram in the center of each E_ϕ or E_θ pattern plot. The power plots do not have the antenna diagram, making it necessary to refer to the previous voltage plot or appropriate site map for the orientation.

In examining the plots, the accuracy limits of the measurement technique should be kept in mind. The details of these limits were discussed previously, but generally, any features of the plot smaller than ±3° azimuth and ±1/2 contour interval are insignificant, due to limited data sampling and to processing errors.

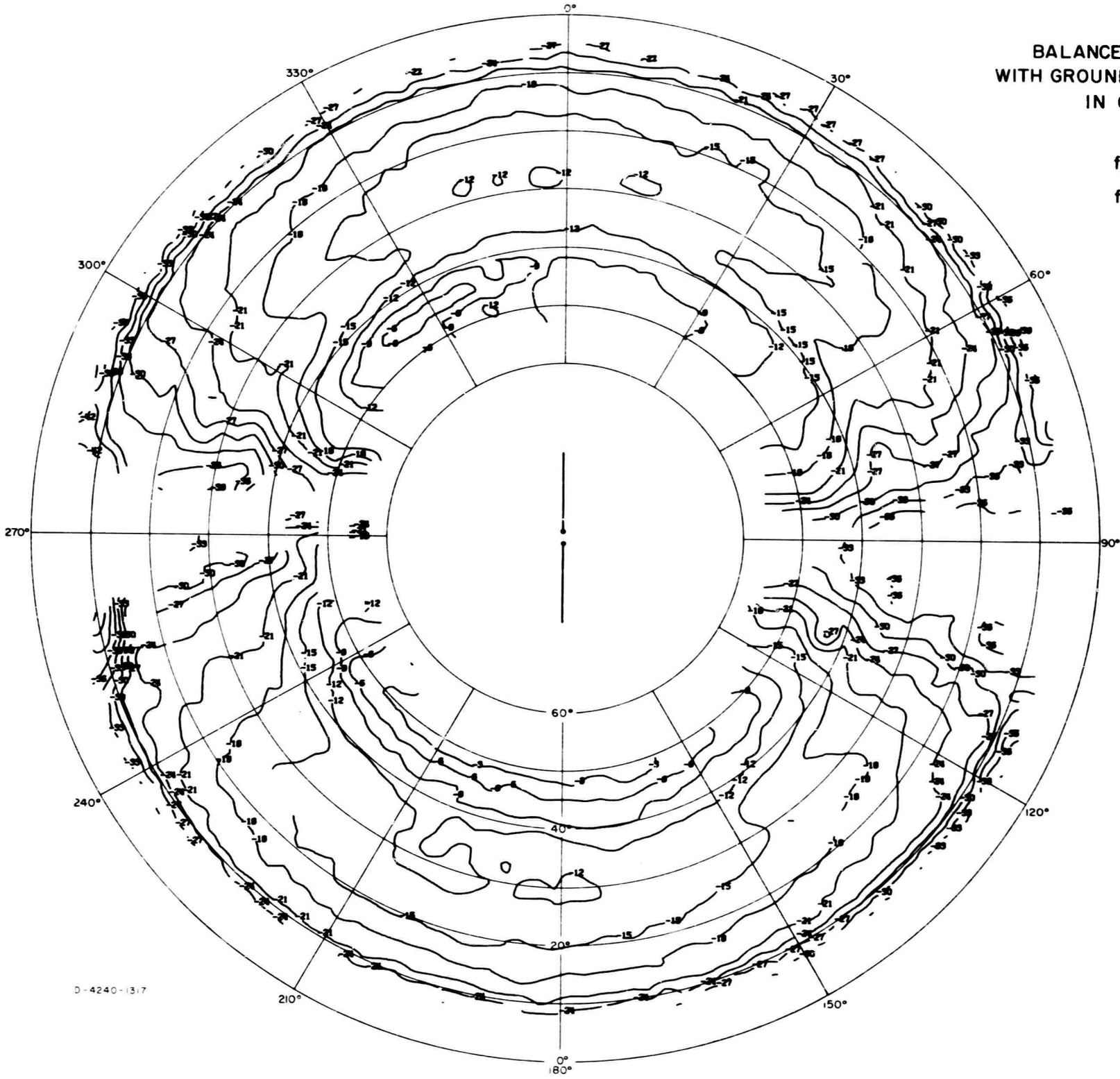

BALANCED DIPOLE
WITH GROUND SCREEN
IN CLEARING

$h_a = 41'$

$f_o = 6$ Mc/s

$f_m = 3$ Mc/s

E_θ

FIG. A-1

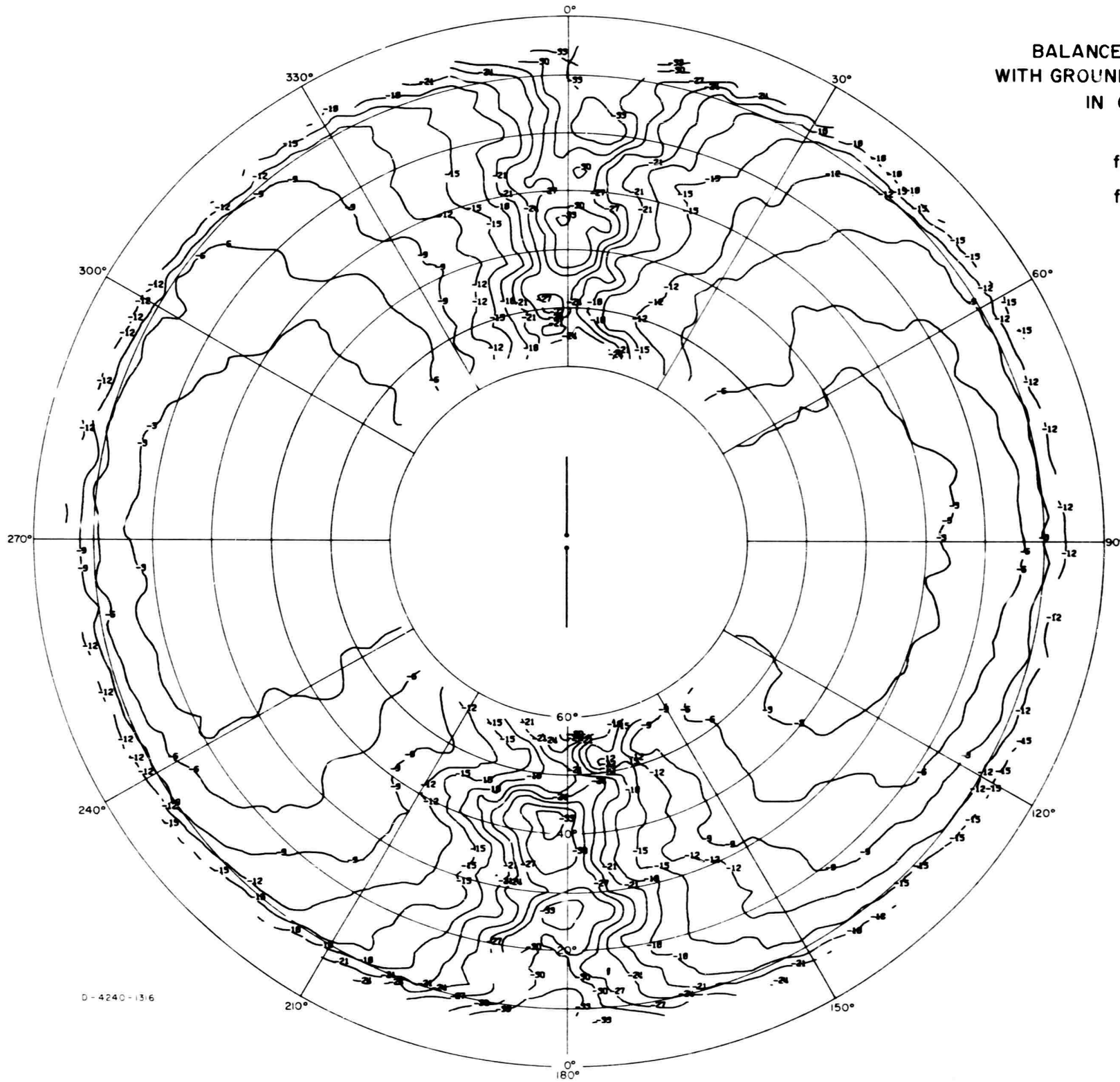

BALANCED DIPOLE
WITH GROUND SCREEN
IN CLEARING

$h_a = 41'$

$f_o = 6$ Mc/s

$f_m = 3$ Mc/s

E_ϕ

FIG. A-2

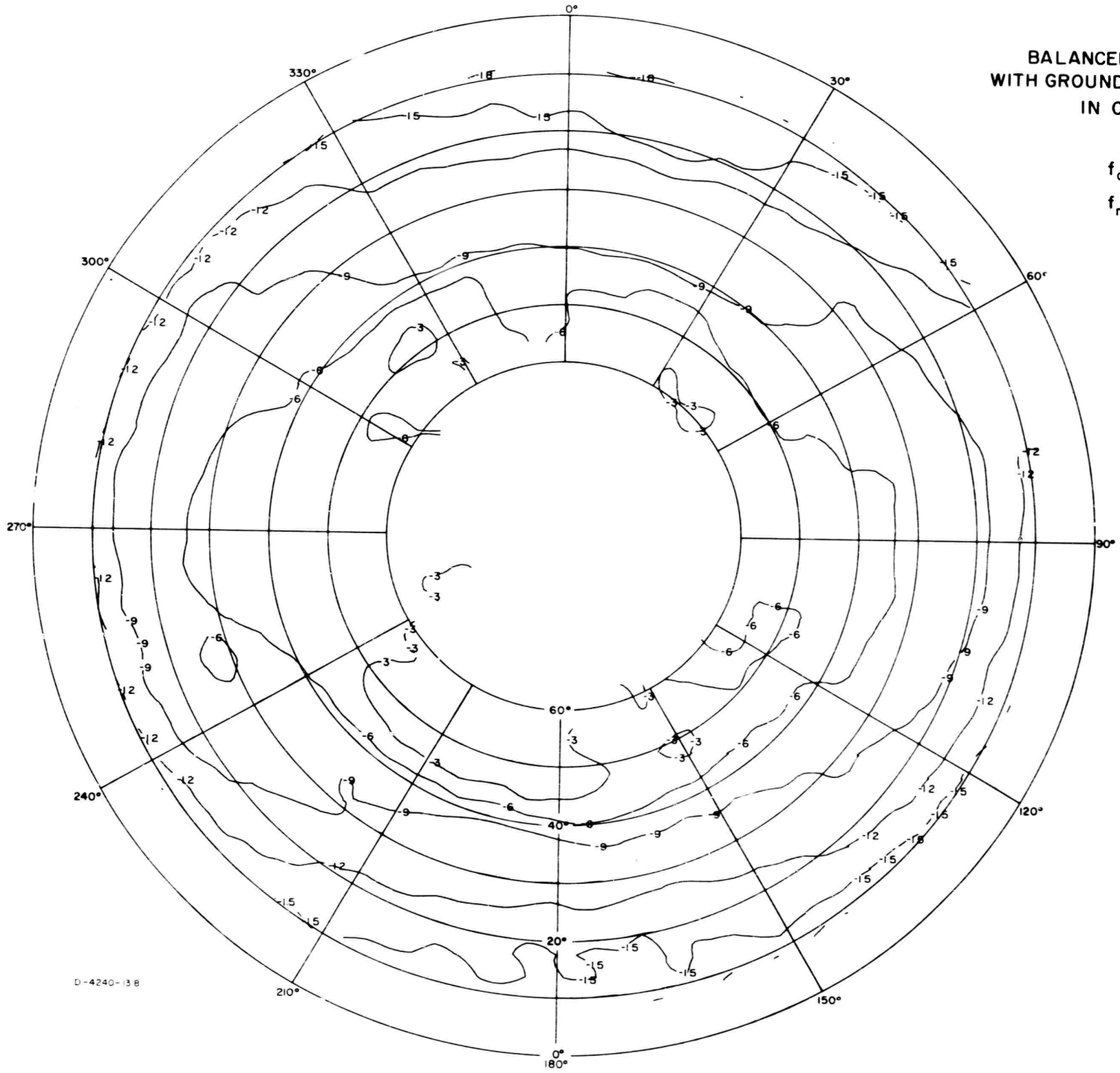

BALANCED DIPOLE
WITH GROUND SCREEN
IN CLEARING

$h_a = 41'$

$f_o = 6$ Mc/s

$f_m = 3$ Mc/s

POWEF

FIG. A-3

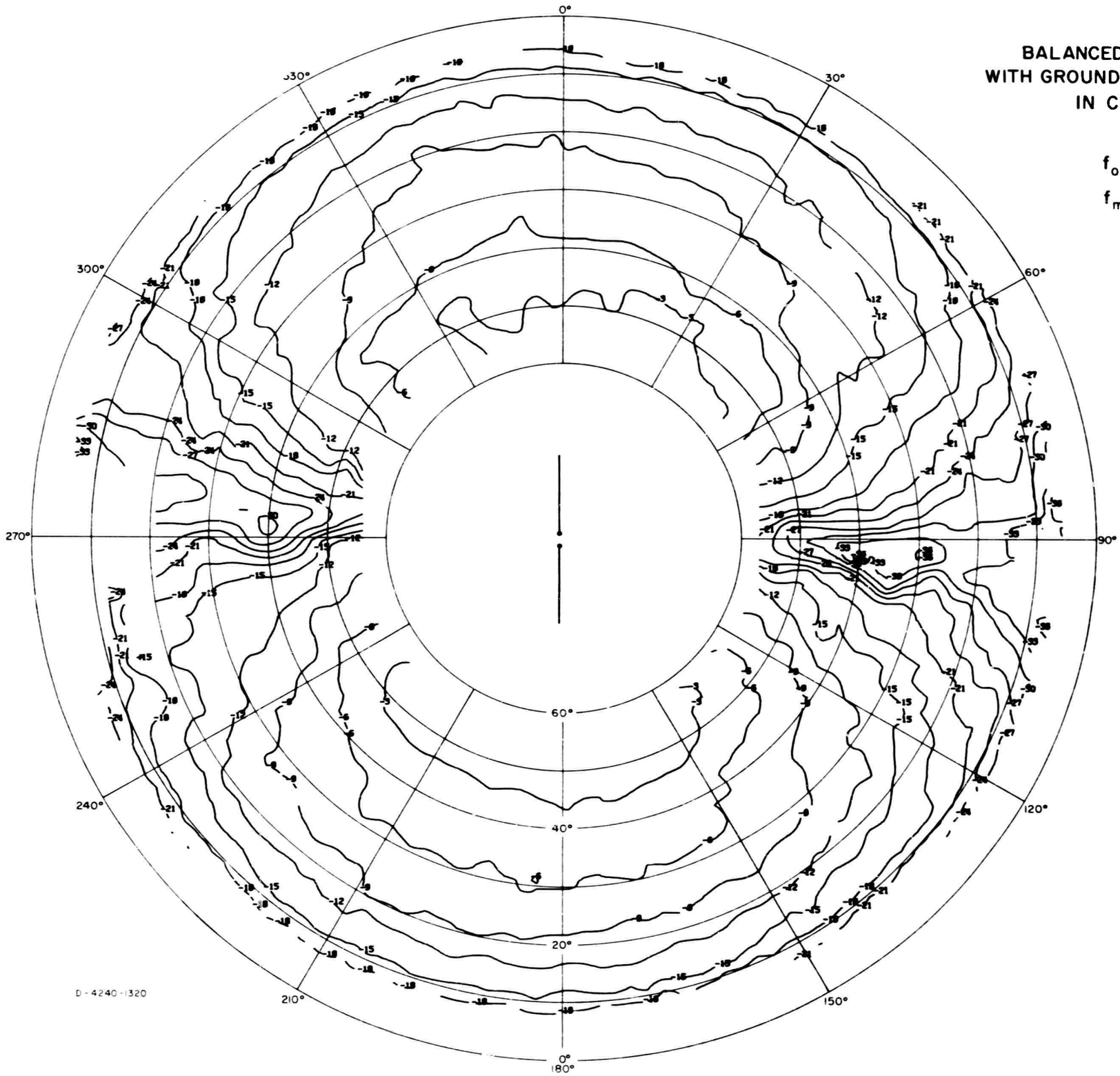

BALANCED DIPOLE
WITH GROUND SCREEN
IN CLEARING

$h_a = 41'$

$f_o = 6$ Mc/s

$f_m = 4$ Mc/s

E_θ

FIG. A-4

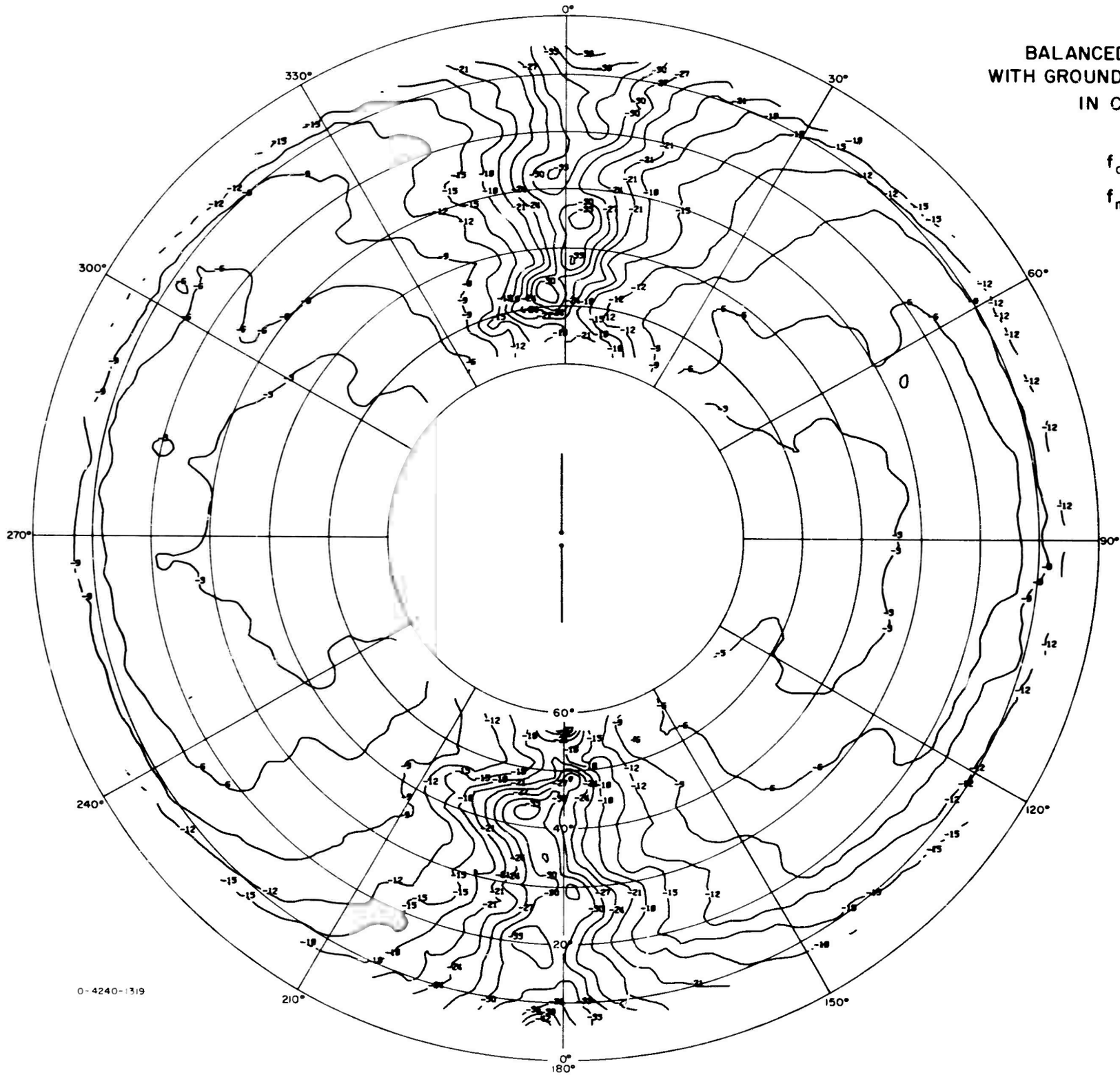

BALANCED DIPOLE
WITH GROUND SCREEN
IN CLEARING

$h_a = 41'$

$f_o = 6$ Mc/s

$f_m = 4$ Mc/s

E_ϕ

FIG. A-5

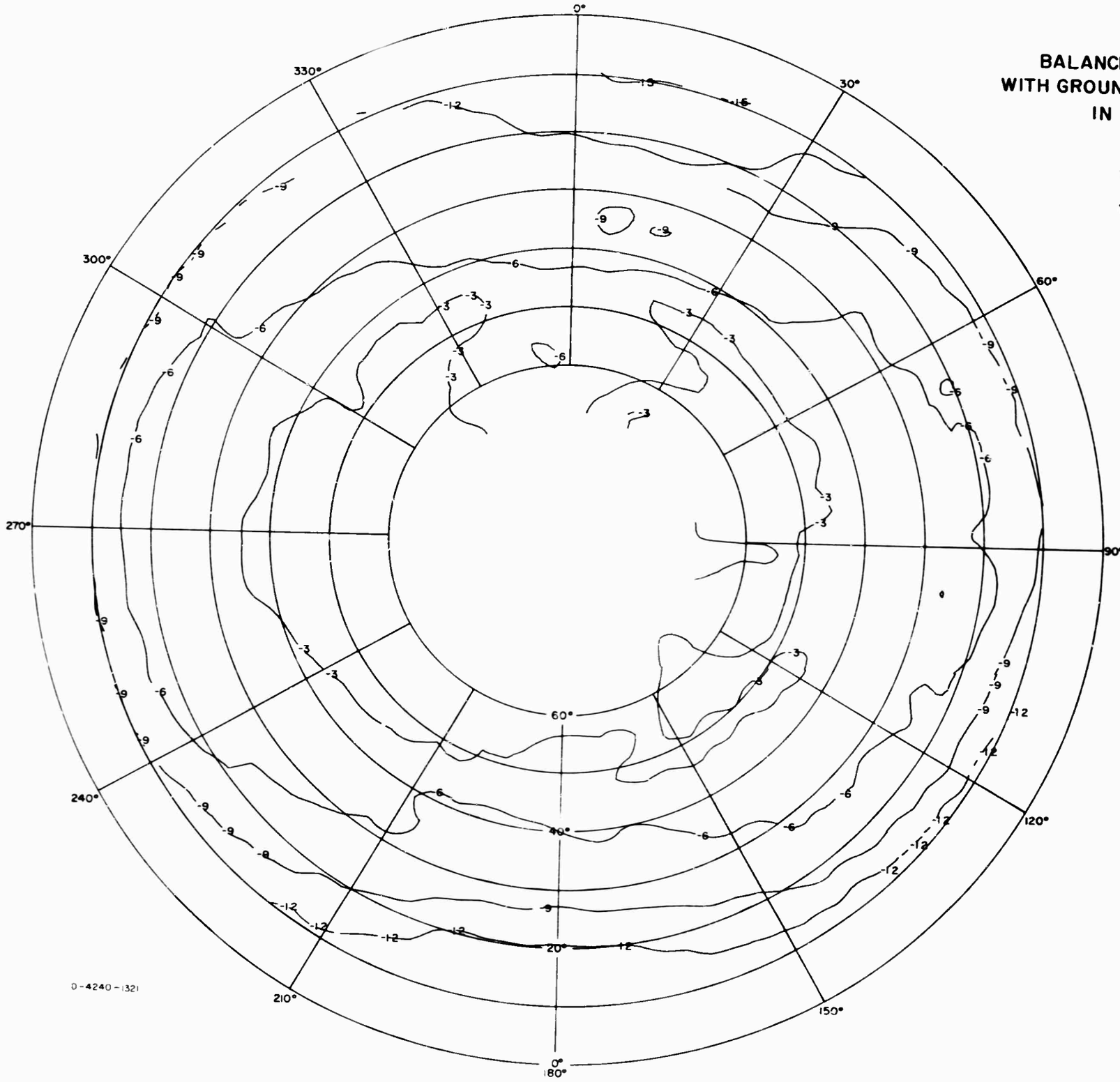

BALANCED DIPOLE
WITH GROUND SCREEN
IN CLEARING

h = 41'

f_o = 6 Mc/s

f_m = 4 Mc/s

POWER

FIG. A-6

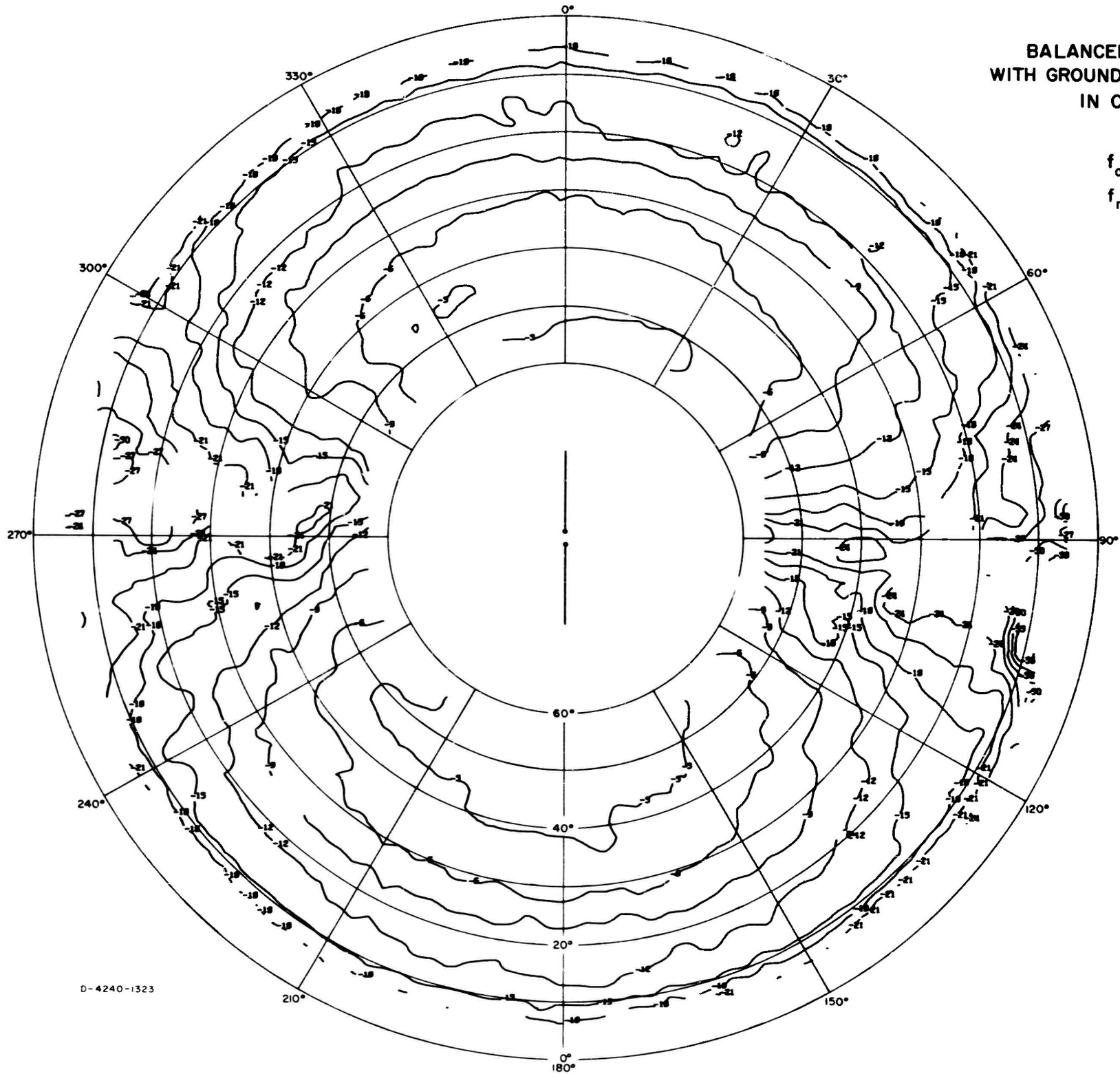

BALANCED DIPOLE
WITH GROUND SCREEN
IN CLEARING

$h_a = 41'$

$f_o = 6$ Mc/s

$f_m = 6$ Mc/s

E_θ

D-4240-1323

FIG. A-7

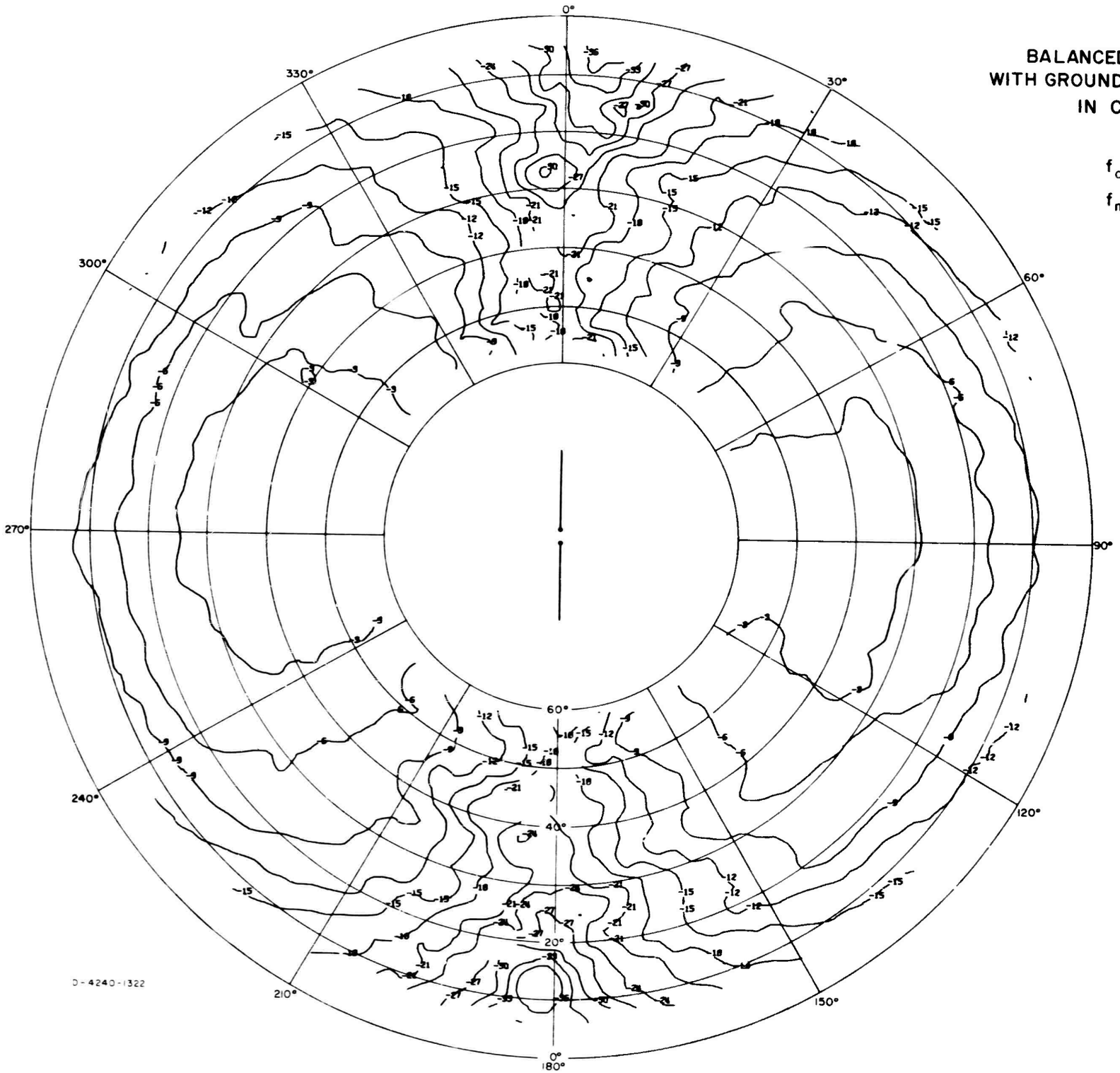

BALANCED DIPOLE
WITH GROUND SCREEN
IN CLEARING

h_a = 41'

f_o = 6 Mc/s

f_m = 6 Mc/s

E_ϕ

FIG. A-8

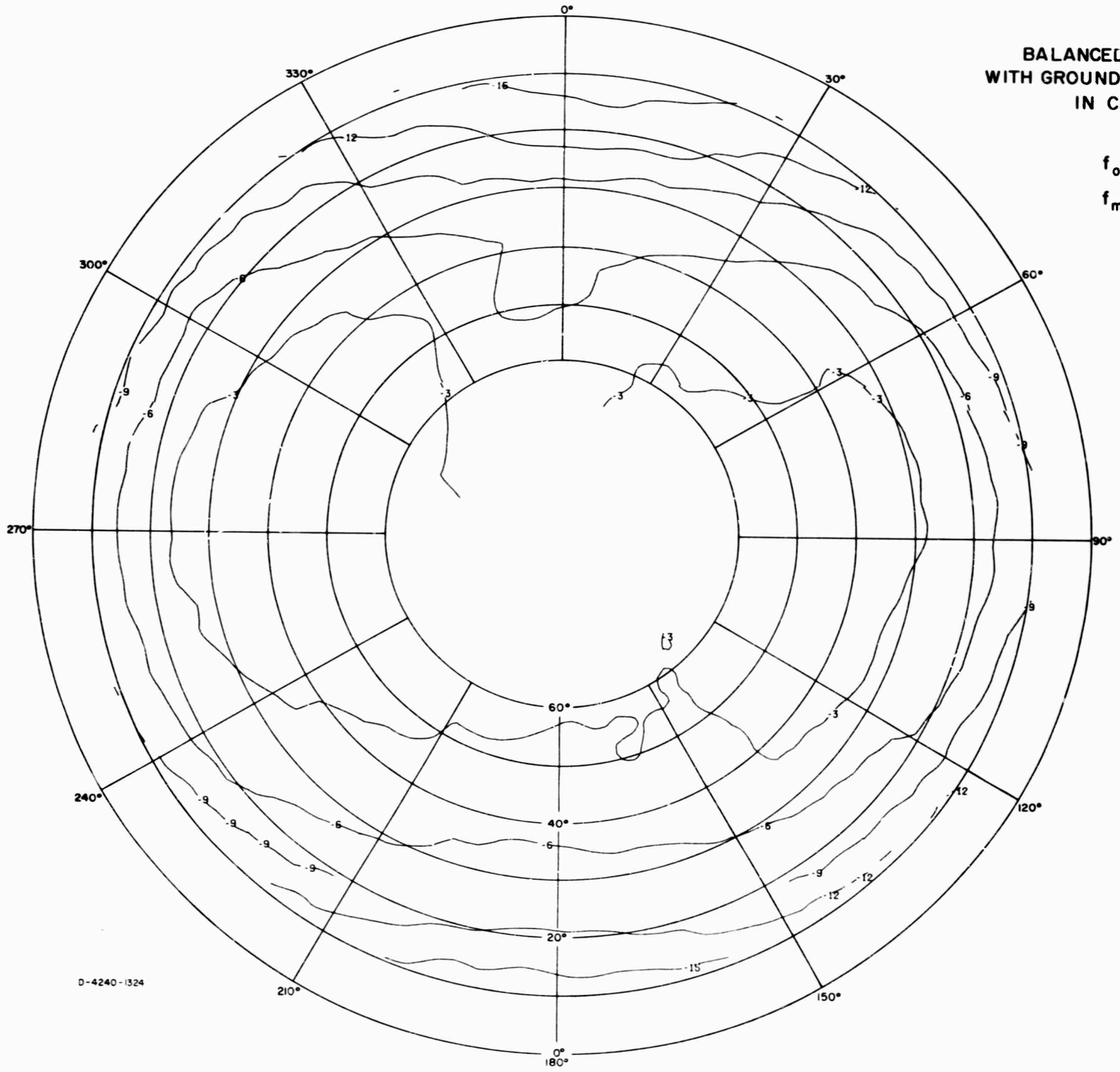

BALANCED DIPOLE
WITH GROUND SCREEN
IN CLEARING

$h_a = 41'$

$f_o = 6$ Mc/s

$f_m = 6$ Mc/s

POWER

FIG. A-9

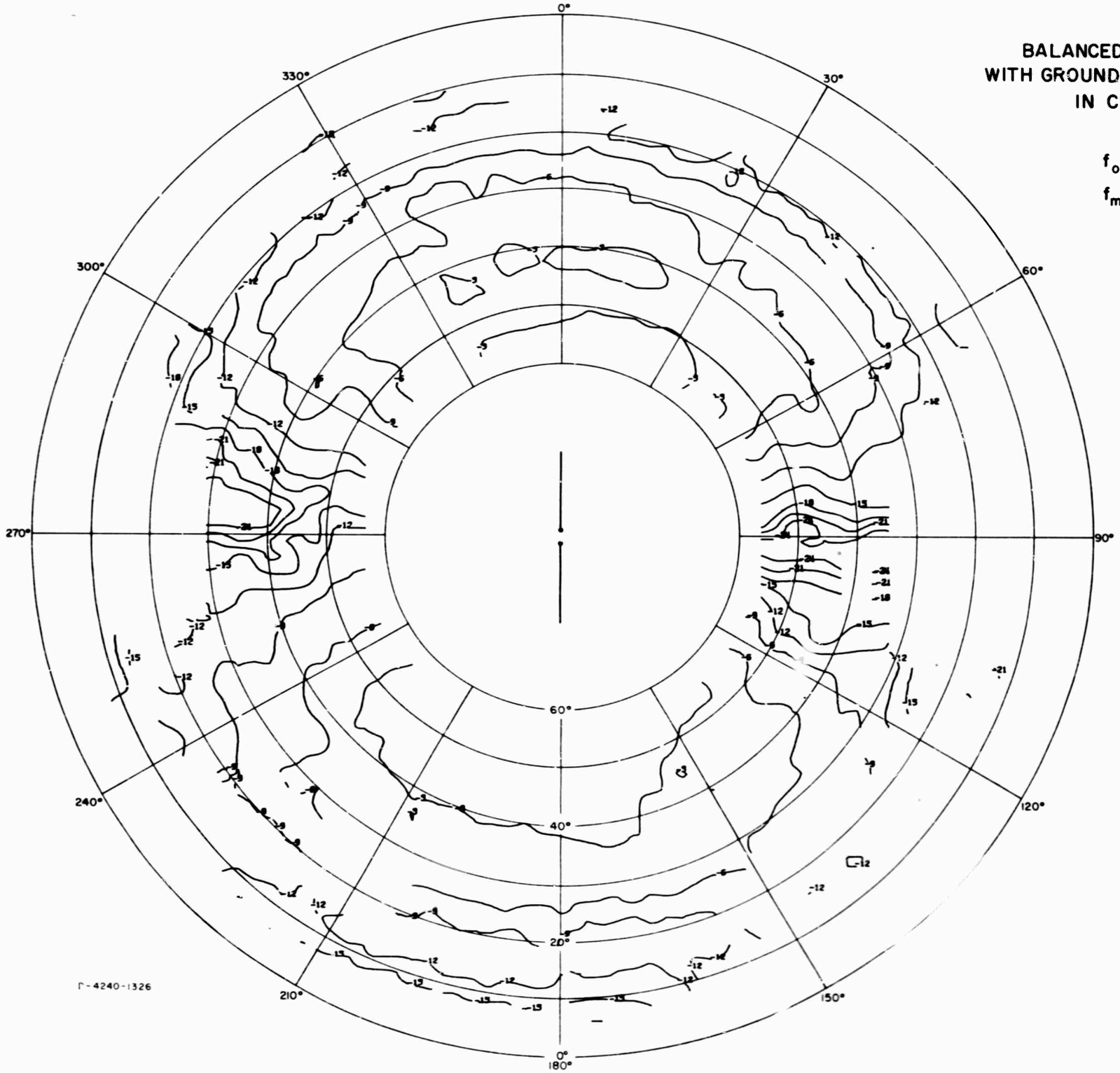

BALANCED DIPOLE
WITH GROUND SCREEN
IN CLEARING

$h_a = 41'$

$f_o = 6$ Mc/s

$f_m = 8$ Mc/s

E_θ

FIG. A-10

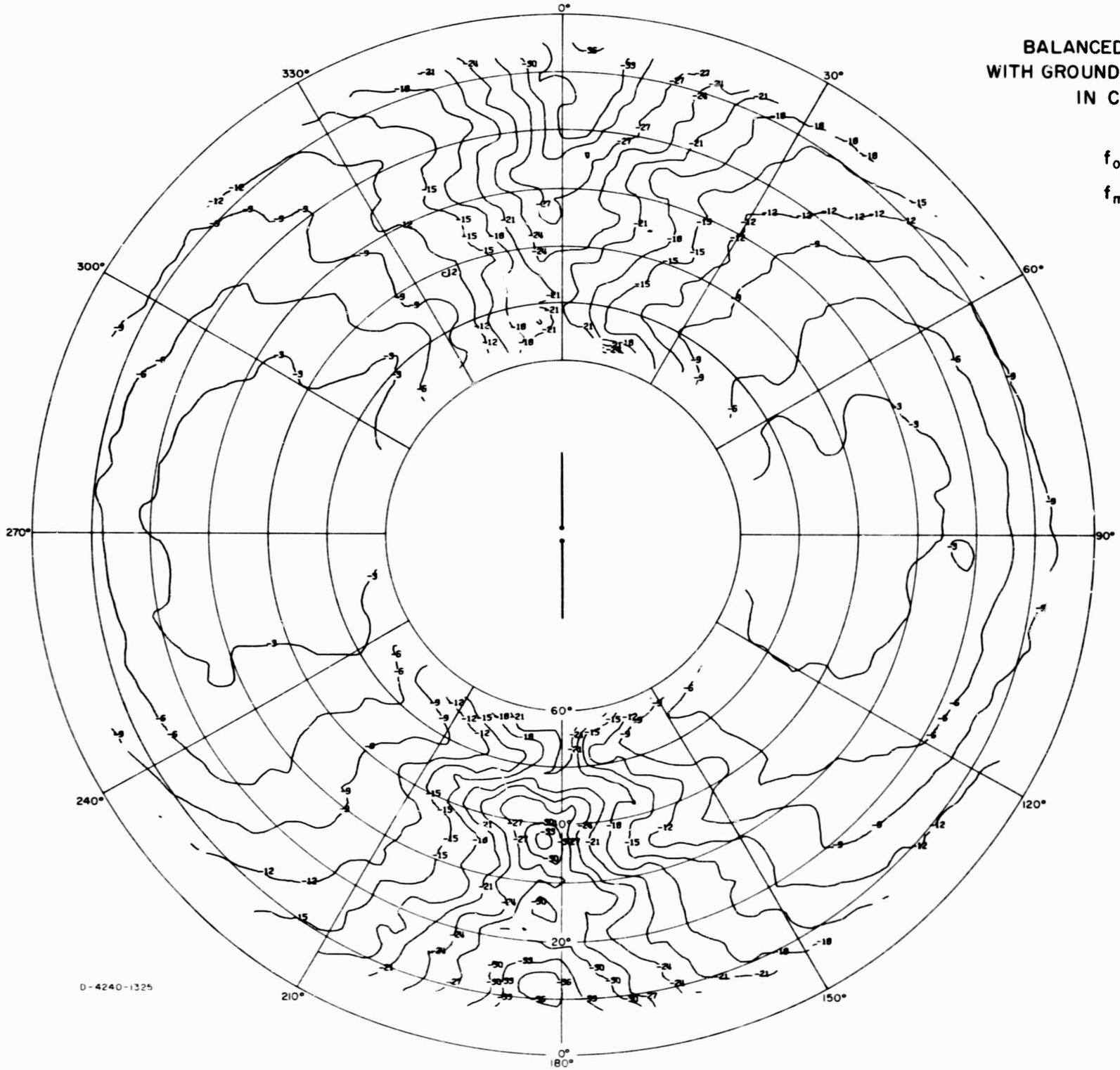

BALANCED DIPOLE
WITH GROUND SCREEN
IN CLEARING

$h_a = 41'$

$f_o = 6$ Mc/s

$f_m = 8$ Mc/s

E_ϕ

D-4240-1325

FIG. A-11

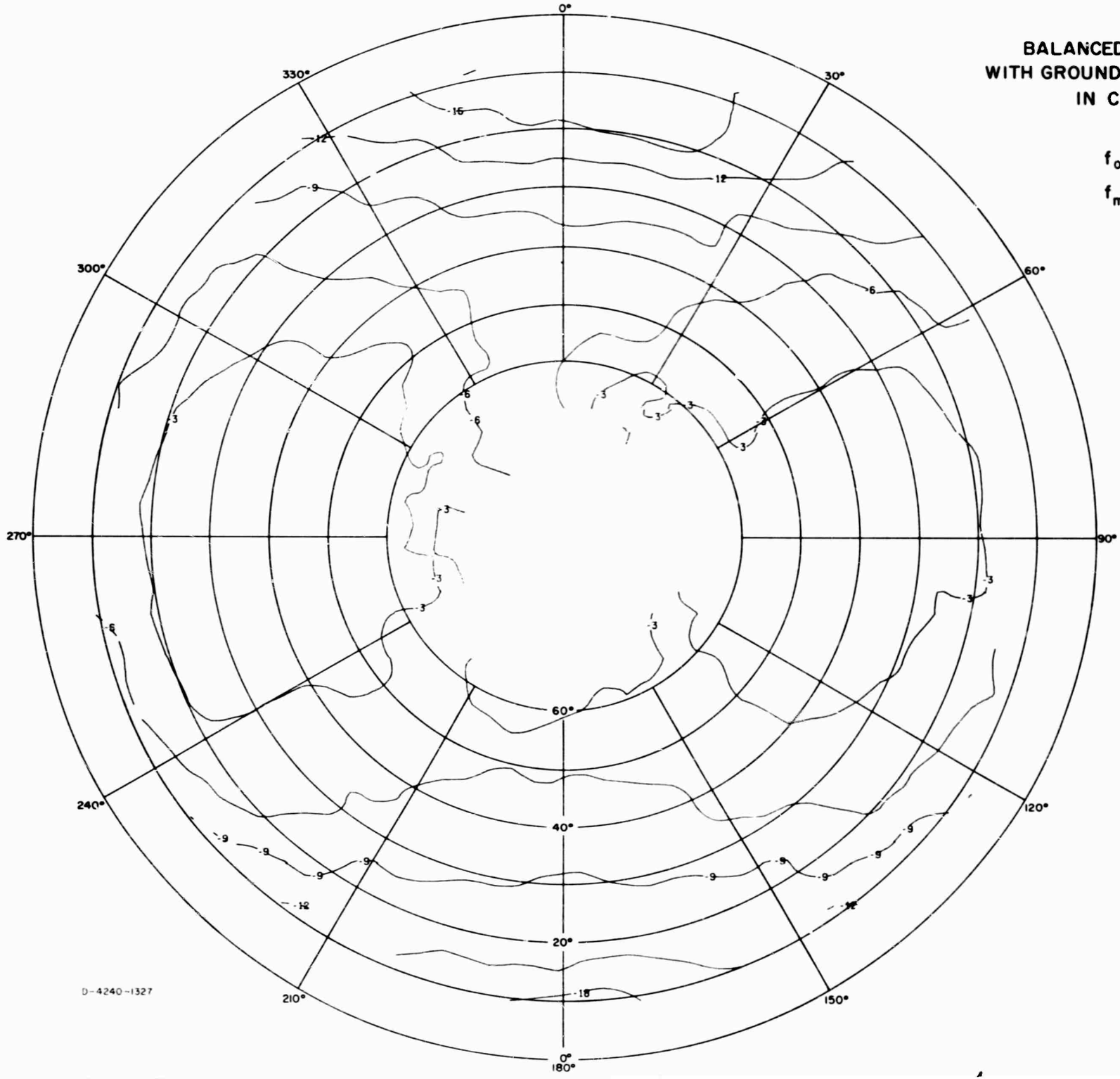

BALANCED DIPOLE
WITH GROUND SCREEN
IN CLEARING

h_a = 41'

f_o = 6 Mc/s

f_m = 8 Mc/s

POWER

FIG. A-12

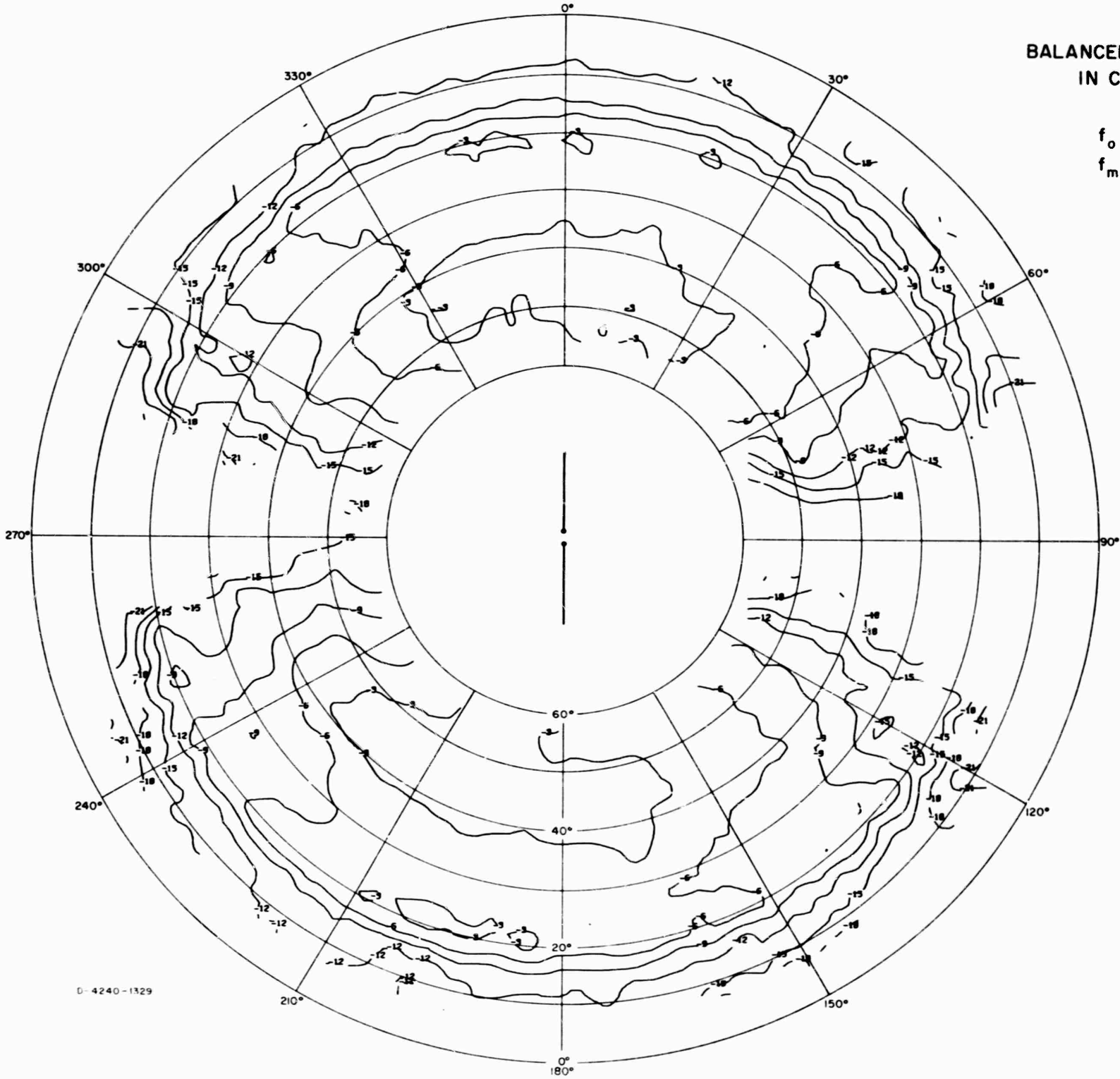

BALANCED DIPOLE
IN CLEARING
$h_a = 41'$
$f_o = 6$ Mc/s
$f_m = 3$ Mc/s
E_θ

FIG. A-13

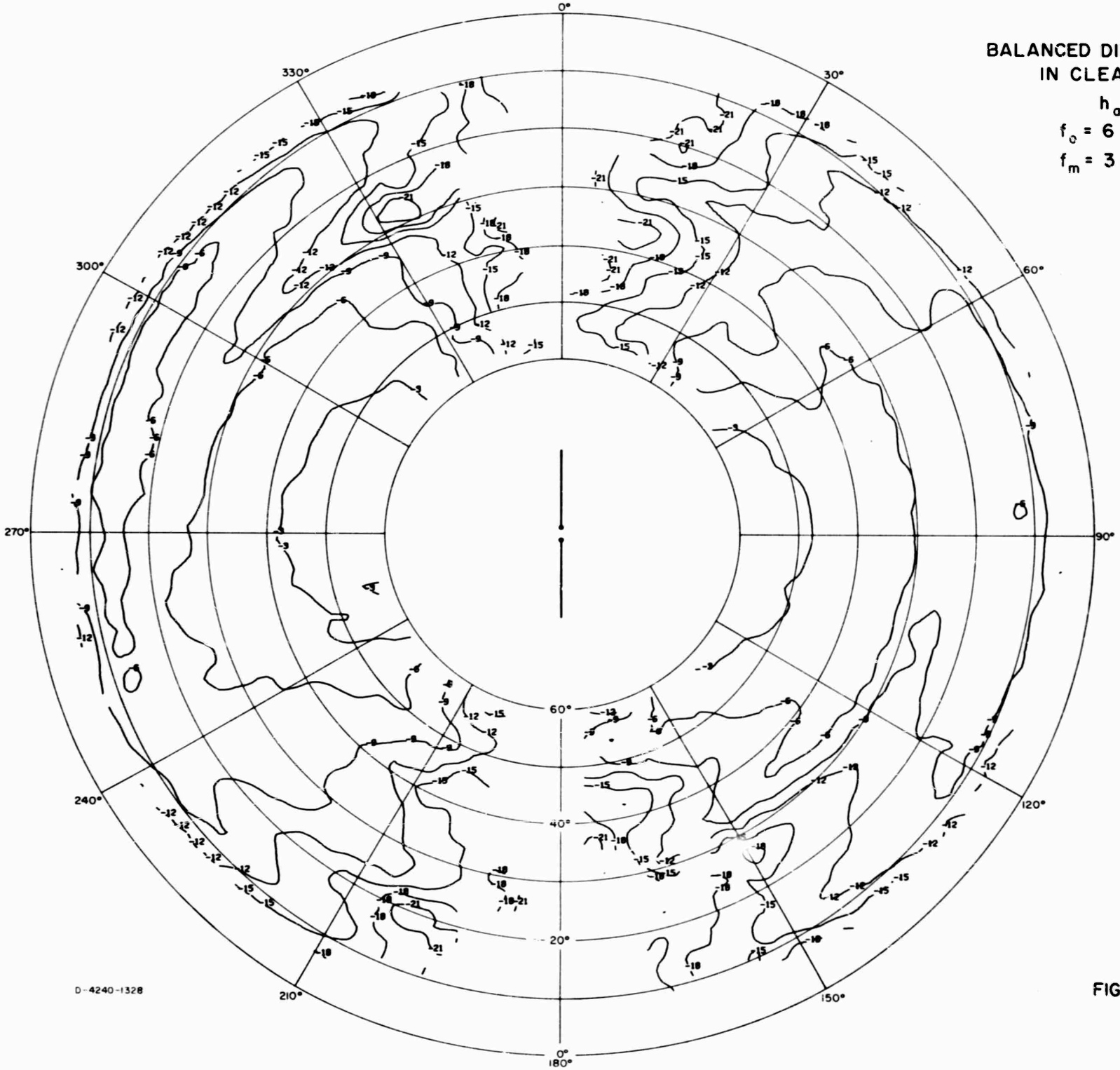

BALANCED DIPOLE
IN CLEARING
h_a = 41'
f_c = 6 Mc/s
f_m = 3 Mc/s
E_ϕ

FIG. A-14

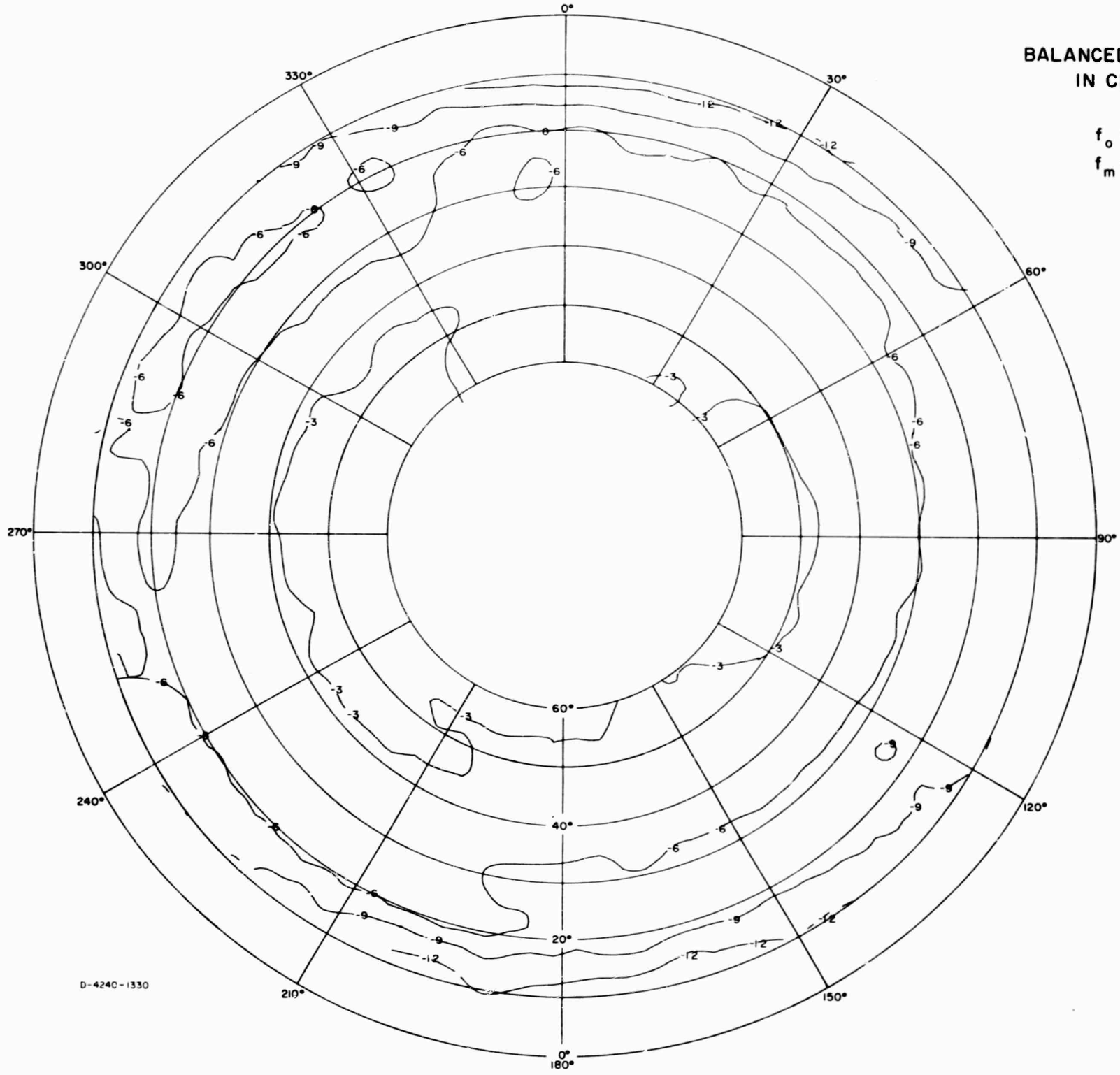

BALANCED DIPOLE
IN CLEARING
$h_a = 41'$
$f_o = 6$ Mc/s
$f_m = 3$ Mc/s
POWER

FIG. A-15

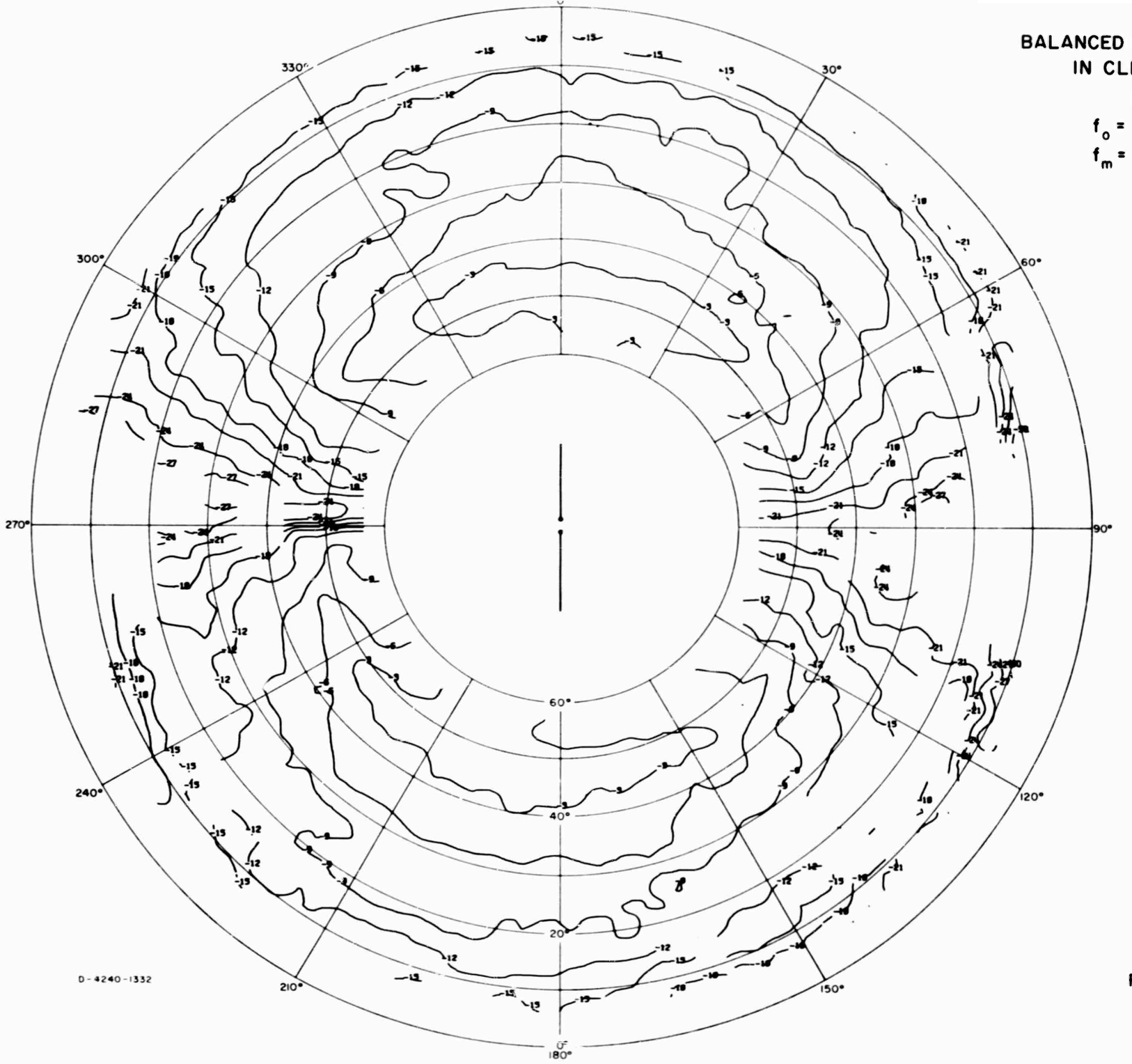
BALANCED DIPOLE
IN CLEARING
h_a = 41'
f_o = 6 Mc/s
f_m = 4 Mc/s
E_θ
0°
30°
60°
90°
120°
150°
180°
210°
240°
270°
300°
330°
60°
40°
20°
D-4240-1332

FIG. A-16

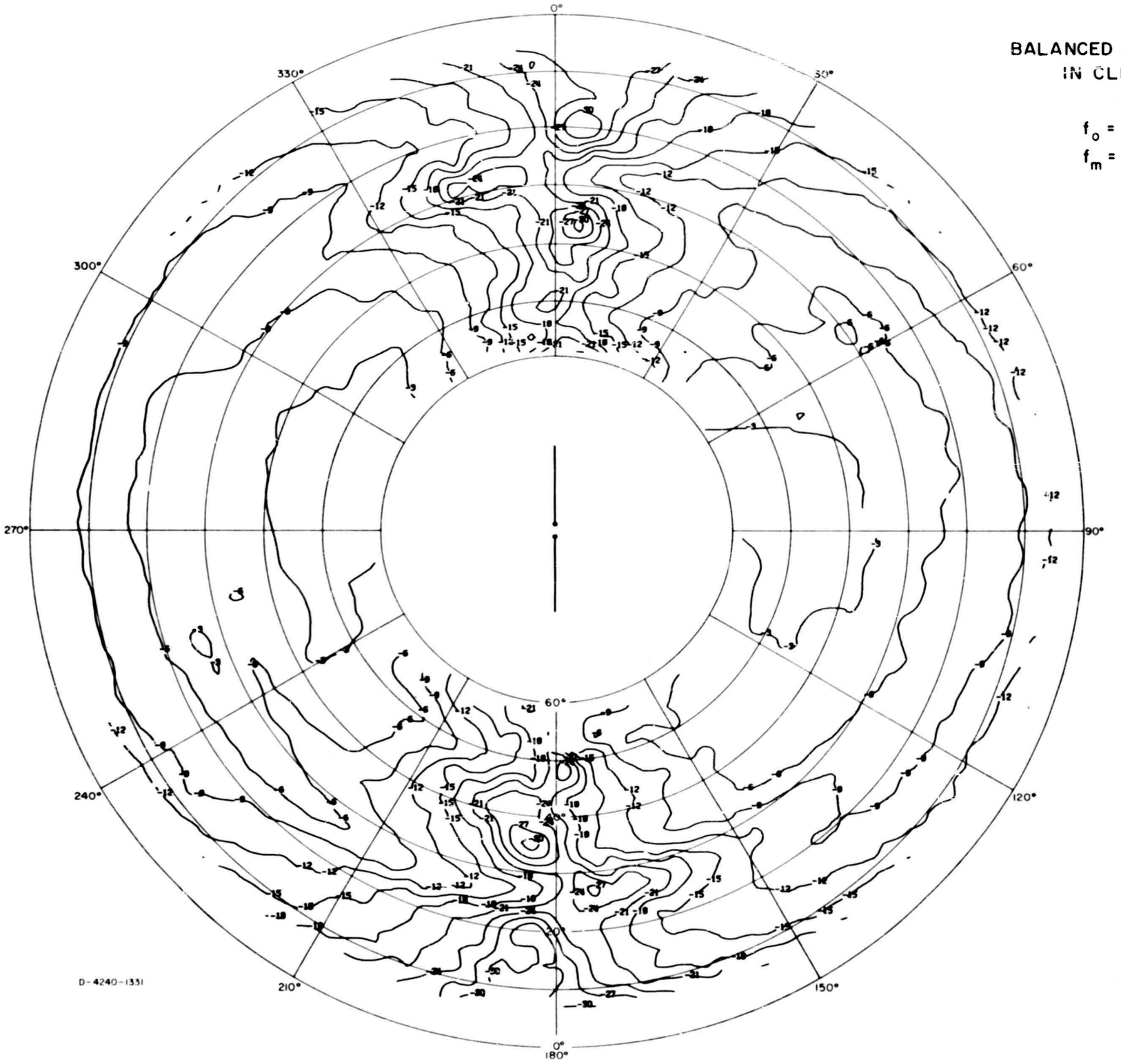

BALANCED DIPOLE
IN CLEARING
$h_a = 41'$
$f_o = 6$ Mc/s
$f_m = 4$ Mc/s
E_ϕ

FIG. A-17

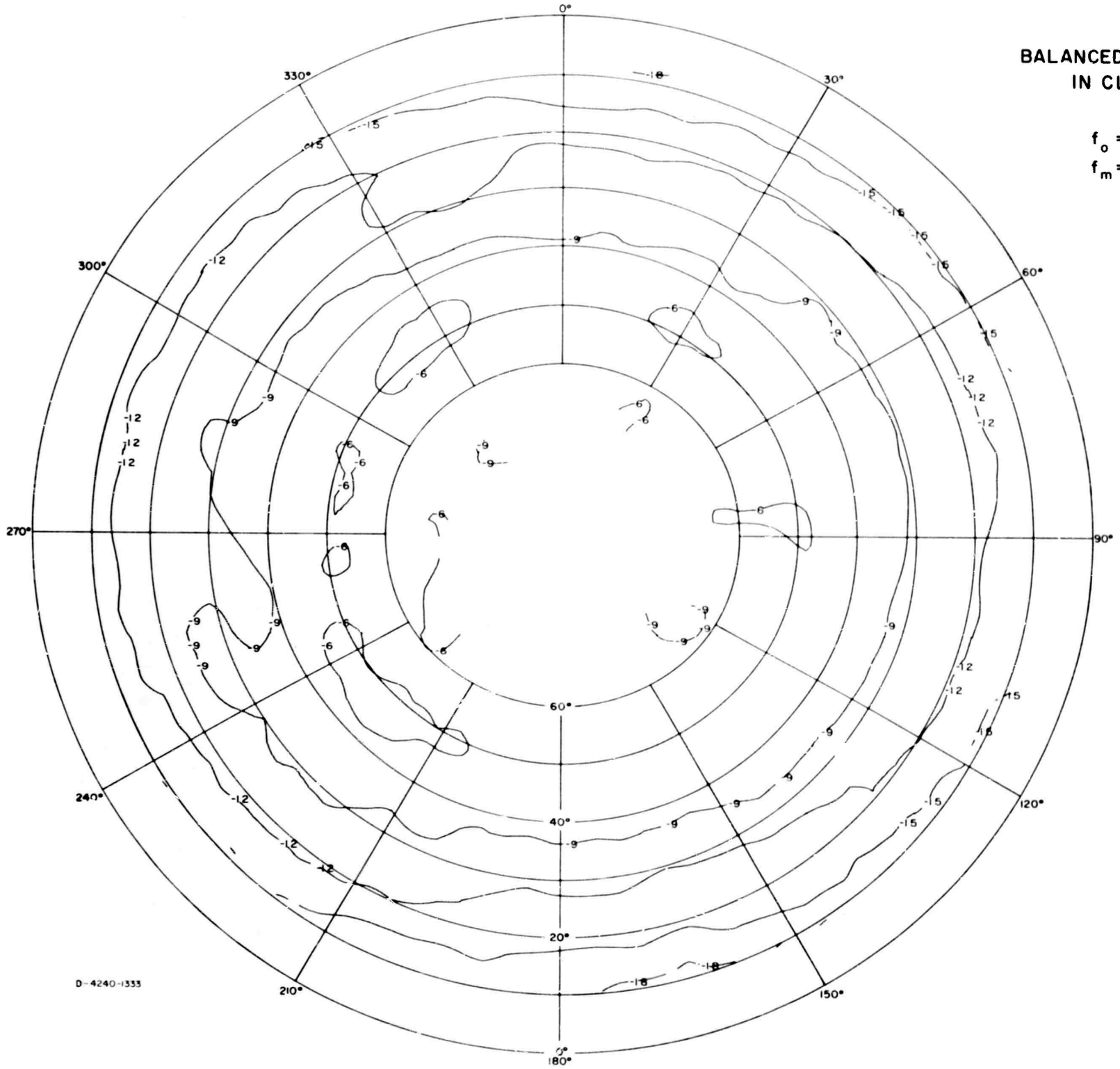

BALANCED DIPOLE
IN CLEARING
$h_a = 41'$
$f_o = 6$ Mc/s
$f_m = 4$ Mc/s
POWER

FIG. A-18

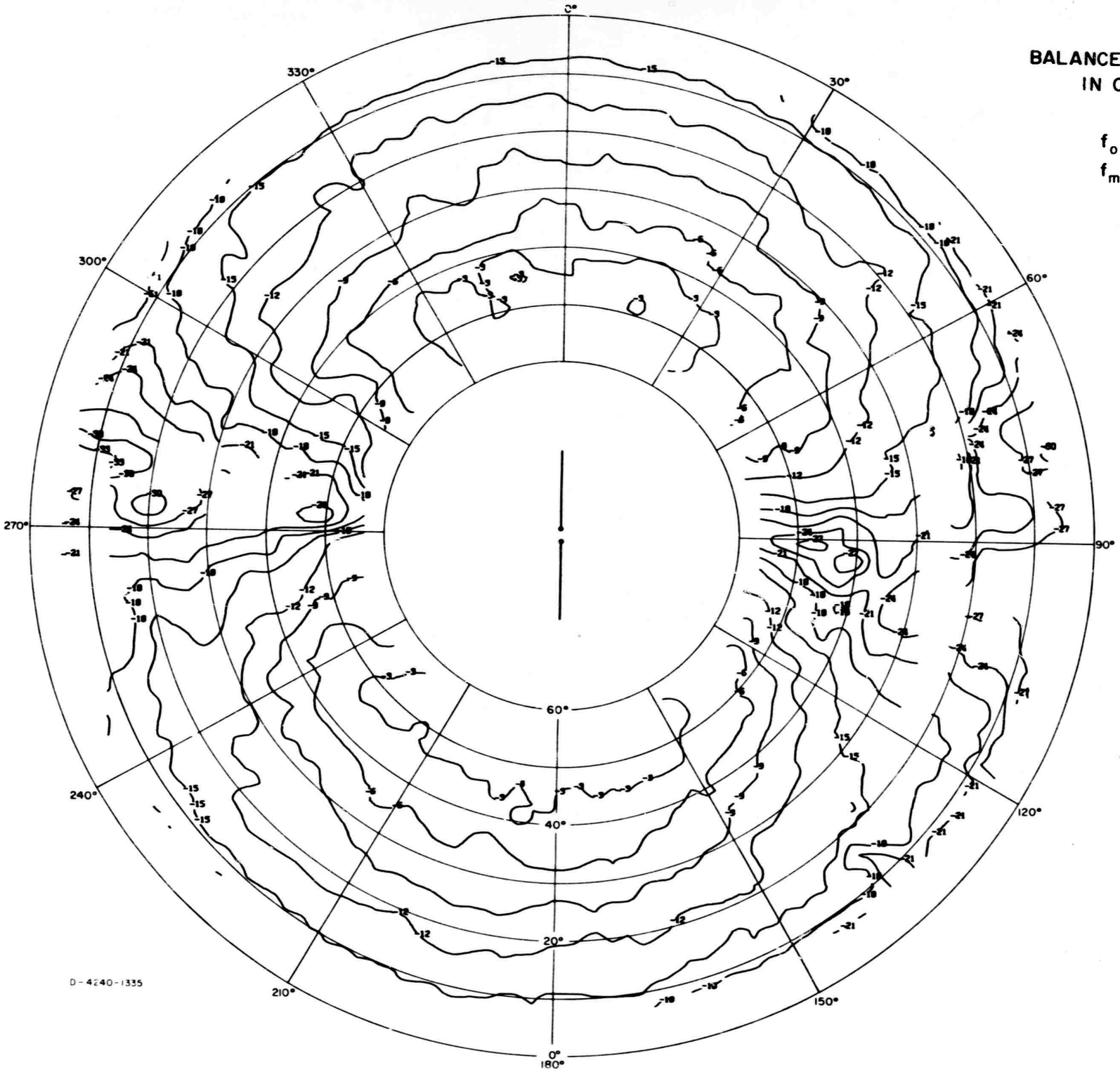

BALANCED DIPOLE
IN CLEARING
$h_a = 41'$
$f_o = 6$ Mc/s
$f_m = 6$ Mc/s
E_θ

D-4240-1335

FIG. A-19

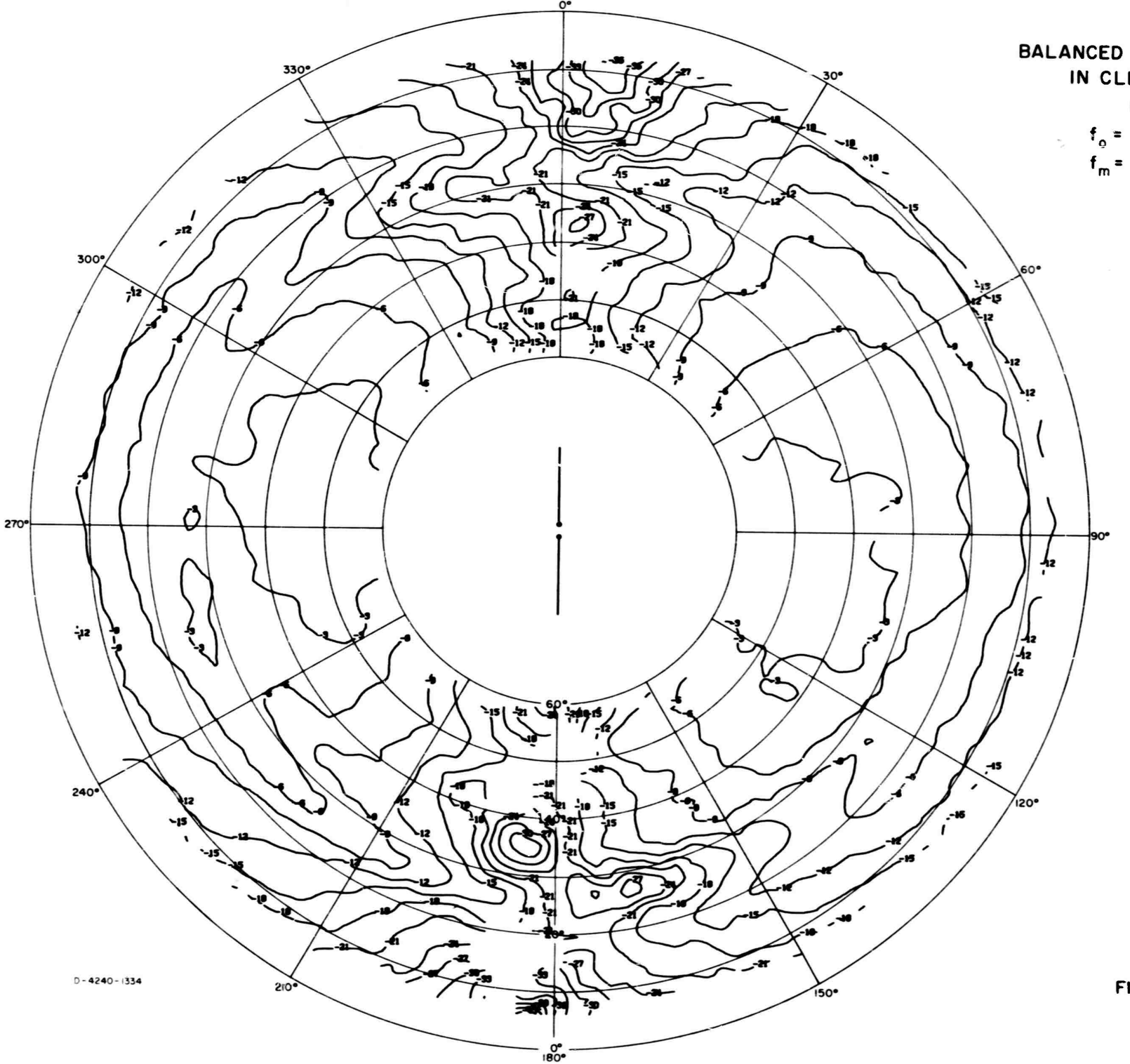

BALANCED DIPOLE
IN CLEARING
$h_a = 41'$
$f_o = 6$ Mc/s
$f_m = 6$ Mc/s
E_ϕ

FIG. A-20

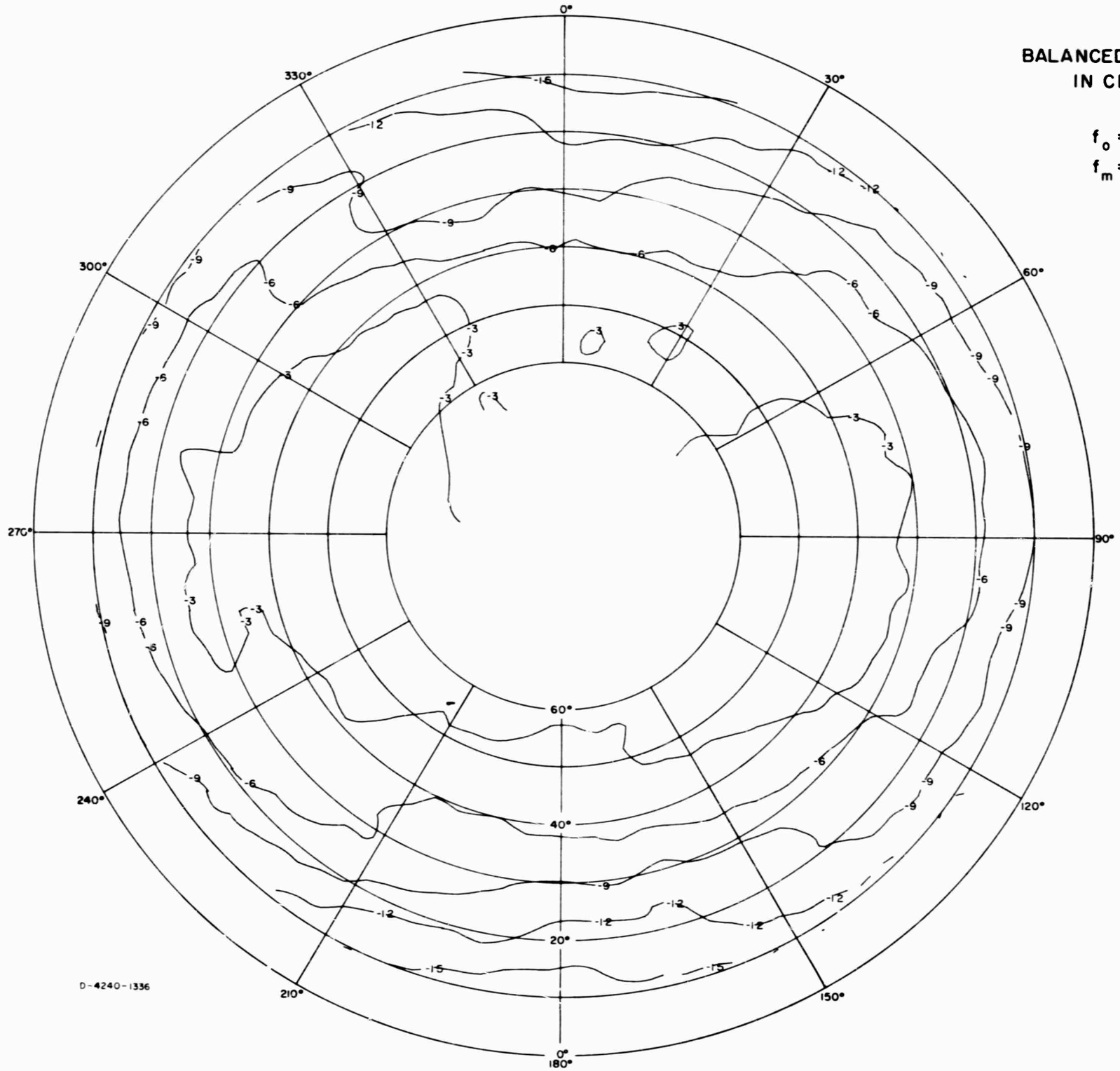

BALANCED DIPOLE
IN CLEARING
h_a = 41'
f_o = 6 Mc/s
f_m = 6 Mc/s
POWER

FIG. A-21

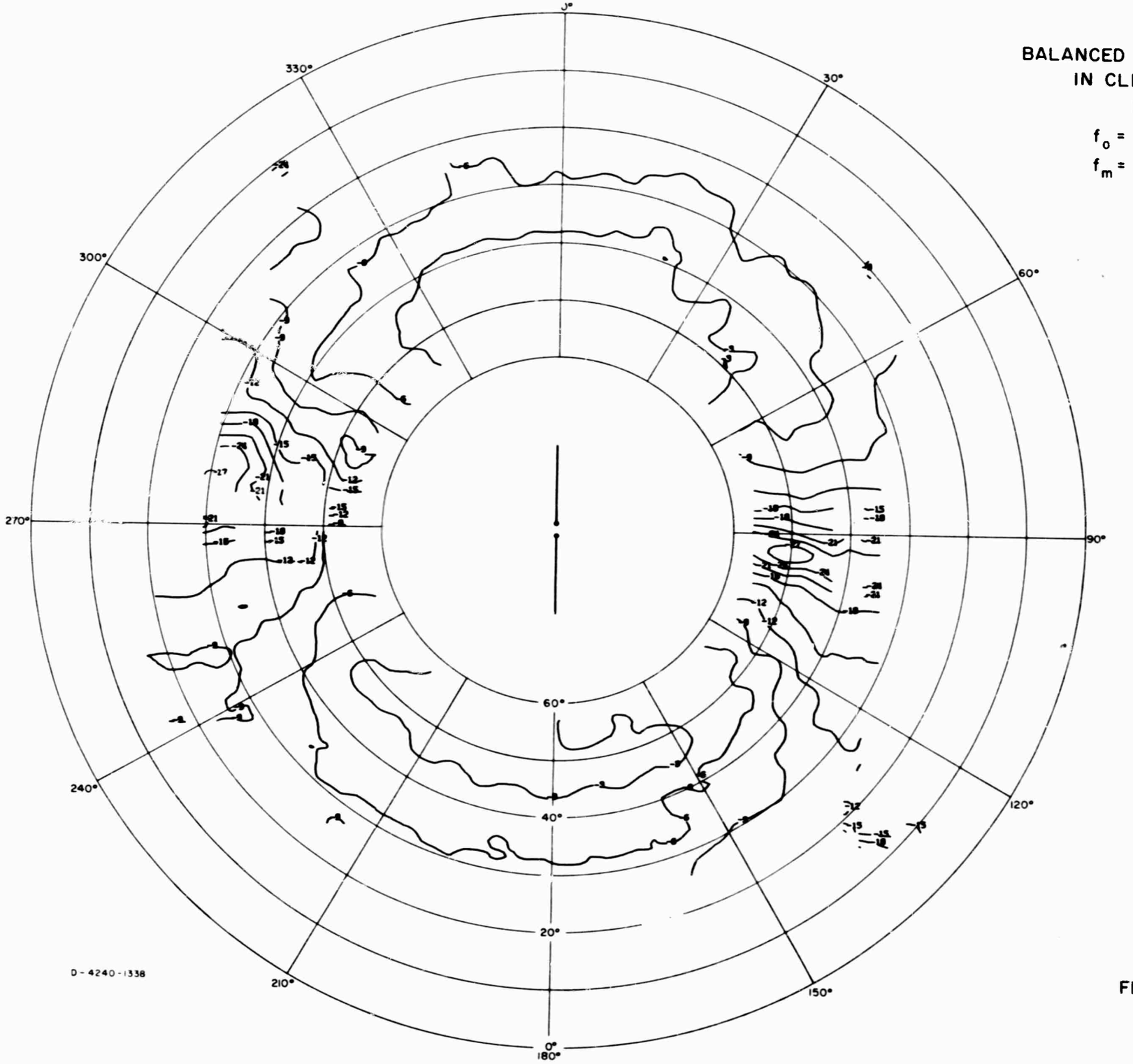

BALANCED DIPOLE
IN CLEARING
$h_a = 41'$
$f_o = 6$ Mc/s
$f_m = 8$ Mc/s
E_θ

FIG. A-22

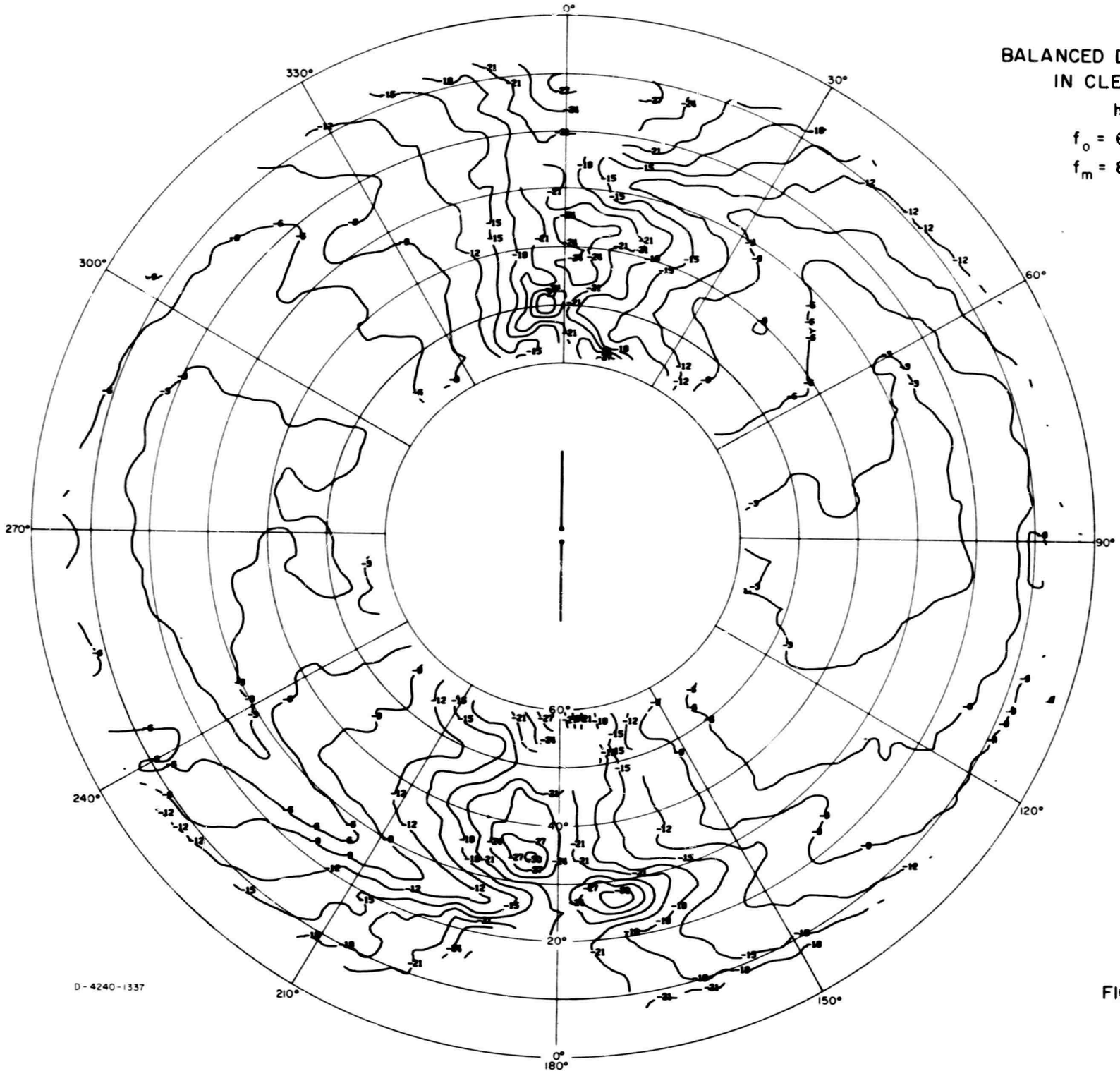

BALANCED DIPOLE
IN CLEARING
$h_a = 41'$
$f_o = 6$ Mc/s
$f_m = 8$ Mc/s
E_ϕ

FIG. A-23

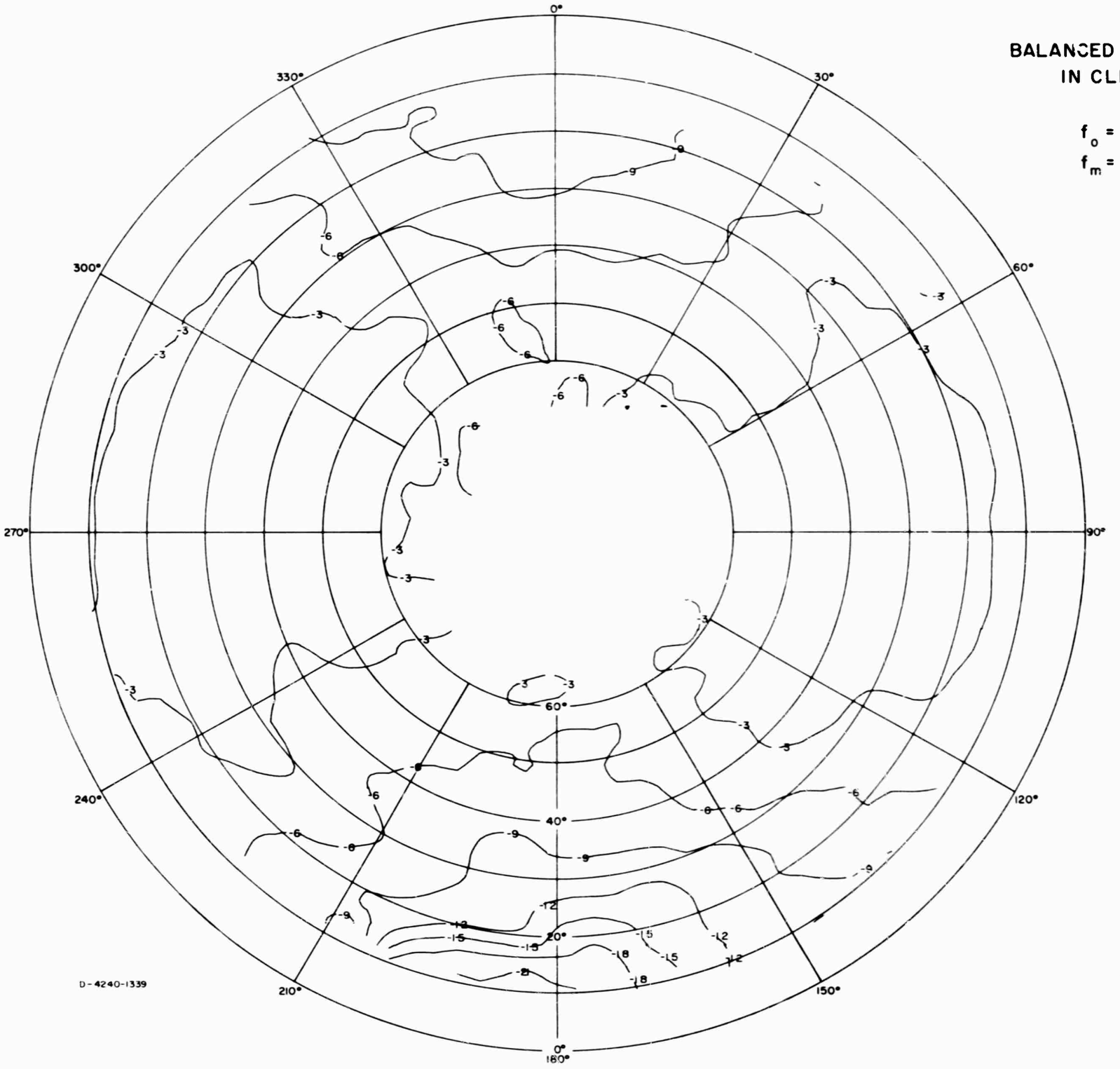

BALANCED DIPOLE
IN CLEARING
$h_a = 41'$
$f_o = 6$ Mc/s
$f_m = 8$ Mc/s
POWER

D-4240-1339

FIG. A-24

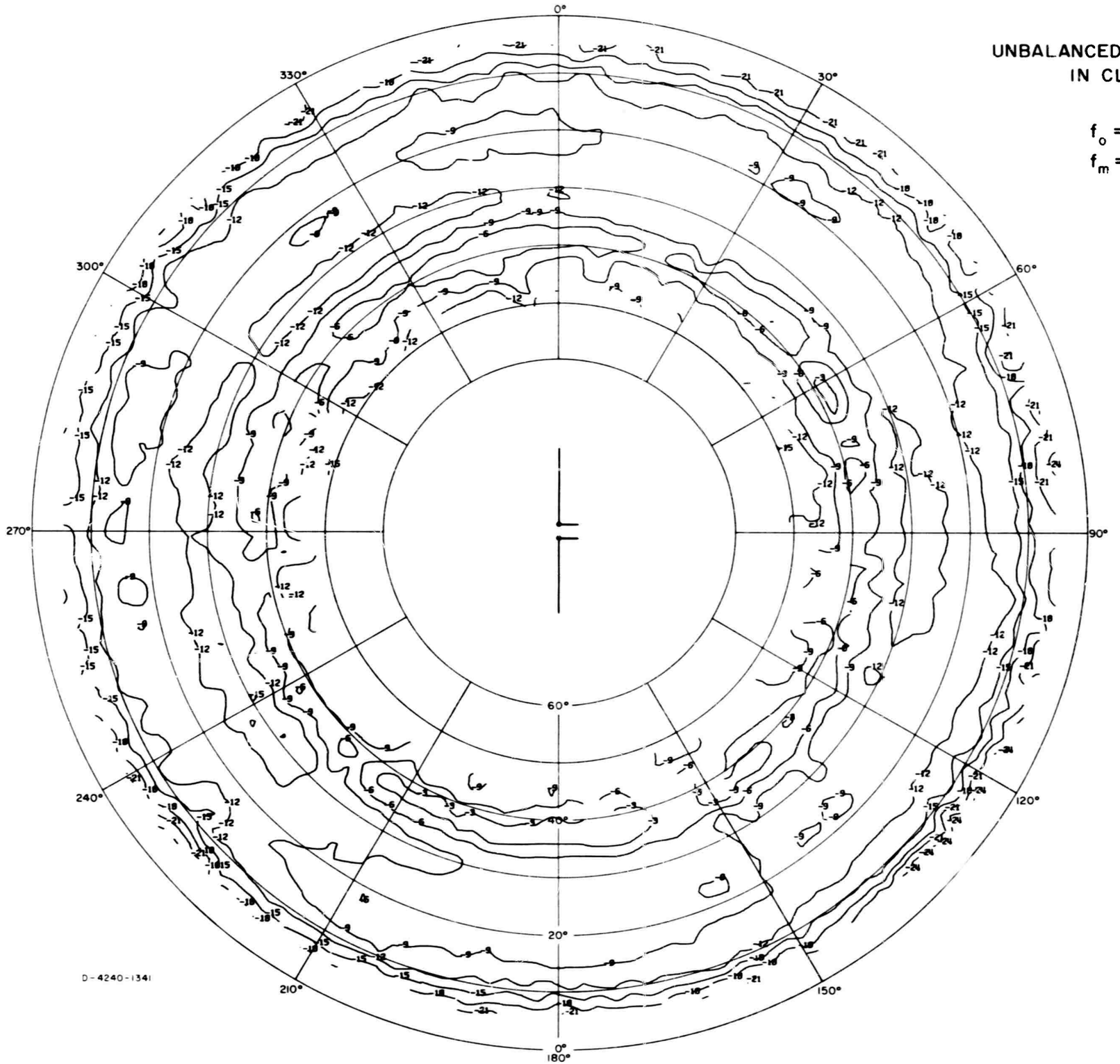

UNBALANCED DIPOLE
IN CLEARING
$h_a = 41'$
$f_o = 6$ Mc/s
$f_m = 3$ Mc/s
E_θ

FIG. A-25

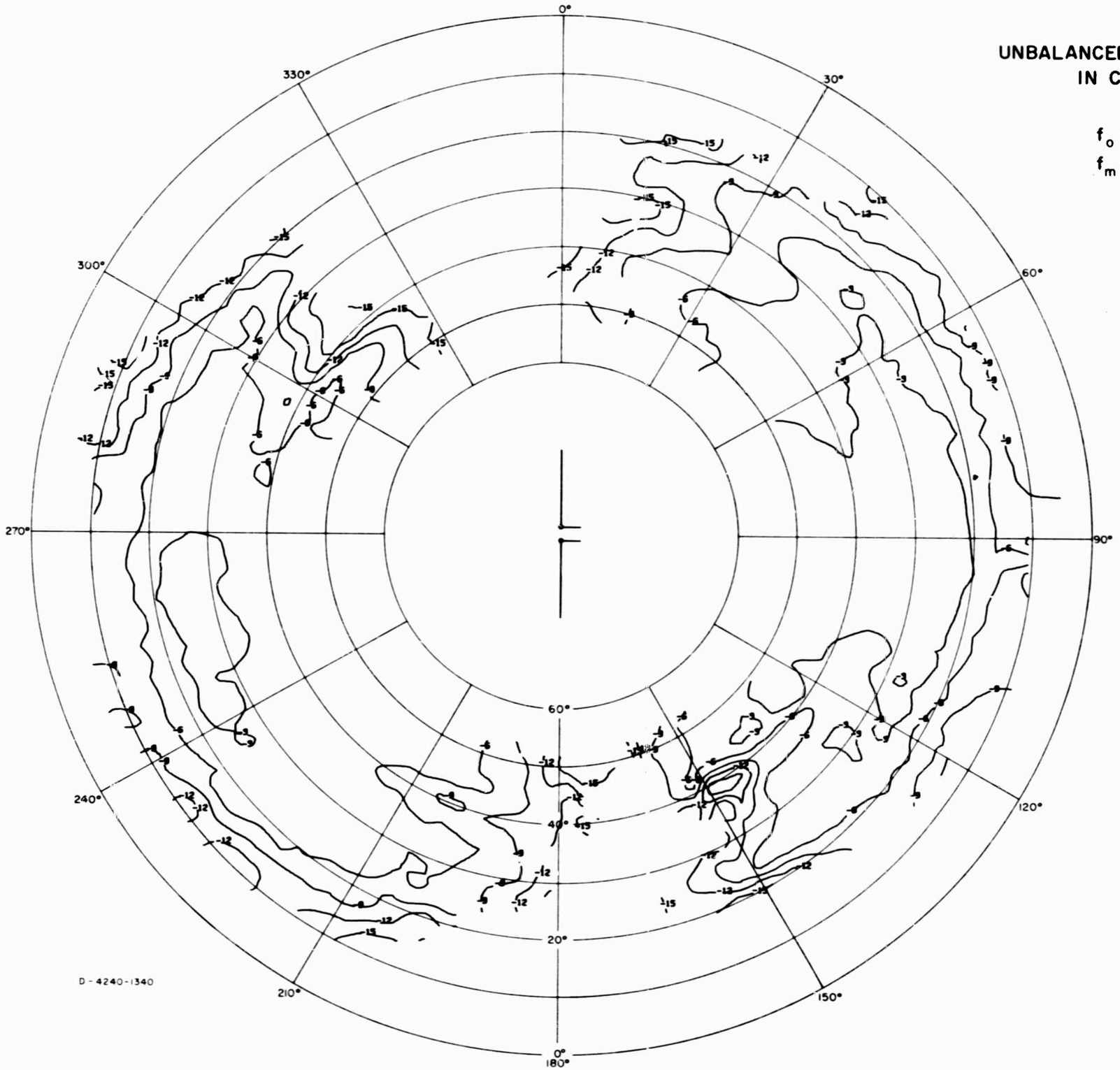

UNBALANCED DIPOLE
IN CLEARING
h_a = 41'
f_o = 6 Mc/s
f_m = 3 Mc/s
E_ϕ

FIG. A-26

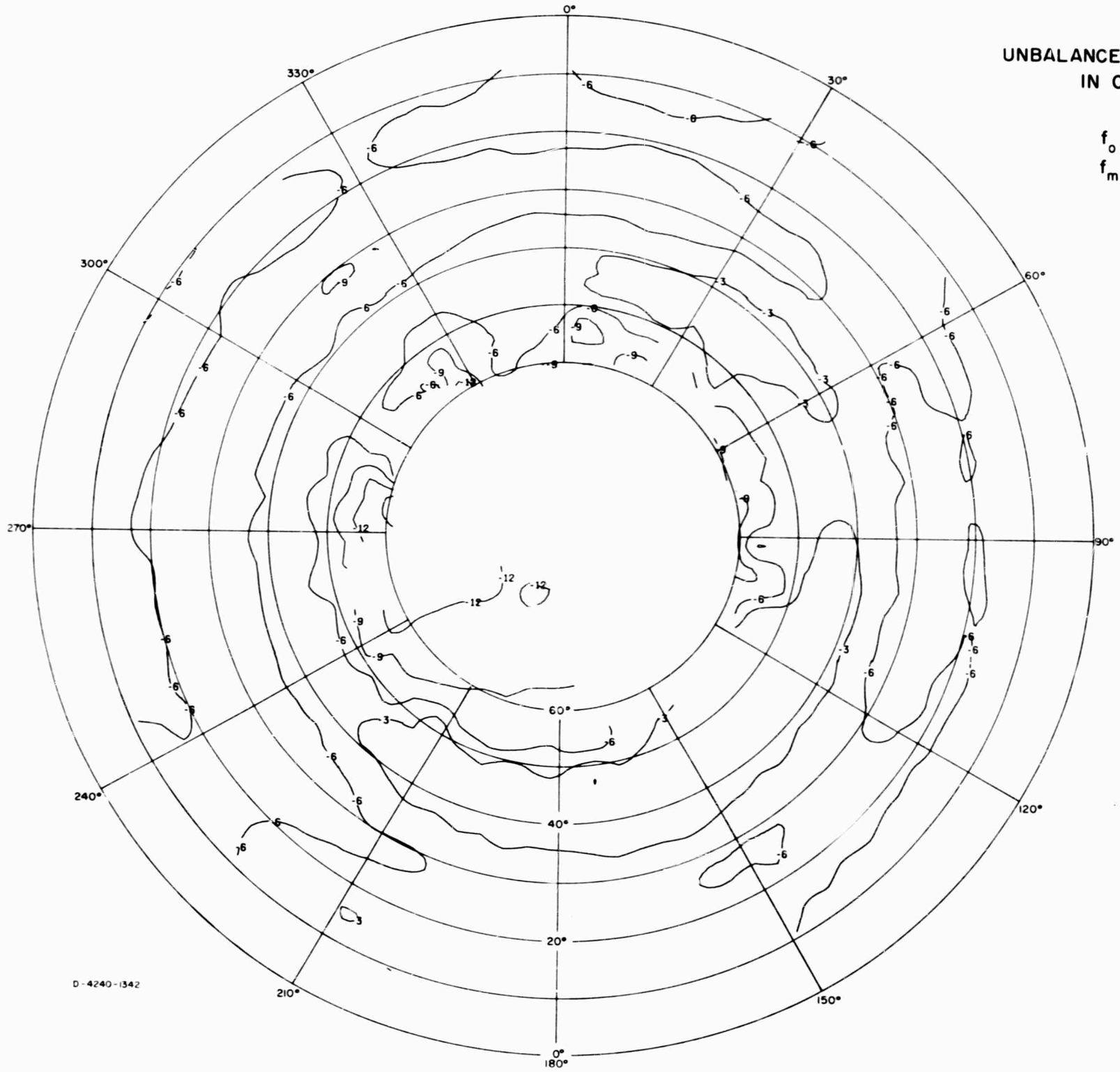

UNBALANCED DIPOLE
IN CLEARING
$h_a = 41'$
$f_o = 6$ Mc/s
$f_m = 3$ Mc/s
POWER

FIG. A-27

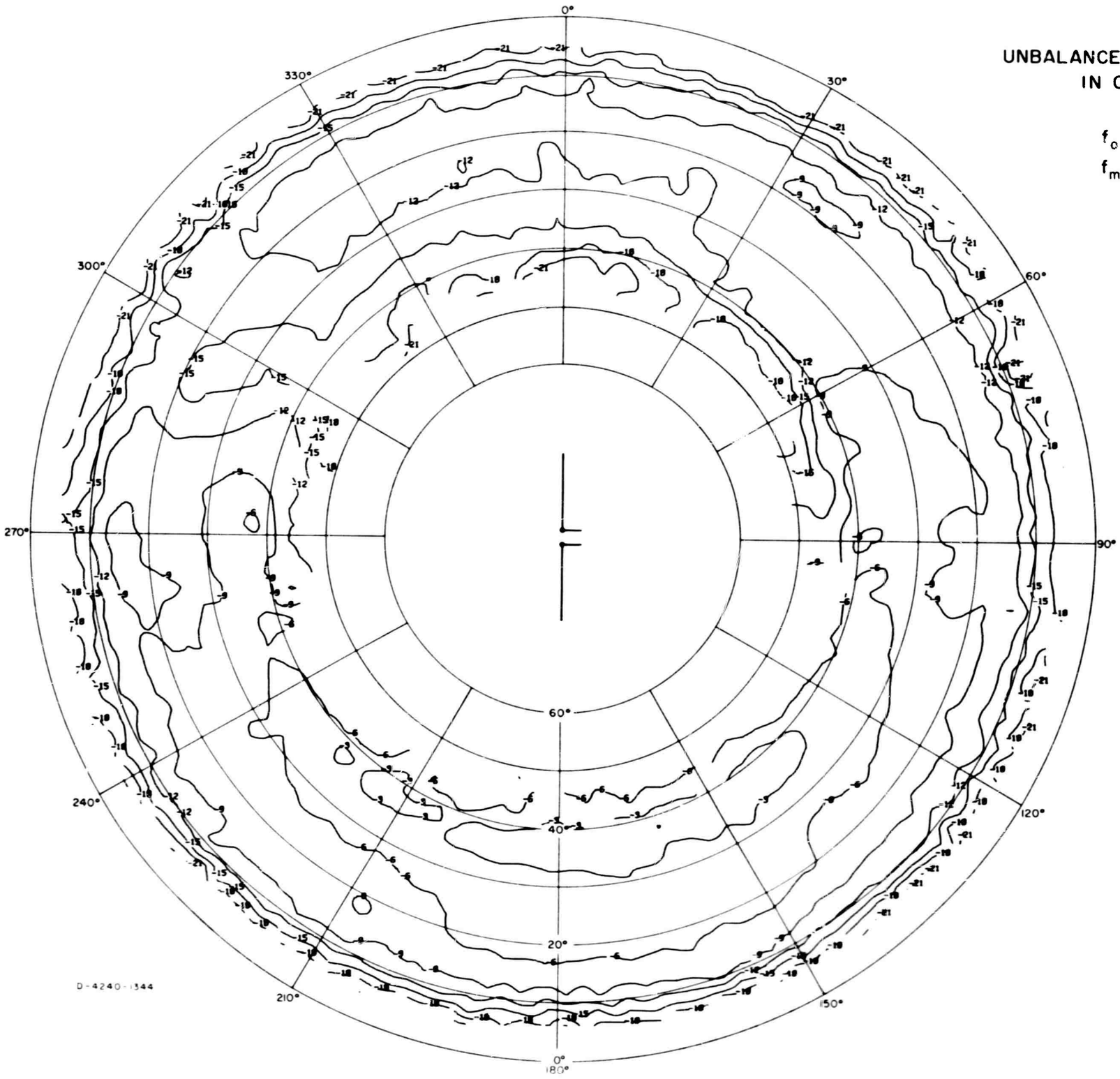

UNBALANCED DIPOLE
IN CLEARING
h_a = 41'
f_c = 6 Mc/s
f_m = 4 Mc/s
E_θ

D-4240-1344

FIG. A-28

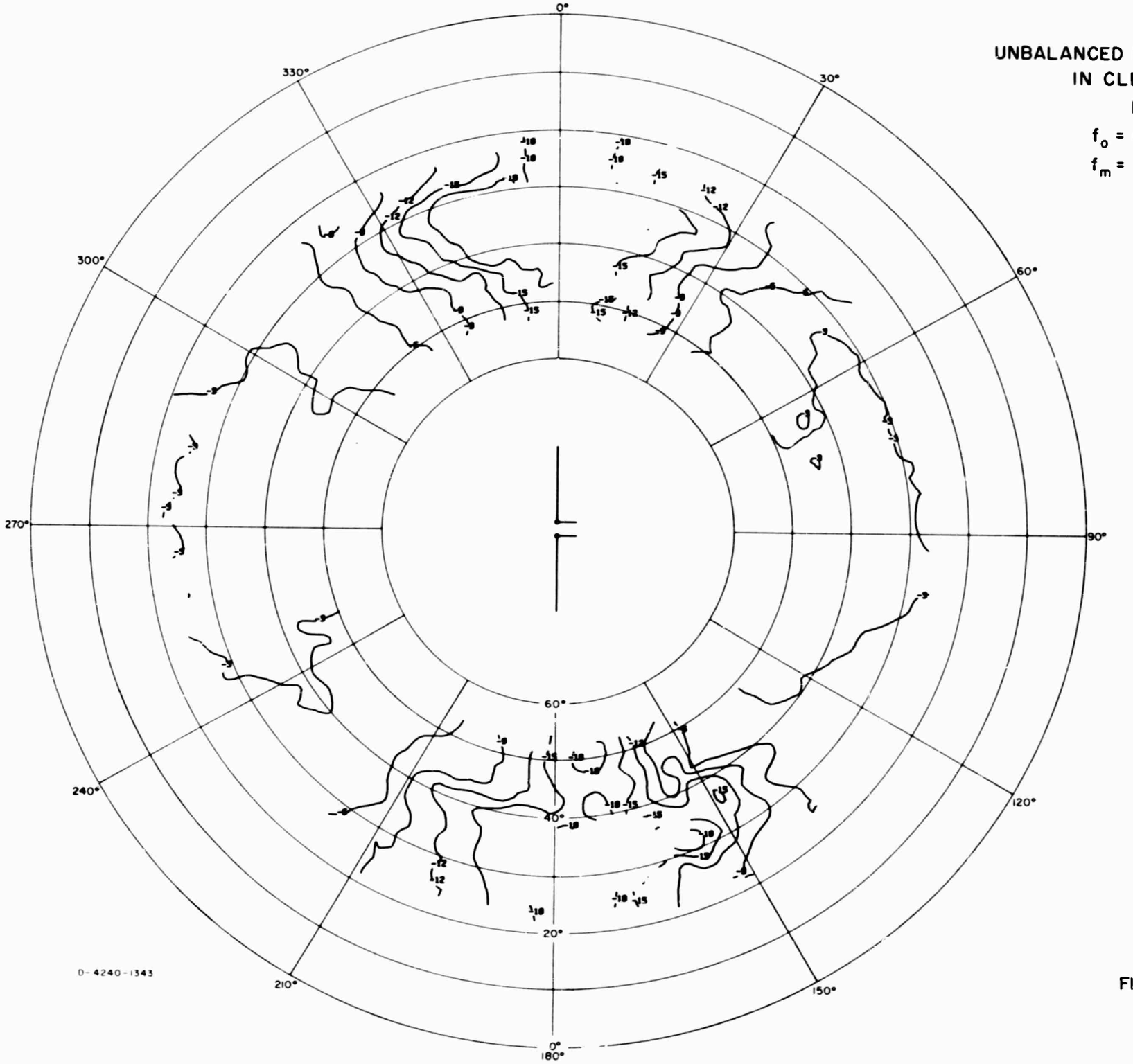

UNBALANCED DIPOLE
IN CLEARING
$h_a = 41'$
$f_o = 6$ Mc/s
$f_m = 4$ Mc/s
E_ϕ

FIG. A-29

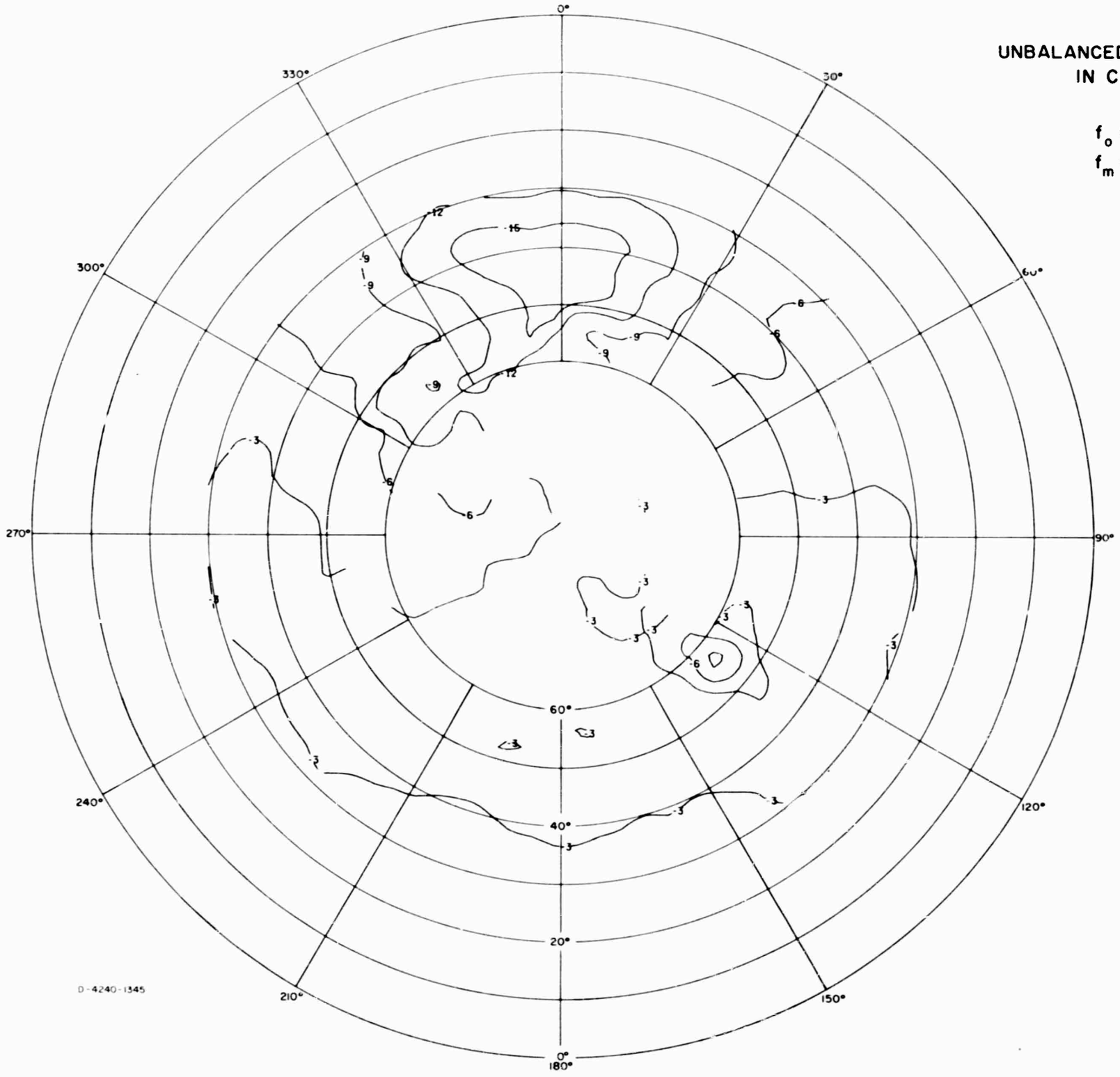

UNBALANCED DIPOLE
IN CLEARING
h_a = 41'
f_o = 6 Mc/s
f_m = 4 Mc/s
POWER

FIG. A-30

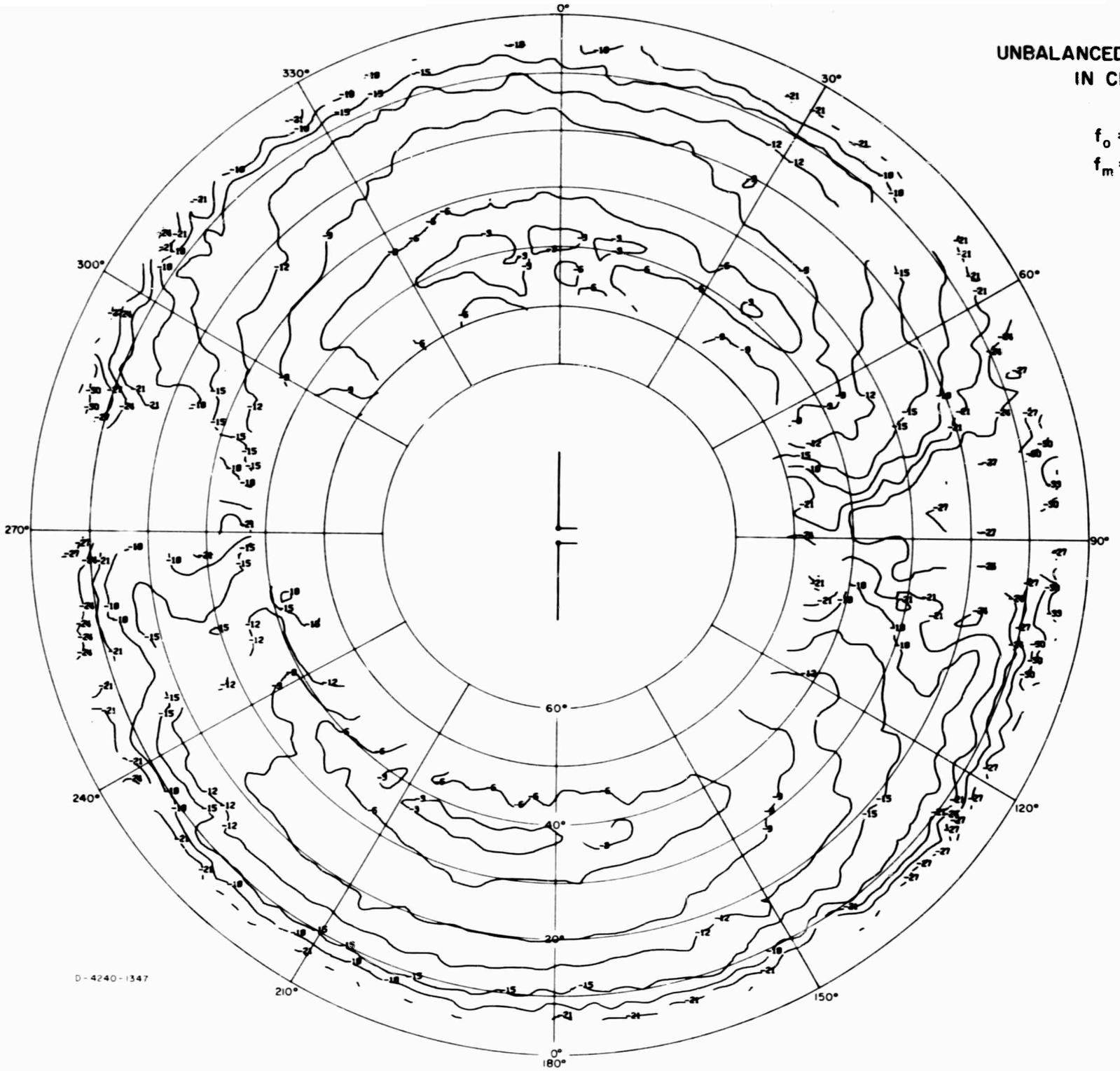

UNBALANCED DIPOLE
IN CLEARING
$h_a = 41'$
$f_o = 6$ Mc/s
$f_m = 6$ Mc/s
E_θ

FIG. A-31

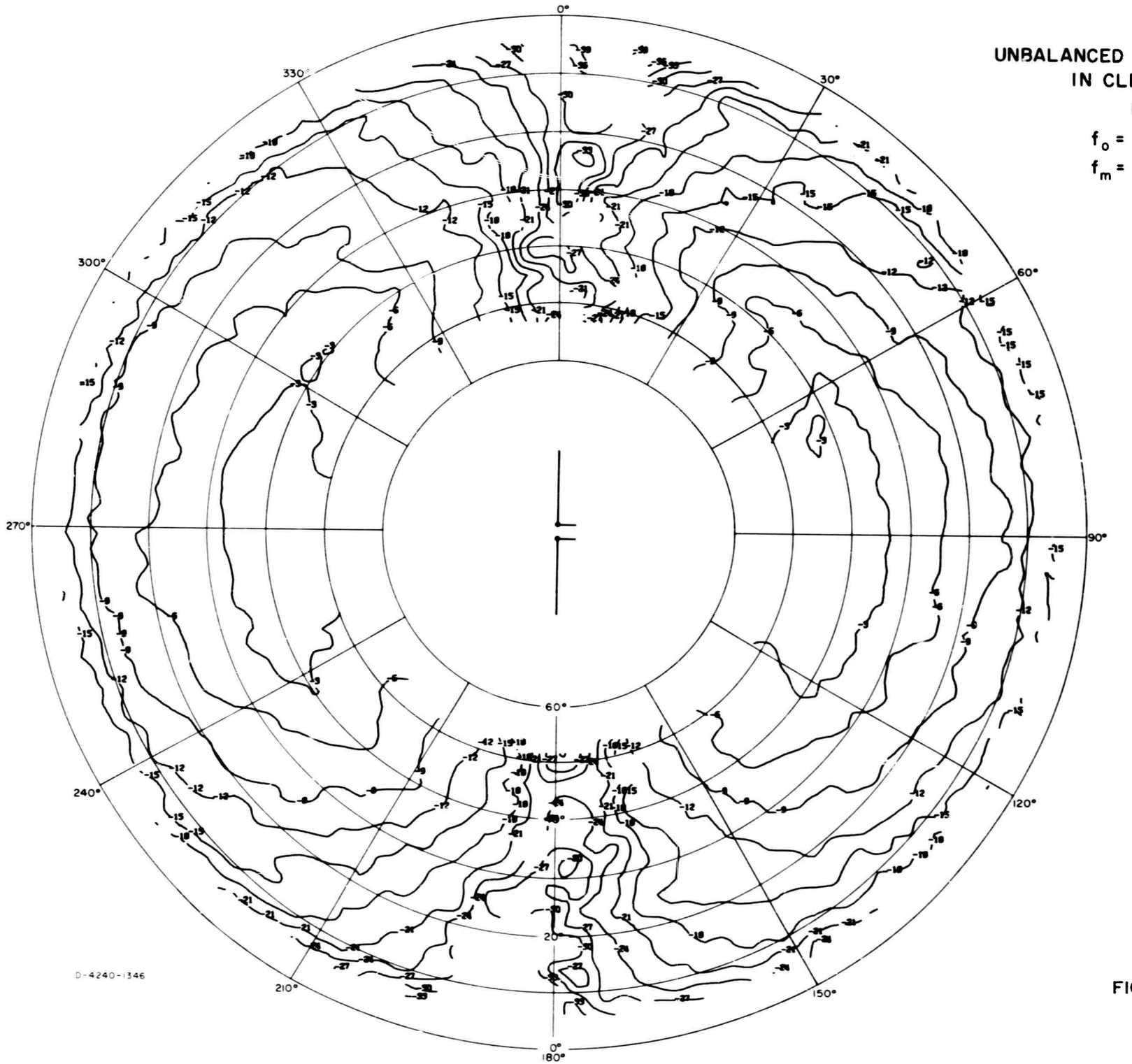

UNBALANCED DIPOLE
IN CLEARING
$h_a = 41'$
$f_o = 6$ Mc/s
$f_m = 6$ Mc/s
E_ϕ

FIG. A-32

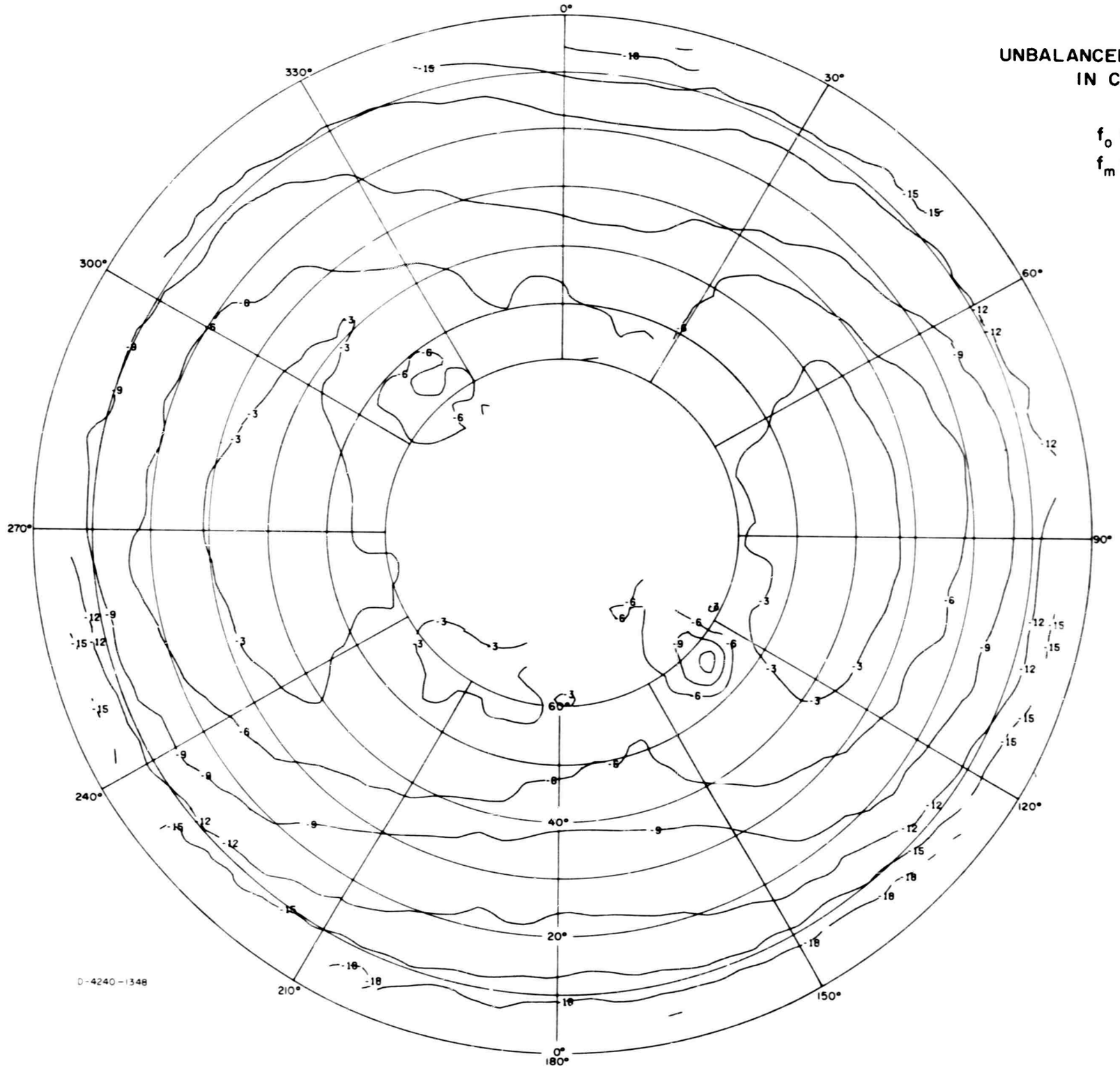

UNBALANCED DIPOLE
IN CLEARING
$h_a = 41'$
$f_o = 6$ Mc/s
$f_m = 6$ Mc/s
POWER

FIG. A-33

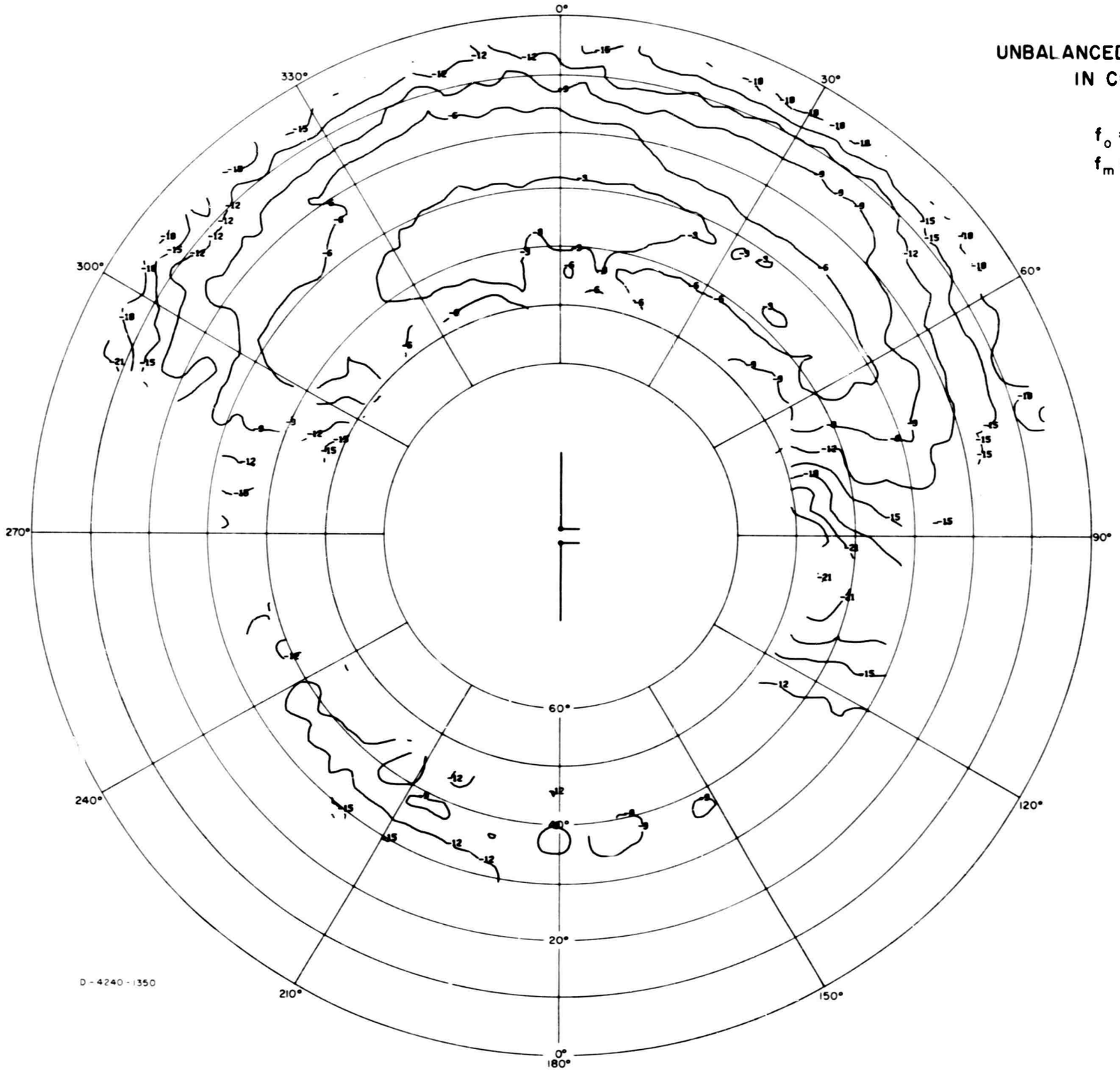

UNBALANCED DIPOLE
IN CLEARING
h_a = 41'
f_o = 6 Mc/s
f_m = 8 Mc/s
E_θ

FIG. A-34

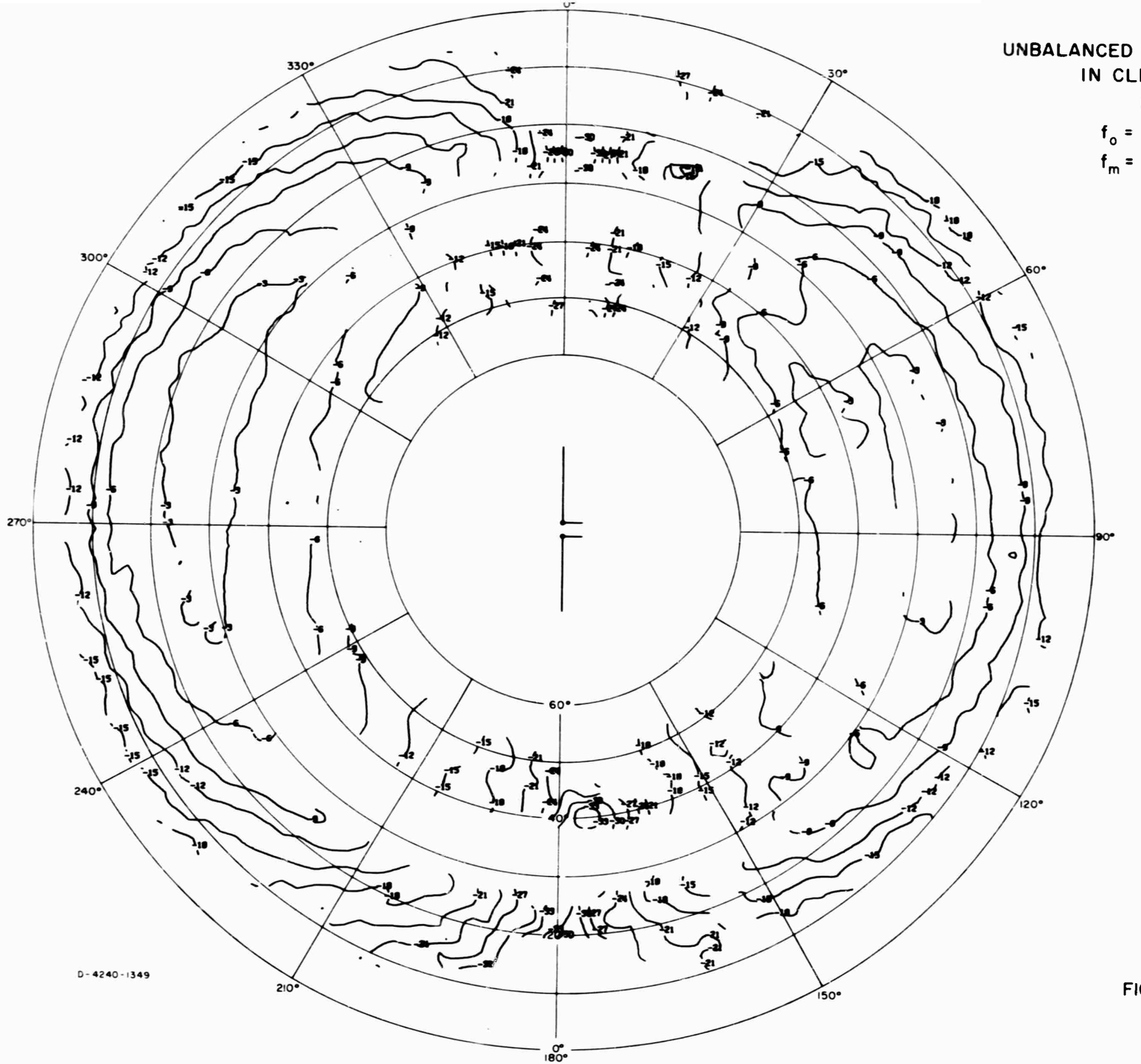

UNBALANCED DIPOLE
IN CLEARING
$h_a = 41'$
$f_o = 6$ Mc/s
$f_m = 8$ Mc/s
E_ϕ

FIG. A-35

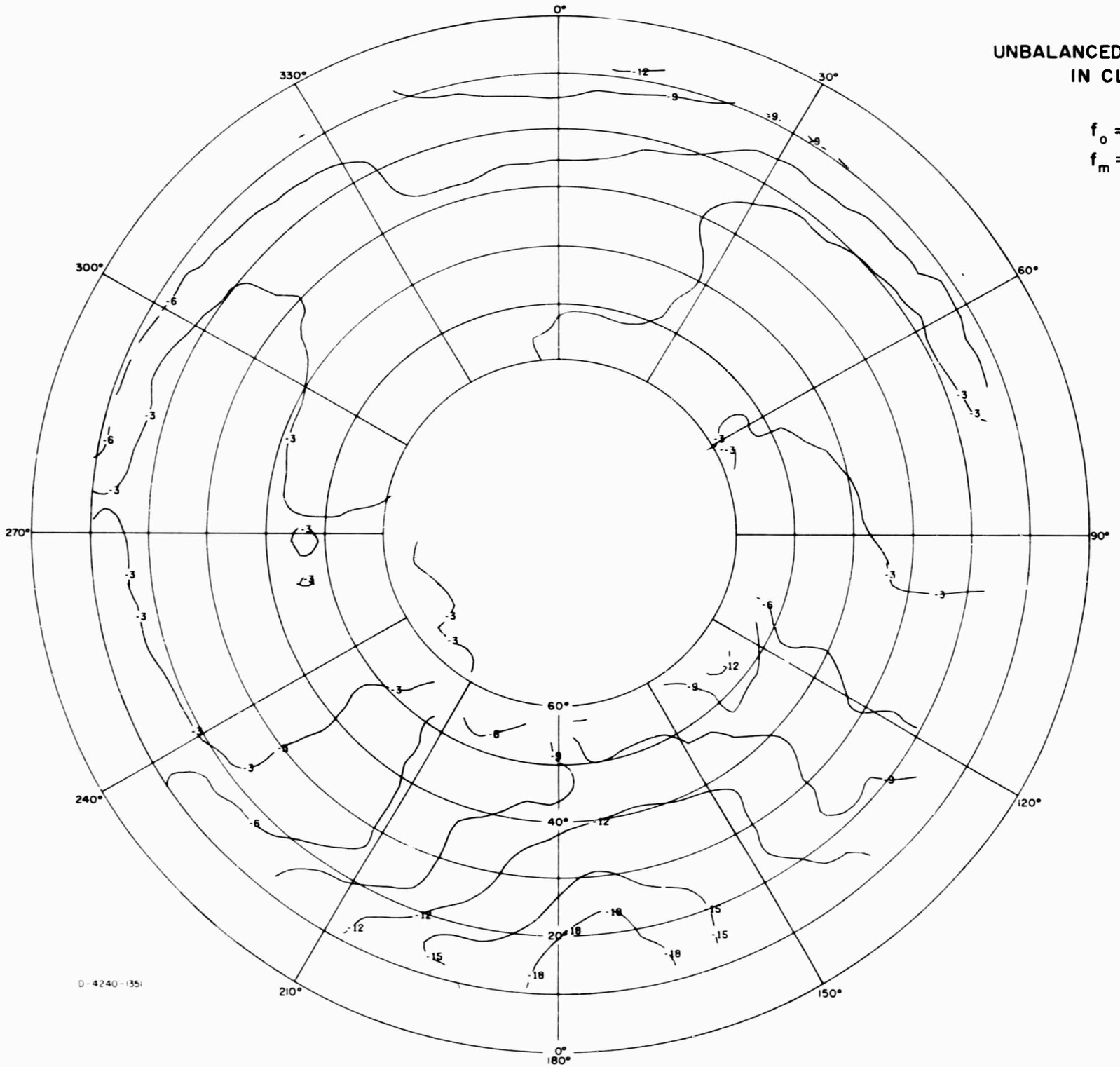

UNBALANCED DIPOLE
IN CLEARING
$h_a = 41'$
$f_o = 6$ Mc/s
$f_m = 8$ Mc/s
POWER

FIG. A-36

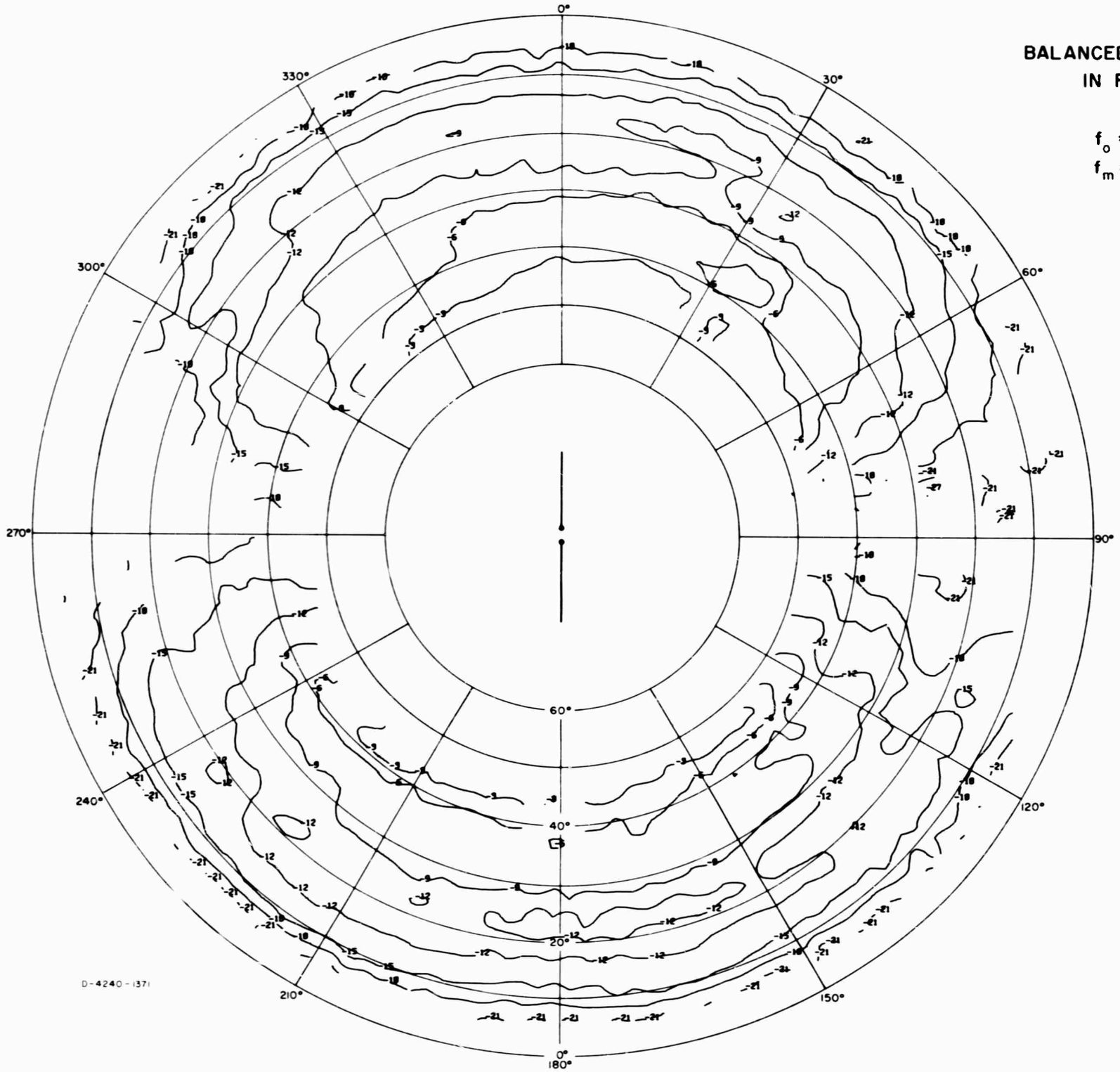

BALANCED DIPOLE
IN FOLIAGE
$h_a = 41'$
$f_o = 6$ Mc/s
$f_m = 6$ Mc/s
$E\theta$

FIG. A-37

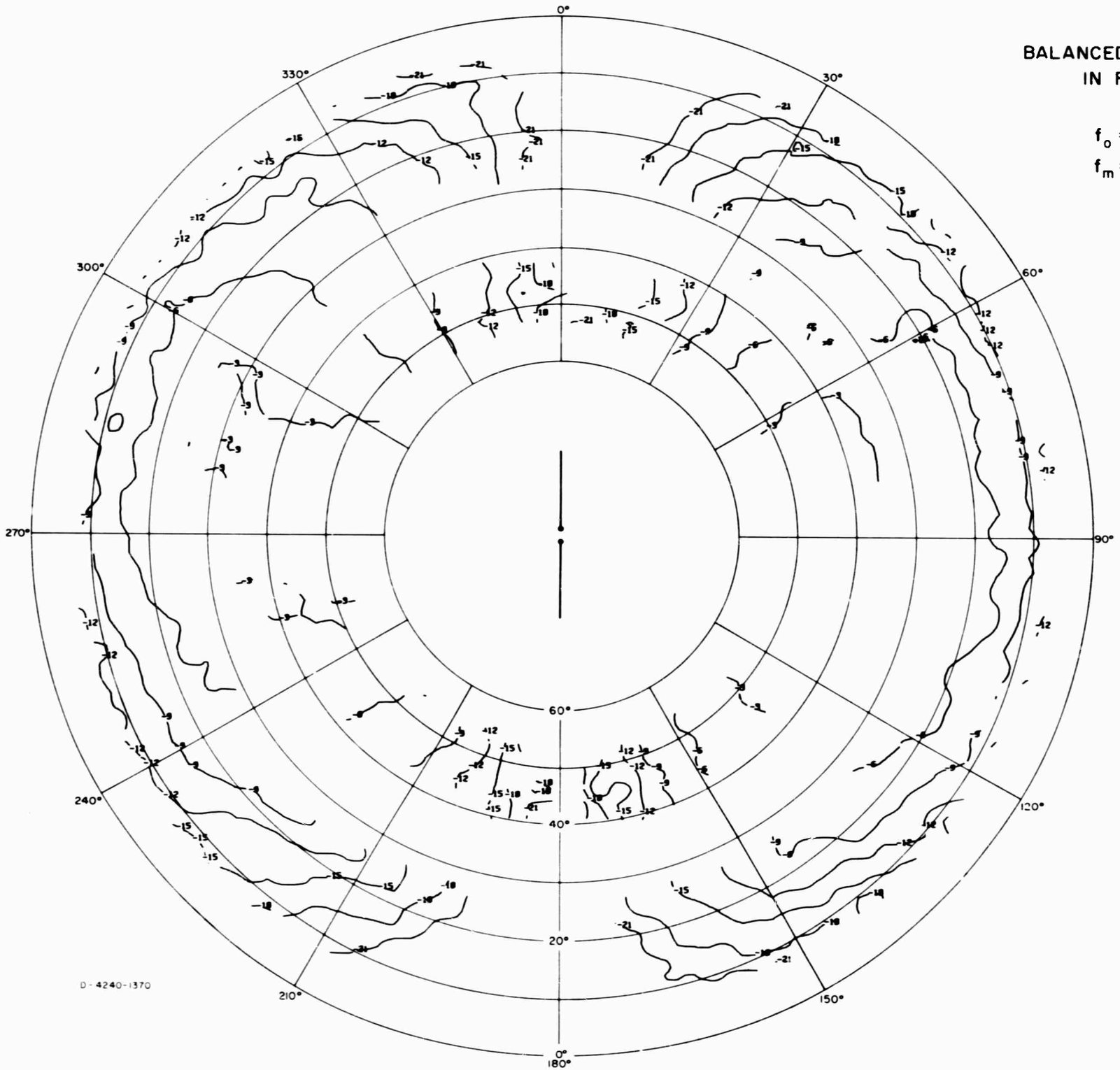

BALANCED DIPOLE
IN FOLIAGE
$h_a = 41'$
$f_o = 6$ Mc/s
$f_m = 6$ Mc/s
E_ϕ

FIG. A-38

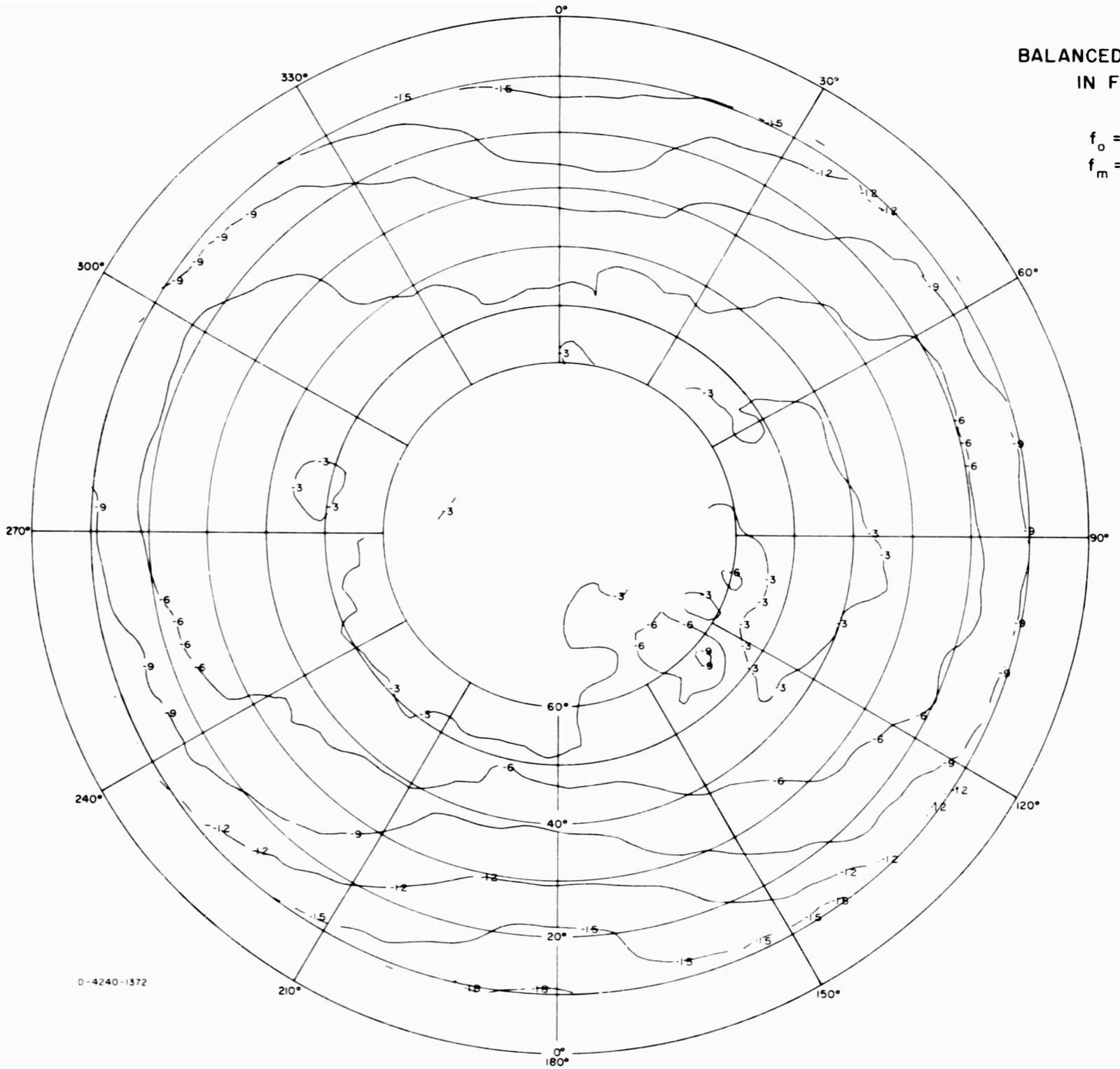

BALANCED DIPOLE
IN FOLIAGE
$h_a = 41'$
$f_o = 6$ Mc/s
$f_m = 6$ Mc/s
POWER

FIG. A-39

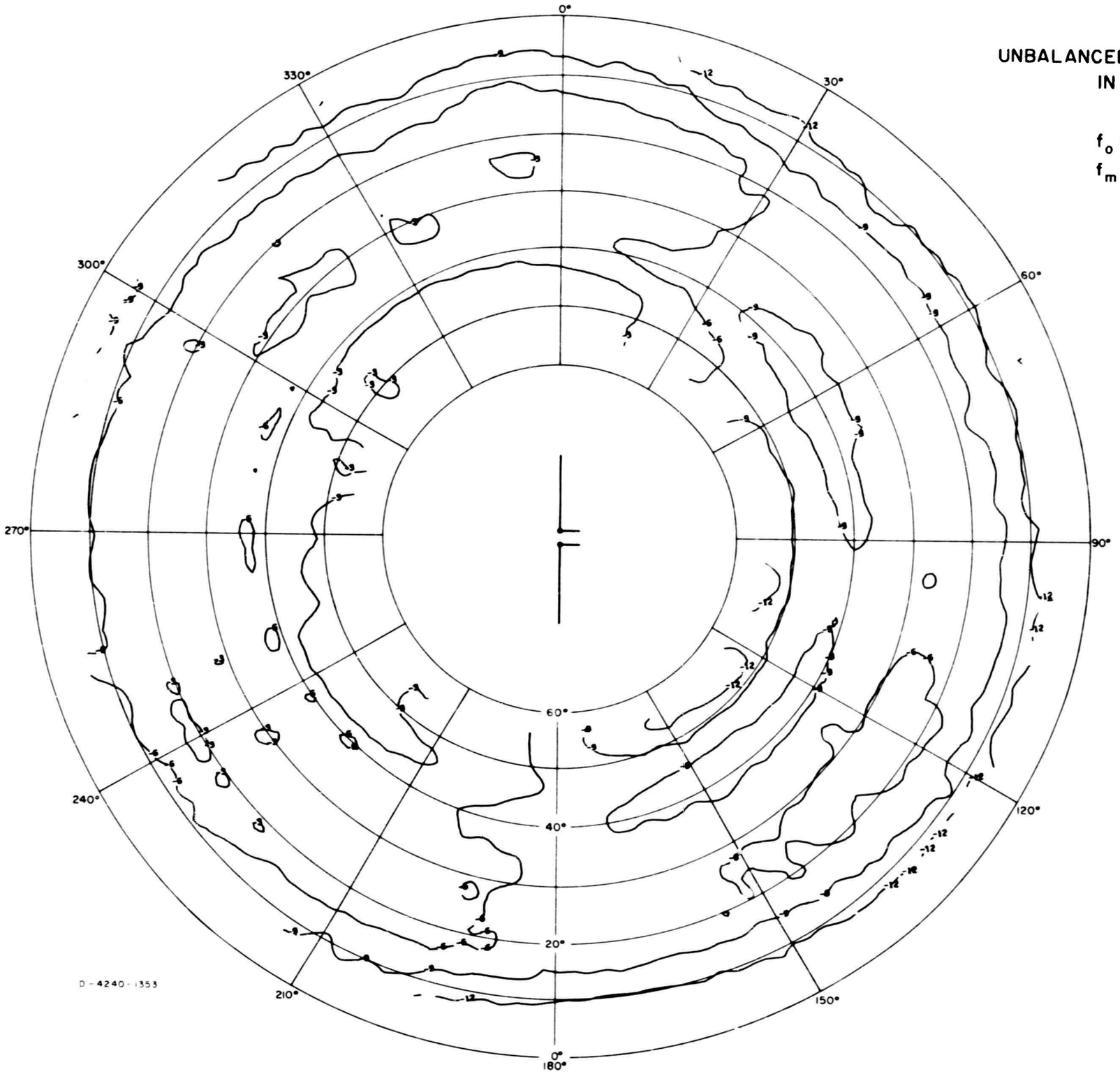

UNBALANCED DIPOLE
IN FOLIAGE
$h_a = 41'$
$f_o = 6$ Mc/s
f_m 3 Mc/s
E_θ

FIG. A-40

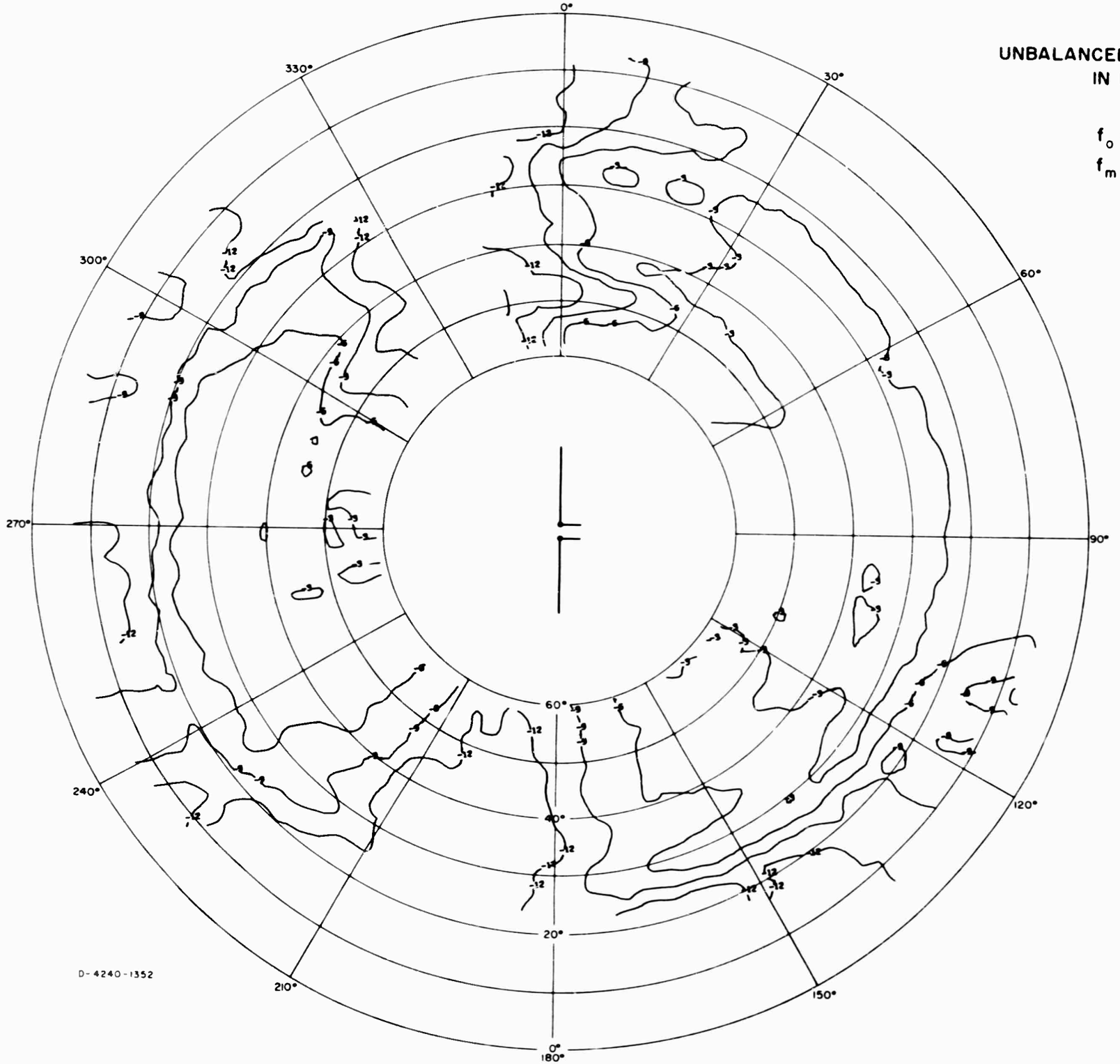

UNBALANCED DIPOLE
IN FOLIAGE
$h_a = 41'$
$f_o = 6$ Mc/s
$f_m = 3$ Mc/s
E_ϕ

D-4240-1352

FIG. A-41

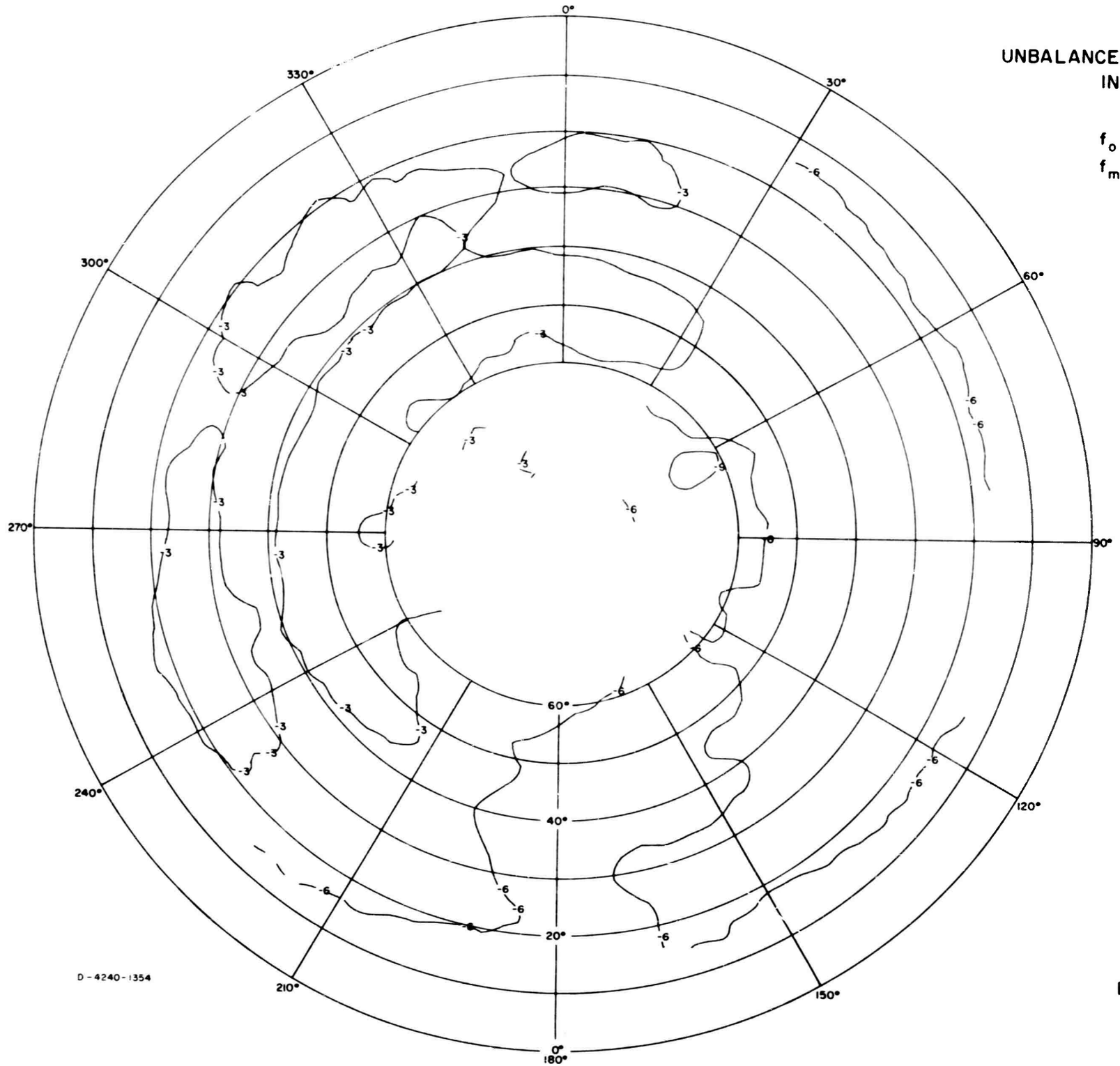

UNBALANCED DIPOLE
IN FOLIAGE
$h_a = 41'$
$f_o = 6$ Mc/s
$f_m = 3$ Mc/s
POWER

FIG. A-42

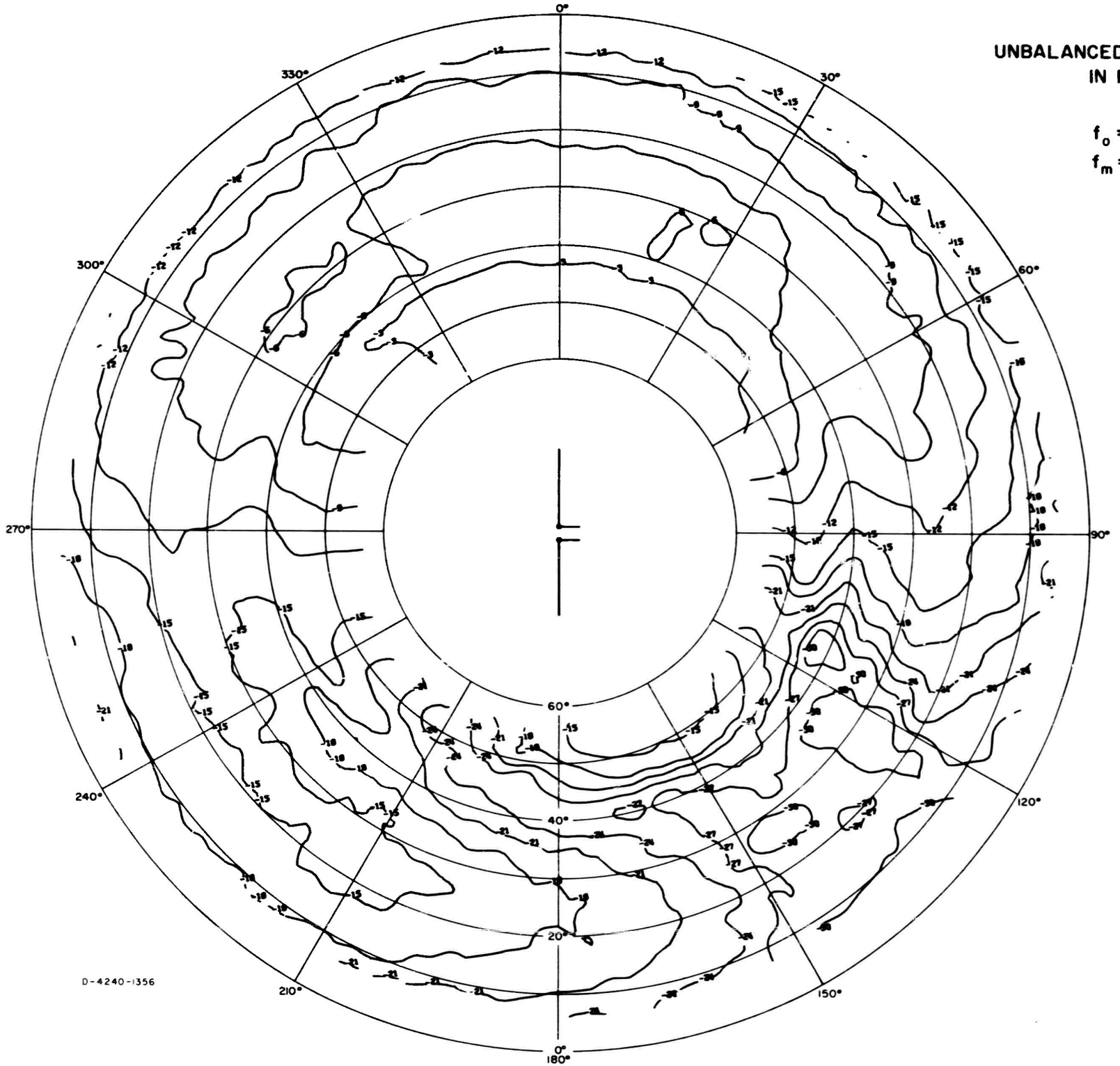

UNBALANCED DIPOLE
IN FOLIAGE
$h_a = 41'$
$f_o = 6$ Mc/s
$f_m = 4$ Mc/s
E_θ

D-4240-1356

FIG. A-43

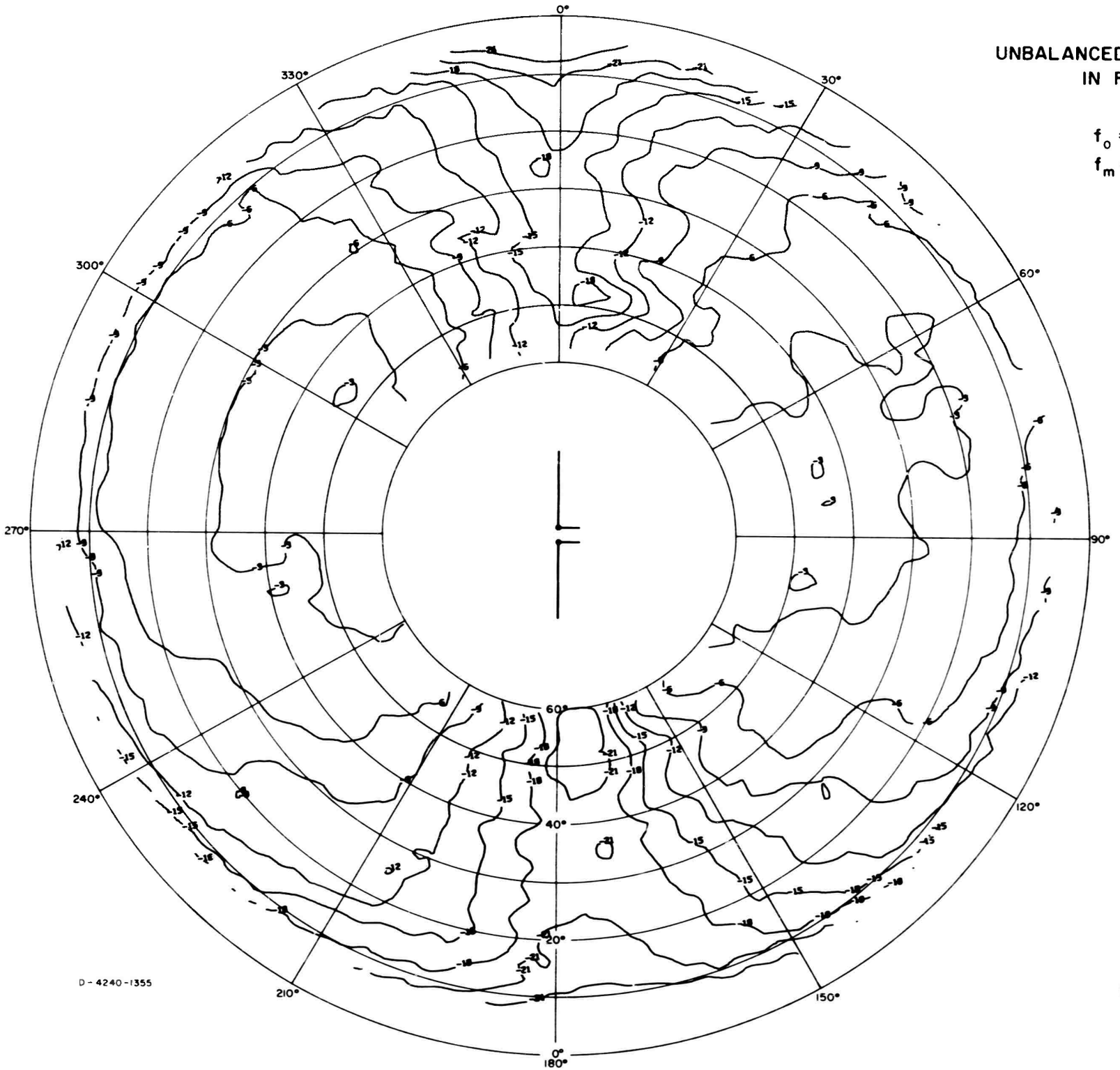

UNBALANCED DIPOLE
IN FOLIAGE
$h_a = 41'$
$f_o = 6$ Mc/s
$f_m = 4$ Mc/s
E_ϕ

D-4240-1355

FIG. A-44

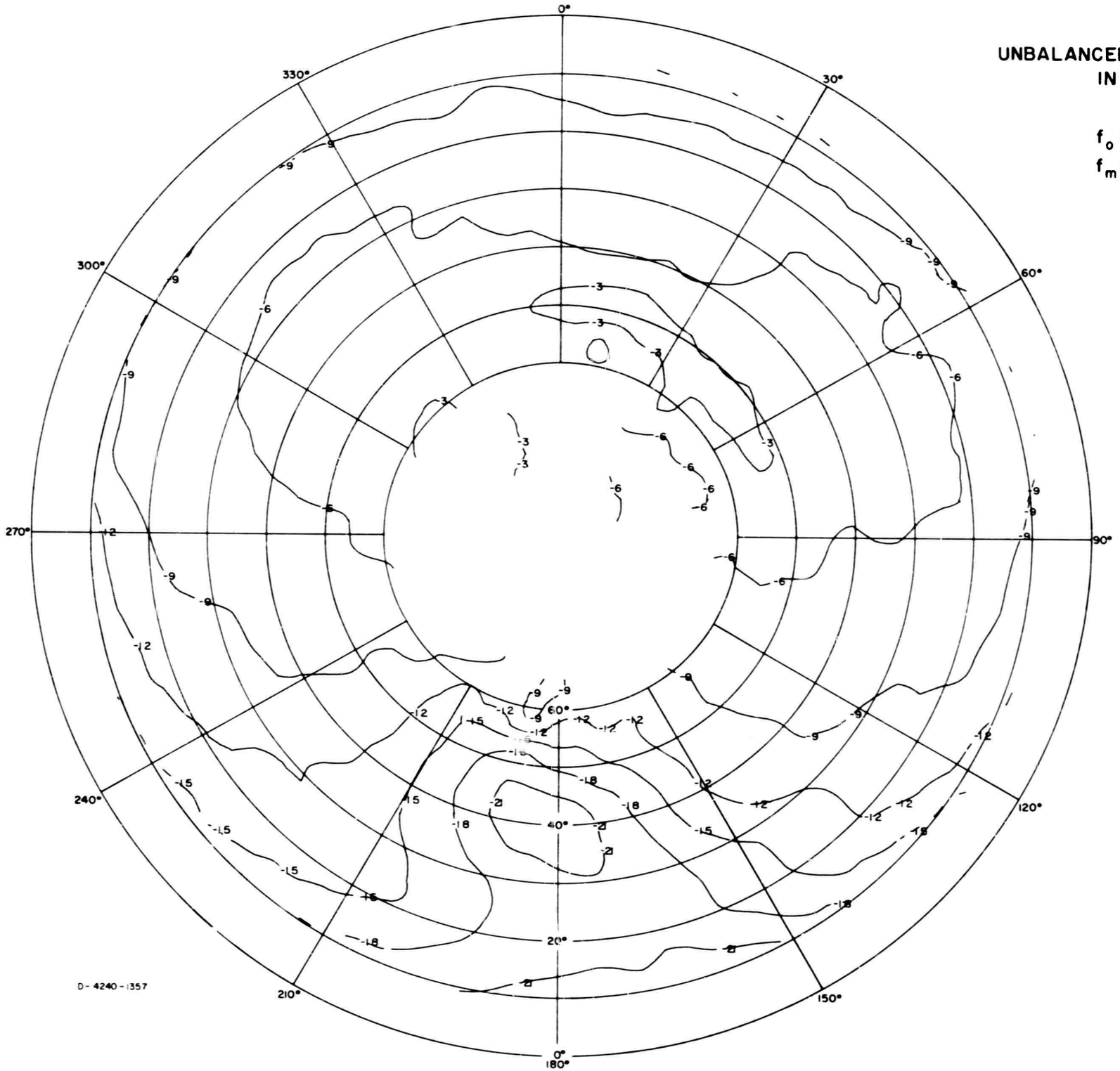

UNBALANCED DIPOLE
IN FOLIAGE
$h_a = 41'$
$f_o = 6$ Mc/s
$f_m = 4$ Mc/s
POWER

FIG. A-45

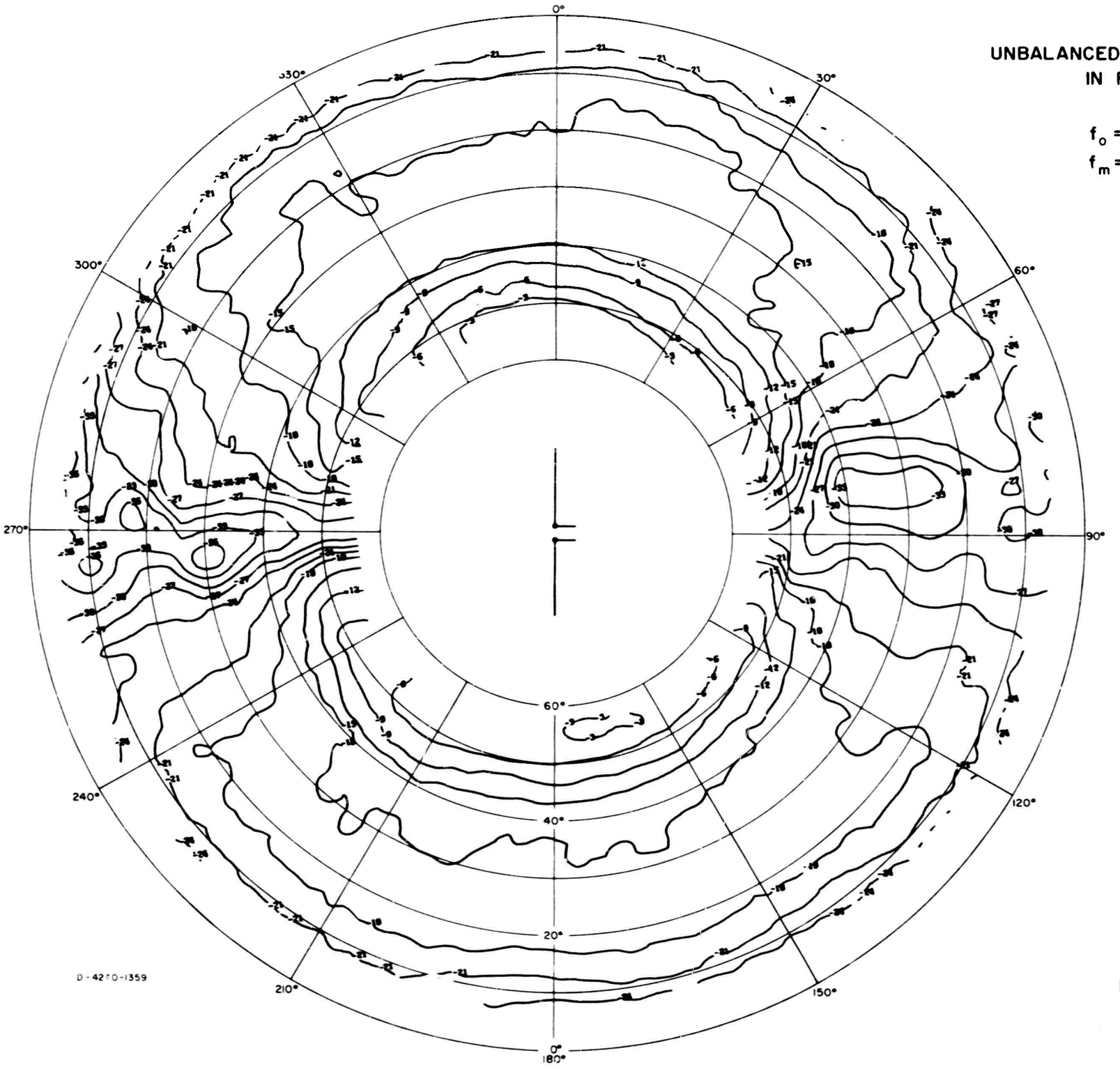

UNBALANCED DIPOLE
IN FOLIAGE
$h_a = 41'$
$f_o = 6$ Mc/s
$f_m = 6$ Mc/s
E_θ

FIG. A-46

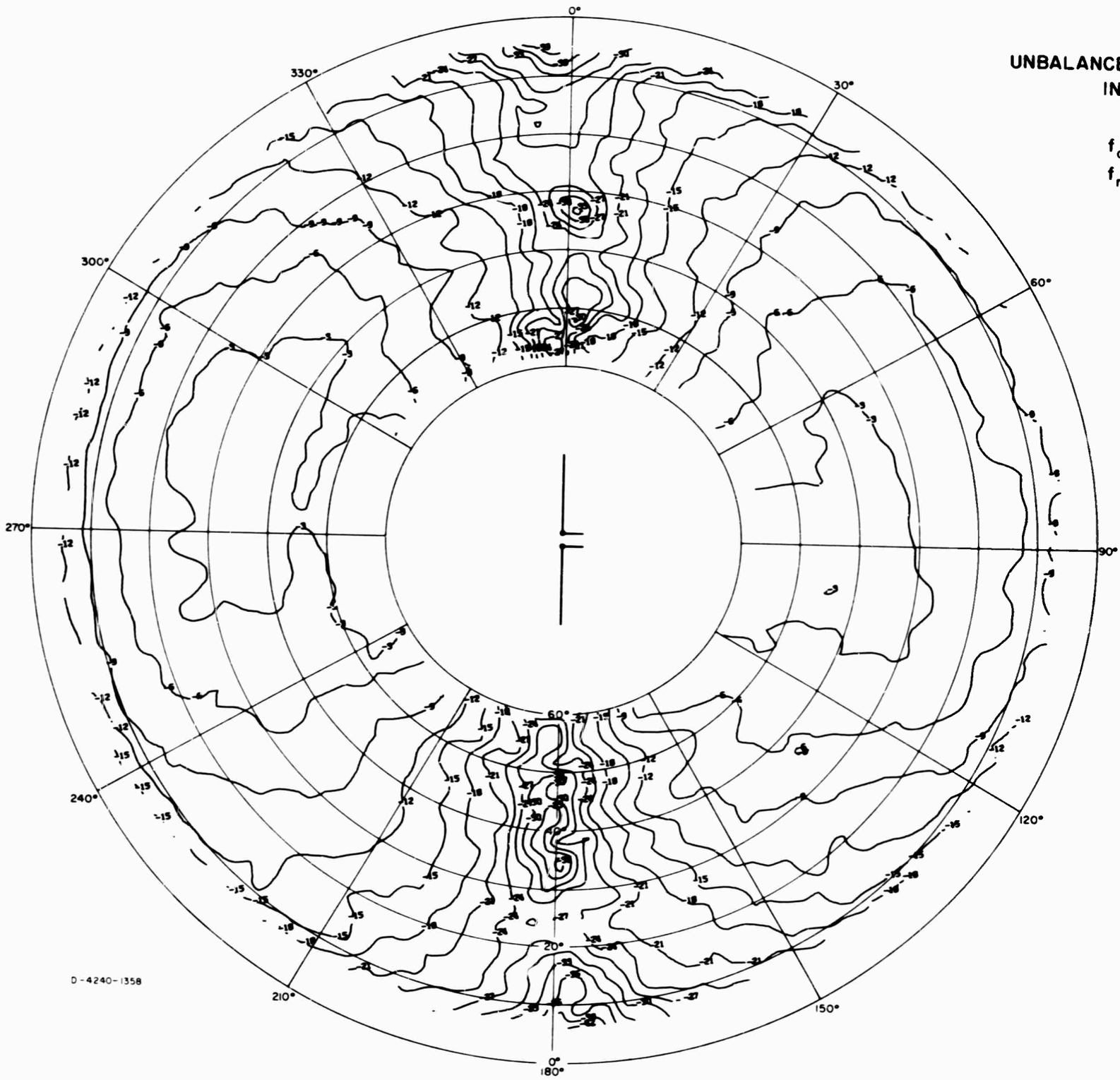

UNBALANCED DIPOLE
IN FOLIAGE
$h_a = 41'$
$f_o = 6$ Mc/s
$f_m = 6$ Mc/s
E_ϕ

FIG. A-47

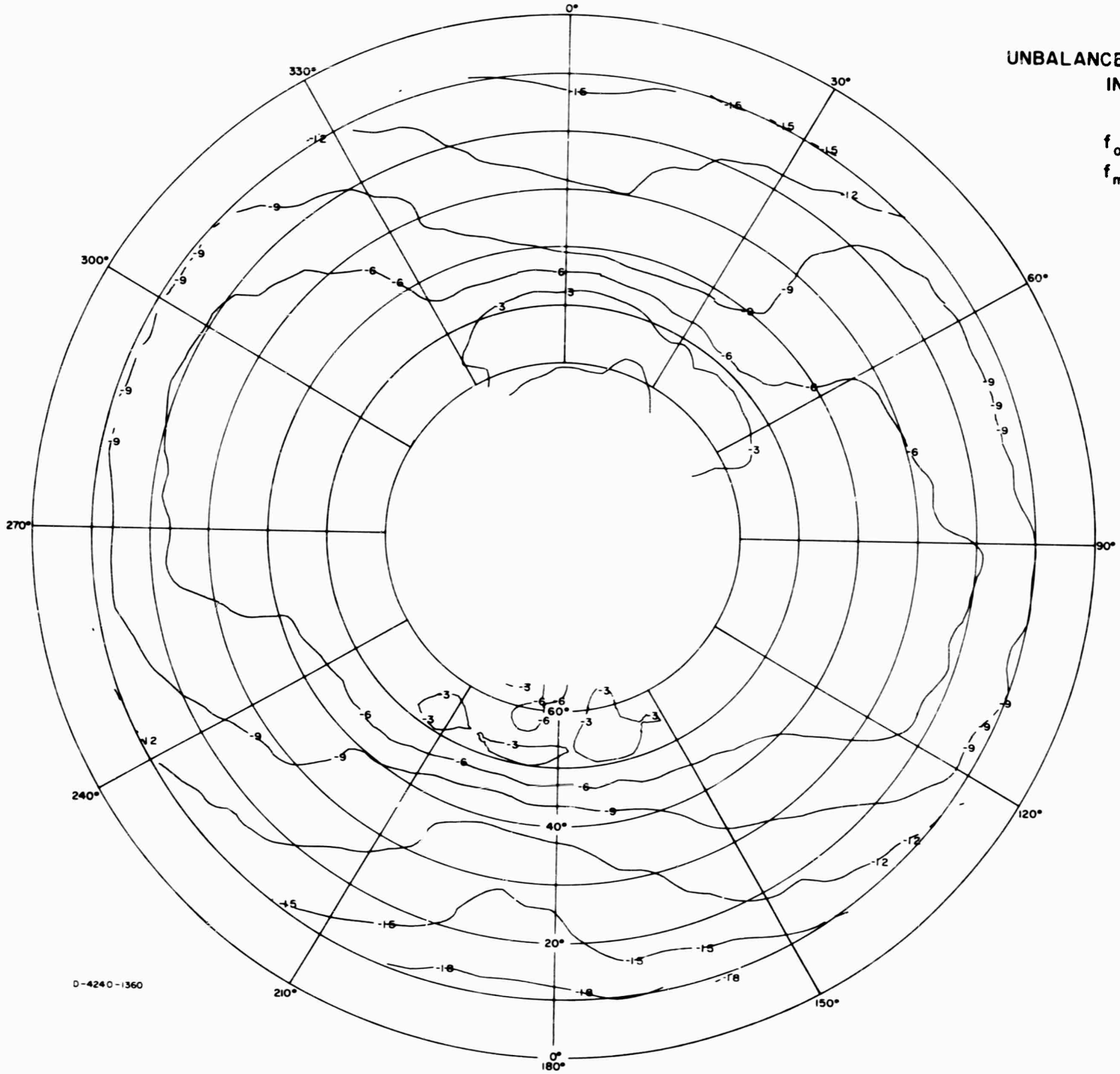

UNBALANCED DIPOLE
IN FOLIAGE
$h_a = 41'$
$f_o = 6$ Mc/s
$f_m = 6$ Mc/s
POWER

FIG. A-48

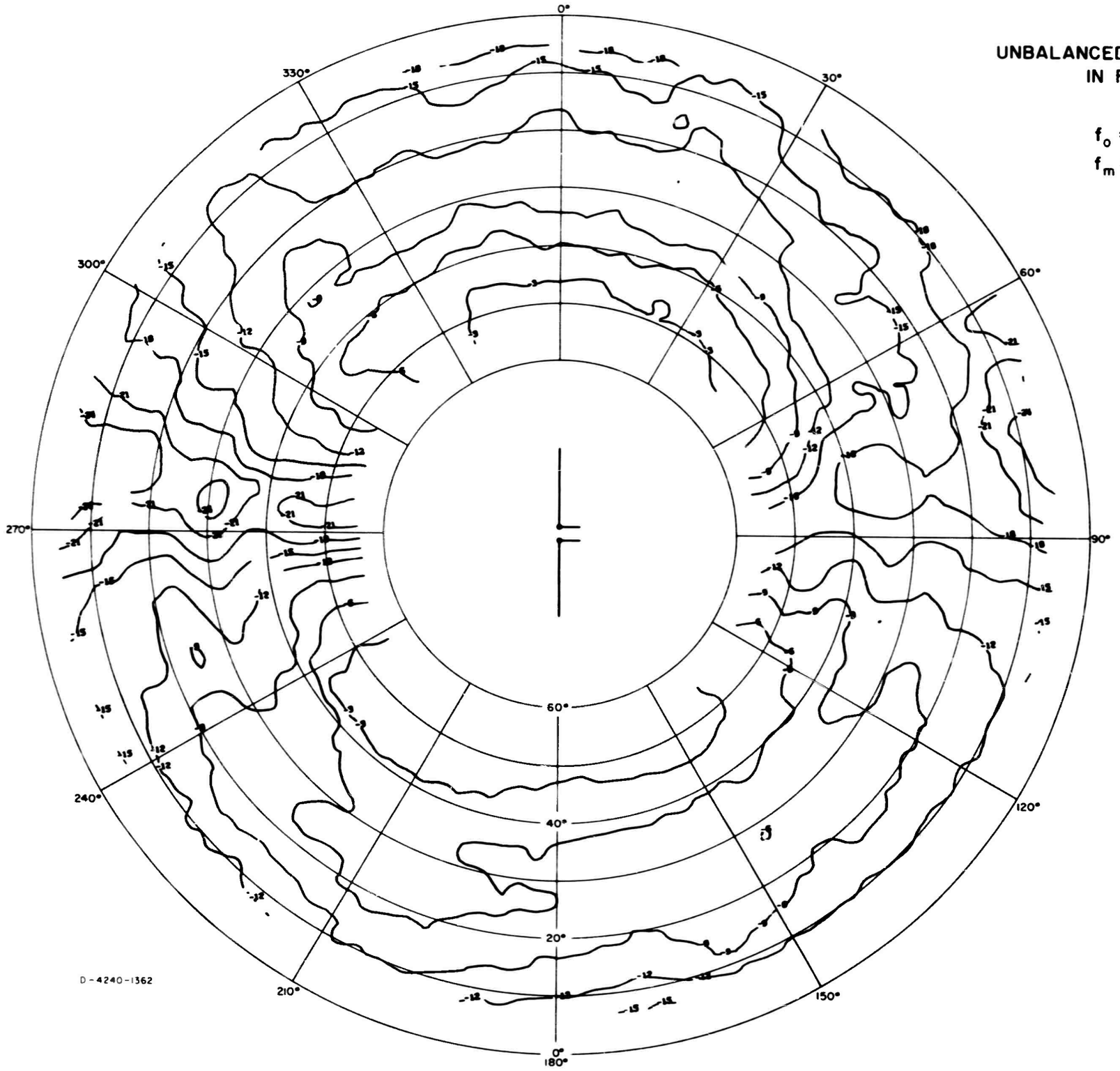

UNBALANCED DIPOLE
IN FOLIAGE
$h_a = 41'$
$f_o = 6$ Mc/s
$f_m = 8$ Mc/s
E_θ

FIG. A-49

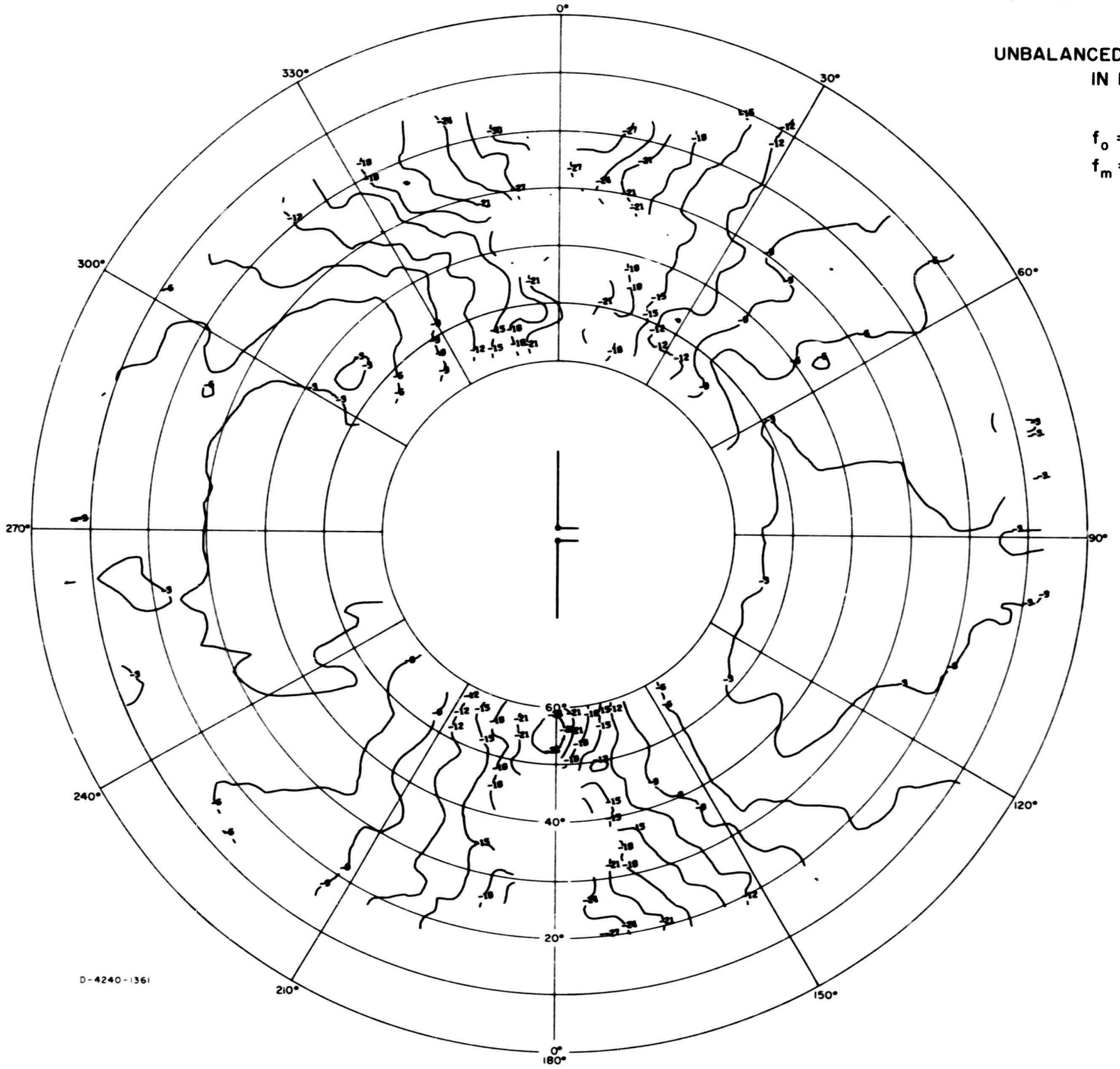

UNBALANCED DIPOLE
IN FOLIAGE
$h_a = 41'$
$f_o = 6$ Mc/s
$f_m = 8$ Mc/s
E_ϕ

FIG. A-50

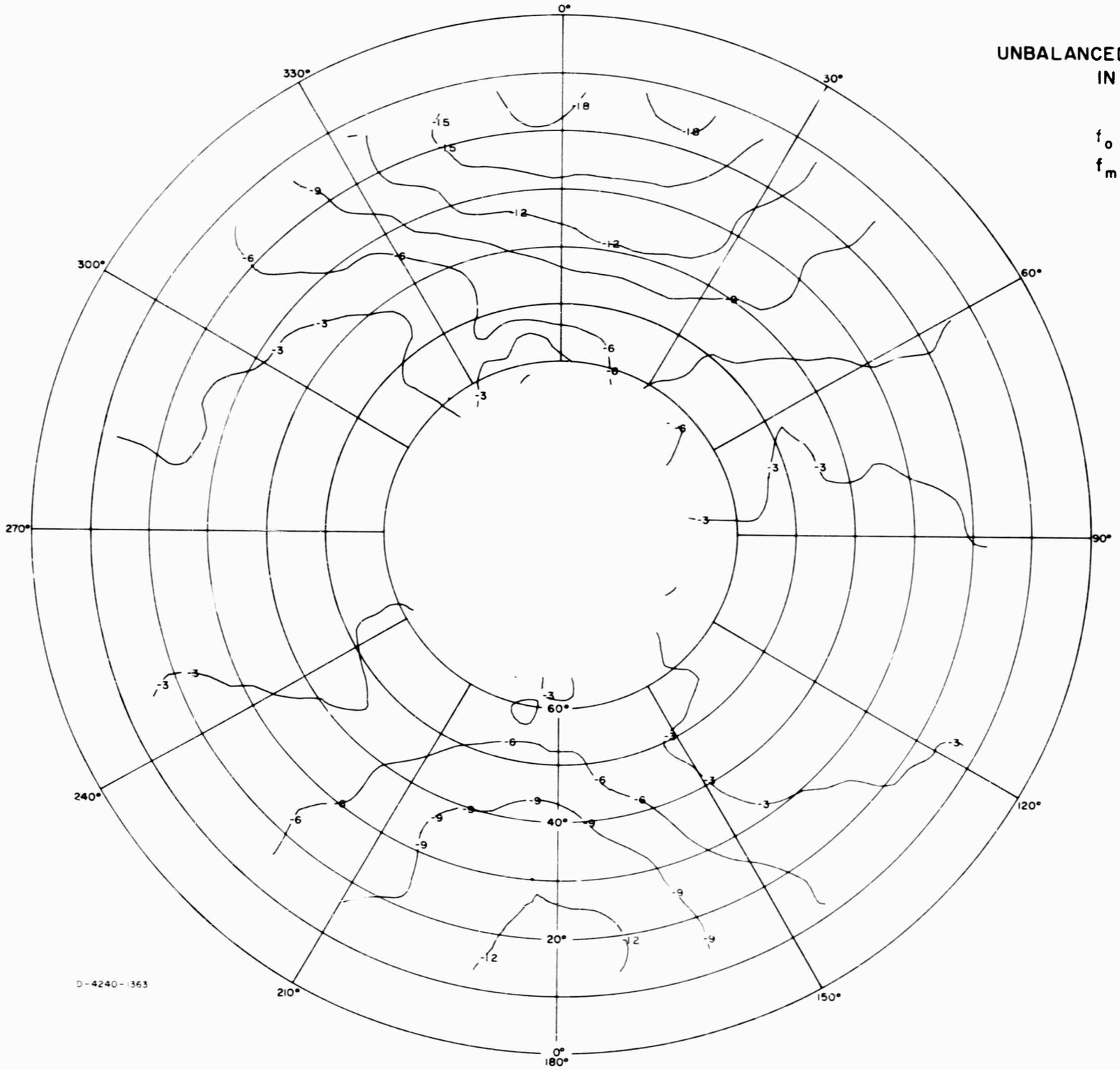

UNBALANCED DIPOLE
IN FOLIAGE
$h_a = 41'$
$f_o = 6$ Mc/s
$f_m = 8$ Mc/s
POWER

FIG. A-51

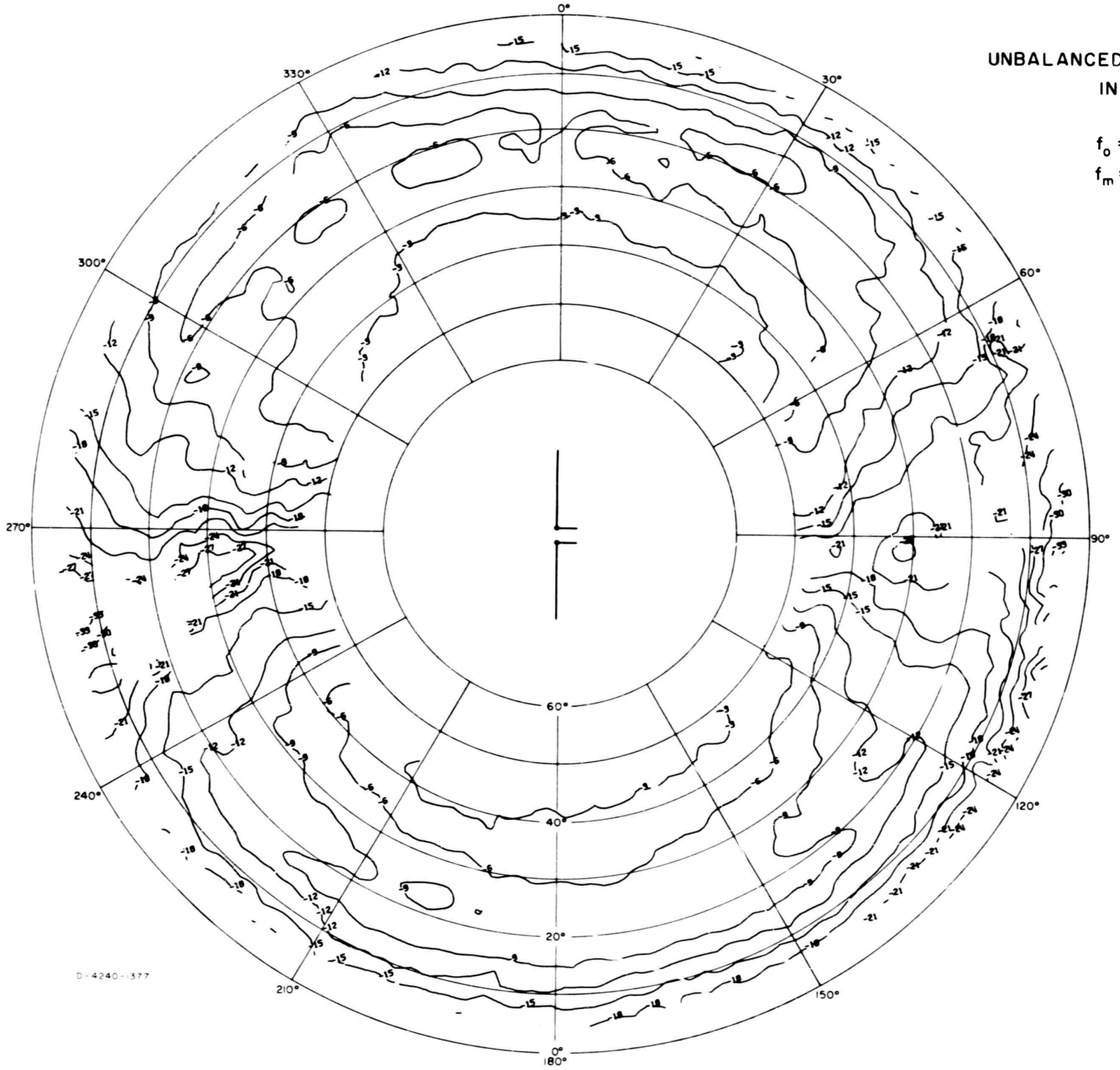

UNBALANCED DIPOLE
IN FOLIAGE
h_a = 16'
f_o = 6 Mc/s
f_m = 6 Mc/s
E_θ

FIG. A-52

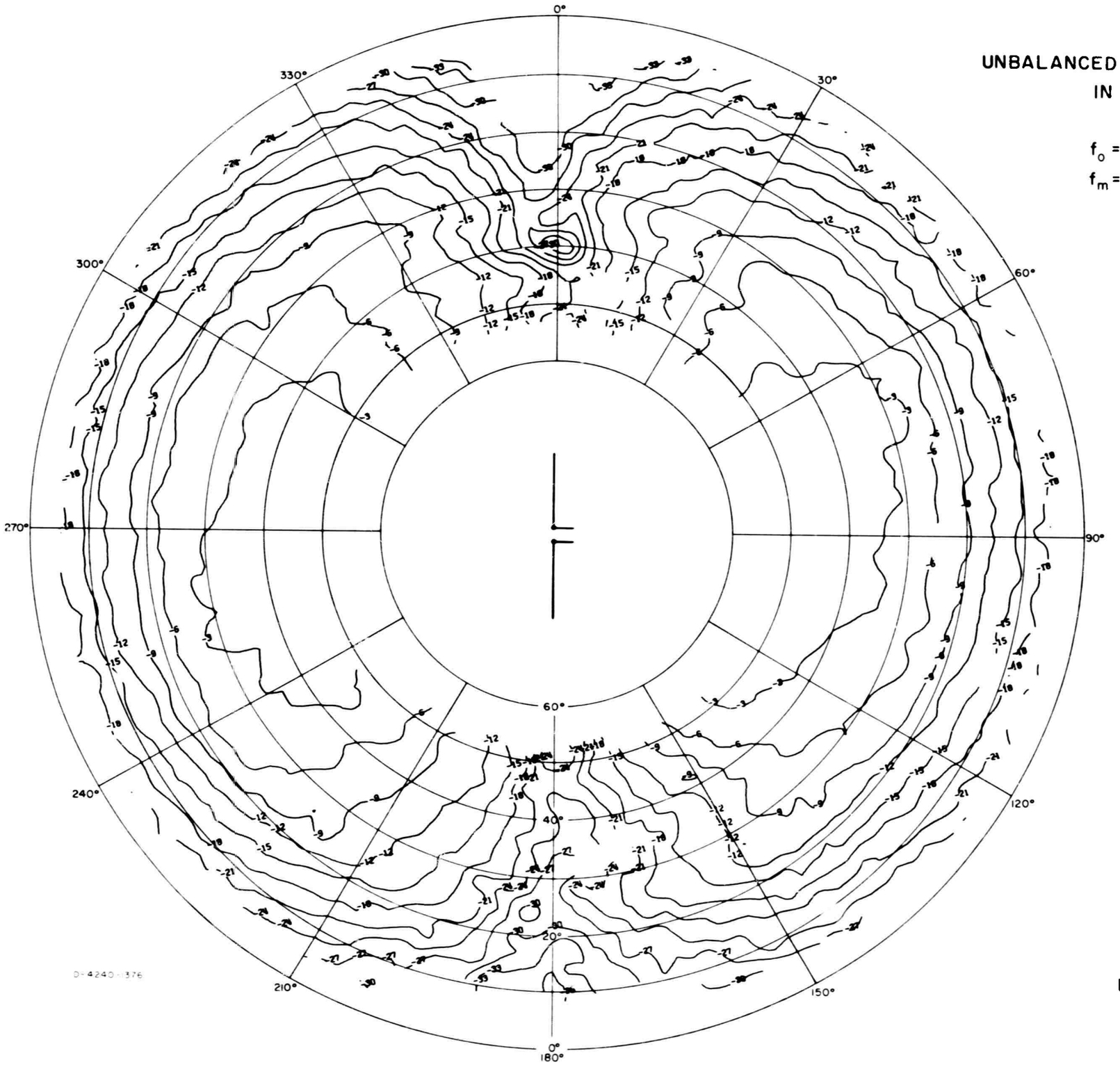

UNBALANCED DIPOLE
IN FOLIAGE
h_a = 16'
f_o = 6 Mc/s
f_m = 6 Mc/s
E_ϕ

FIG. A-53

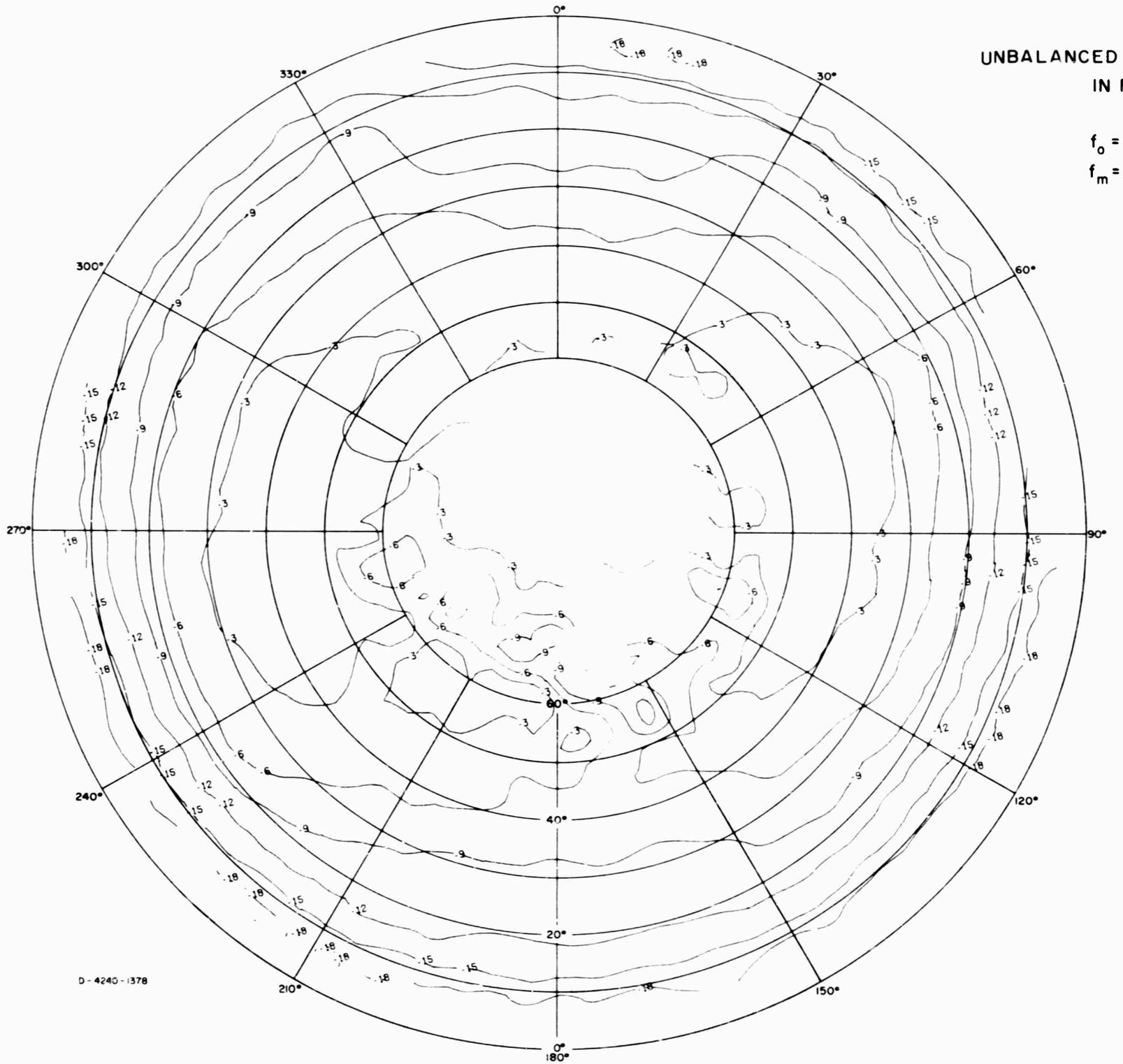
0°
30°
60°
90°
120°
150°
180°
210°
240°
270°
300°
330°
UNBALANCED DIPOLE
IN FOLIAGE
h_a = 16'
f_o = 6 Mc/s
f_m = 6 Mc/s
POWER
D-4240-1378

FIG. A-54

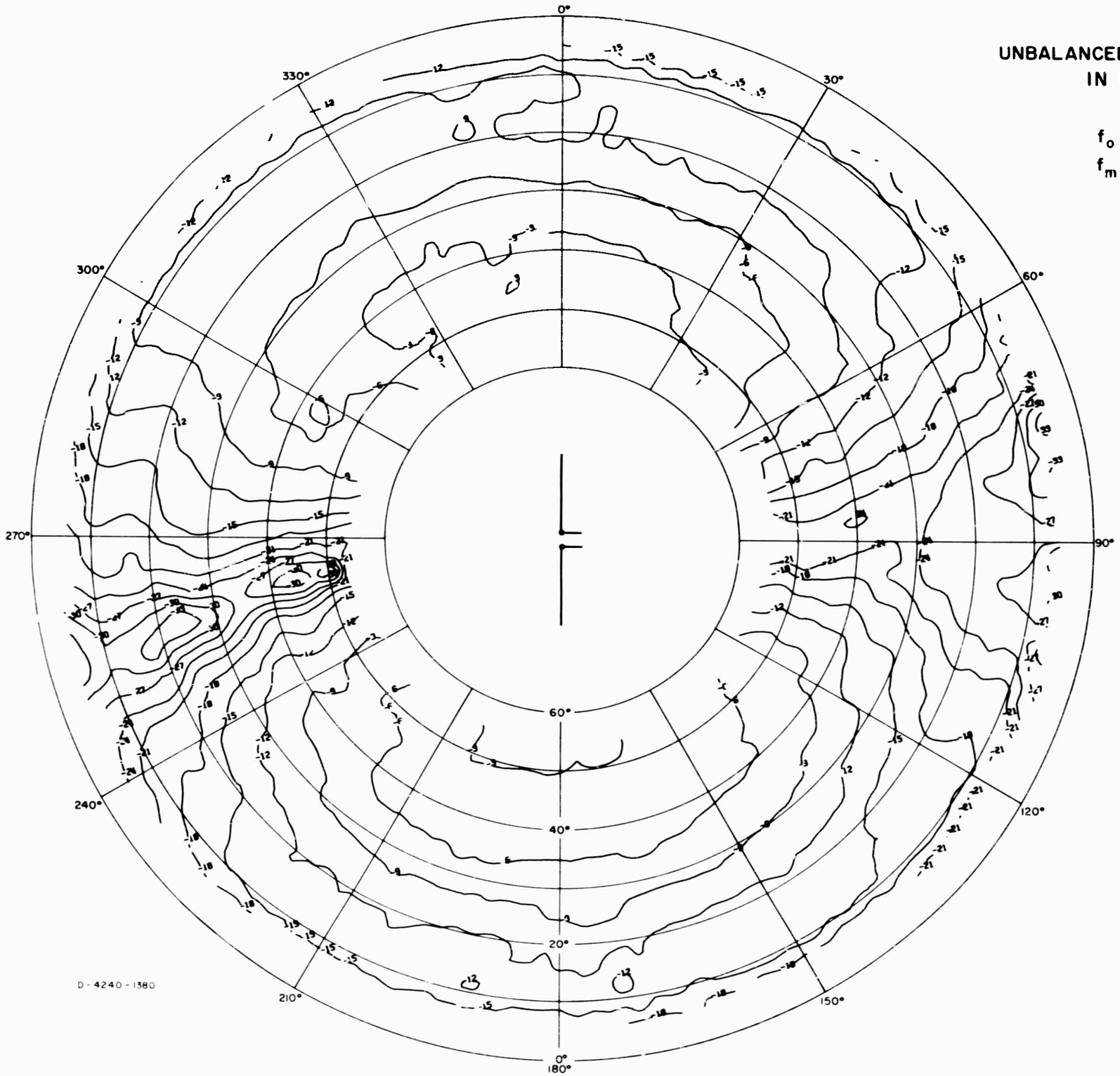

UNBALANCED DIPOLE
IN FOLIAGE
$h_a = 8'$
$f_o = 6$ Mc/s
$f_m = 6$ Mc/s
E_θ

D-4240-1380

FIG. A-55

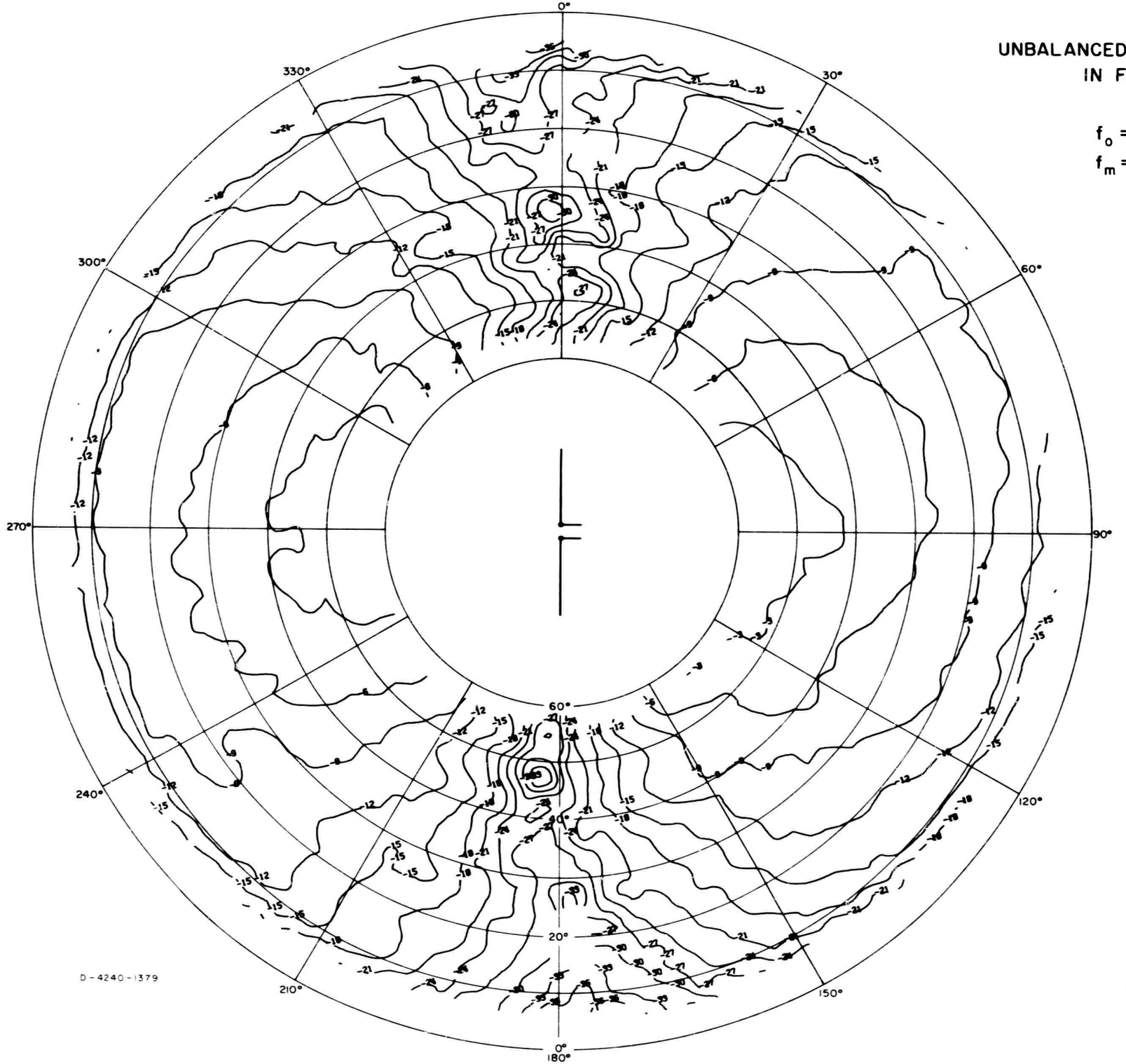

UNBALANCED DIPOLE
IN FOLIAGE
$h_a = 8'$
$f_o = 6$ Mc/s
$f_m = 6$ Mc/s
E_ϕ

D-4240-1379

FIG. A-56

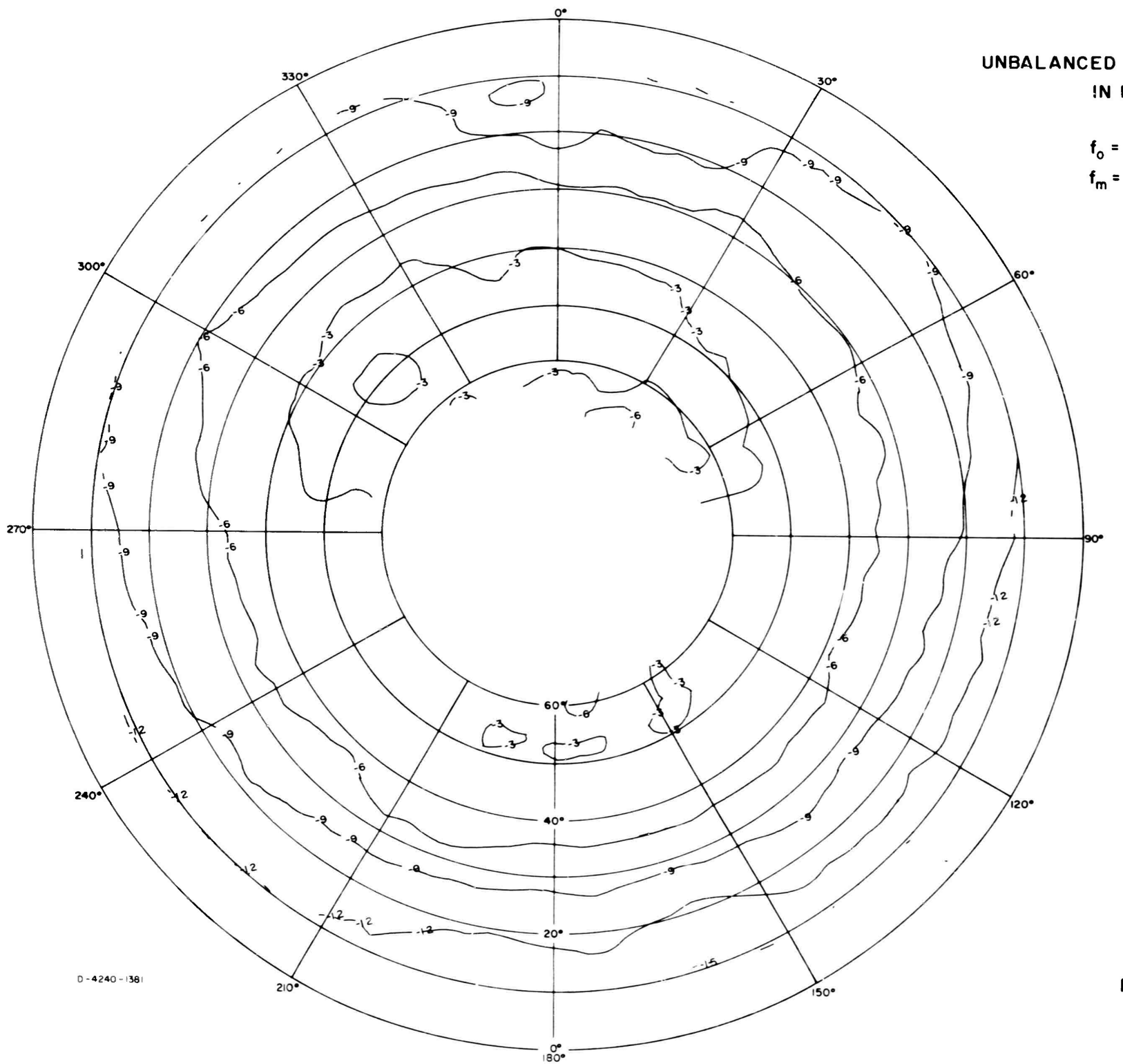

UNBALANCED DIPOLE
IN FOLIAGE
$h_a = 8'$
$f_o = 6$ Mc/s
$f_m = 6$ Mc/s
POWER

FIG. A-57

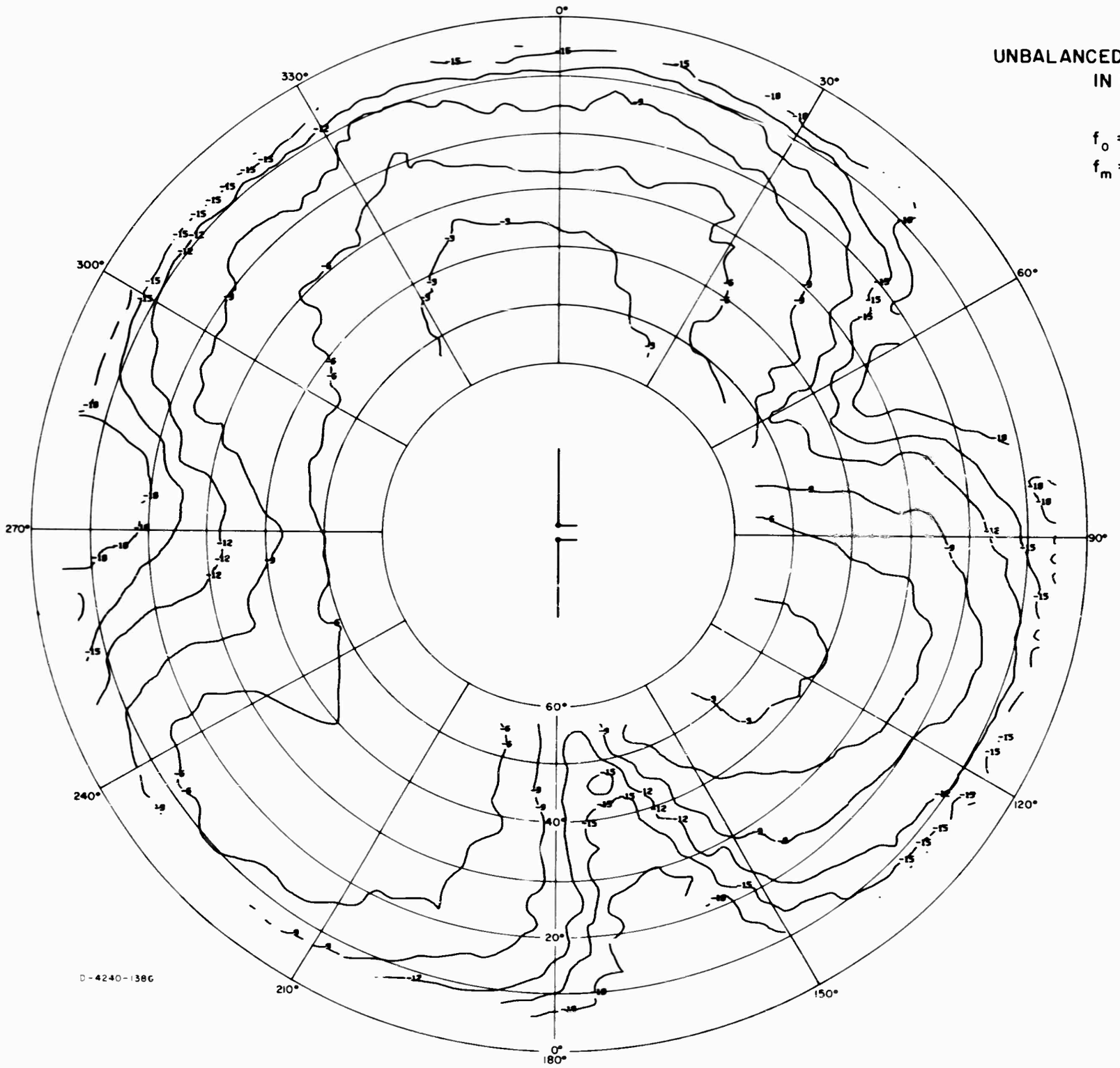

UNBALANCED DIPOLE
IN FOLIAGE
h_a = 2'
f_o = 6 Mc/s
f_m = 4 Mc/s
E_θ

FIG. A-58

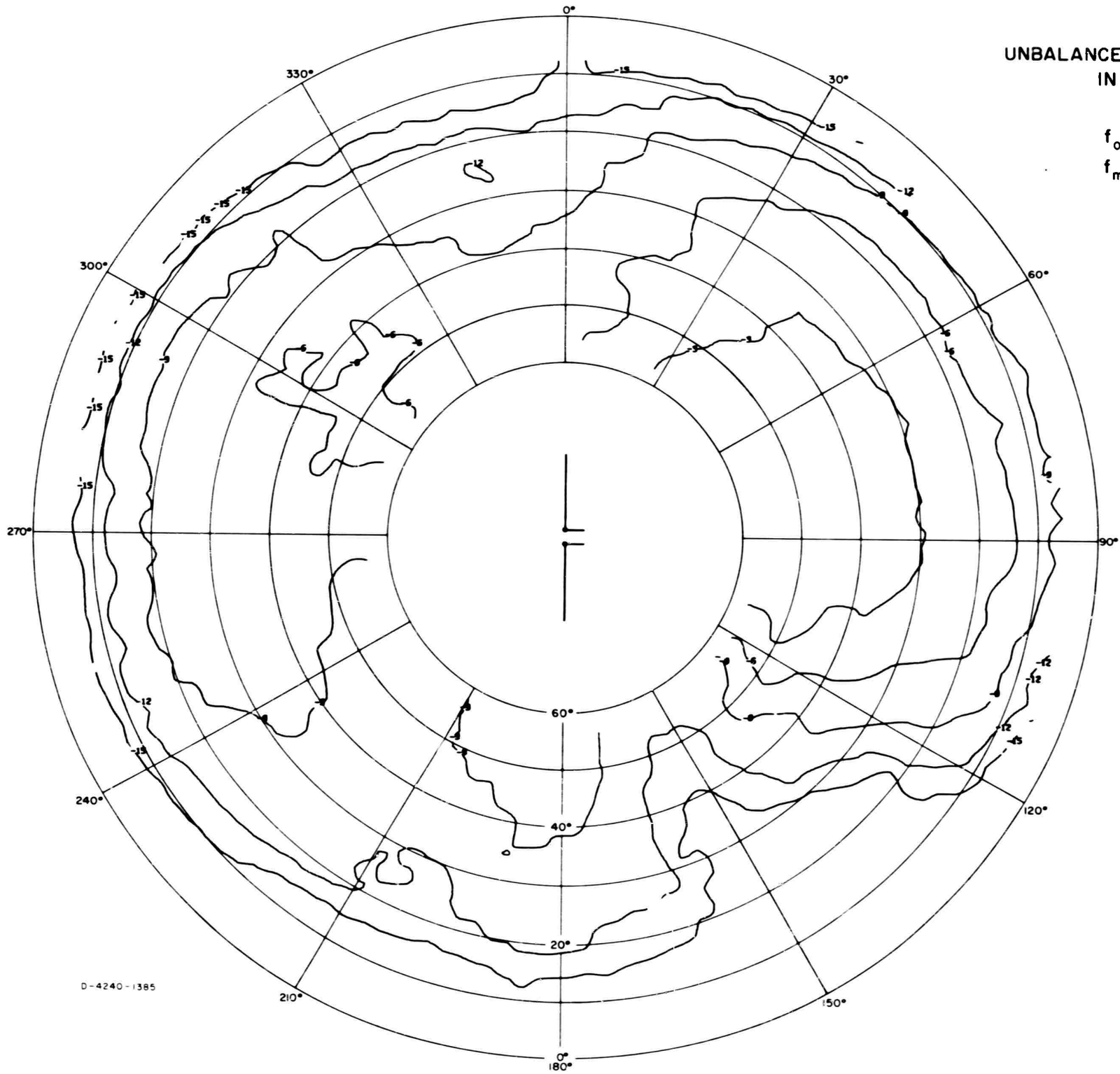

UNBALANCED DIPOLE
IN FOLIAGE
$h_a = 2'$
$f_o = 6$ Mc/s
$f_m = 4$ Mc/s
E_ϕ

FIG. A-59

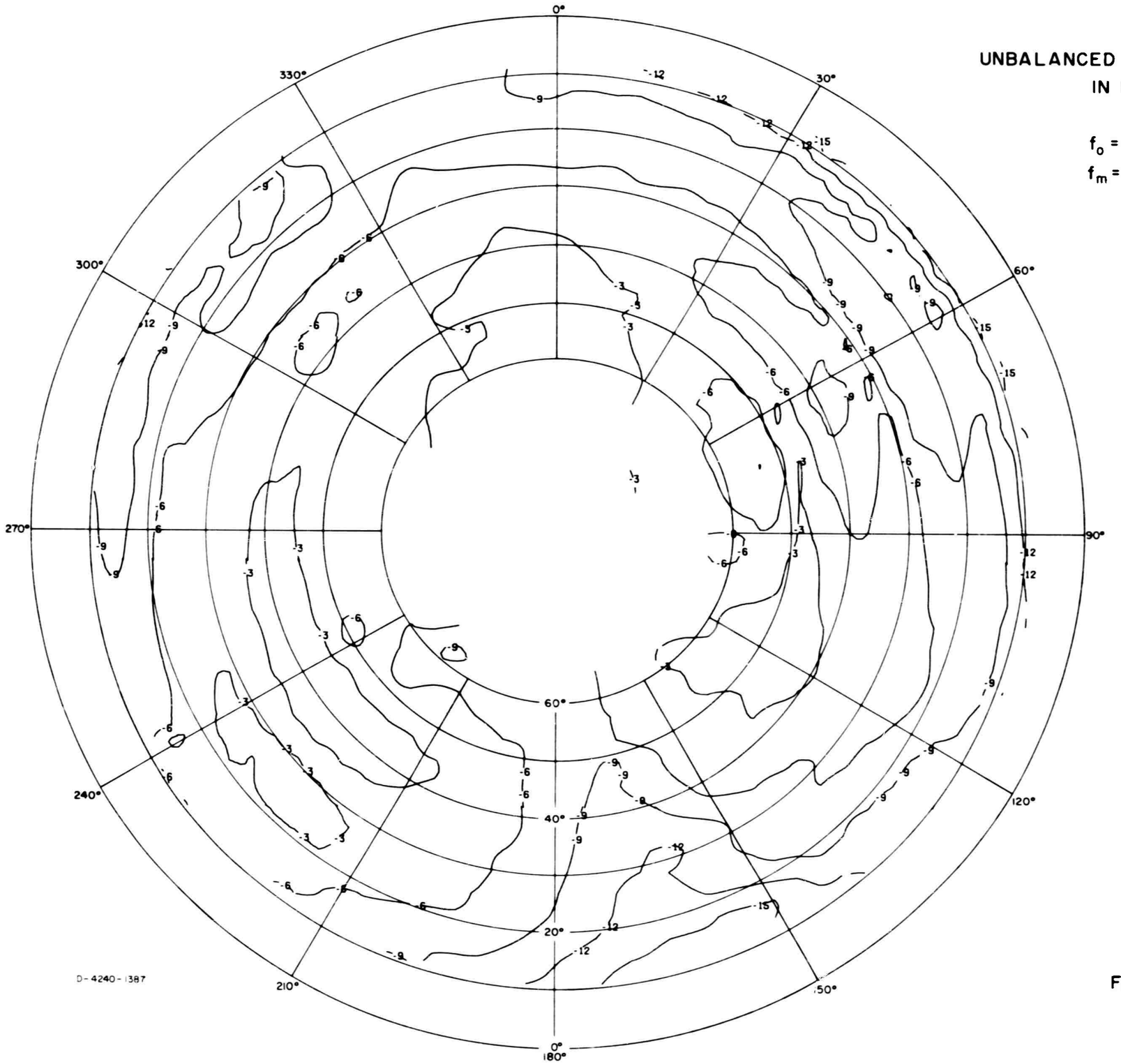

UNBALANCED DIPOLE
IN FOLIAGE
$h_a = 2'$
$f_o = 6$ Mc/s
$f_m = 4$ Mc/s
POWER

D-4240-1387

FIG. A-60

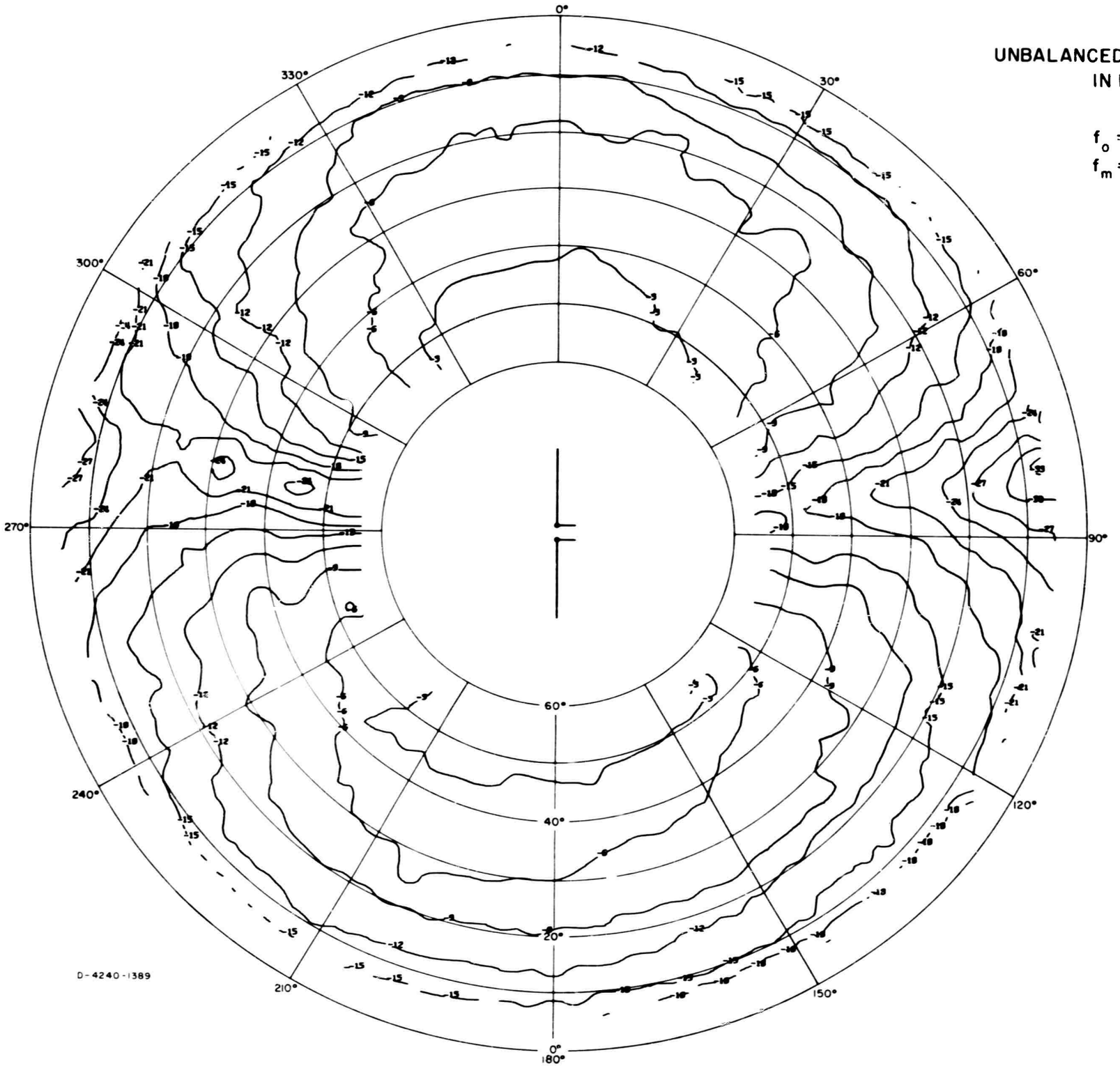

UNBALANCED DIPOLE
IN FOLIAGE
$h_a = 2'$
$f_o = 6$ Mc/s
$f_m = 6$ Mc/s
E_θ

FIG. A-61

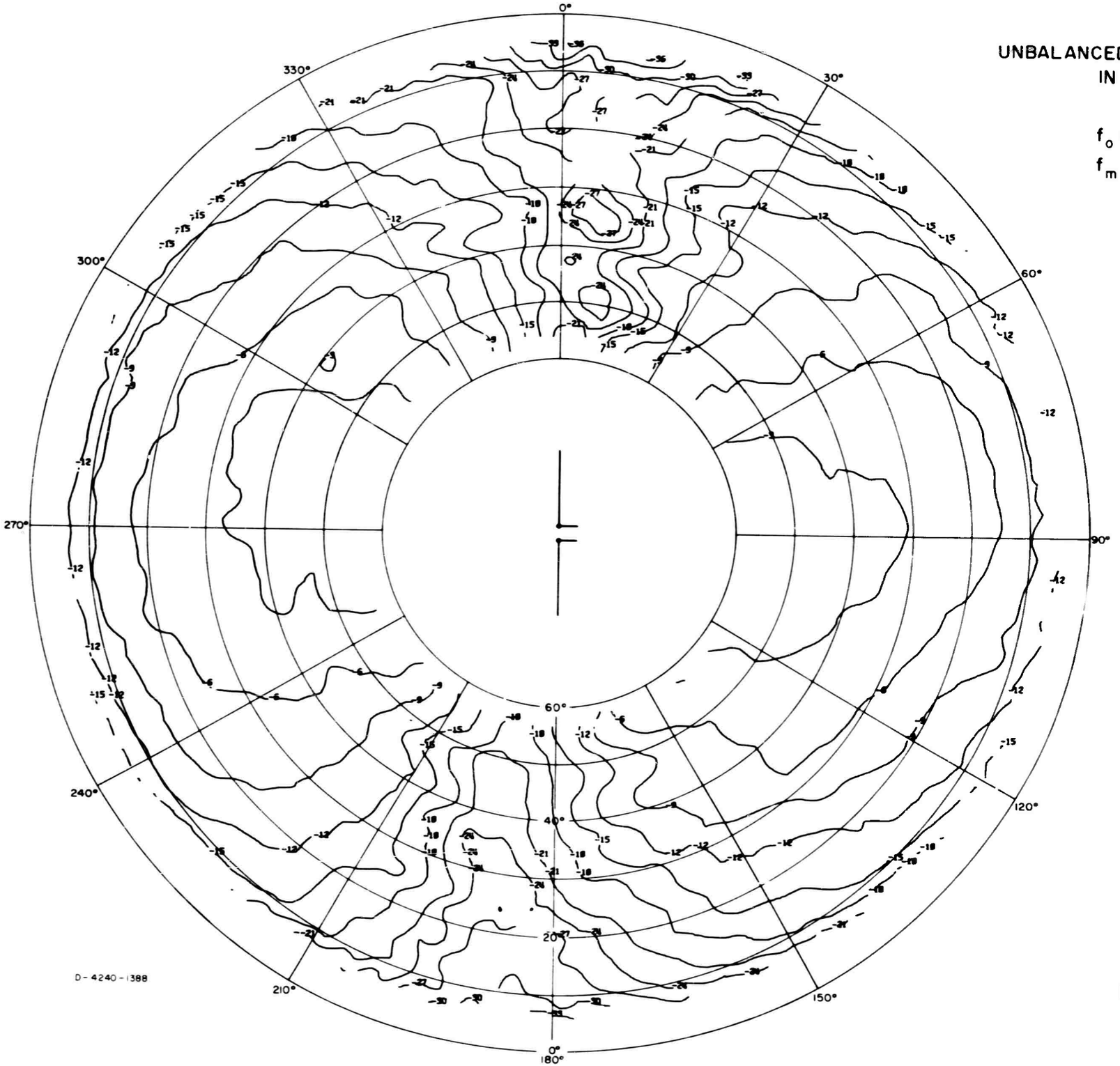

UNBALANCED DIPOLE
IN FOLIAGE
$h_a = 2'$
$f_o = 6$ Mc/s
$f_m = 6$ Mc/s
E_ϕ

FIG. A-62

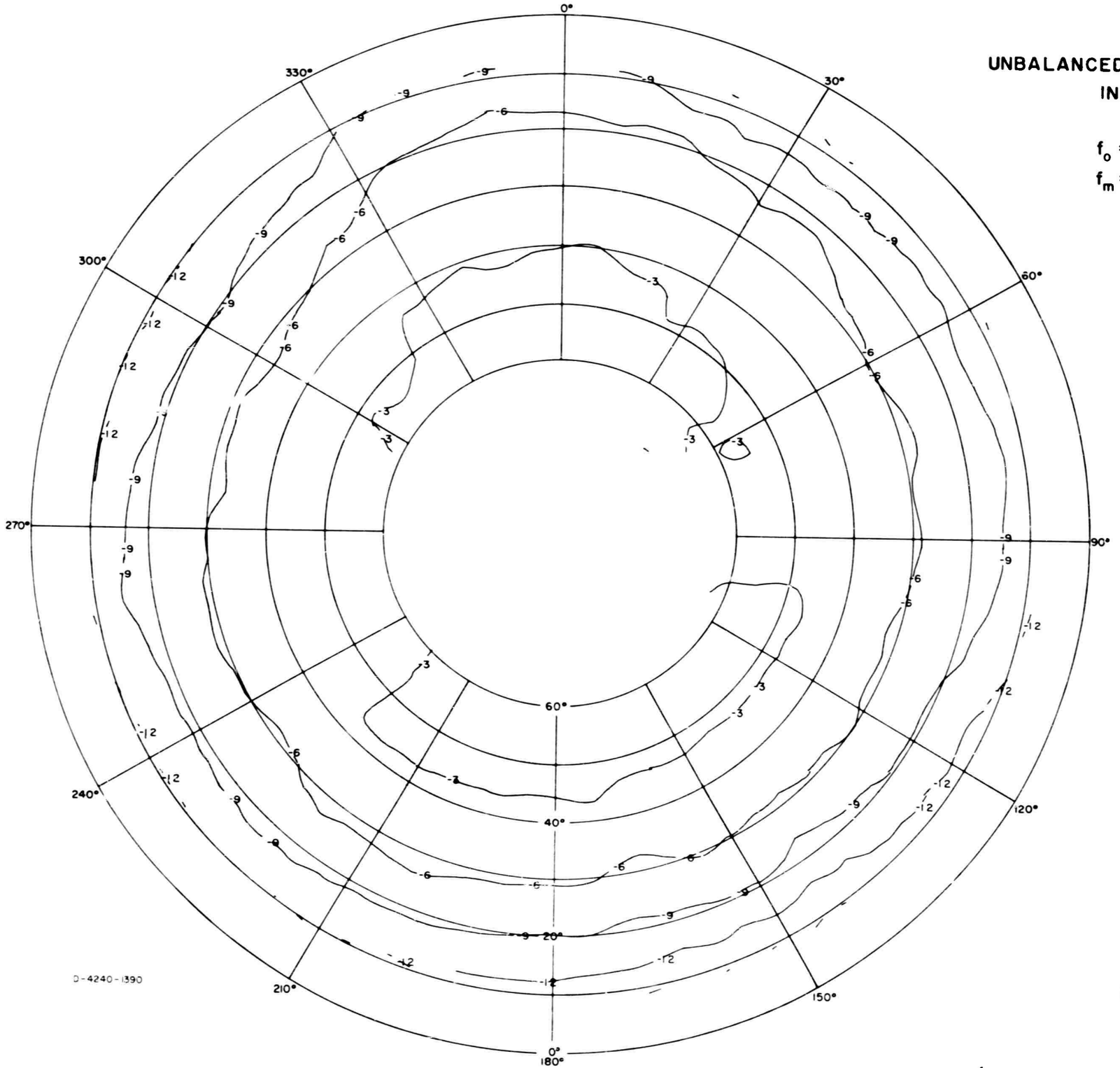

UNBALANCED DIPOLE
IN FOLIAGE
$h_a = 2'$
$f_o = 6$ Mc/s
$f_m = 6$ Mc/s
POWER

FIG. A-63

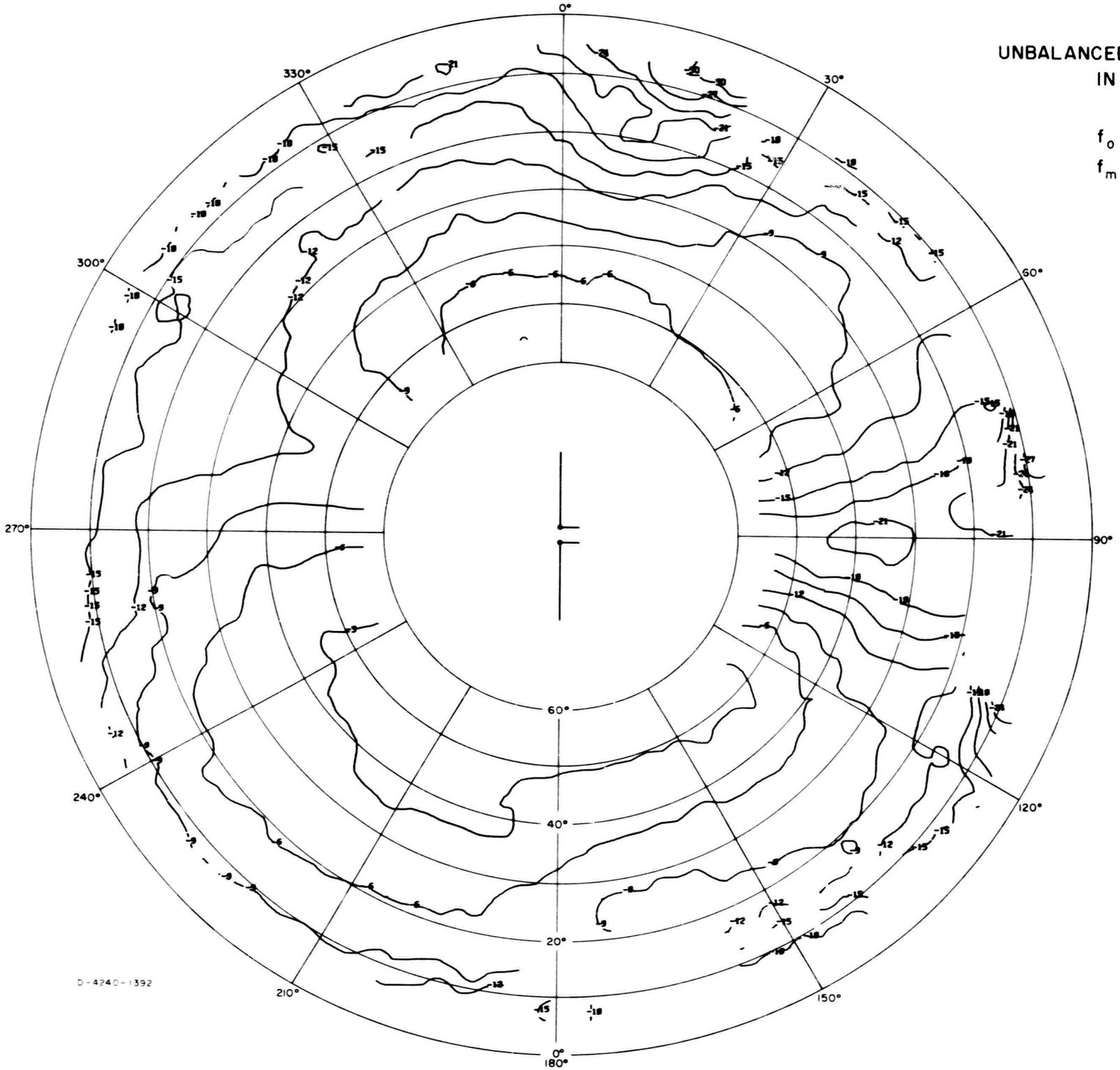

UNBALANCED DIPOLE
IN FOLIAGE
$h_a = 2'$
$f_o = 6$ Mc/s
$f_m = 8$ Mc/s
E_θ

FIG. A-64

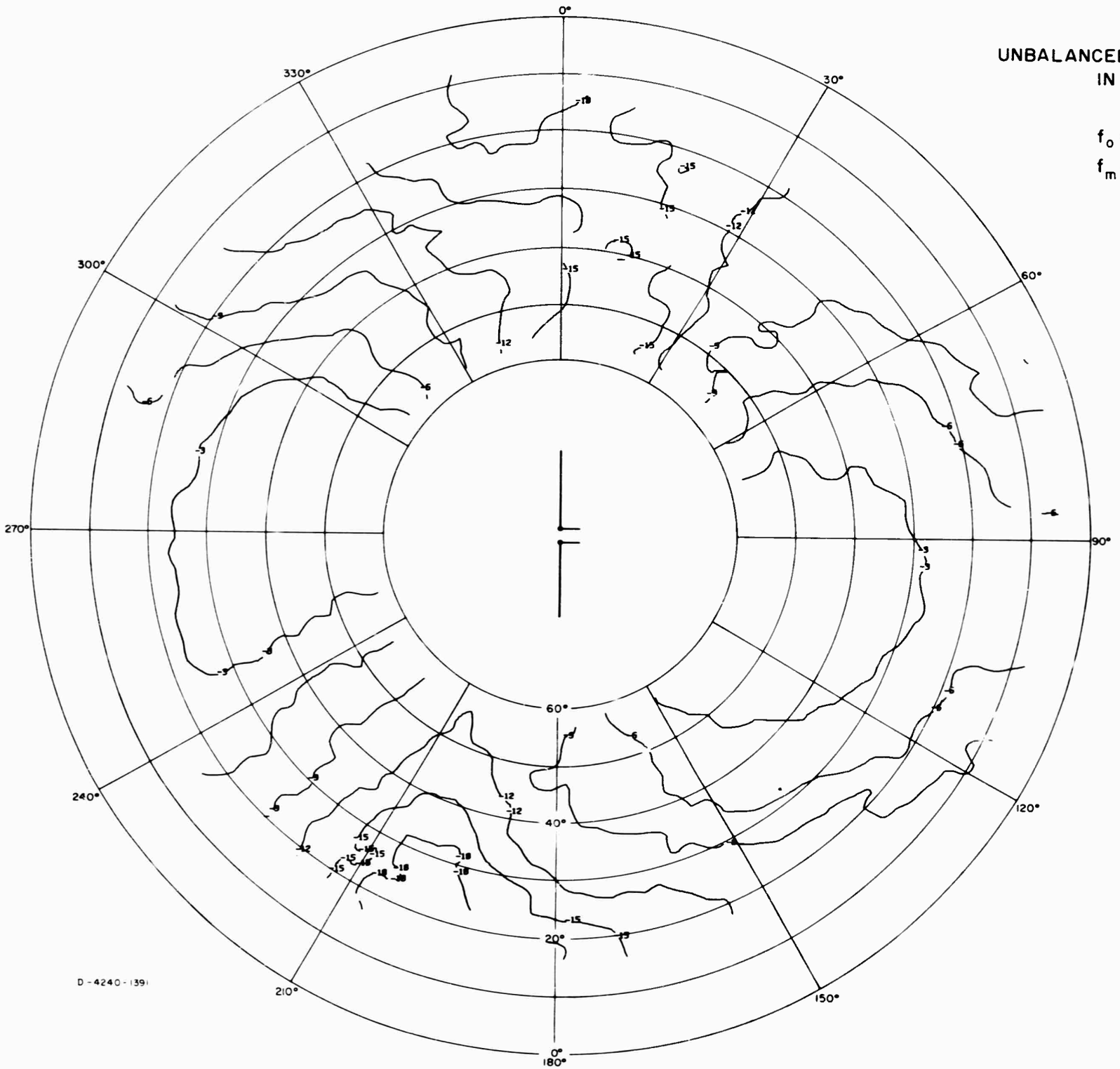

UNBALANCED DIPOLE
IN FOLIAGE
$h_a = 2'$
$f_o = 6$ Mc/s
$f_m = 8$ Mc/s
$\bar{E}_\phi$

D-4240-1391

FIG. A-65

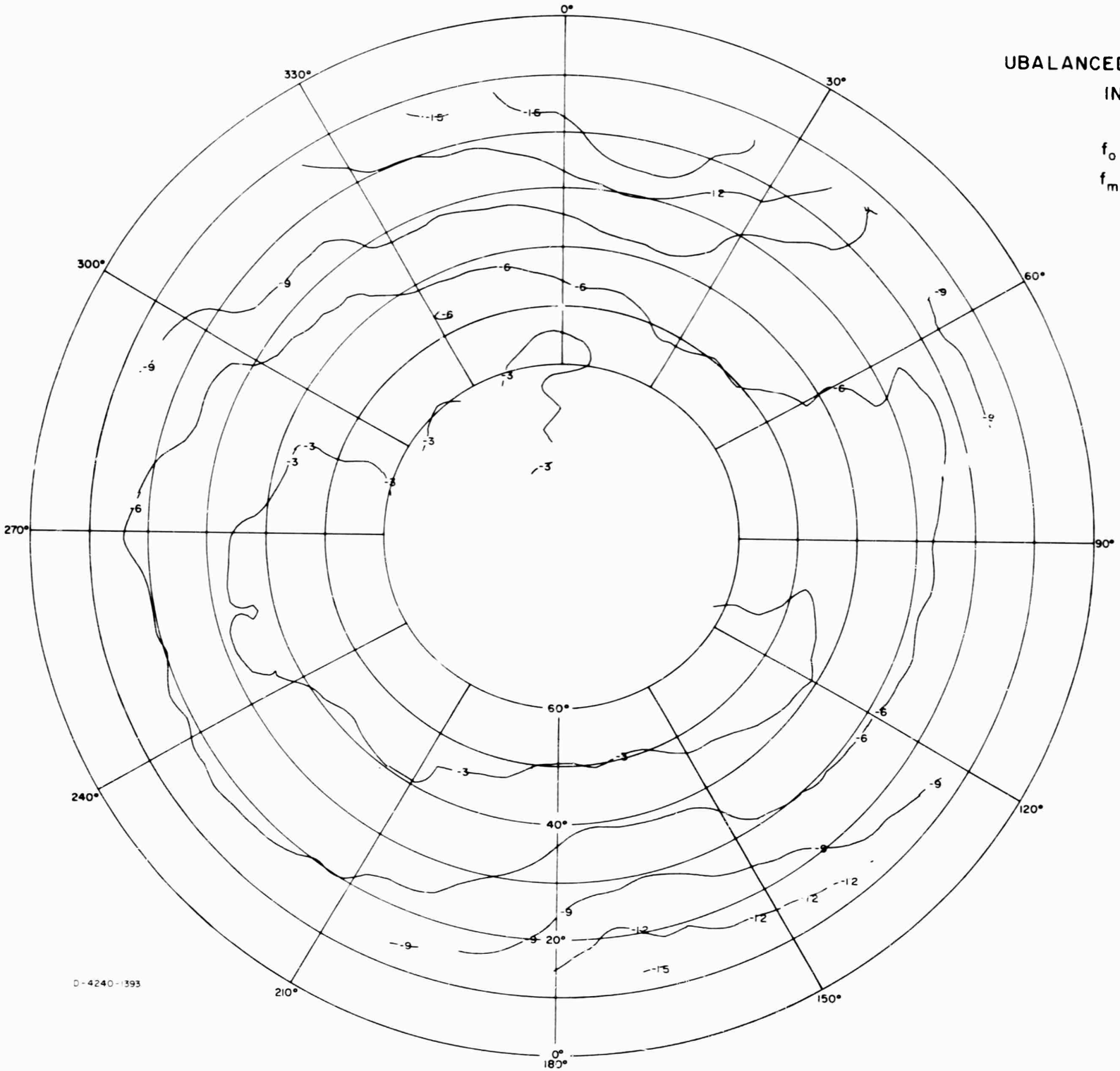

UBALANCED DIPOLE
IN FOLIAGE
$h_a = 2'$
$f_o = 6$ Mc/s
$f_m = 8$ Mc/s
POWER

FIG. A-66

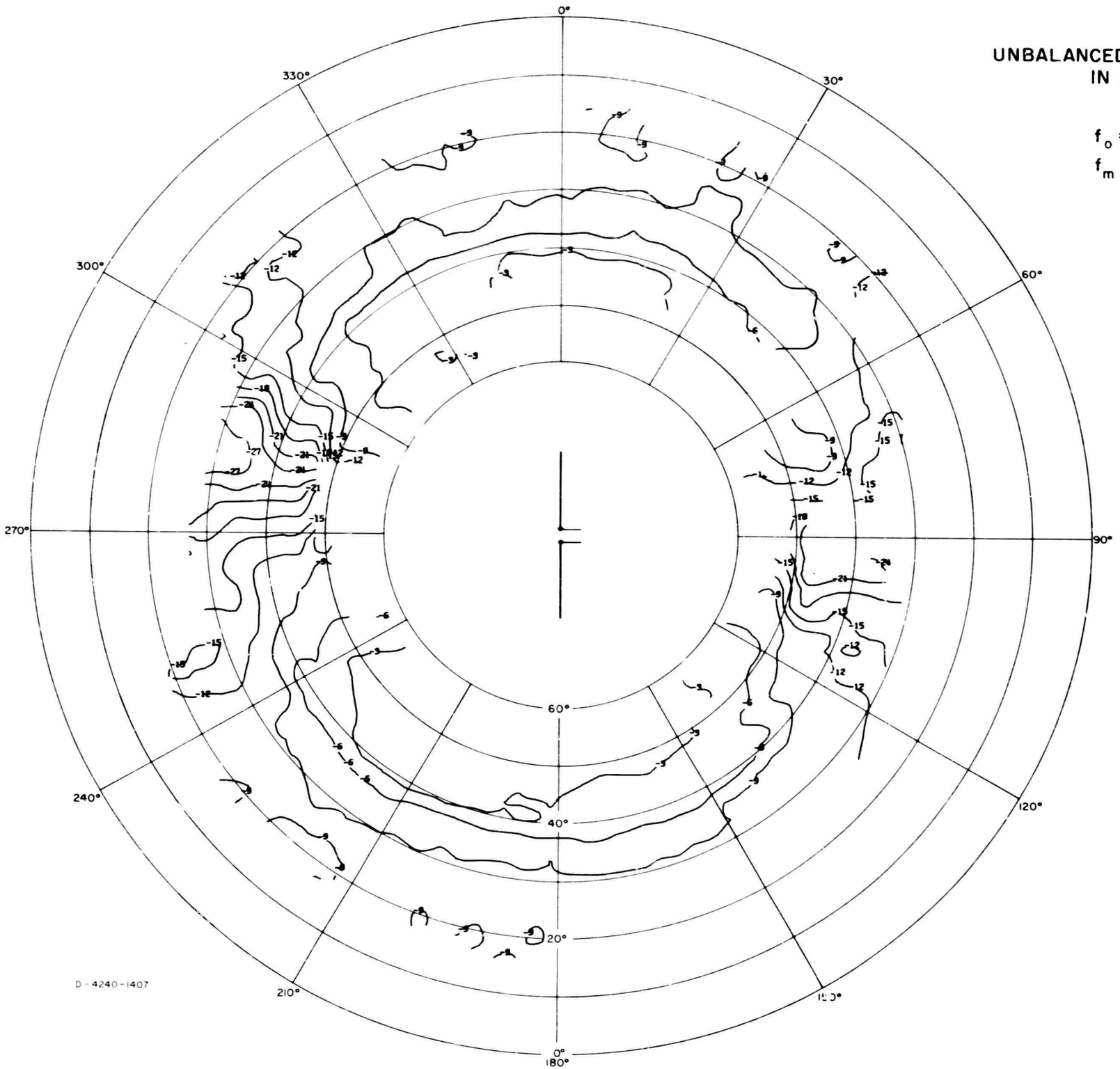

UNBALANCED DIPOLE
IN FOLIAGE

h_a = 23'

f_o = 8 Mc/s

f_m = 8 Mc/s

E_θ

D-4240-1407

FIG. A-67

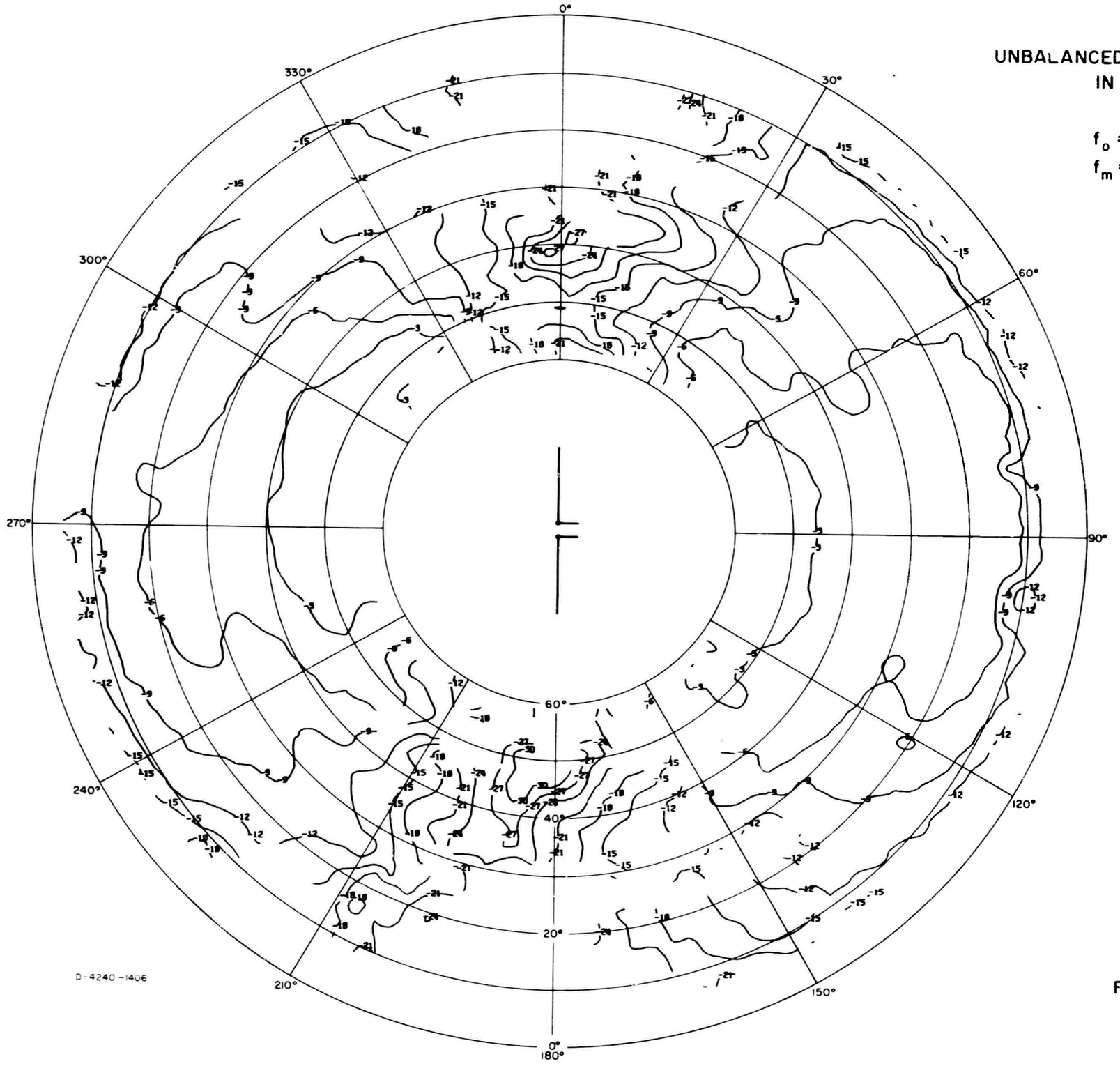

UNBALANCED DIPOLE
IN FOLIAGE
h_a = 23'
f_o = 8 Mc/s
f_m = 8 Mc/s
E_ϕ

FIG. A-68

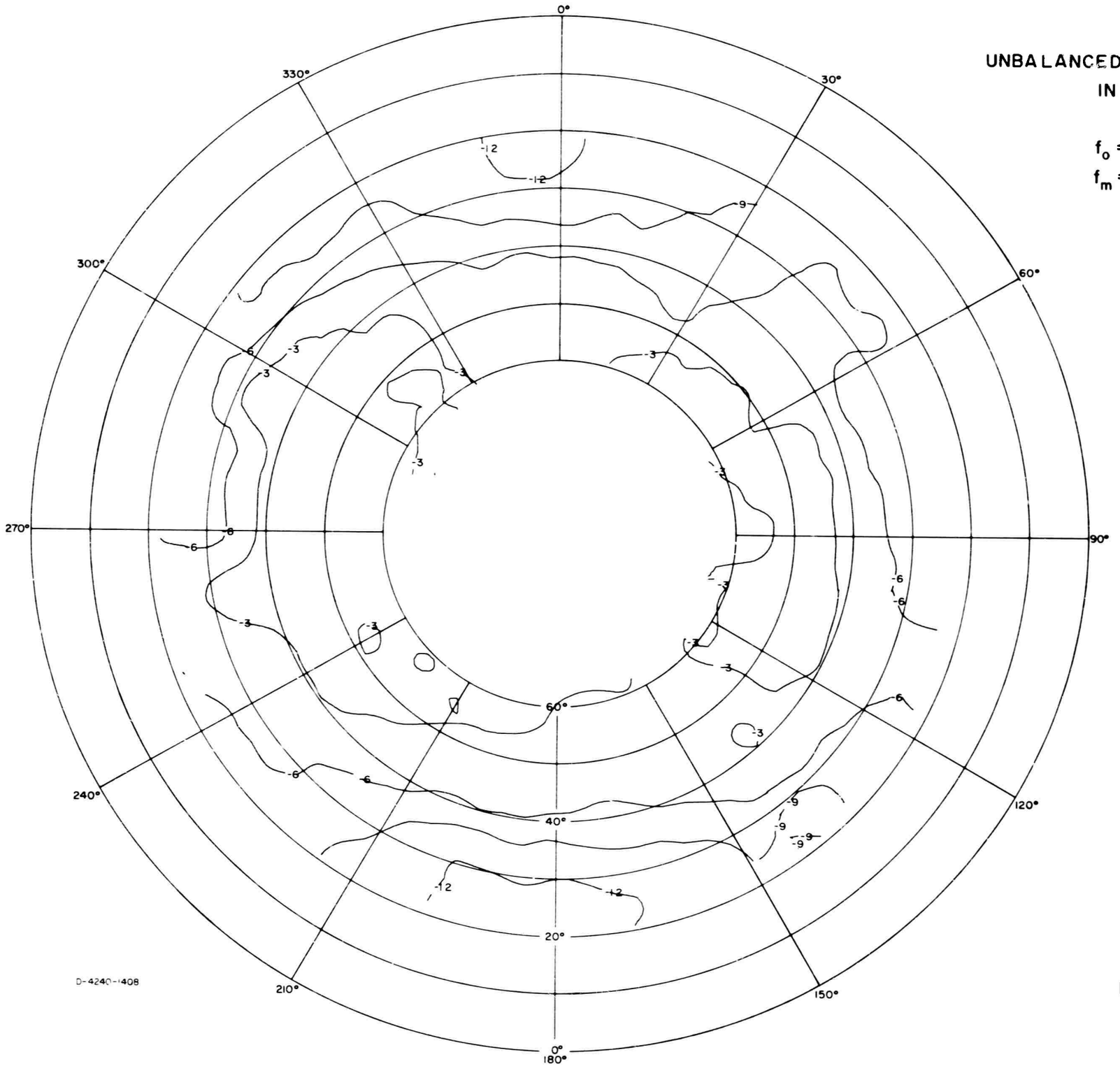

UNBALANCED DIPOLE
IN FOLIAGE
$h_a = 23'$
$f_o = 8$ Mc/s
$f_m = 8$ Mc/s
POWER

D-4240-1408

FIG. A-69

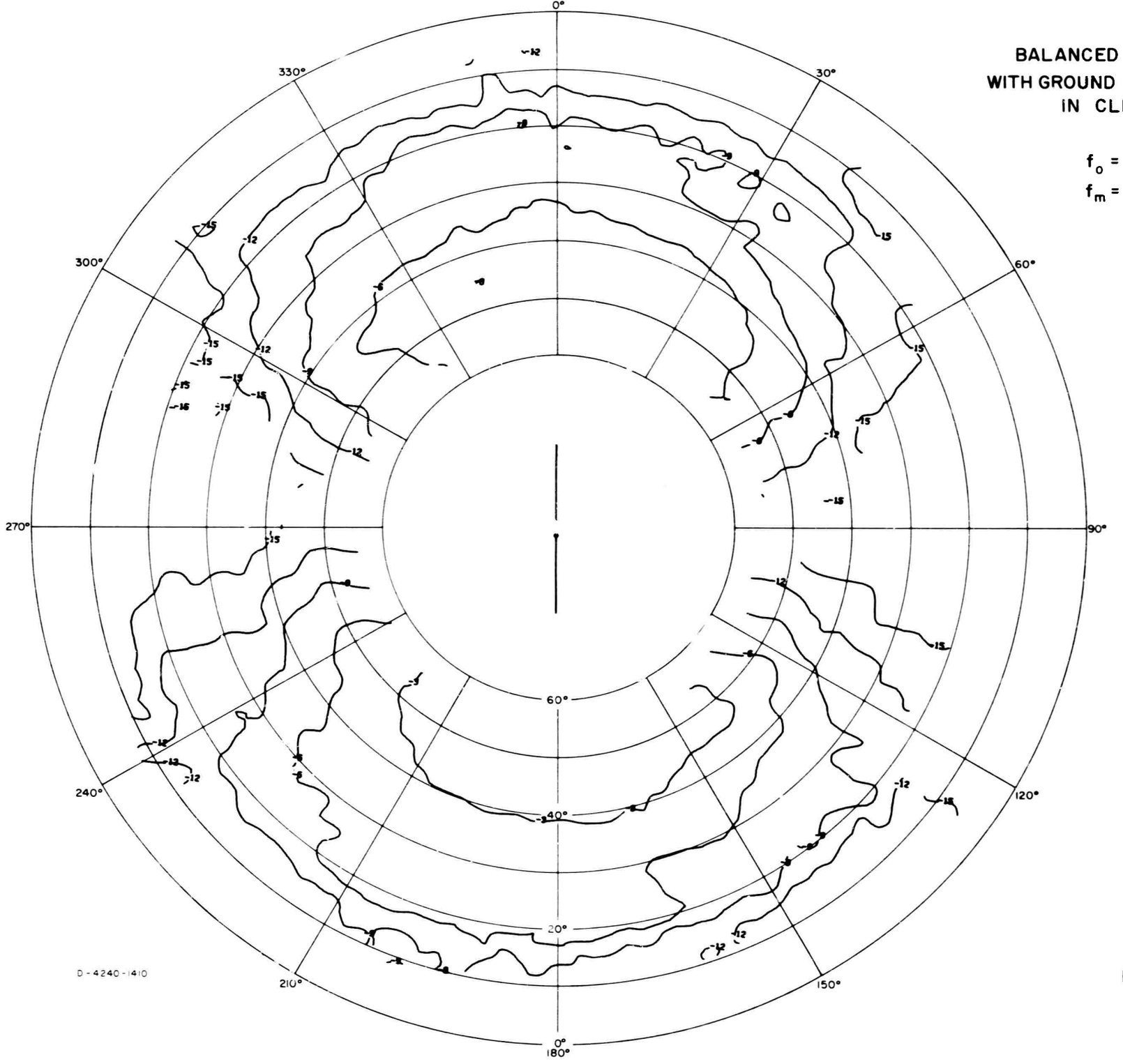

BALANCED DIPOLE
WITH GROUND SCREEN
IN CLEARING

$h_a = 16.4'$

$f_o = 15$ Mc/s

$f_m = 4$ Mc/s

E_θ

FIG. A-70

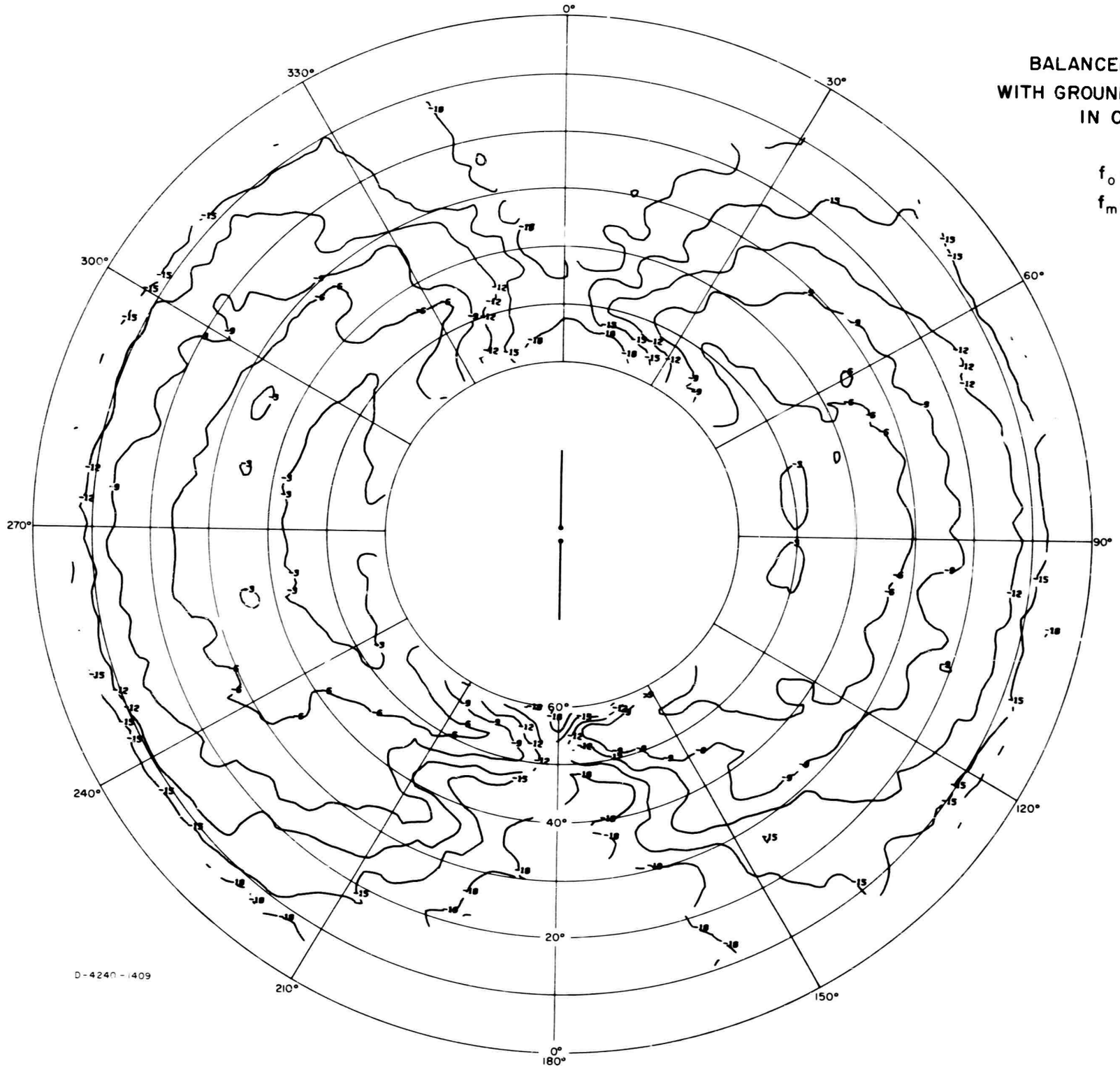

BALANCED DIPOLE
WITH GROUND SCREEN
IN CLEARING
$h_a = 16.4'$
$f_o = 15$ Mc/s
$f_m = 4$ Mc/s
E_ϕ

FIG. A-71

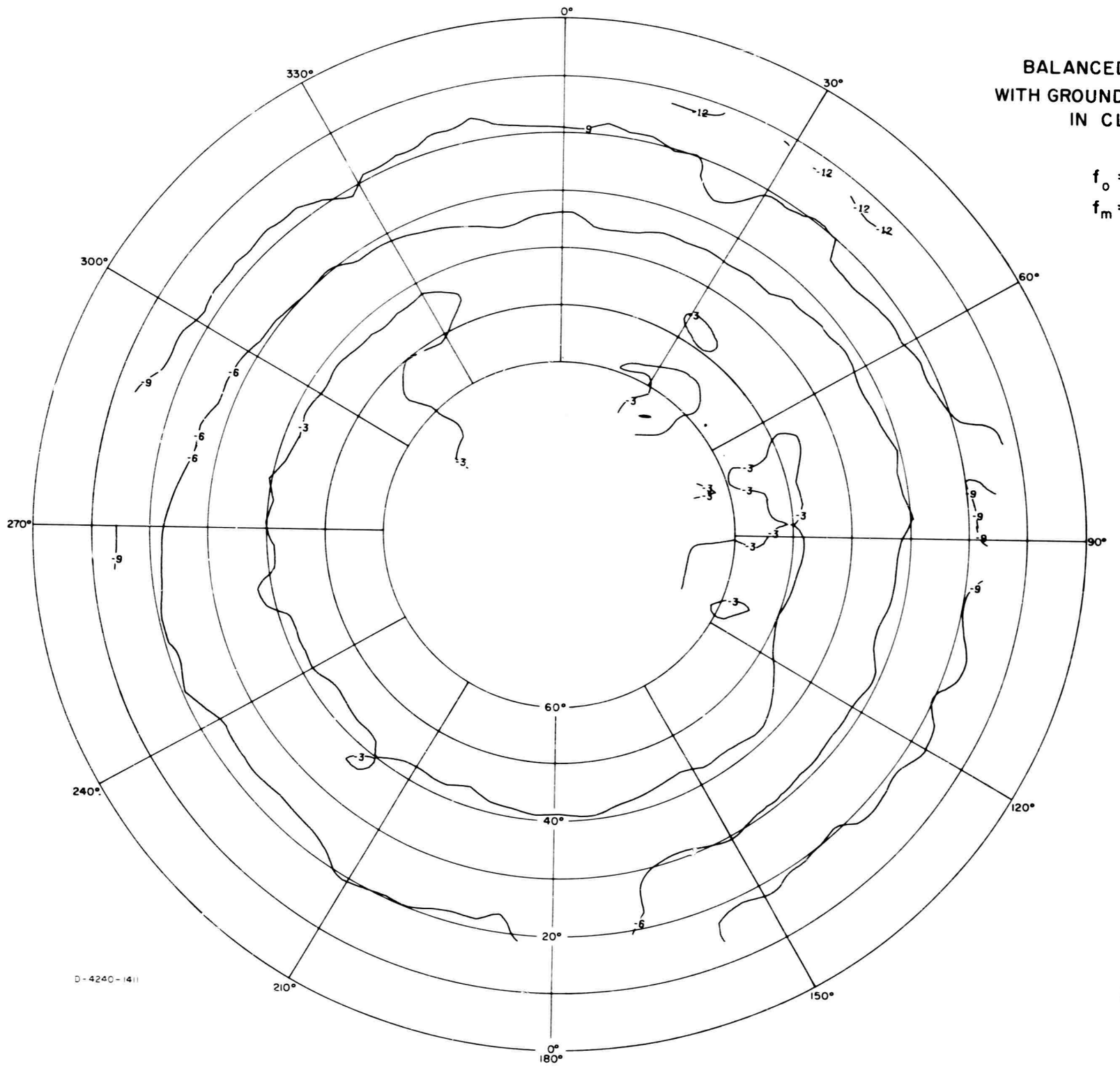

BALANCED DIPOLE
WITH GROUND SCREEN
IN CLEARING
$h_a = 16.4'$
$f_o = 15$ Mc/s
$f_m = 4$ Mc/s
POWER

FIG. A-72

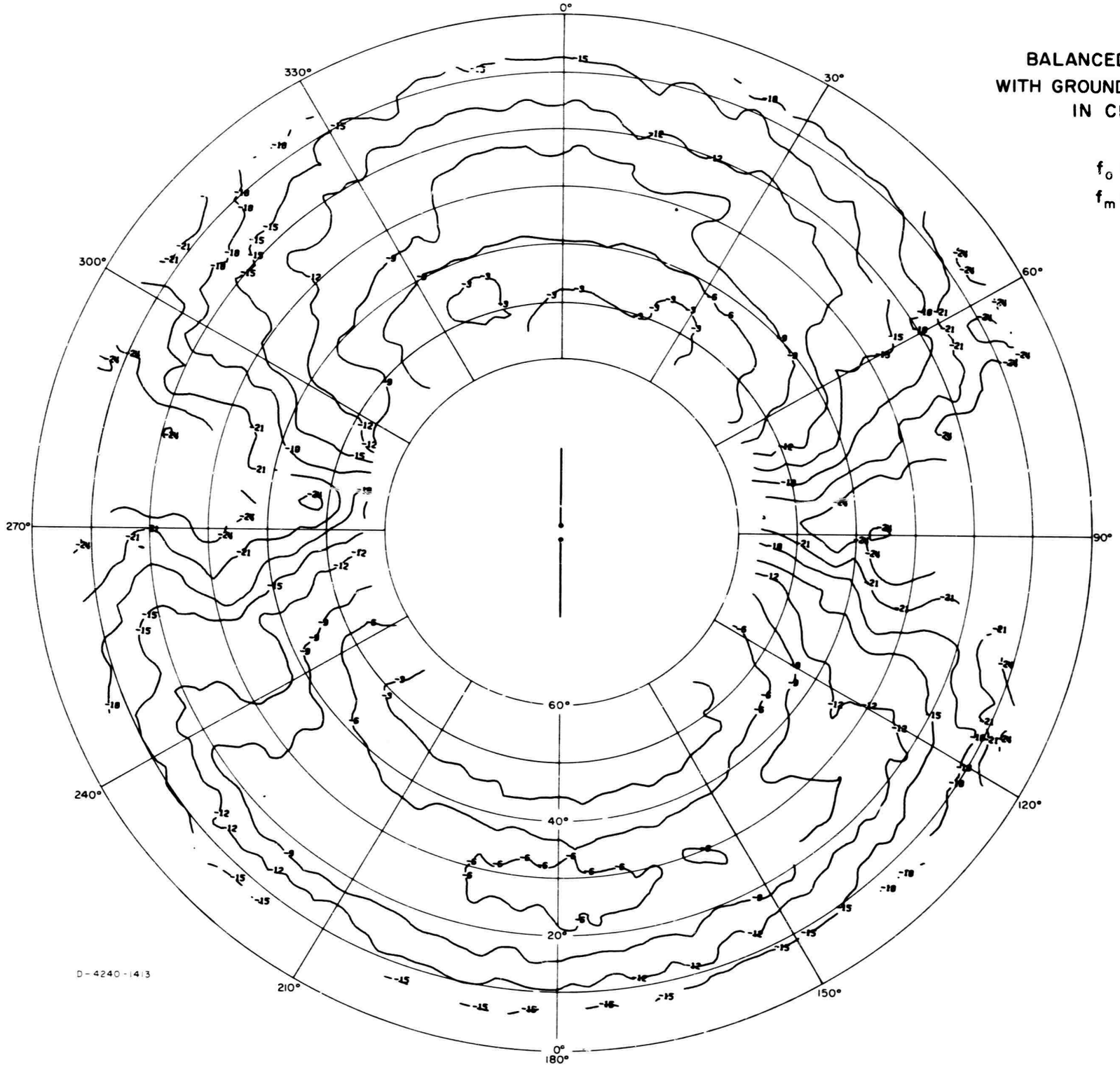

BALANCED DIPOLE
WITH GROUND SCREEN
IN CLEARING
$h_a = 16.4'$
$f_o = 15$ Mc/s
$f_m = 6$ Mc/s
$E\theta$

FIG. A-73

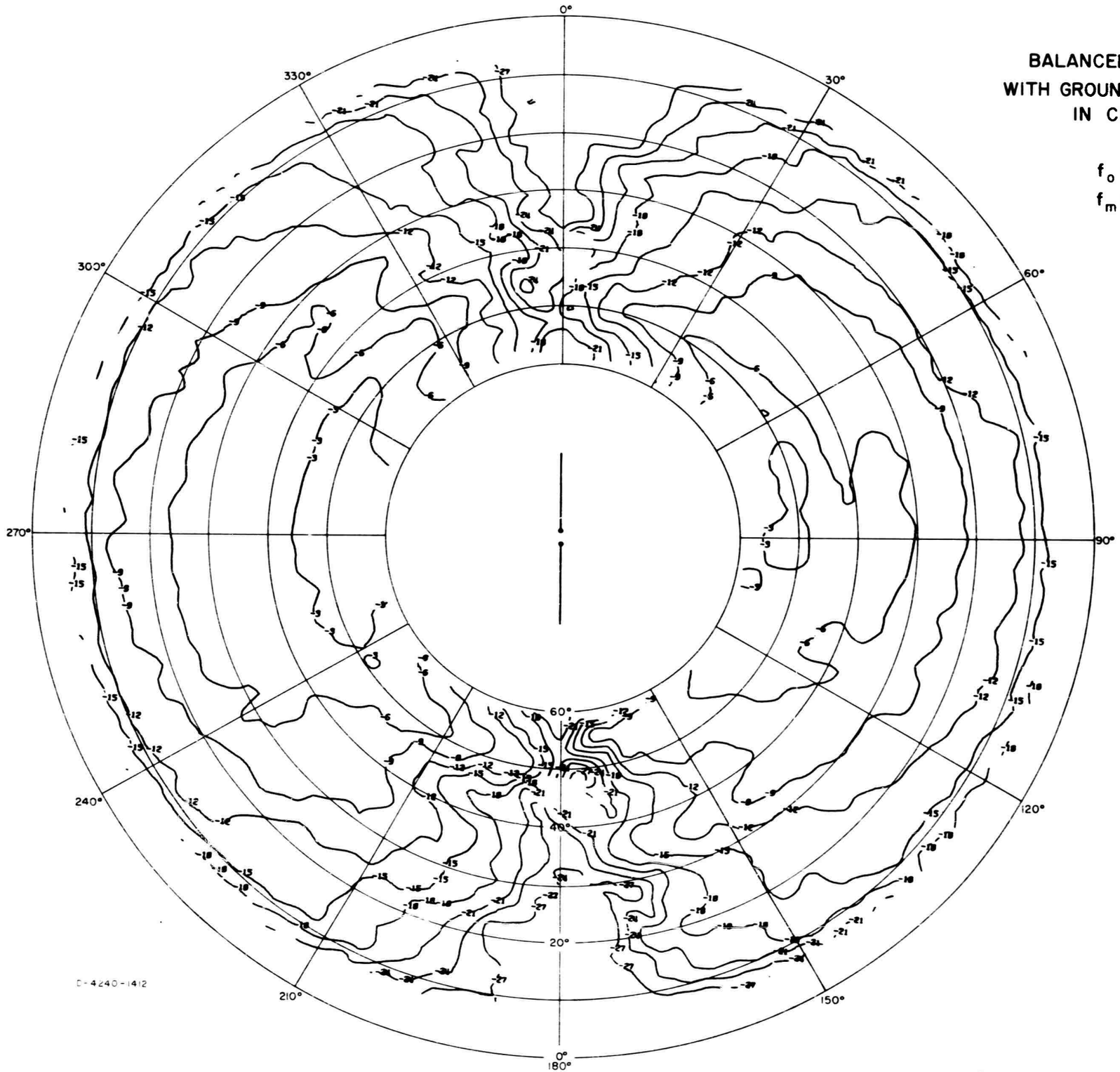

BALANCED DIPOLE
WITH GROUND SCREEN
IN CLEARING
$h_a = 16.4'$
$f_o = 15$ Mc/s
$f_m = 6$ Mc/s
E_ϕ

FIG. A-74

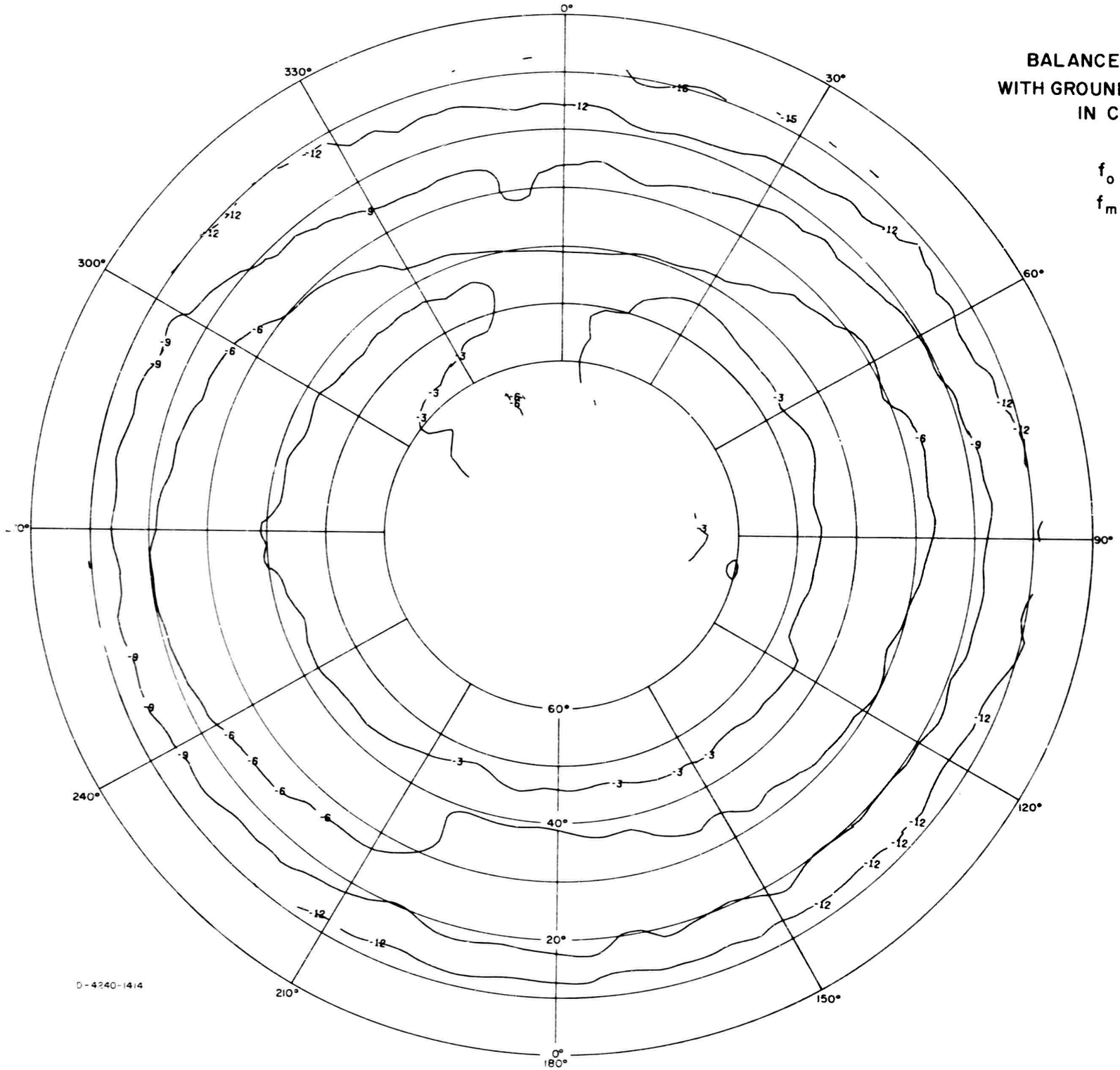

BALANCED DIPOLE
WITH GROUND SCREEN
IN CLEARING
$h_a = 16.4'$
$f_o = 15$ Mc/s
$f_m = 6$ Mc/s
POWER

FIG. A-75

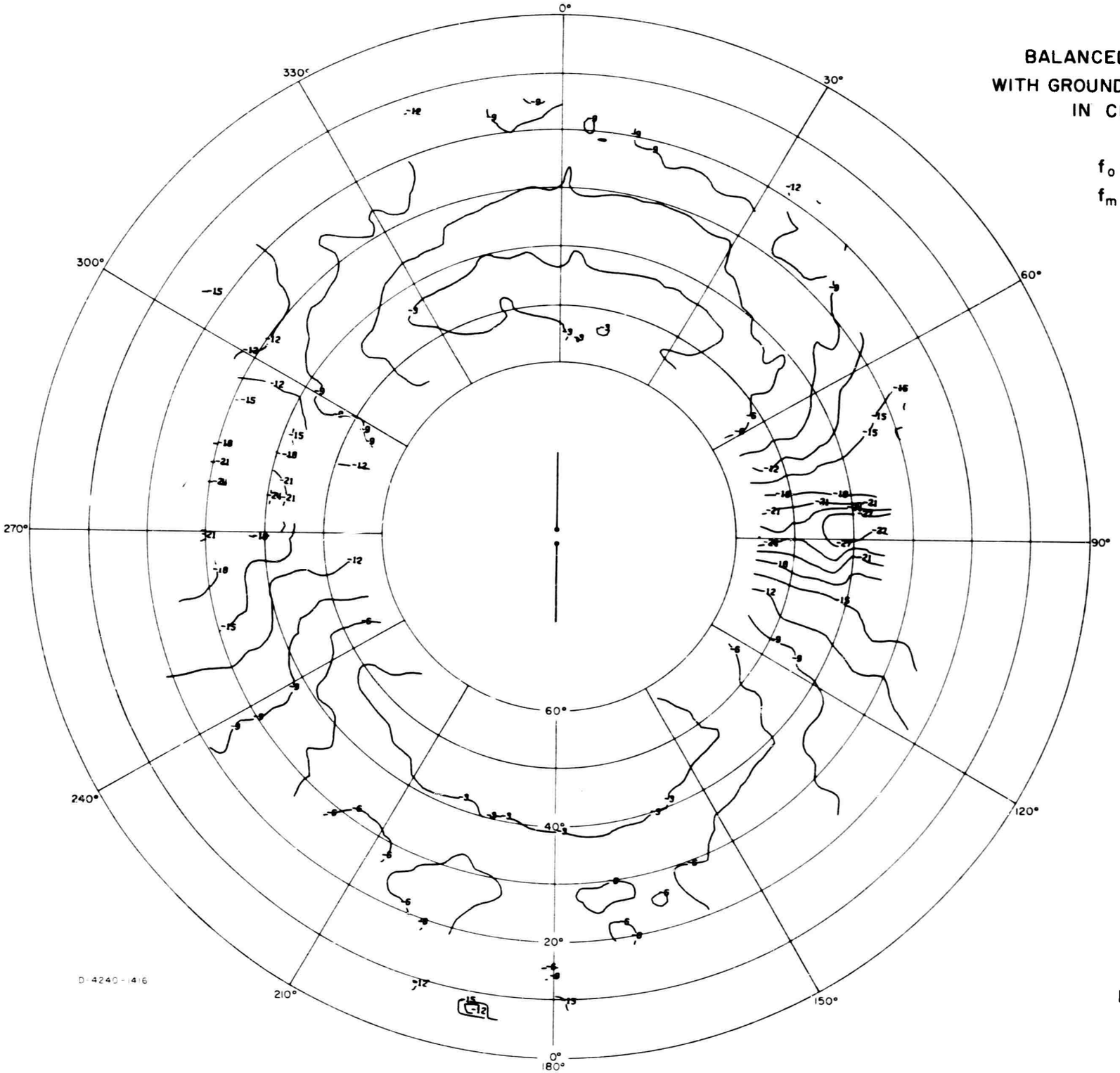

BALANCED DIPOLE
WITH GROUND SCREEN
IN CLEARING
$h_a = 16.4'$
$f_0 = 15$ Mc/s
$f_m = 8$ Mc/s
E_θ

FIG. A-76

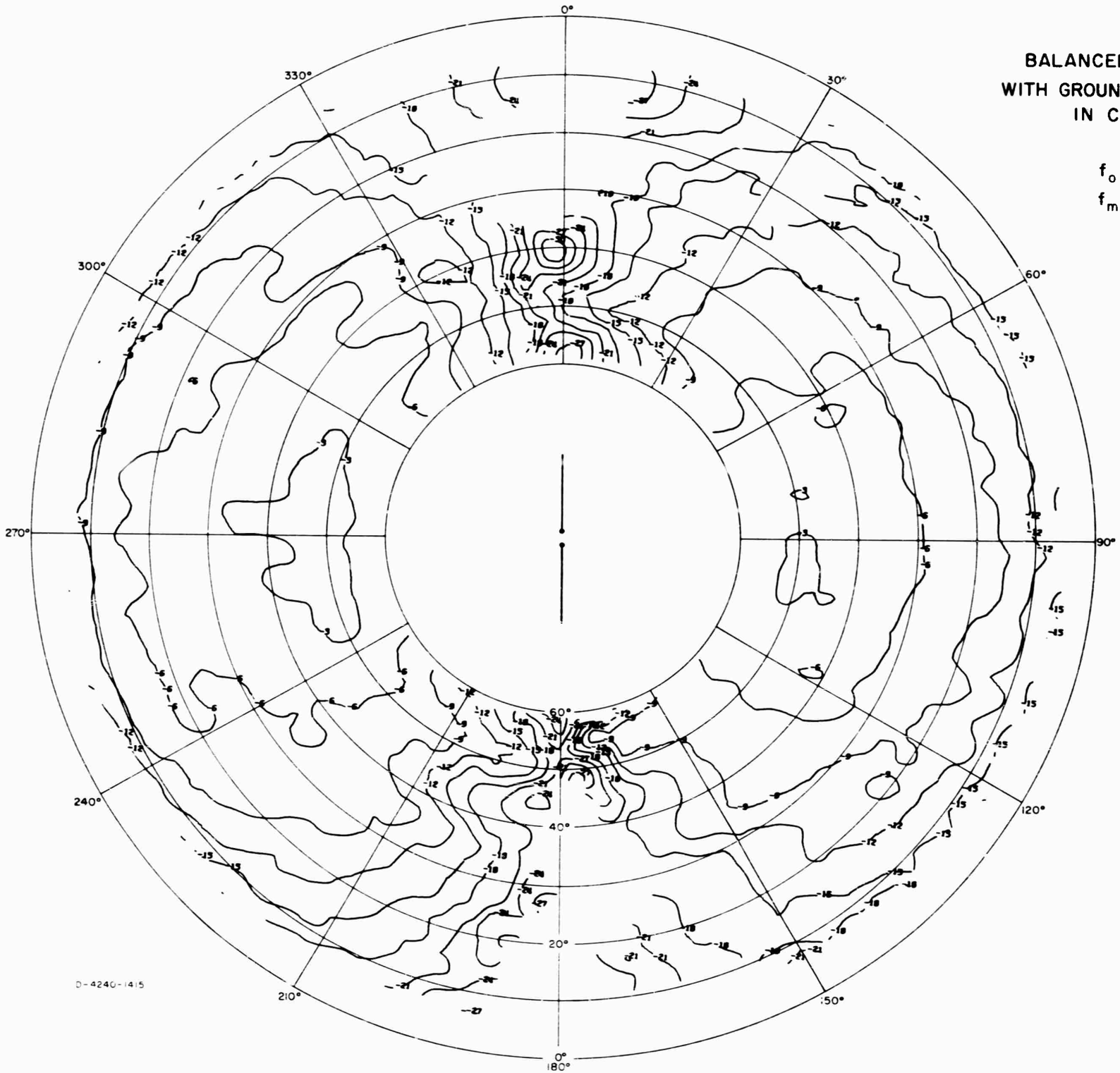

BALANCED DIPOLE
WITH GROUND SCREEN
IN CLEARING
$h_a = 16.4'$
$f_o = 15$ Mc/s
$f_m = 8$ Mc/s
E_ϕ

FIG. A-77

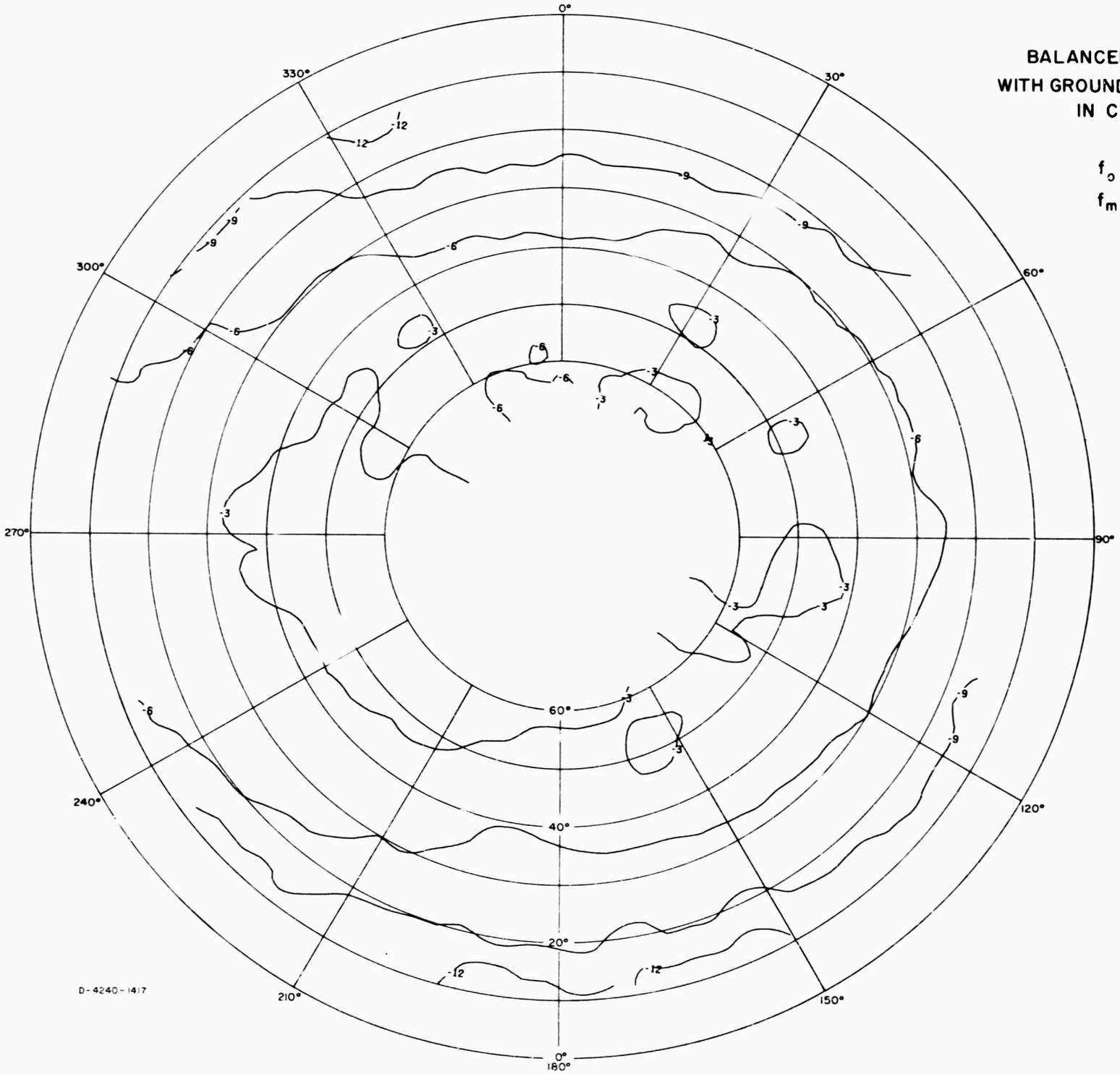

BALANCED DIPOLE
WITH GROUND SCREEN
IN CLEARING
h_a = 16.4'
f_o = 15 Mc/s
f_m = 8 Mc/s
POWER

FIG. A-78

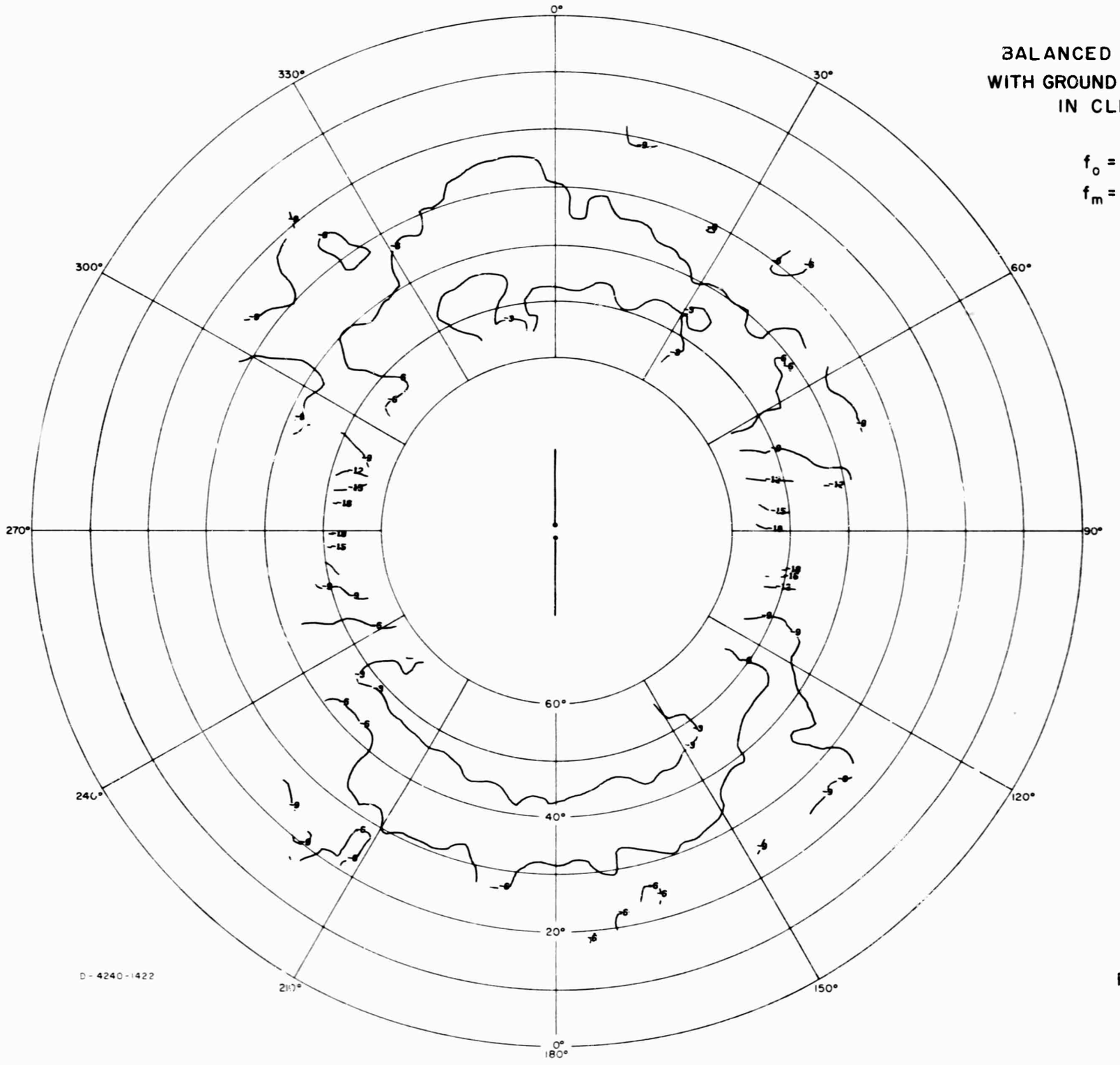

BALANCED DIPOLE
WITH GROUND SCREEN
IN CLEARING
$h_a = 16.4'$
$f_o = 15$ Mc/s
$f_m = 12$ Mc/s
E_θ

FIG. A-79

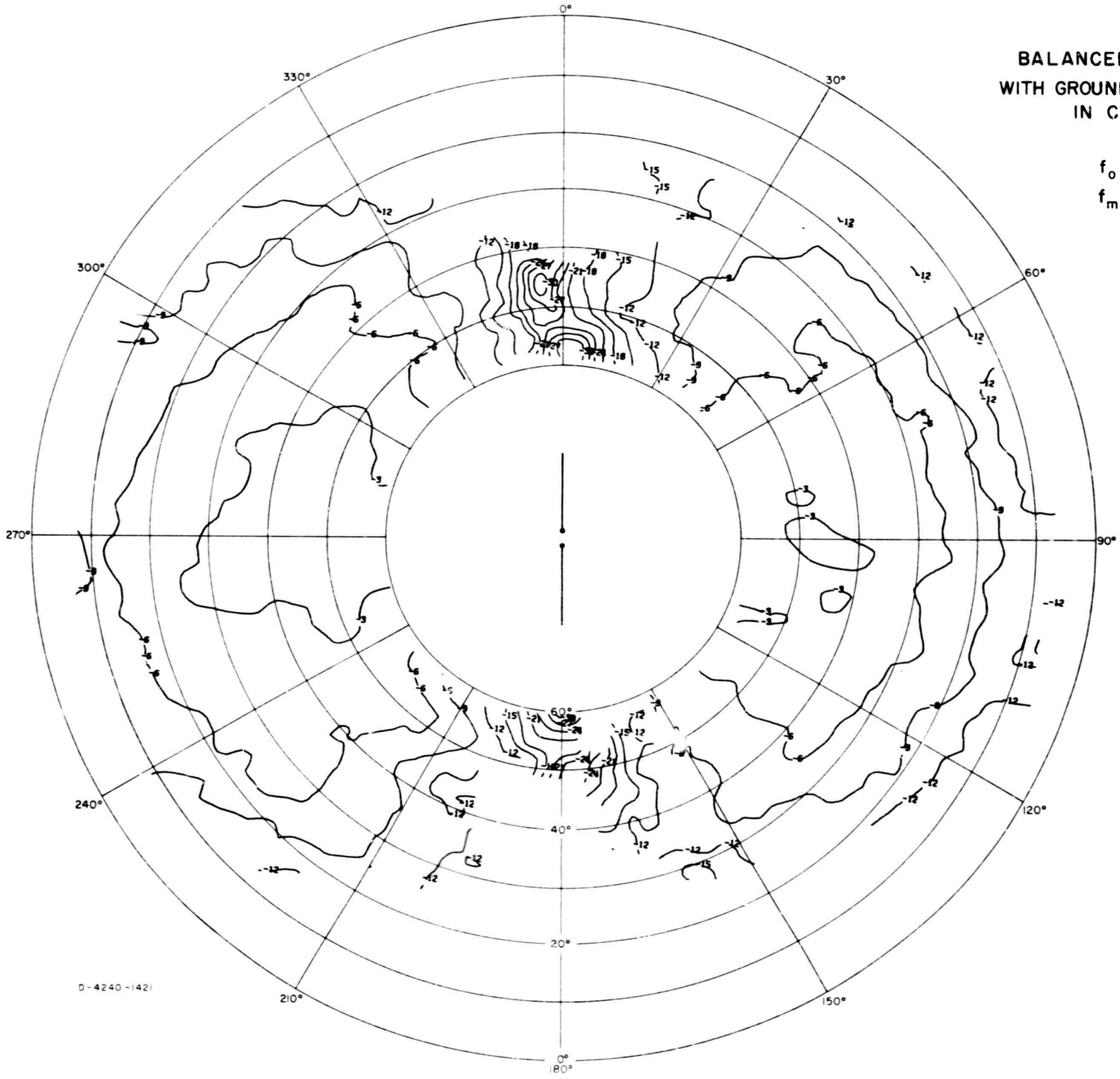

BALANCED DIPOLE
WITH GROUND SCREEN
IN CLEARING
$h_a = 16.4'$
$f_o = 15$ Mc/s
$f_m = 12$ Mc/s
E_ϕ

D-4240-1421

FIG. A-80

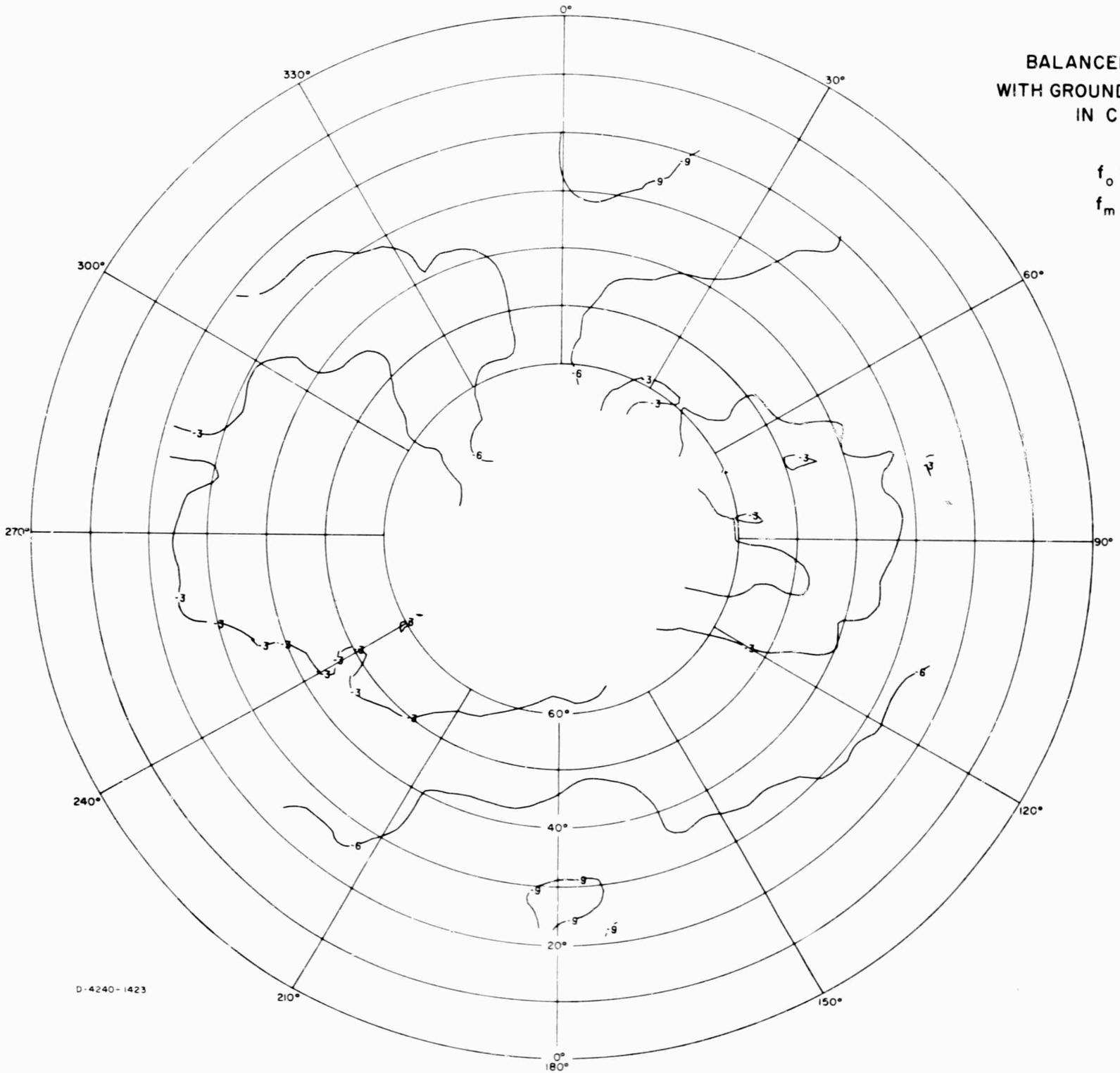

BALANCED DIPOLE
WITH GROUND SCREEN
IN CLEARING

$h_a = 16.4'$

$f_o = 15$ Mc/s

$f_m = 12$ Mc/s

POWER

D-4240-1423

FIG. A-81

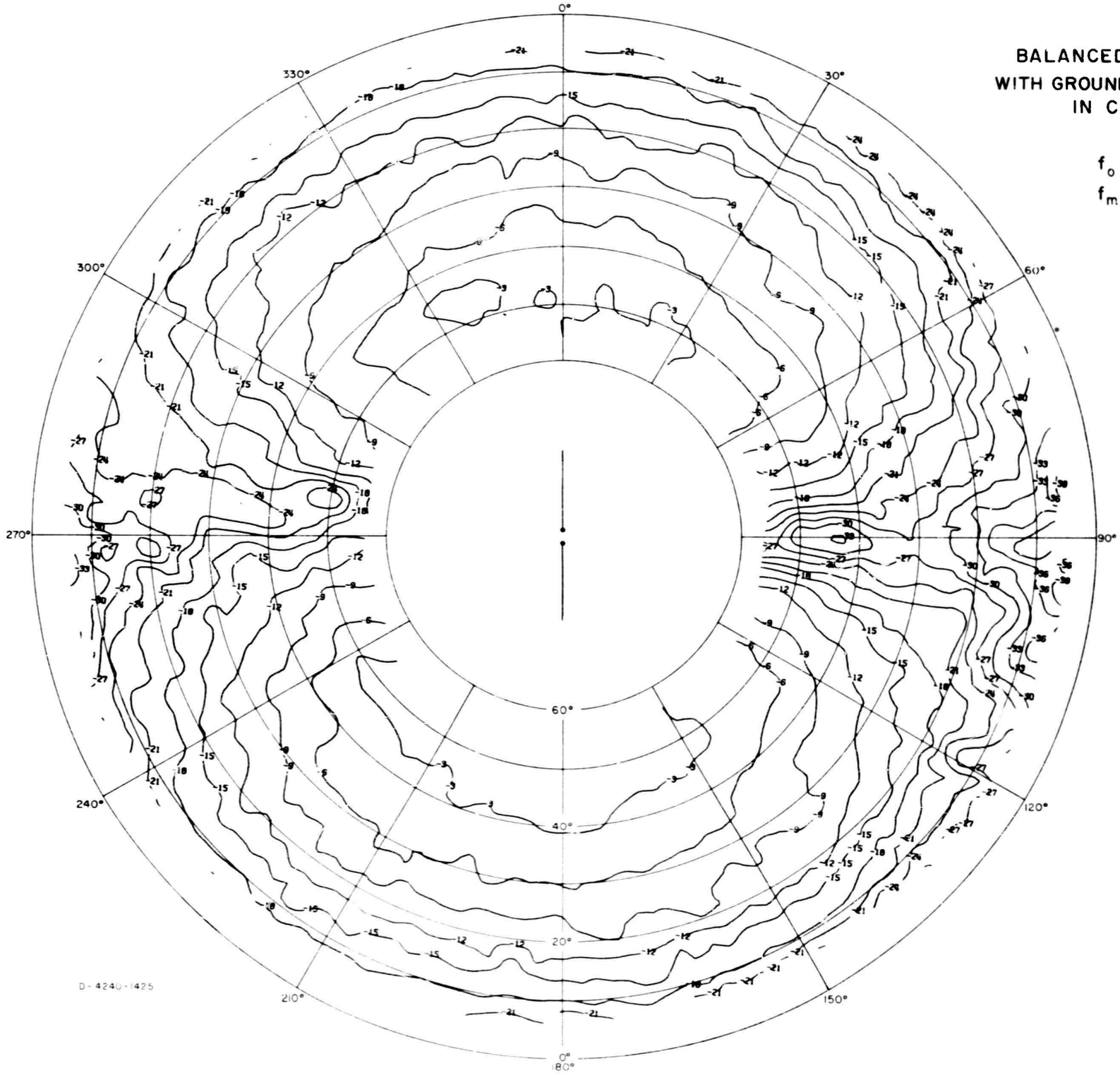

BALANCED DIPOLE
WITH GROUND SCREEN
IN CLEARING
$h_a = 16.4'$
$f_o = 15$ Mc/s
$f_m = 15$ Mc/s
E_θ

D-4240-1425

FIG. A-82

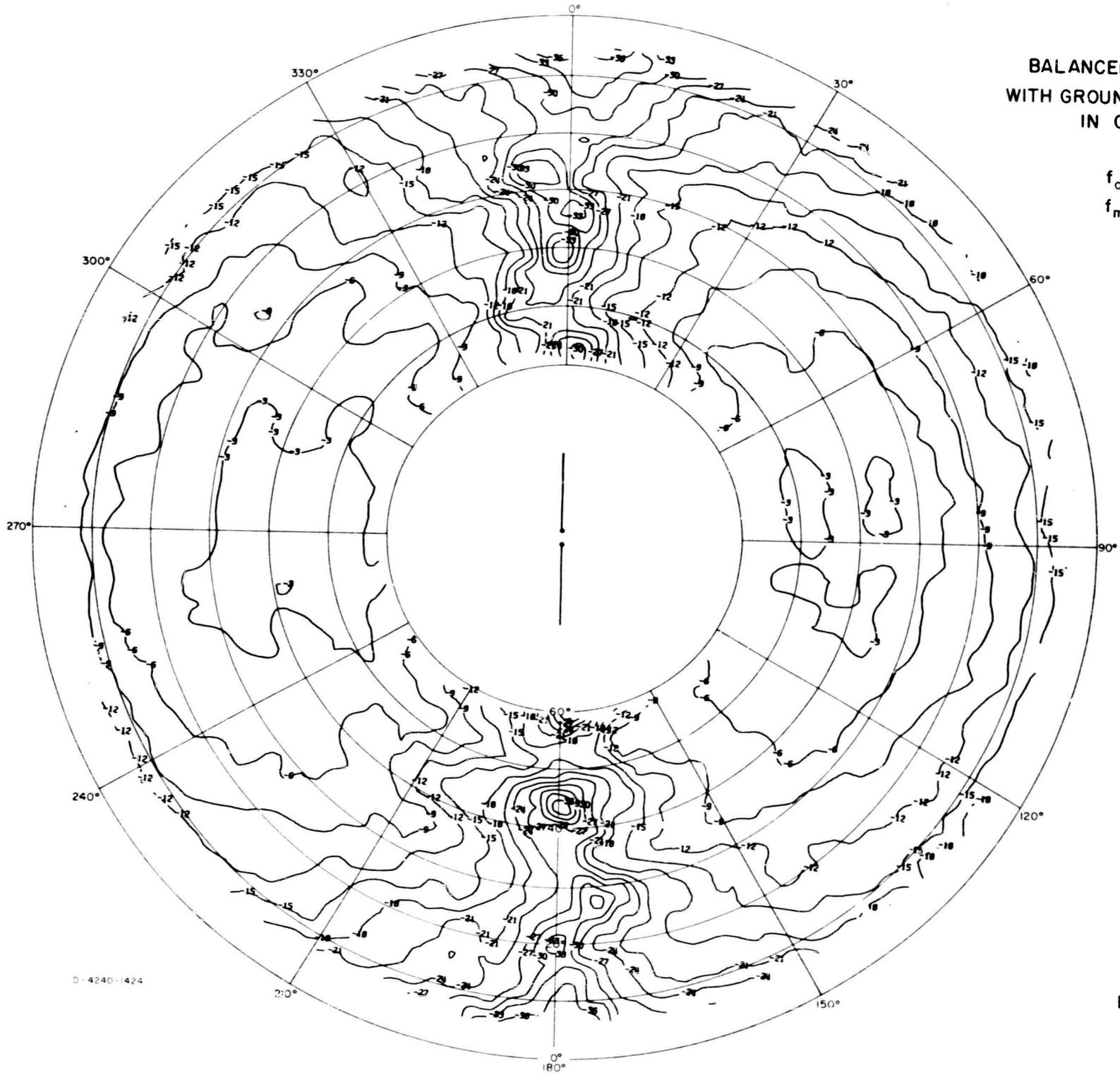

BALANCED DIPOLE
WITH GROUND SCREEN
IN CLEARING
$h_a = 164'$
$f_o = 15$ Mc/s
$f_m = 15$ Mc/s
E_ϕ

FIG. A-83

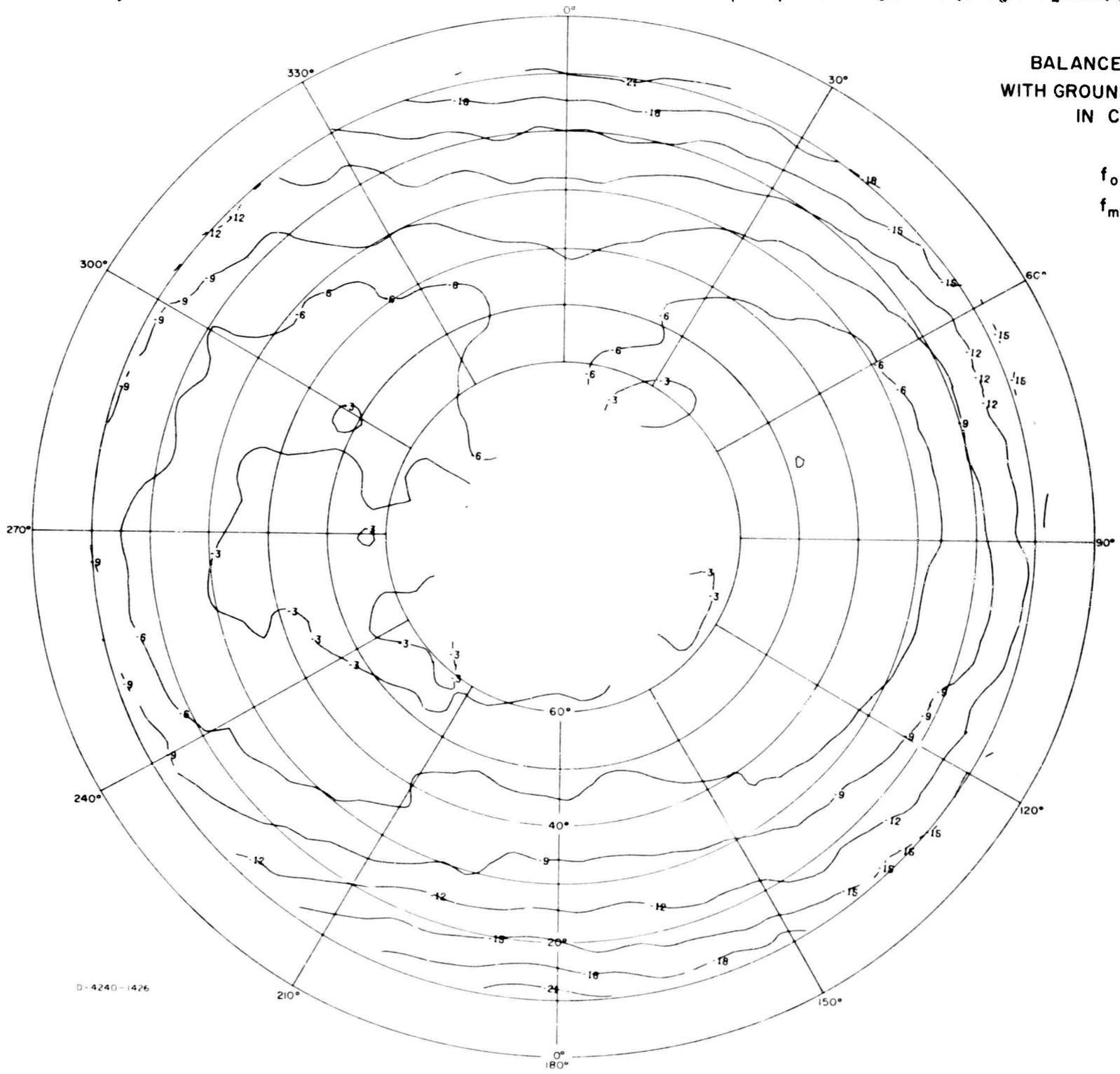

BALANCED DIPOLE
WITH GROUND SCREEN
IN CLEARING
$h_a = 16.4'$
$f_o = 15$ Mc/s
$f_m = 15$ Mc/s
POWER

FIG. A-84

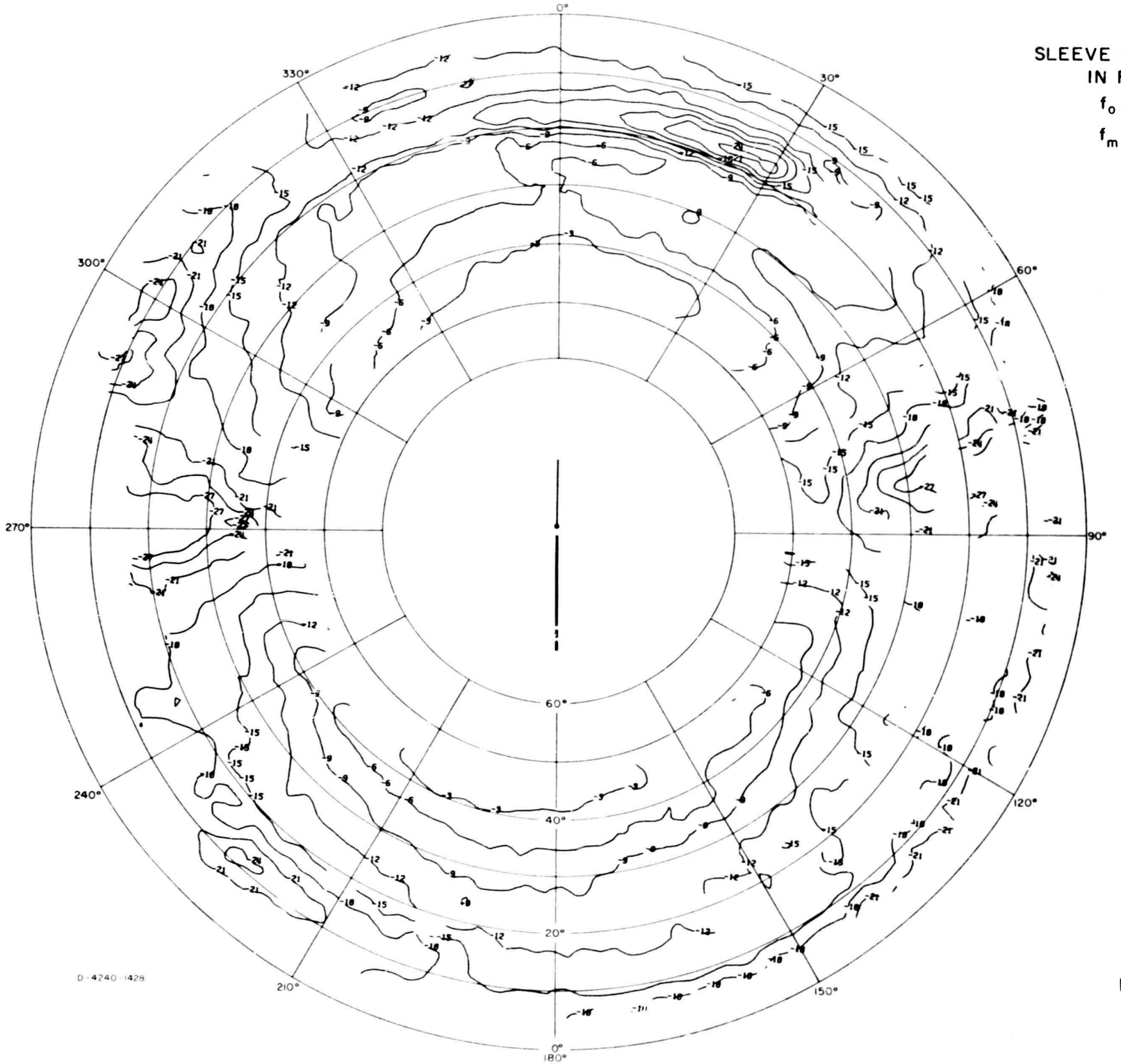

SLEEVE DIPOLE
IN FOLIAGE
f_o = 6 Mc/s
f_m = 6 Mc/s
E_θ

FIG. A-85

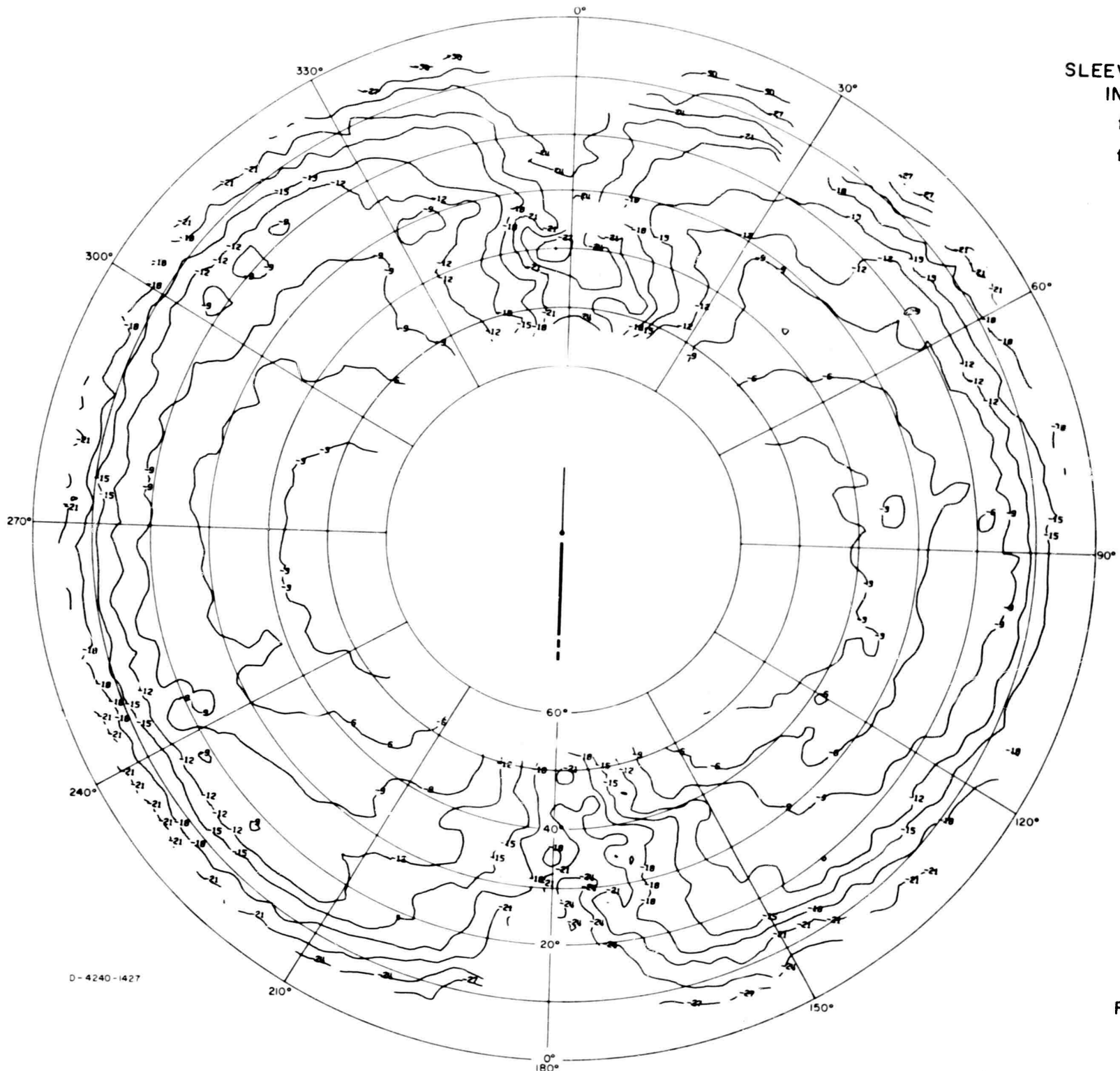

SLEEVE DIPOLE
IN FOLIAGE
f_o = 6 Mc/s
f_m = 6 Mc/s
E_ϕ

FIG. A-86

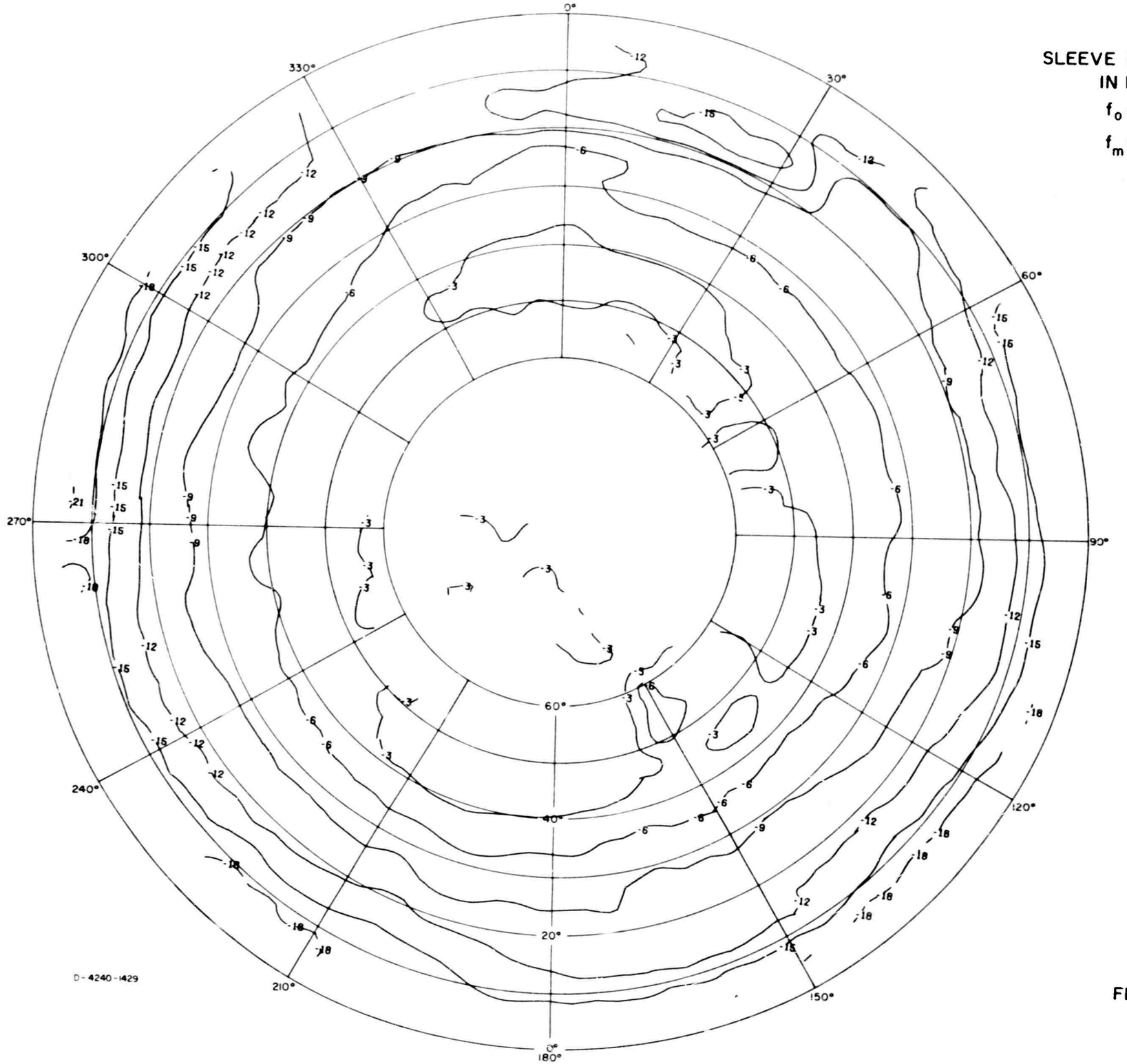

SLEEVE DIPOLE
IN FOLIAGE
f_0 = 6 Mc/s
f_m = 6 Mc/s
POWER

FIG. A-87

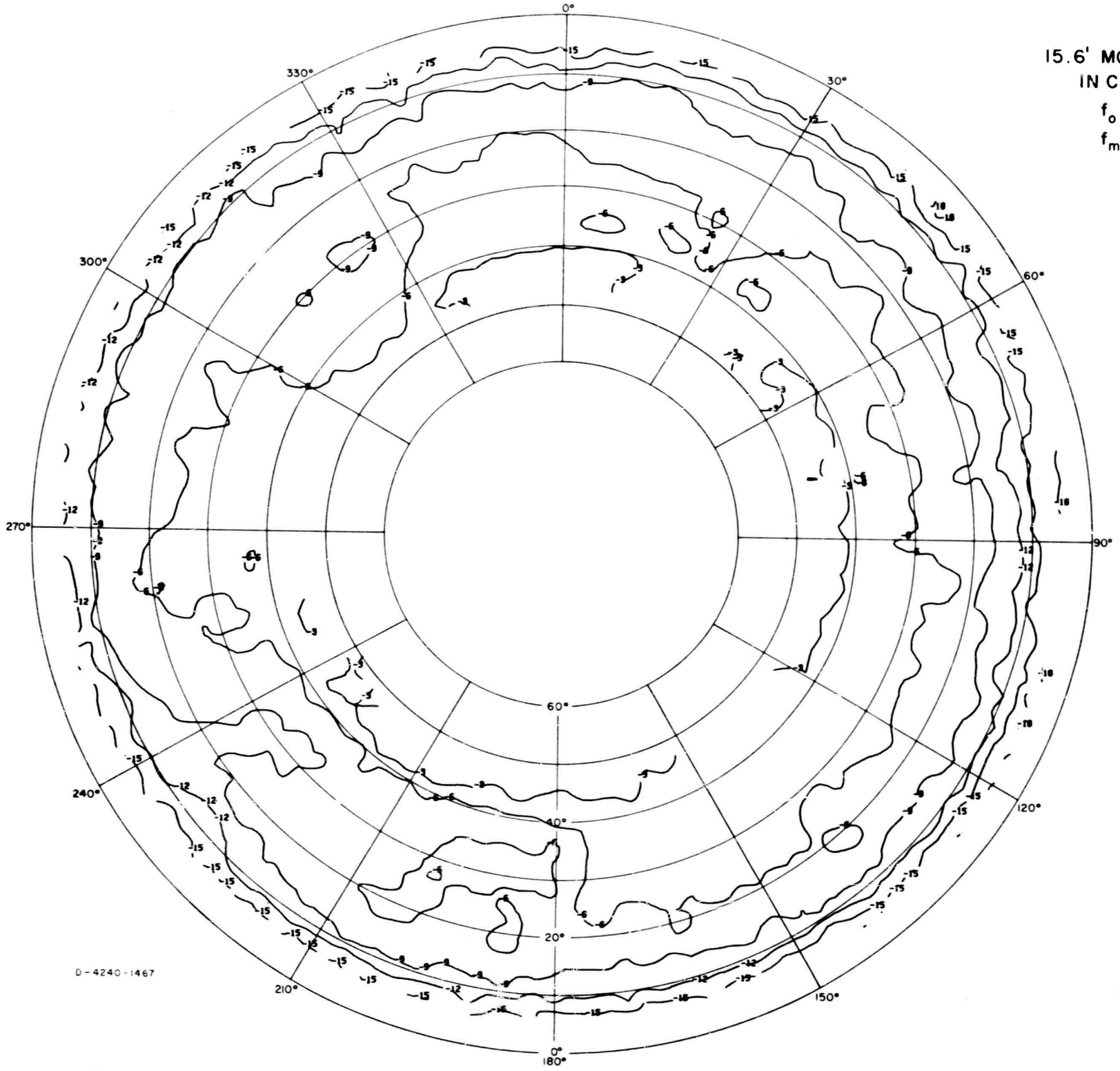

15.6' MONOPOLE
IN CLEARING
f_o = 6 Mc/s
f_m = 6 Mc/s
E_θ

FIG. A-88

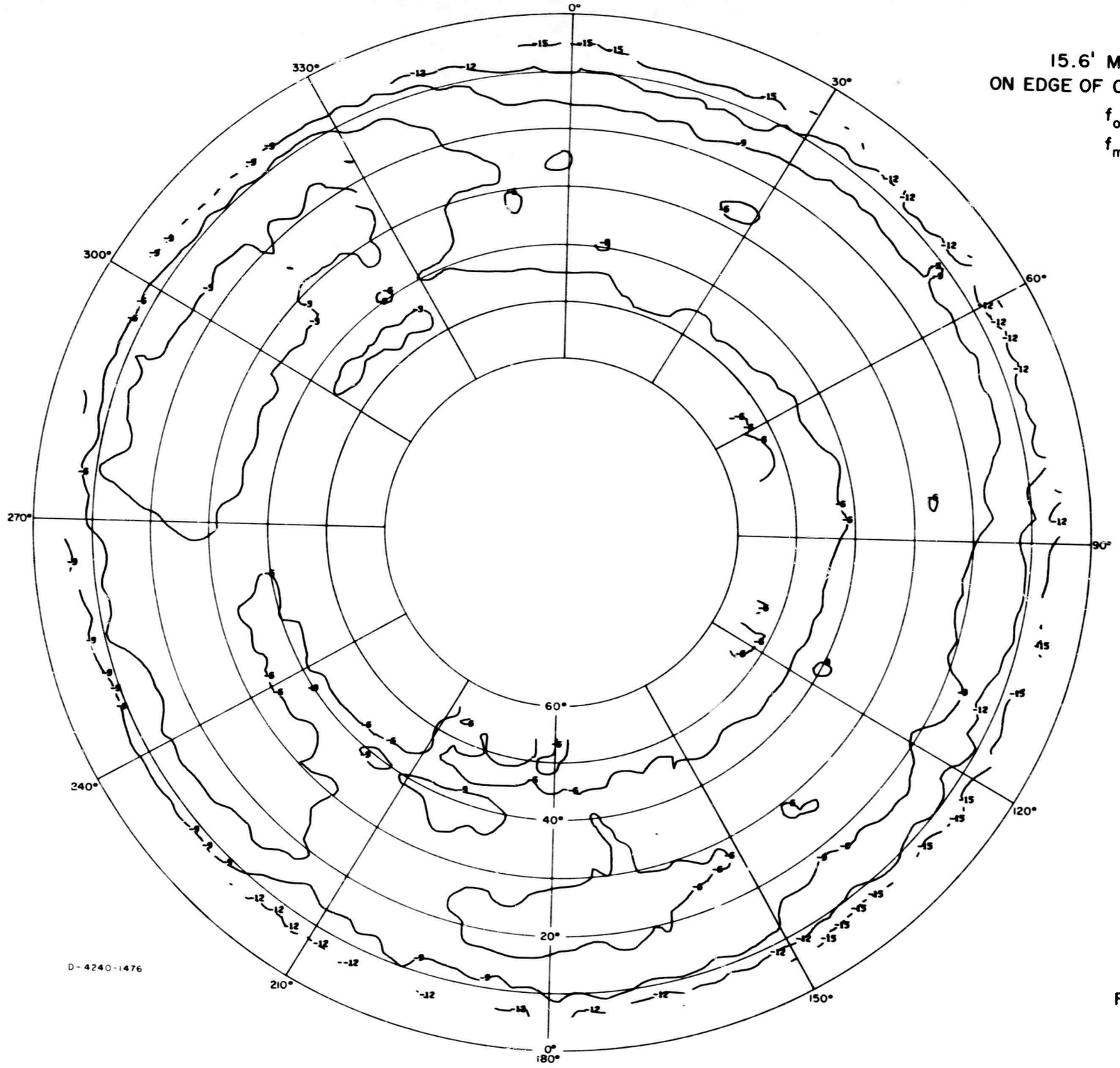

15.6' MONOPOLE
ON EDGE OF CLEARING
f_o = 6 Mc/s
f_m = 4 Mc/s
E_θ

FIG. A-89

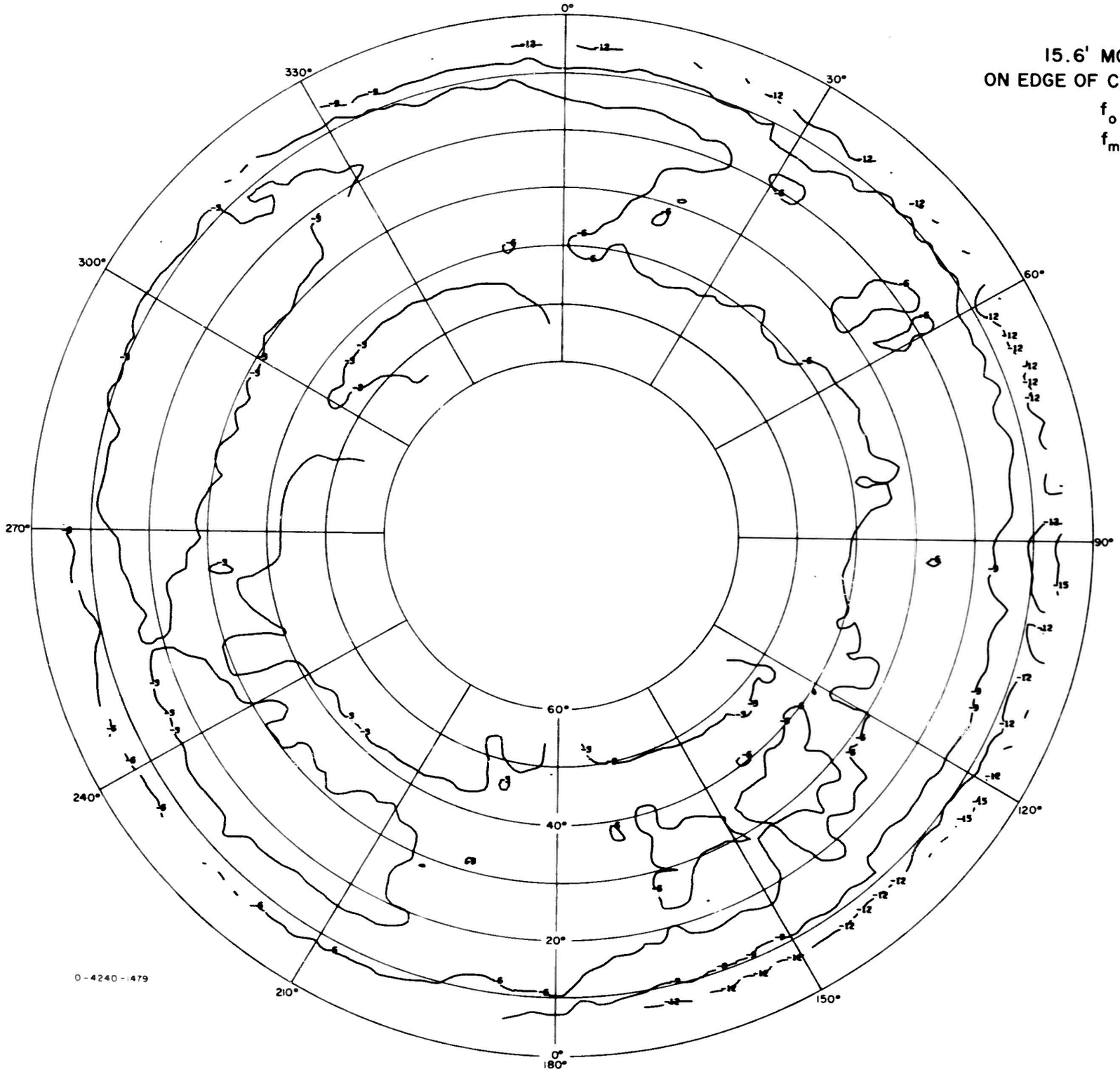

15.6' MONOPOLE
ON EDGE OF CLEARING
f_o = 6 Mc/s
f_m = 6 Mc/s
E_θ

FIG. A-90

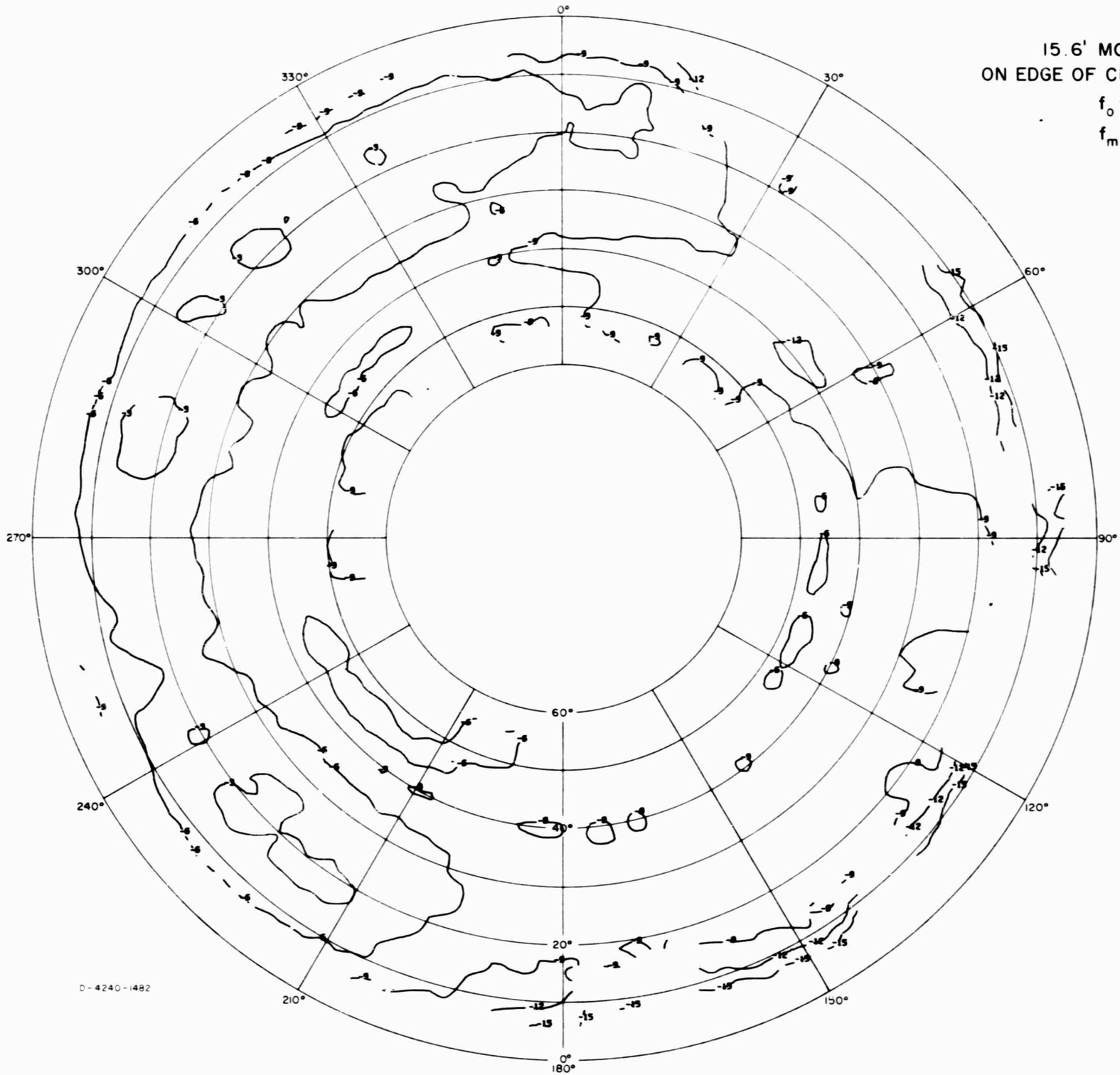

15.6' MONOPOLE
ON EDGE OF CLEARING
f_0 = 6 Mc/s
f_m = 8 Mc/s
E_θ

FIG. A-91

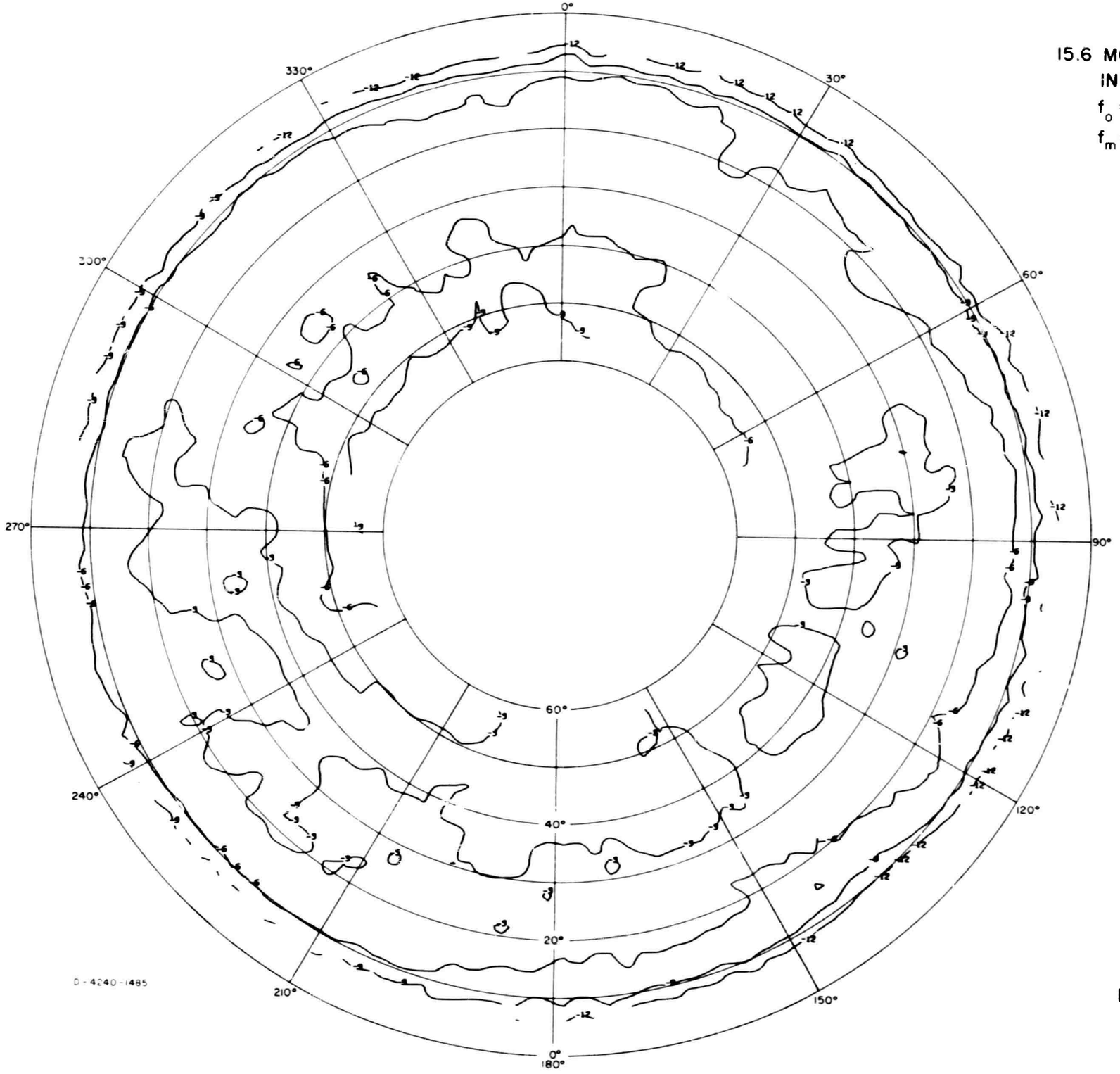

15.6 MONOPOLE
IN FOLIAGE
f_o = 6 Mc/s
f_m = 4 Mc/s
E_θ

FIG. A-92

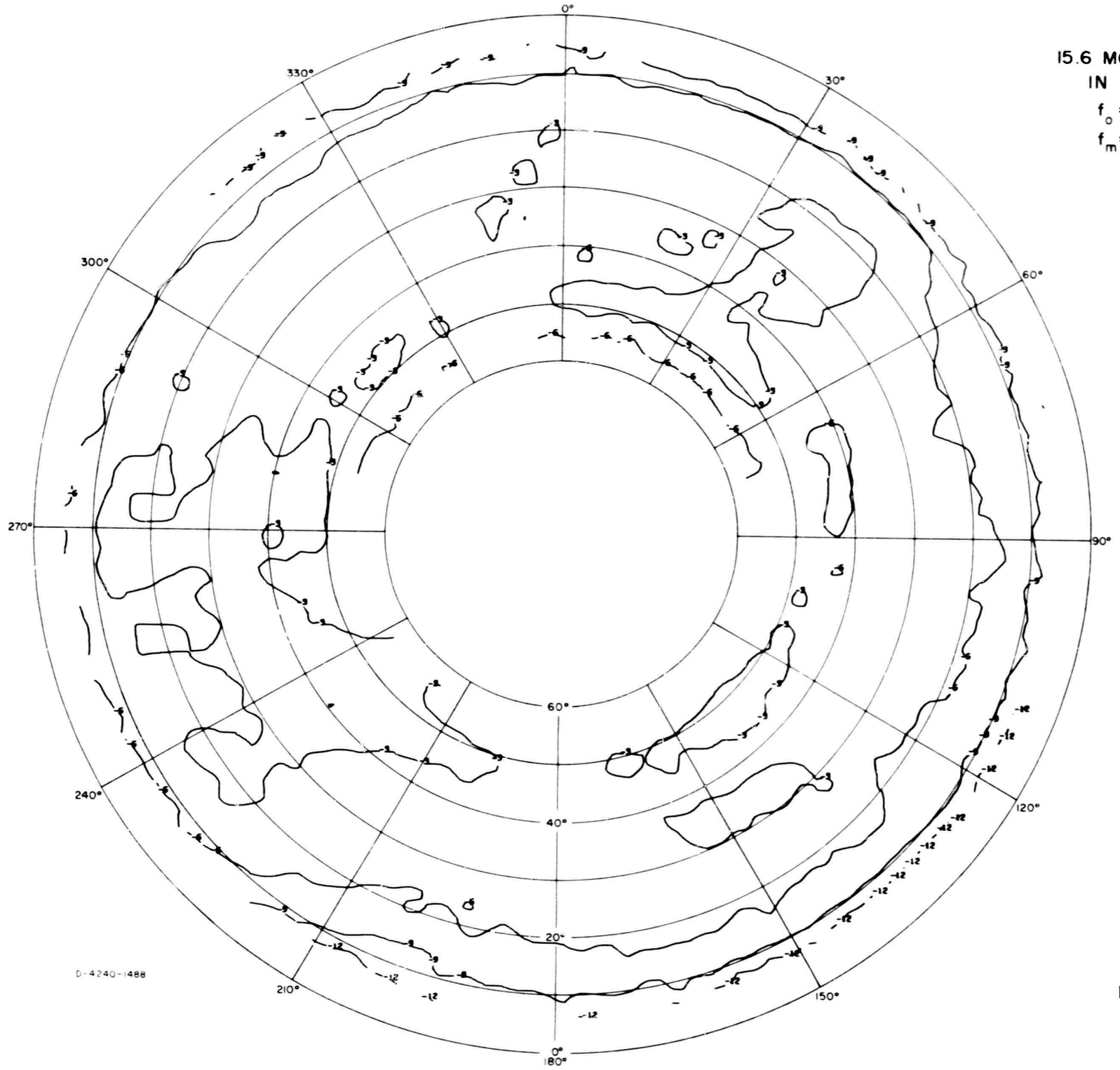

15.6 MONOPOLE
IN FOLIAGE
f_o = 6 Mc/s
f_m = 6 Mc/s
E_θ

FIG. A-93

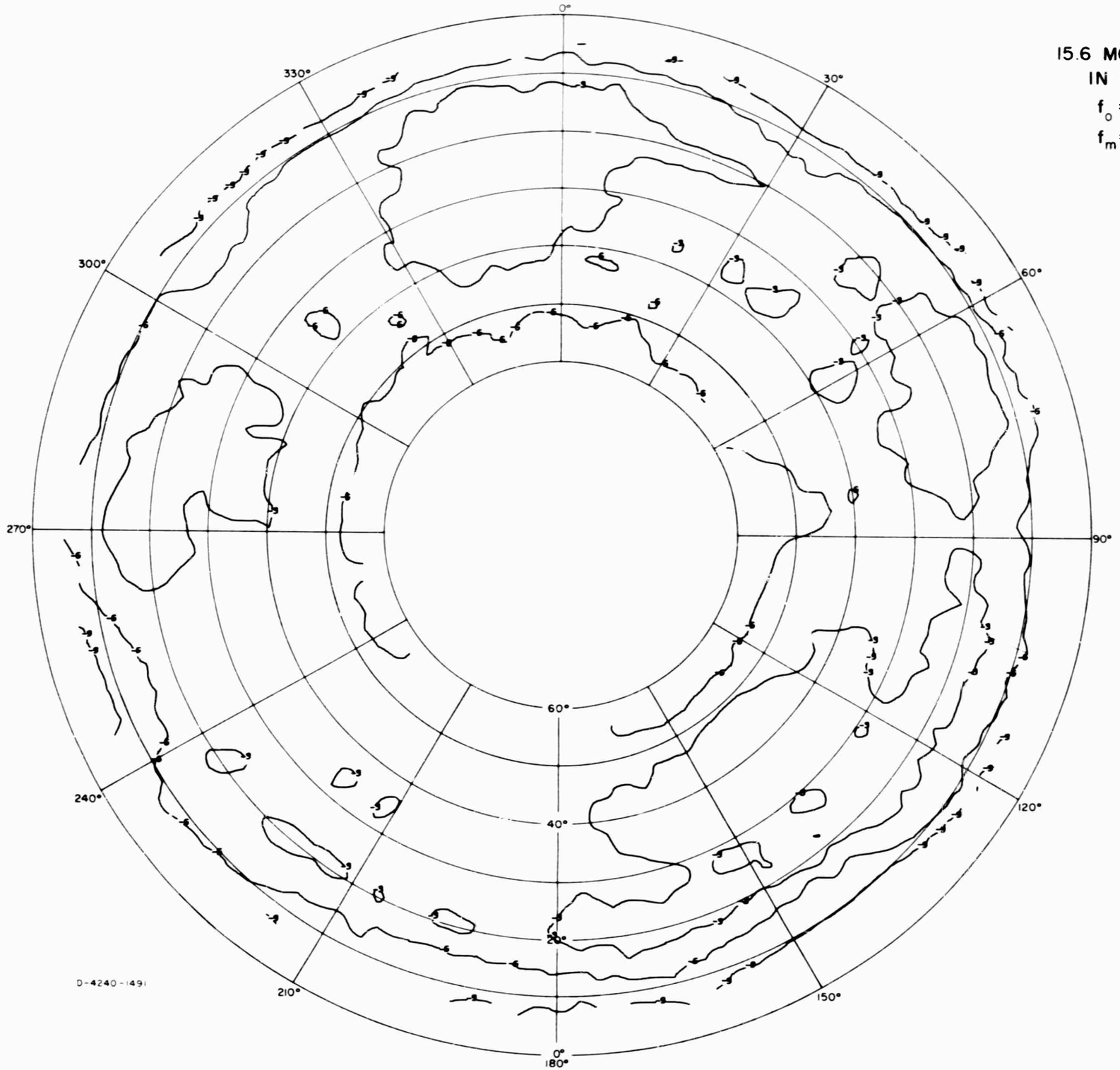

15.6 MONOPOLE
IN FOLIAGE
f_o = 6 Mc/s
f_m = 8 Mc/s
E_θ

FIG. A-94

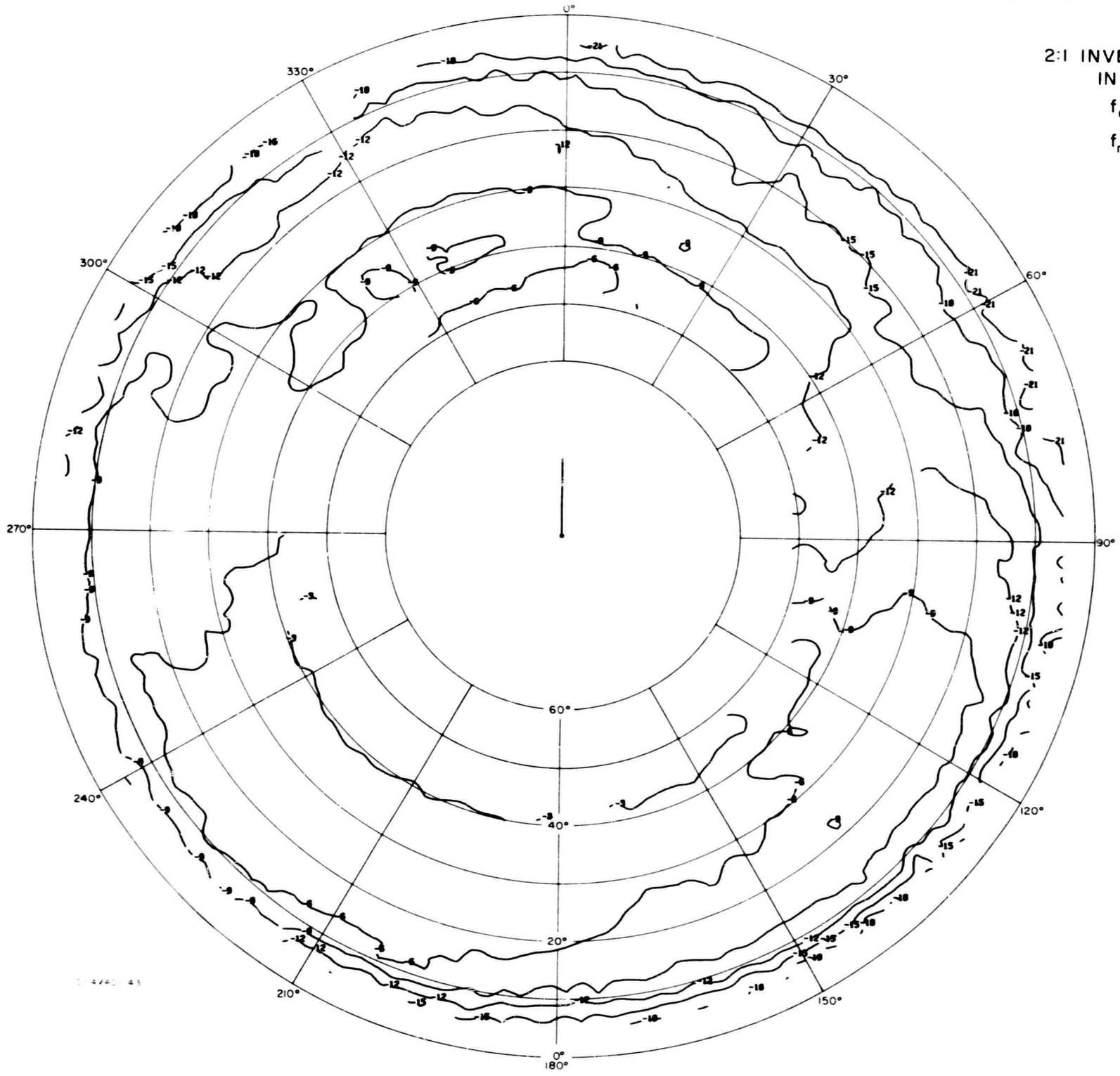

2:1 INVERTED-L
IN FOLIAGE
f_0 = 6 Mc/s
f_m = 3 Mc/s
E_θ

FIG. A-95

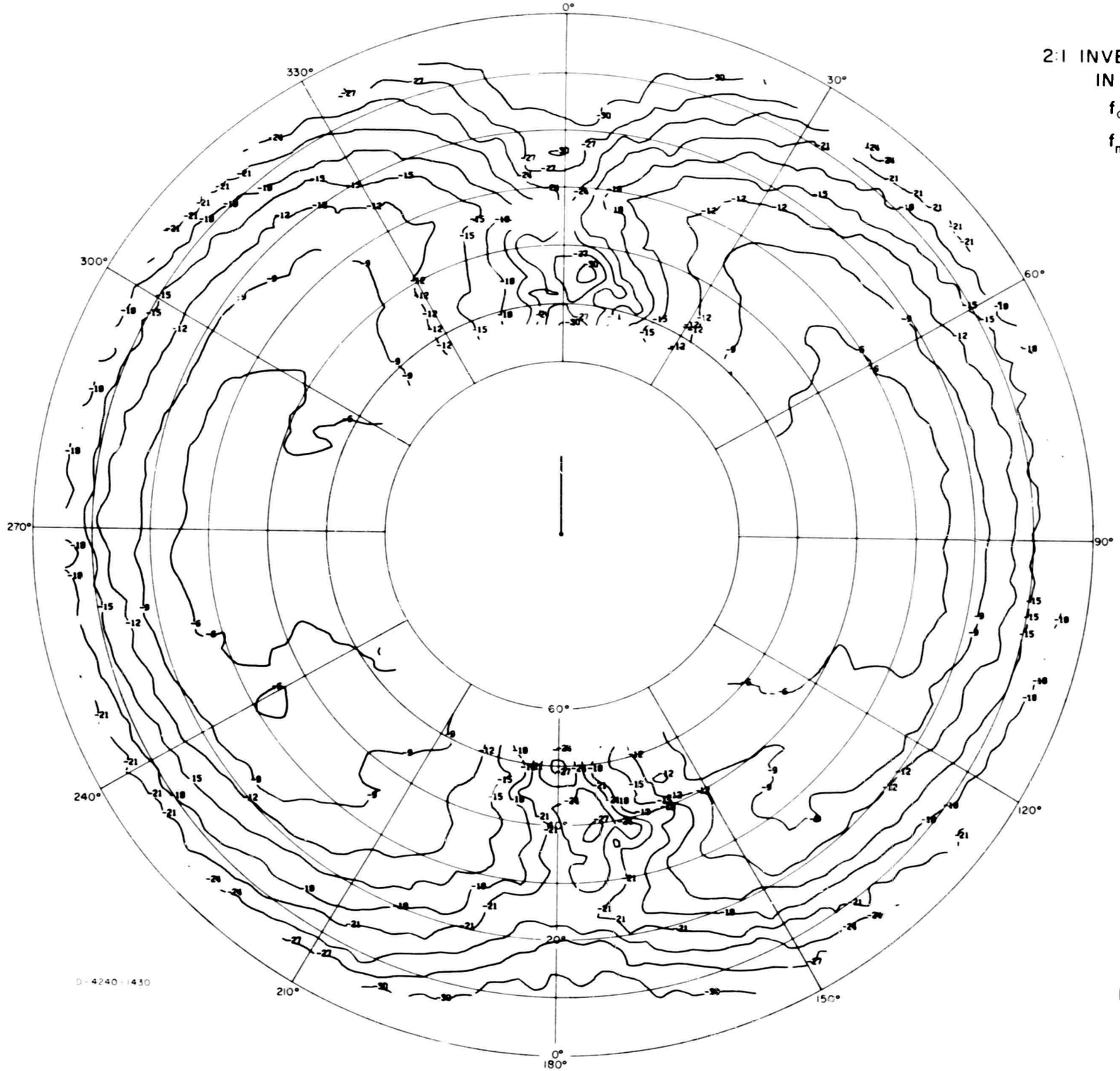

2:1 INVERTED-L
IN FOLIAGE
f_0 = 6 Mc/s
f_m = 3 Mc/s
E_ϕ

FIG. A-96

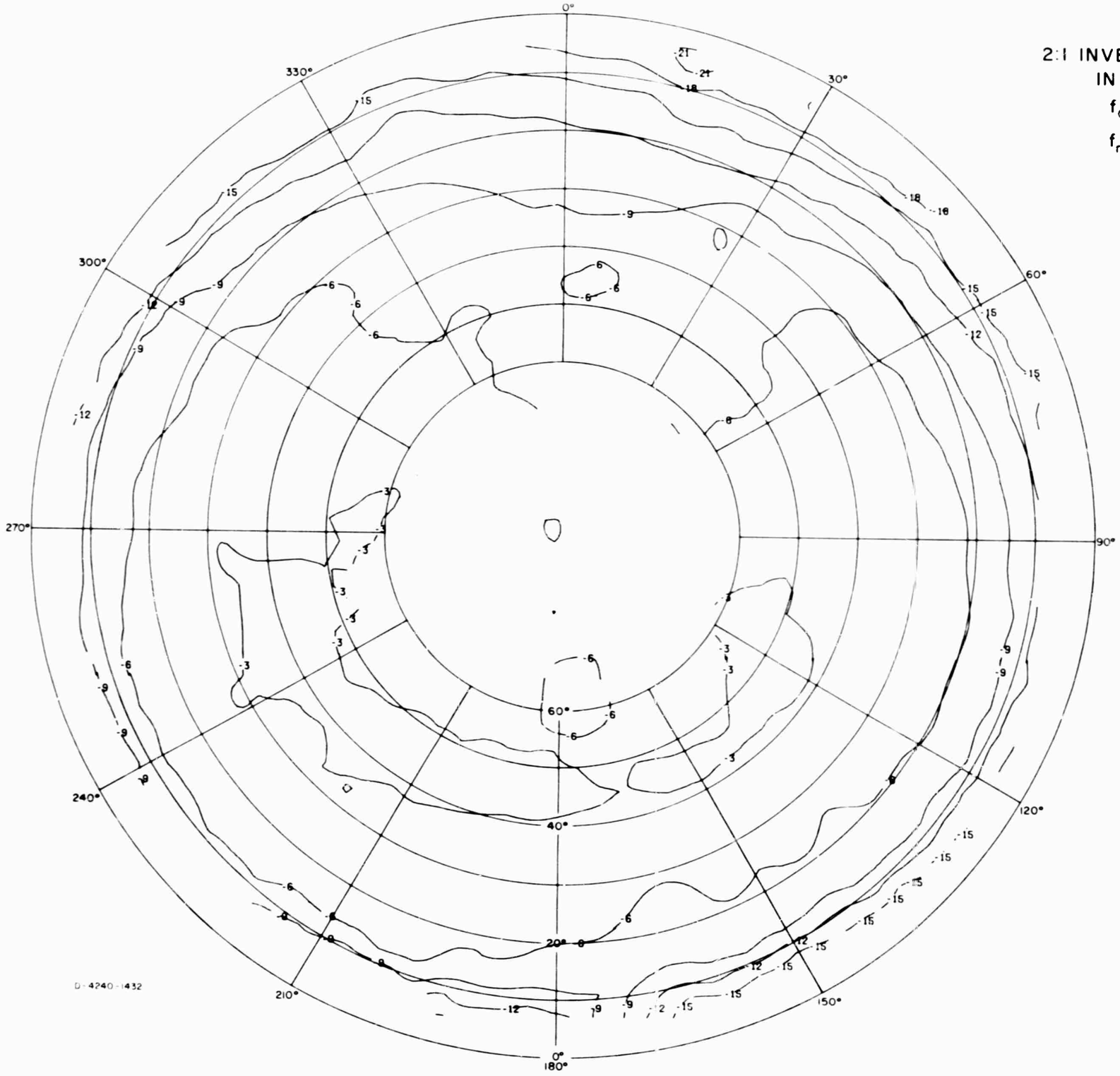

2:1 INVERTED-L
IN FOLIAGE
f_0 = 6 Mc/s
f_m = 3 Mc/s
POWER

FIG. A-97

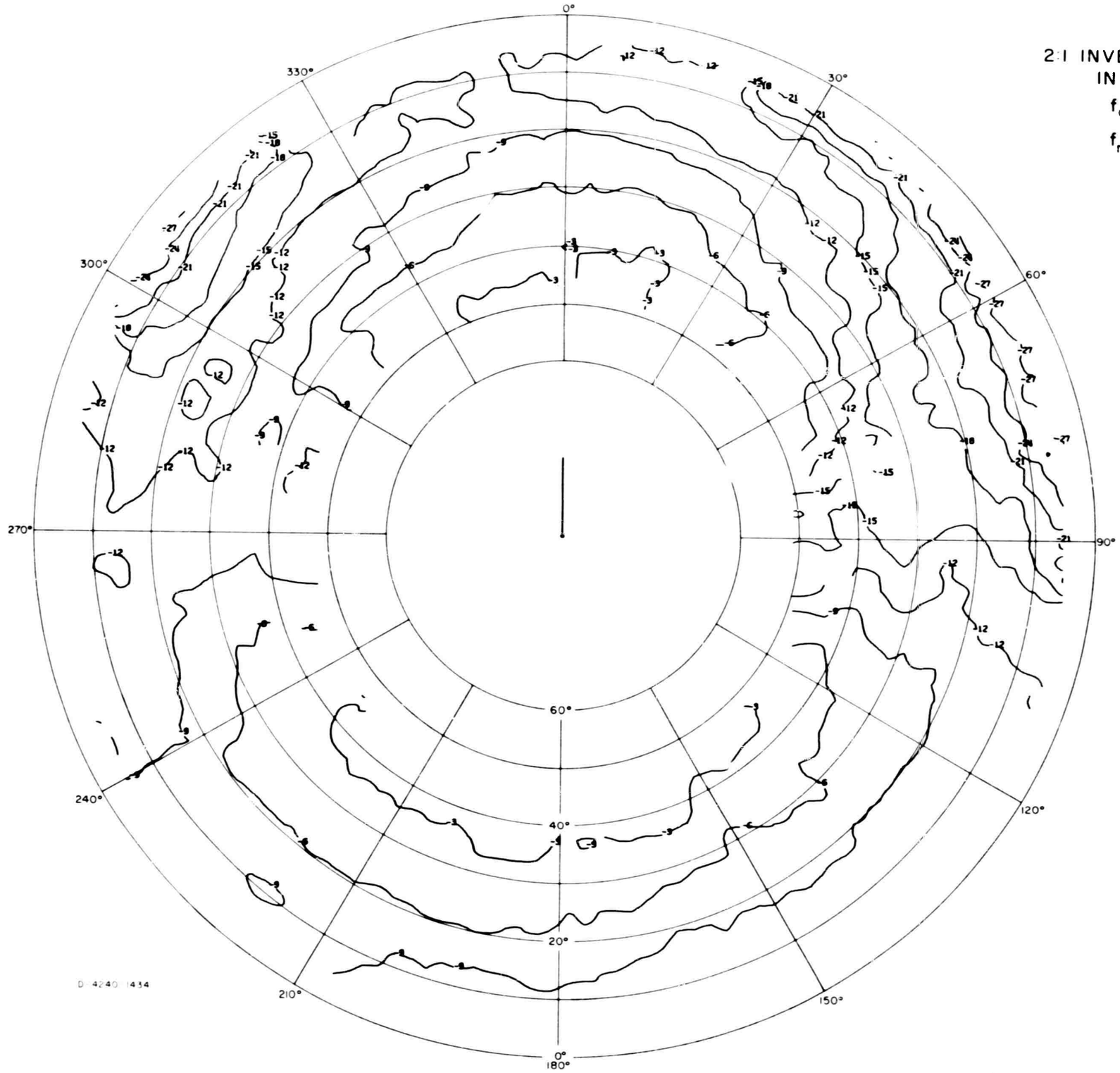

2-1 INVERTED-L
IN FOLIAGE
f_o = 6 Mc/s
f_m = 4 Mc/s
E_θ

FIG. A-98

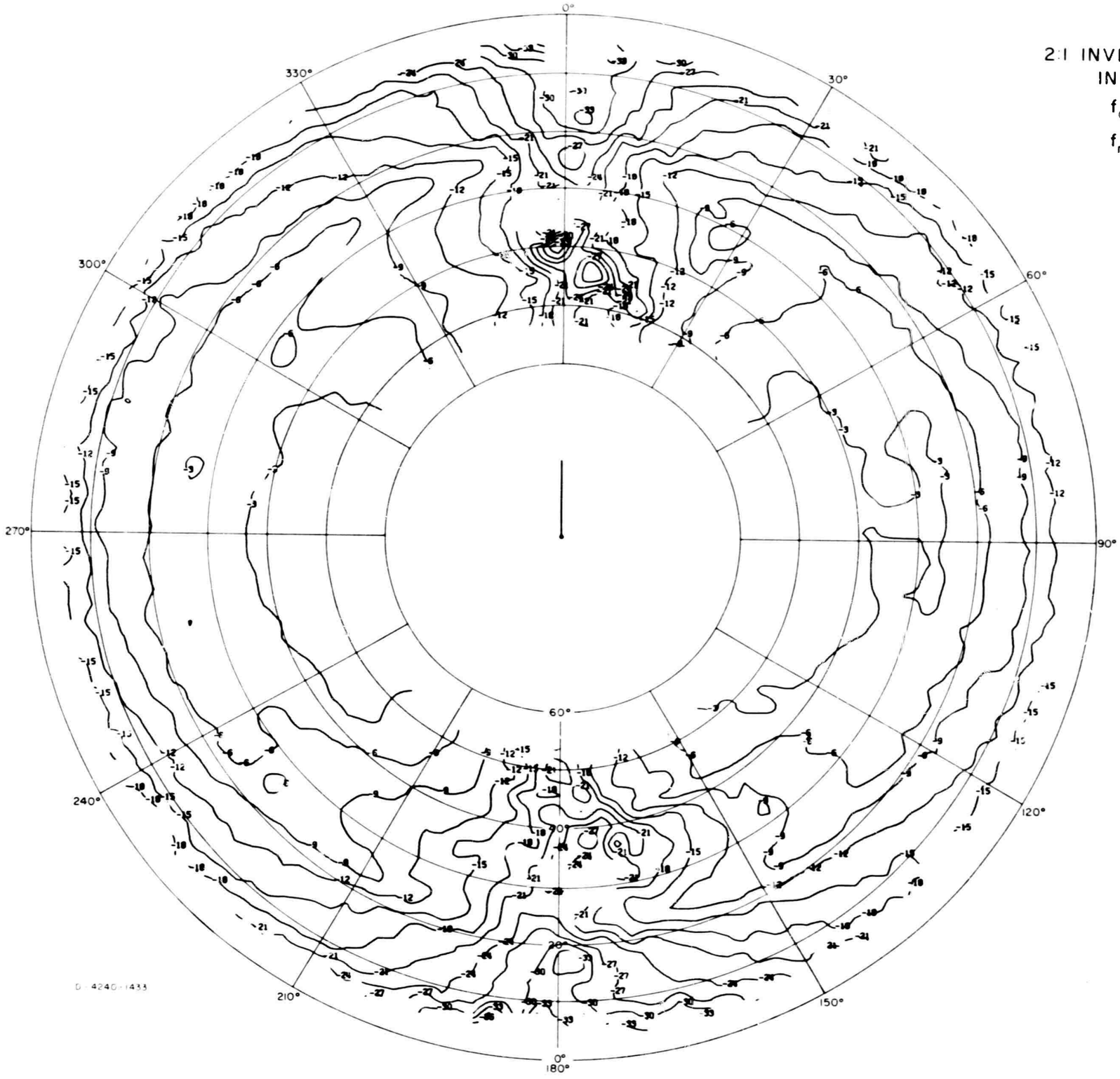

2:1 INVERTED-L
IN FOLIAGE
f_0 = 6 Mc/s
f_m = 4 Mc/s
E_ϕ

FIG. A-99

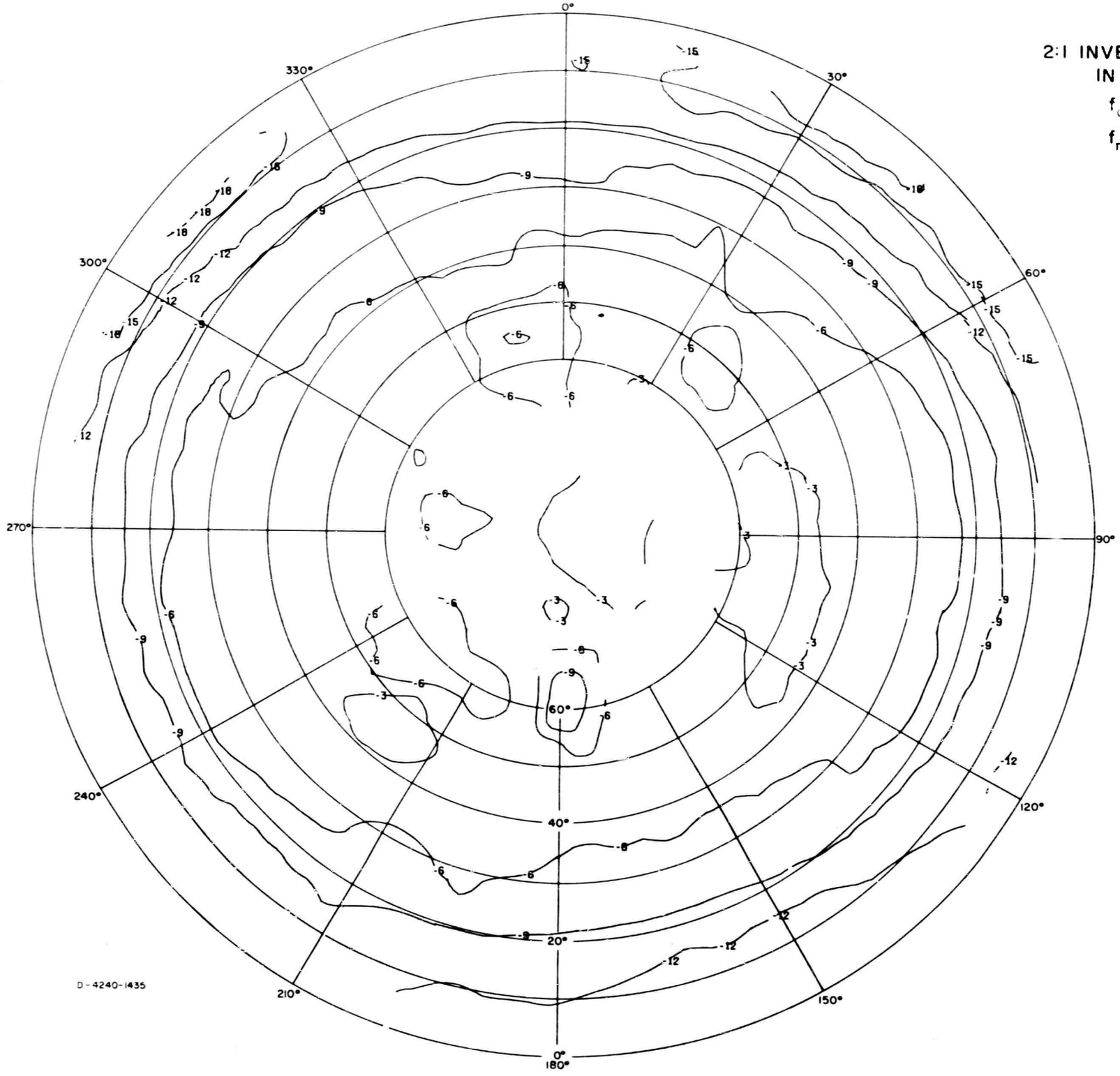

2:1 INVERTED-L
IN FOLIAGE
f_o = 6 Mc/s
f_m = 4 Mc/s
POWER

FIG. A-100

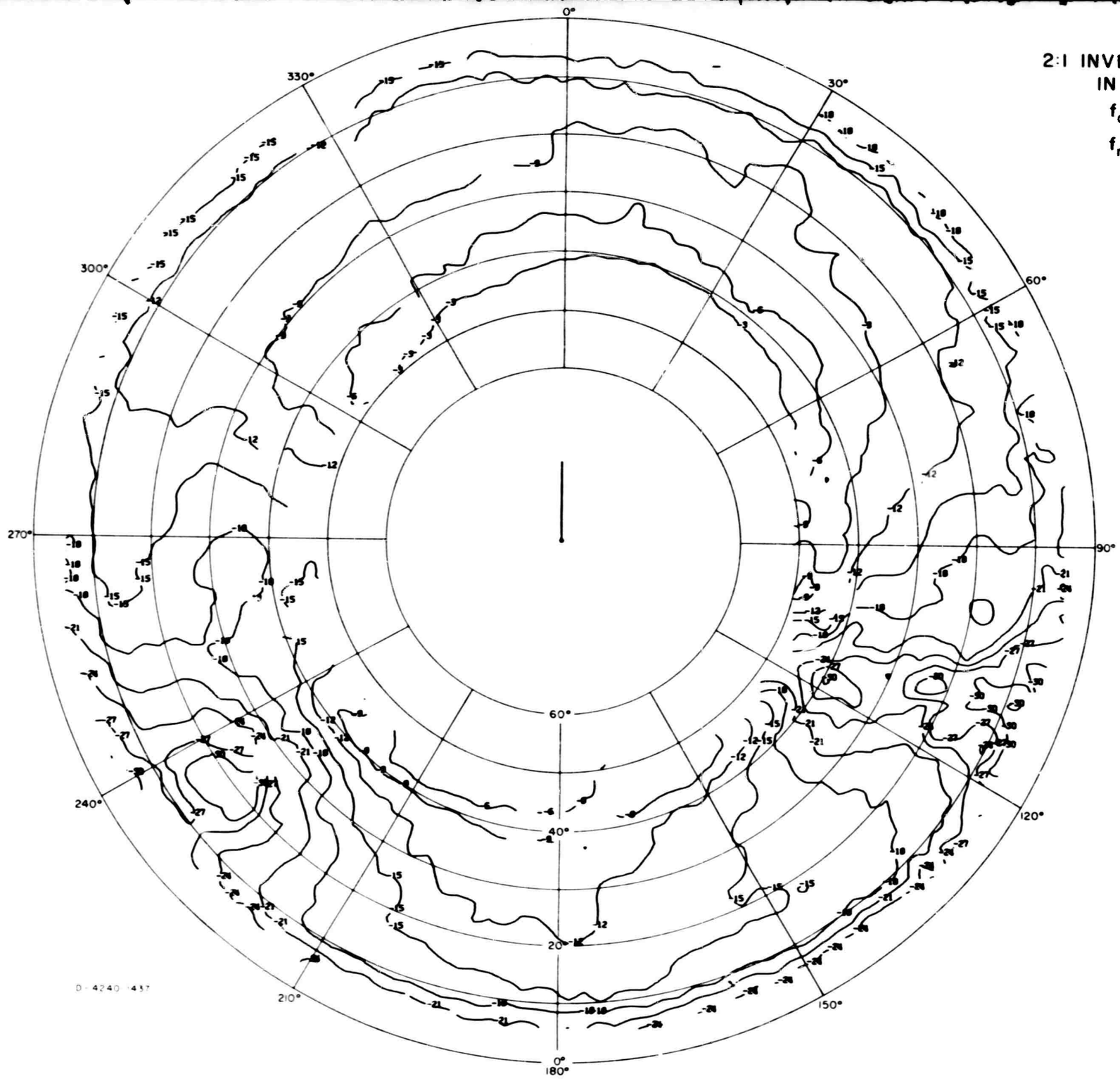

2:1 INVERTED-L
IN FOLIAGE
f_o = 6 Mc/s
f_m = 6 Mc/s
E_θ

FIG. A-101

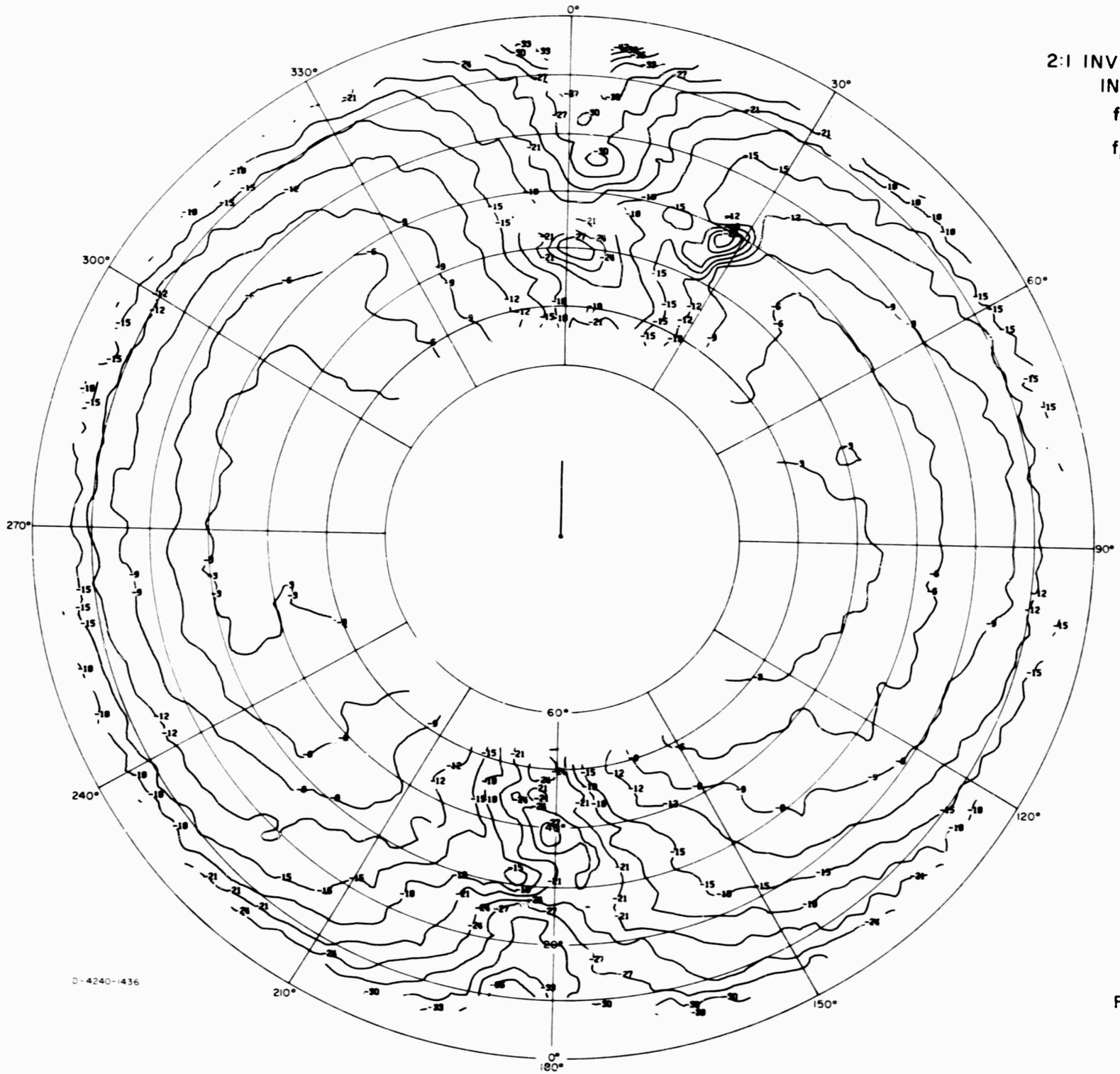

2:1 INVERTED-L
IN FOLIAGE
f_o = 6 Mc/s
f_m = 6 Mc/s
E_ϕ

FIG. A-102

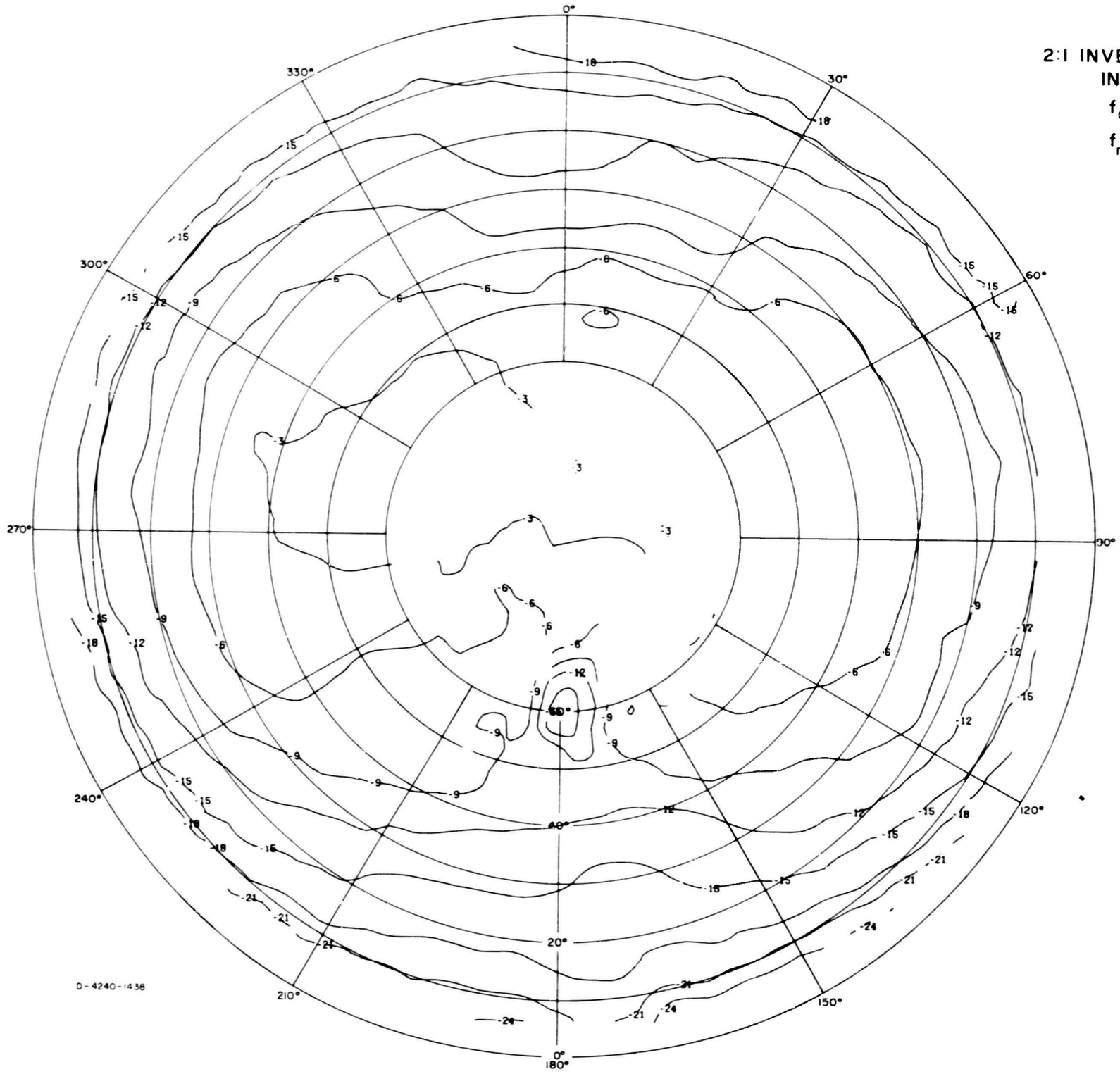

2:1 INVERTED-L
IN FOLIAGE
f_o = 6 Mc/s
f_m = 6 Mc/s
POWER

FIG. A-103

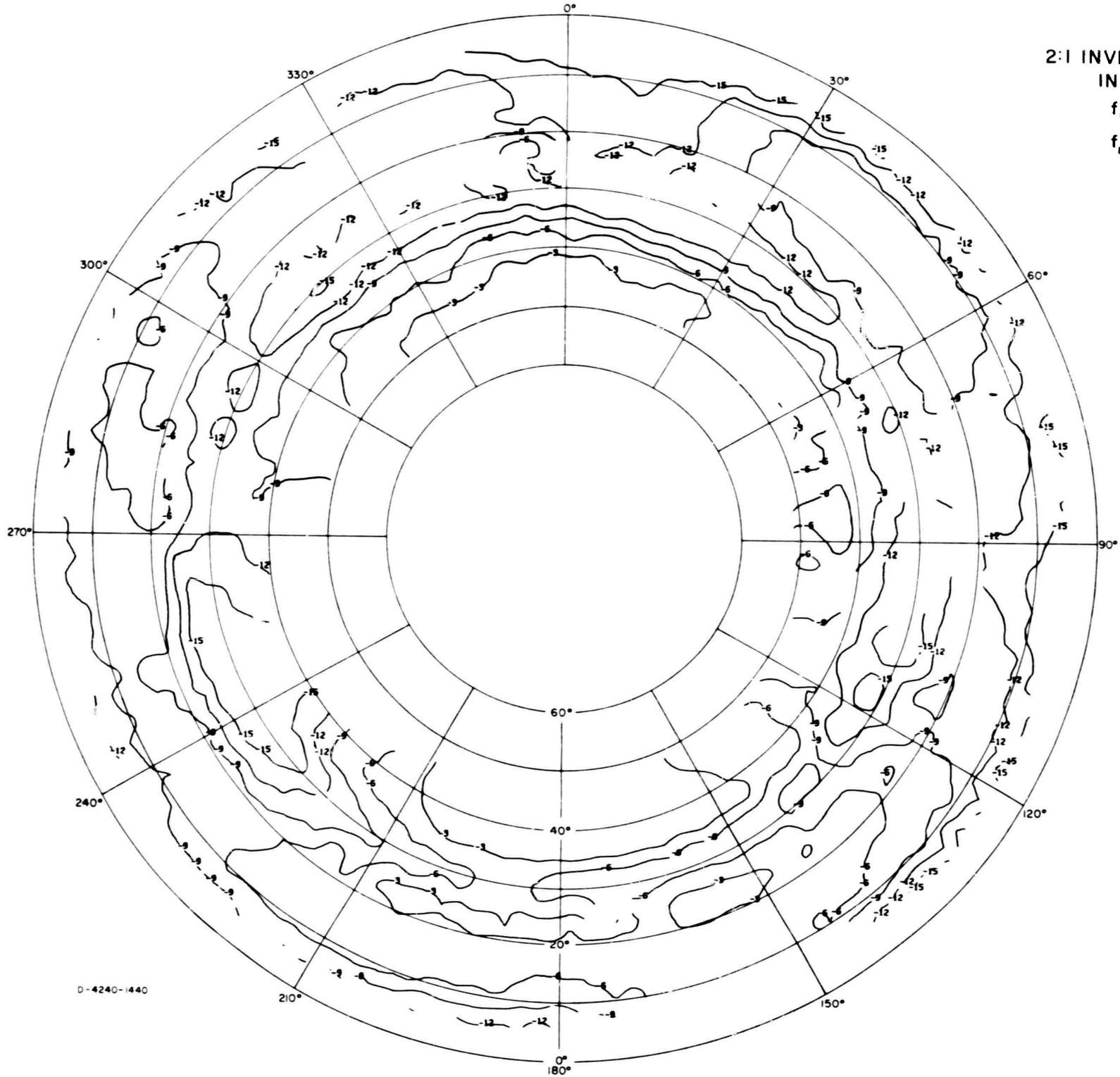

2:1 INVERTED-L
IN FOLIAGE
f_o = 6 Mc/s
f_m = 8 Mc/s
E_θ

FIG. A-104

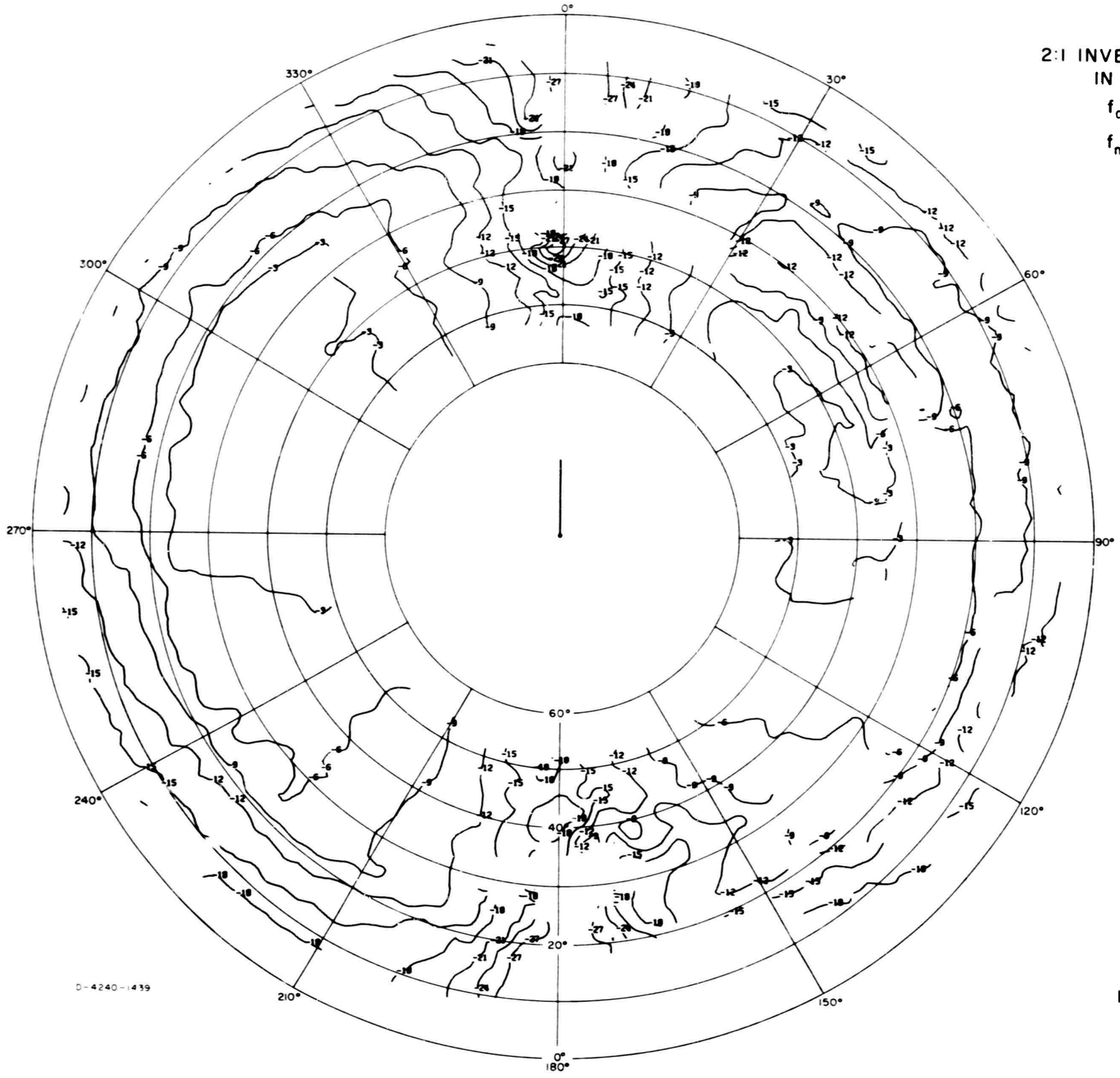

2:1 INVERTED-L
IN FOLIAGE
$f_o = 6$ Mc/s
$f_m = 8$ Mc/s
E_ϕ

FIG. A-105

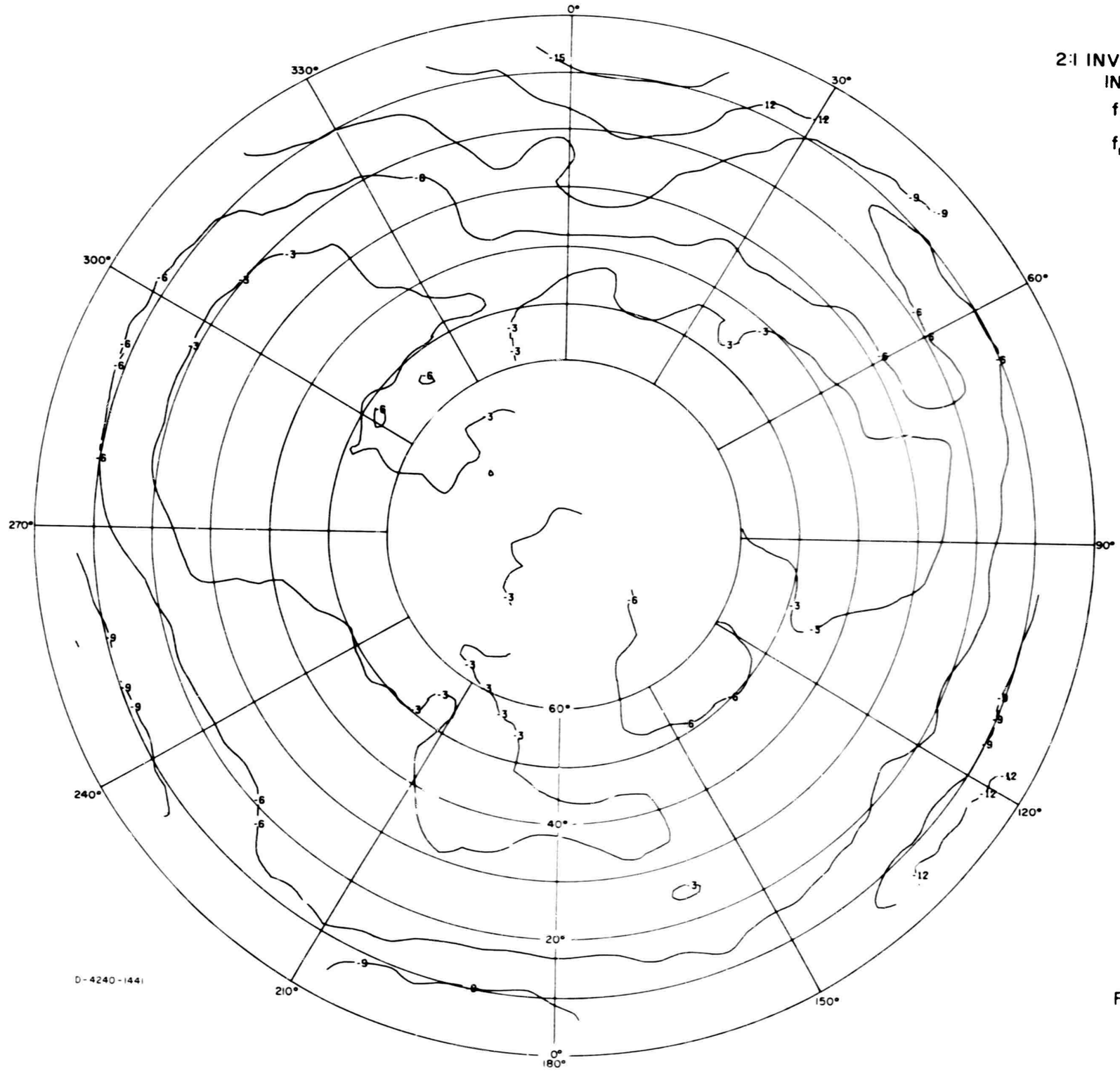

2:1 INVERTED-L
IN FOLIAGE
f_o = 6 Mc/s
f_m = 8 Mc/s
POWER

FIG. A-106

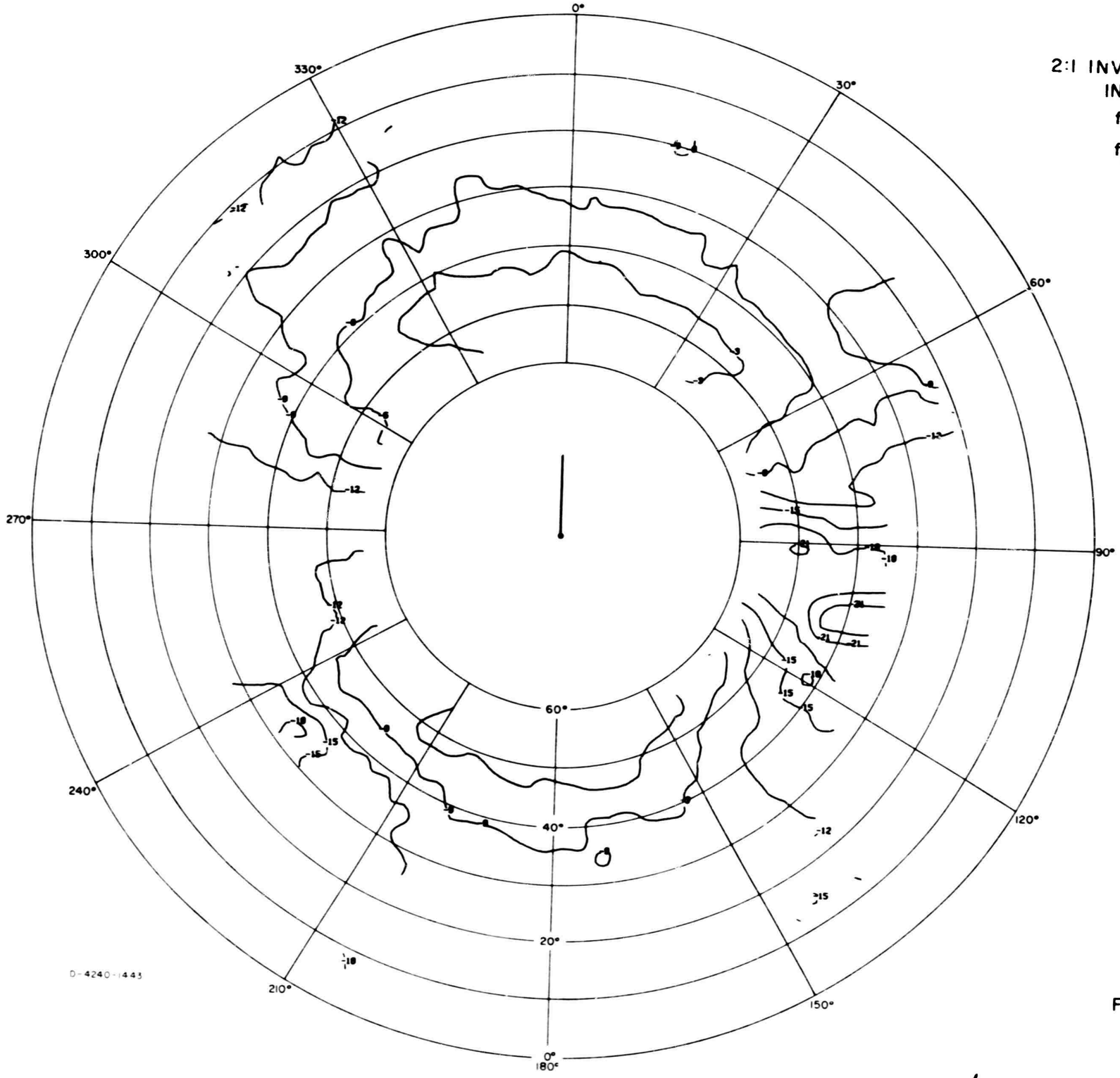

2:1 INVERTED-L
IN FOLIAGE
f_o = 8 Mc/s
f_m = 8 Mc/s
E_θ

FIG. A-107

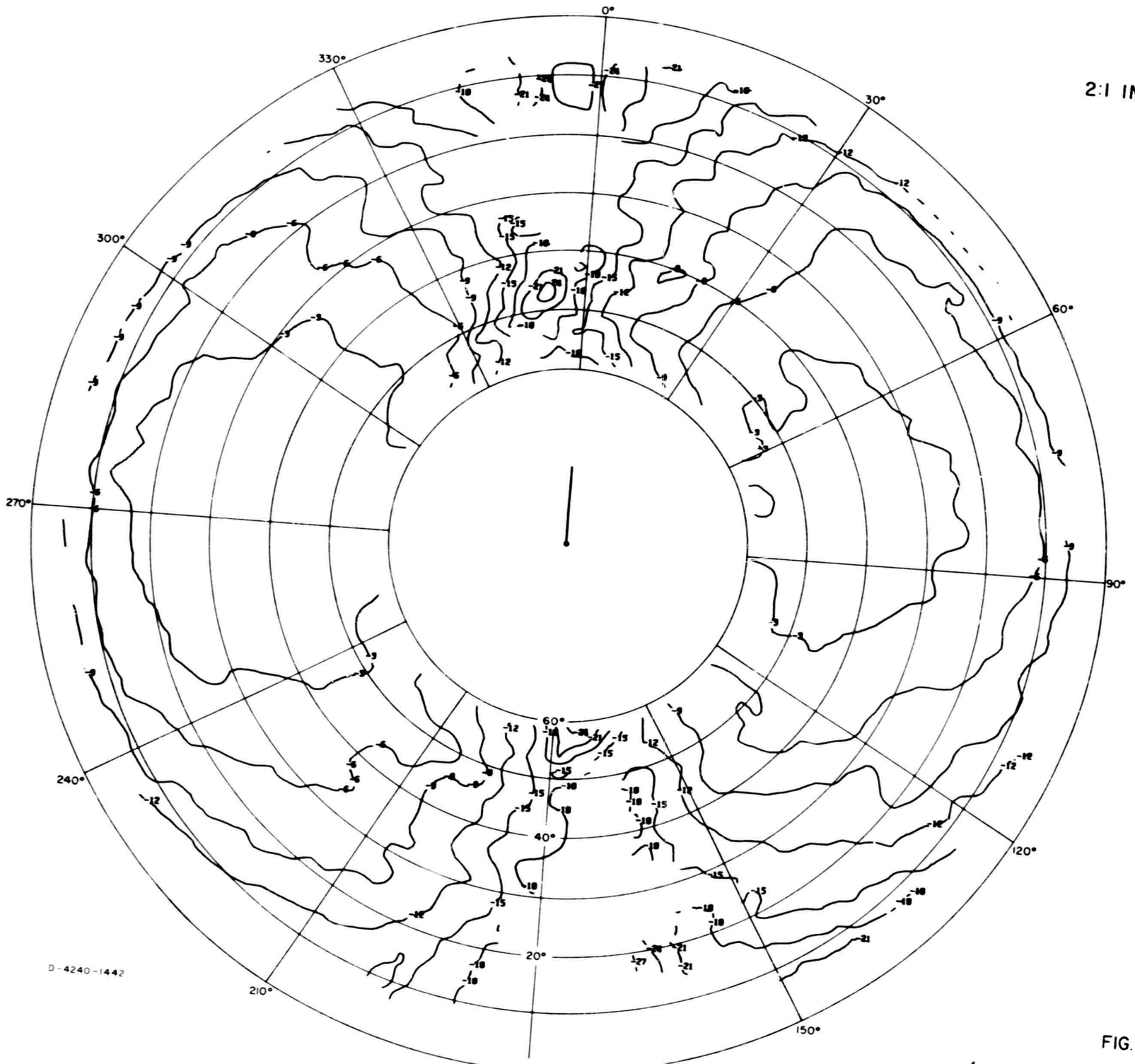

2:1 INVERTED-L
IN FOLIAGE
$f_o = 8$ Mc/s
$f_m = 8$ Mc/s
E_ϕ

FIG. A-108

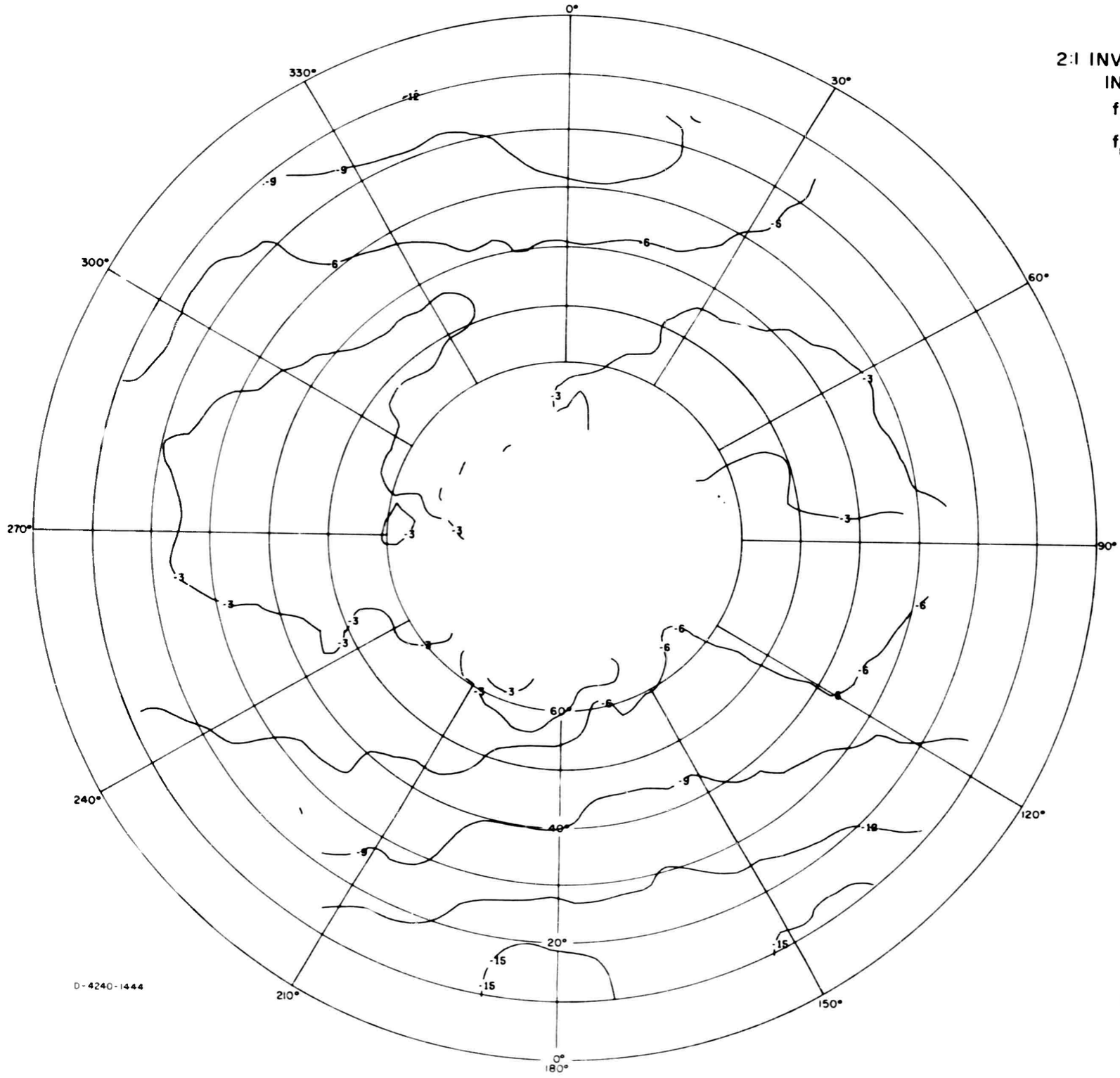

2:1 INVERTED-L
IN FOLIAGE
f_o = 8 Mc/s
f_m = 8 Mc/s
POWER

FIG. A-109

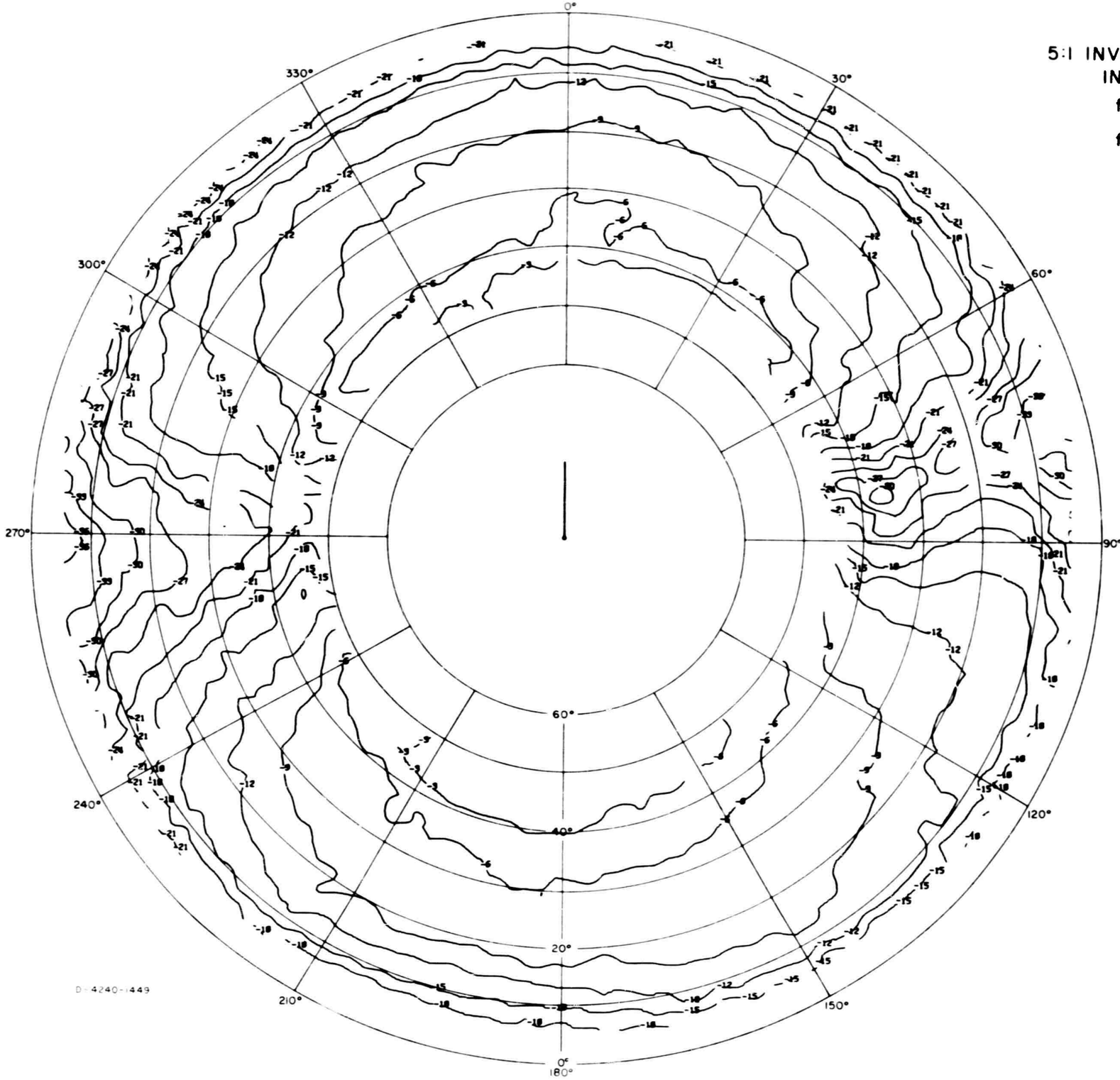

5:1 INVERTED-L
IN FOLIAGE
f_o = 6 Mc/s
f_m = 4 Mc/s
E_θ

FIG A-110

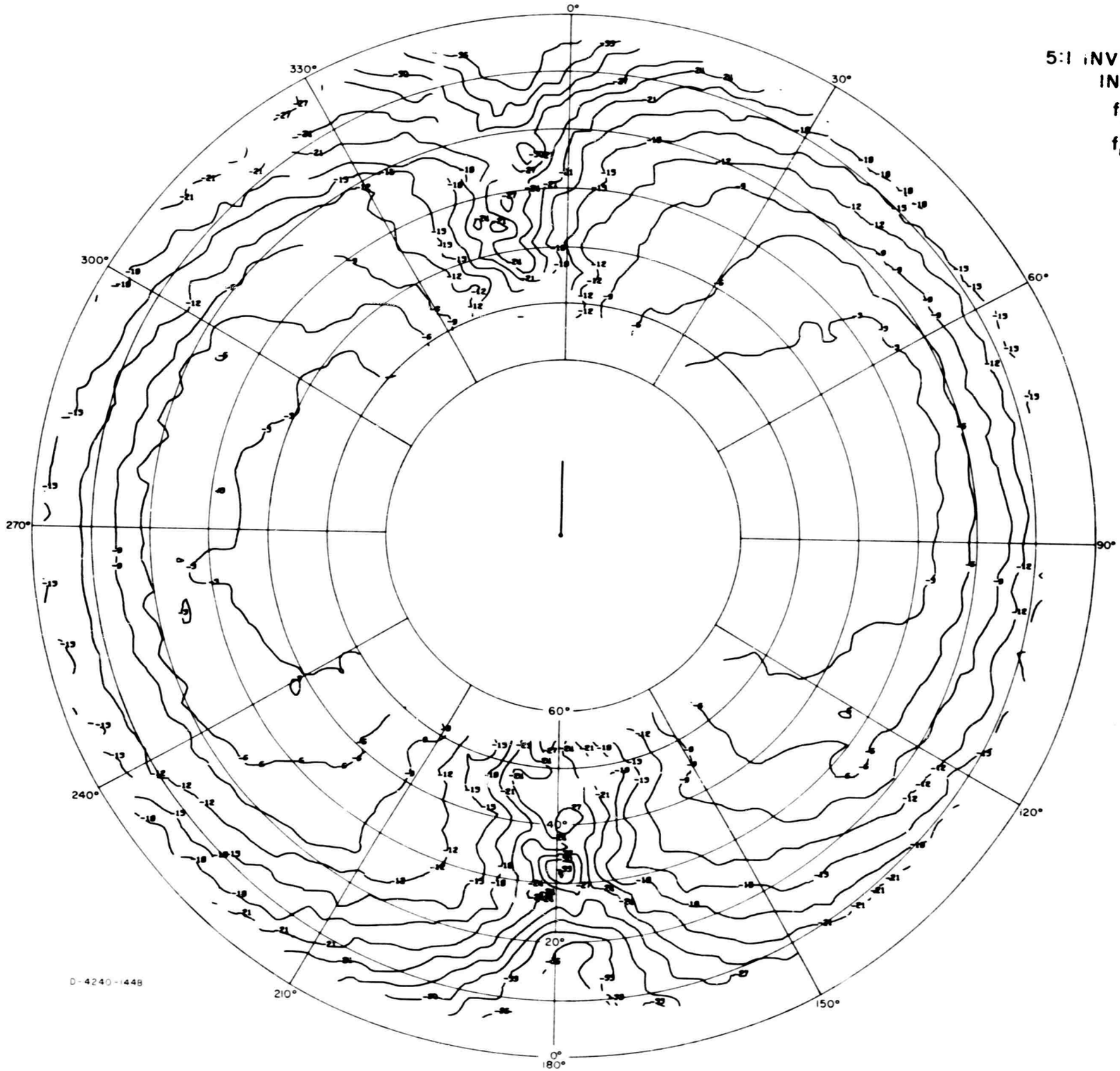

5:1 INVERTED-L
IN FOLIAGE
$f_0 = 6$ Mc/s
$f_m = 4$ Mc/s
E_ϕ

FIG. A-111

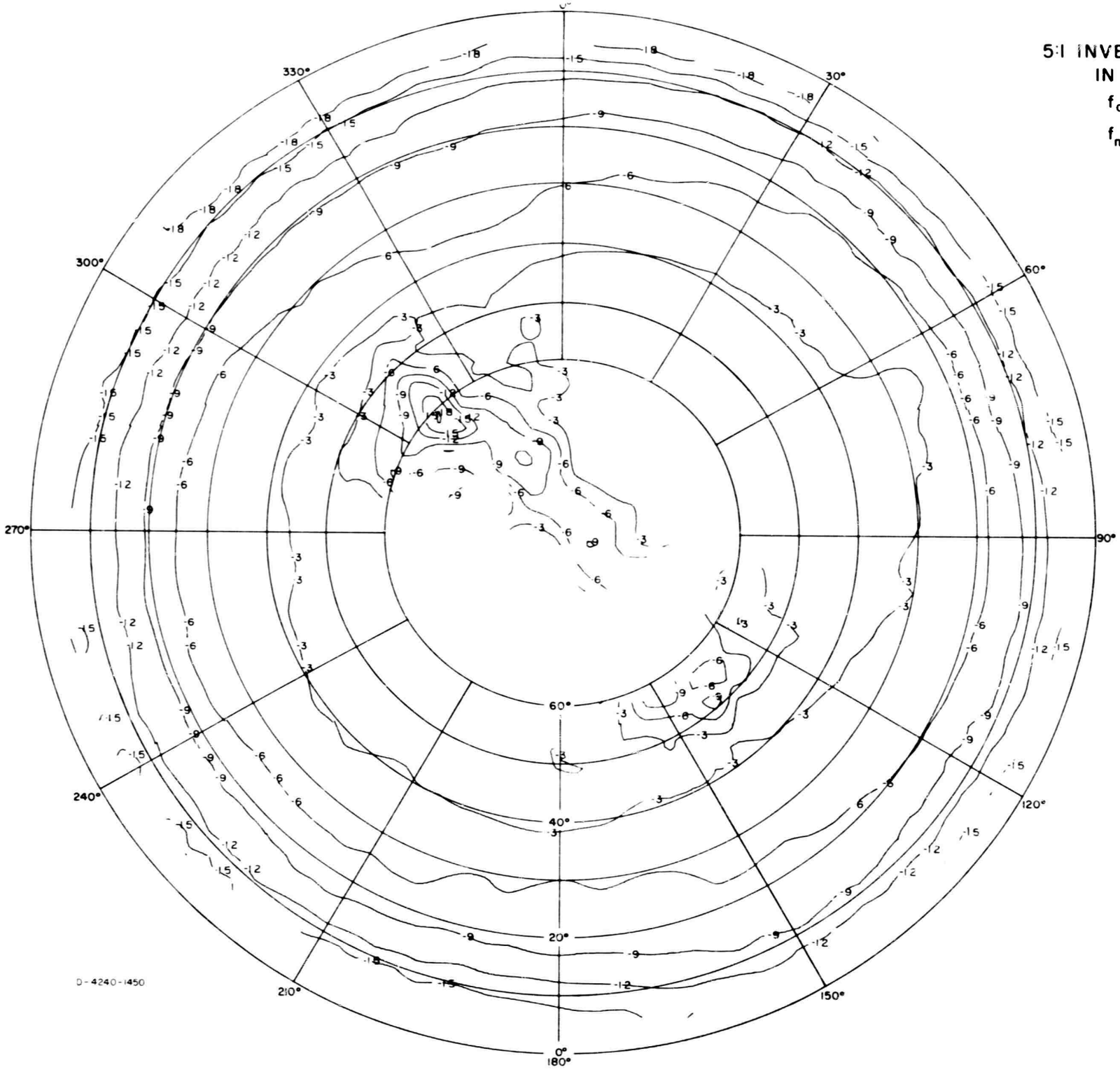
5:1 INVERTED-L
IN FOLIAGE
f_o = 6 Mc/s
f_m = 4 Mc/s
POWER
0°
30°
60°
90°
120°
150°
180°
210°
240°
270°
300°
330°
20°
40°
60°
D-4240-1450

FIG. A-112

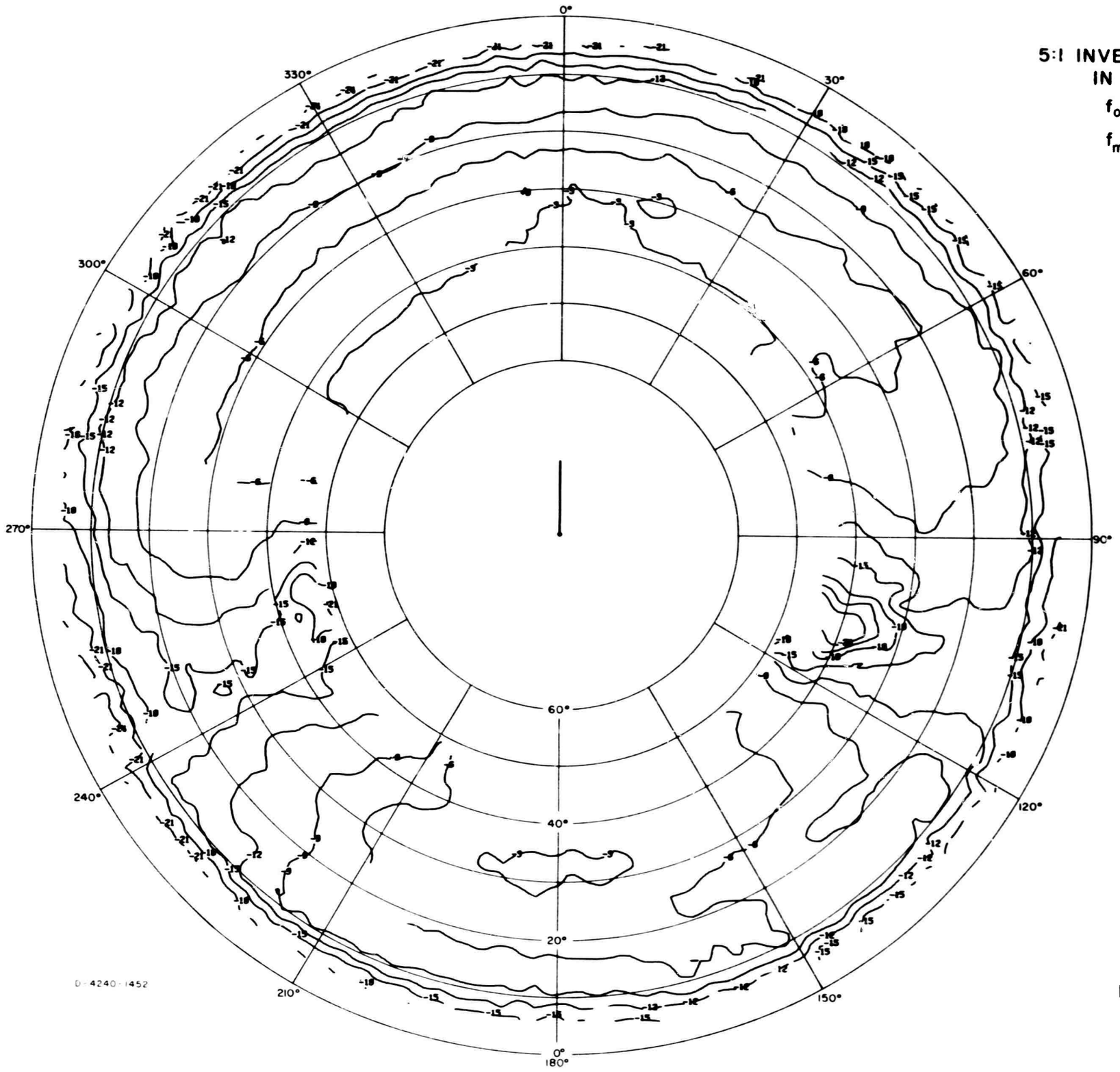

5:1 INVERTED-L
IN FOLIAGE
f_o = 6 Mc/s
f_m = 6 Mc/s
E_θ

FIG. A-113

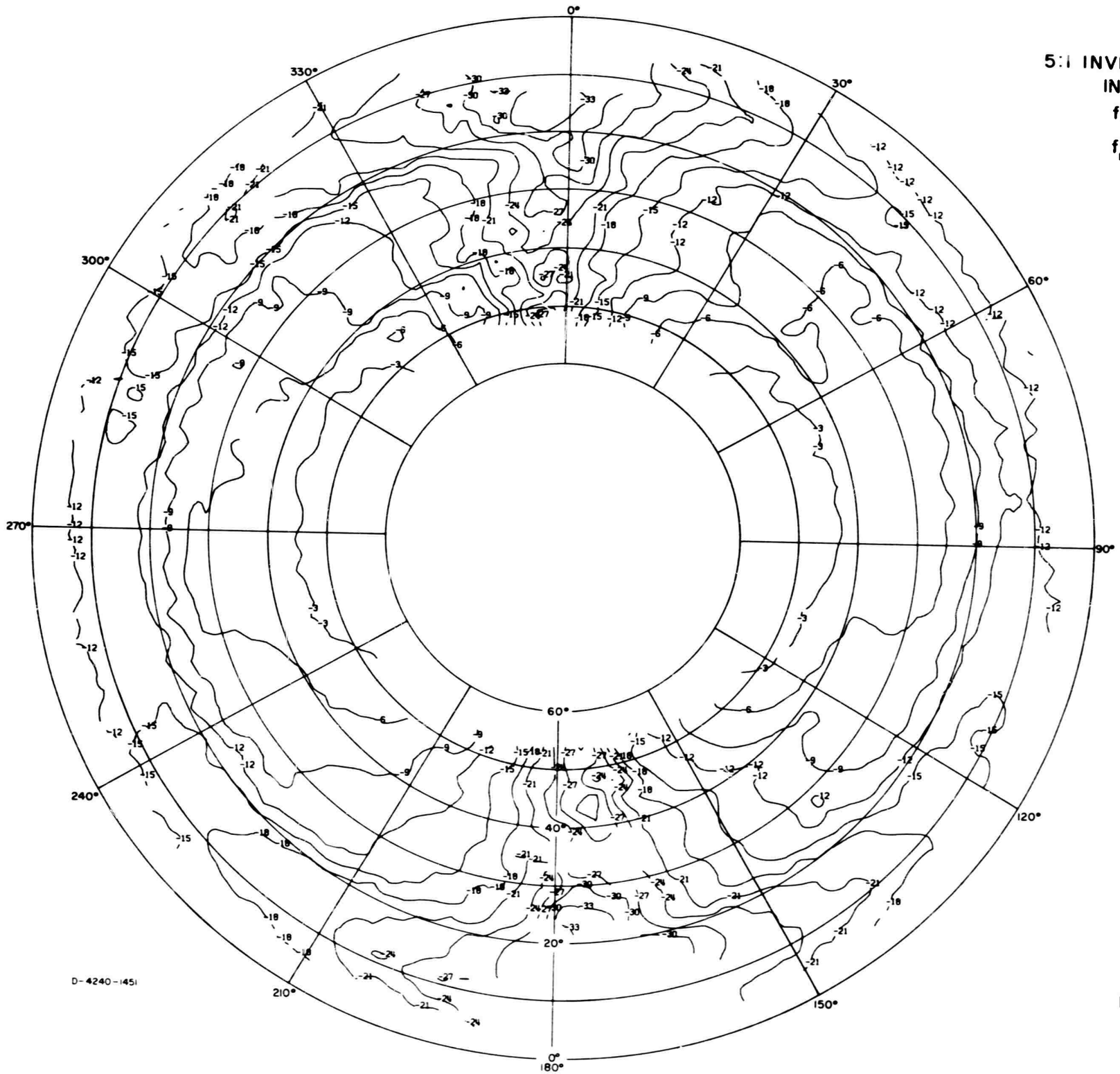

5:1 INVERTED-L
IN FOLIAGE
f_o = 6 Mc/s
f_m = 6 Mc/s
E_ϕ

FIG. A-114

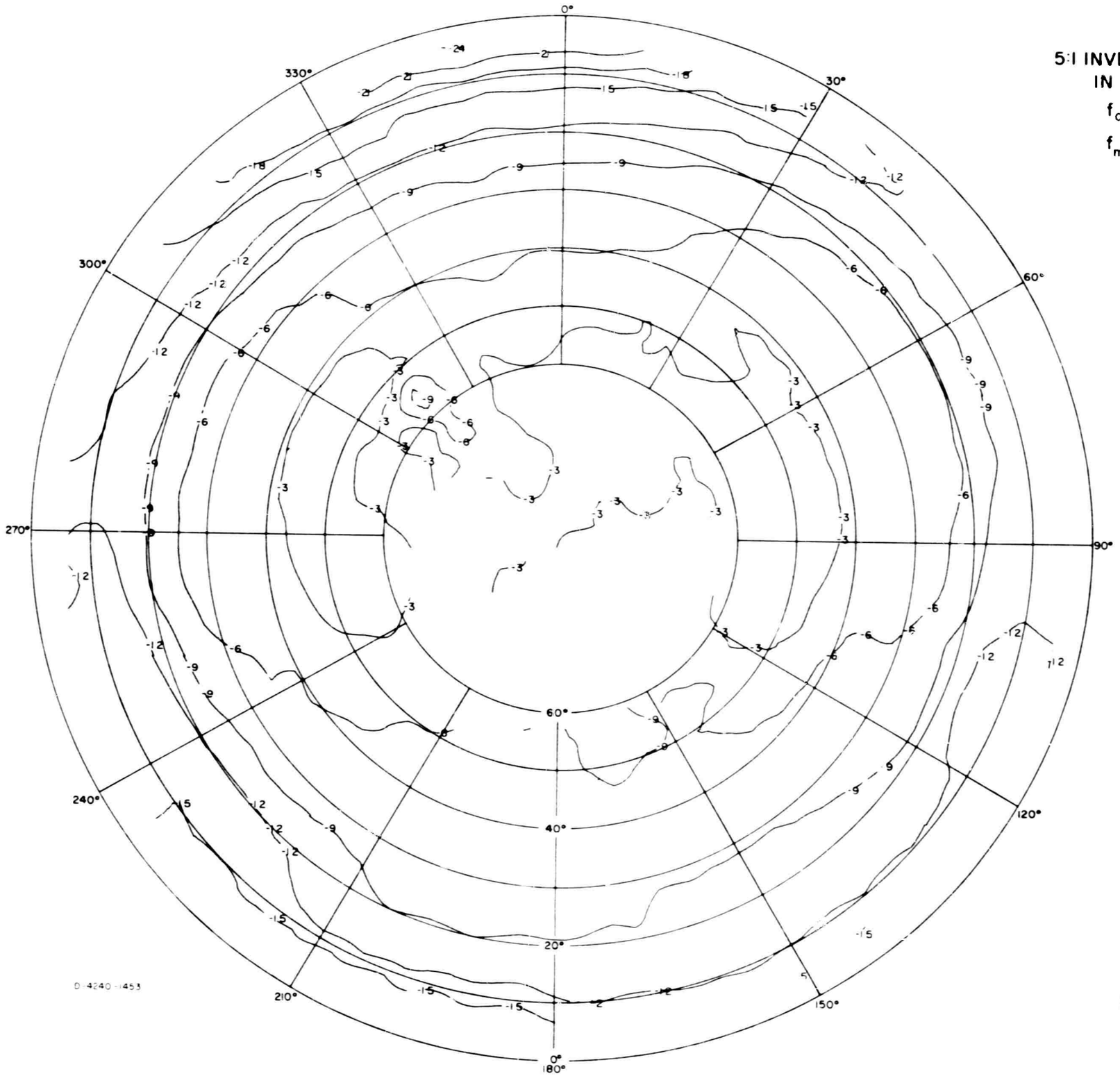

5:1 INVERTED-L
IN FOLIAGE
f_o = 6 Mc/s
f_m = 6 Mc/s
POWER

FIG. A-115

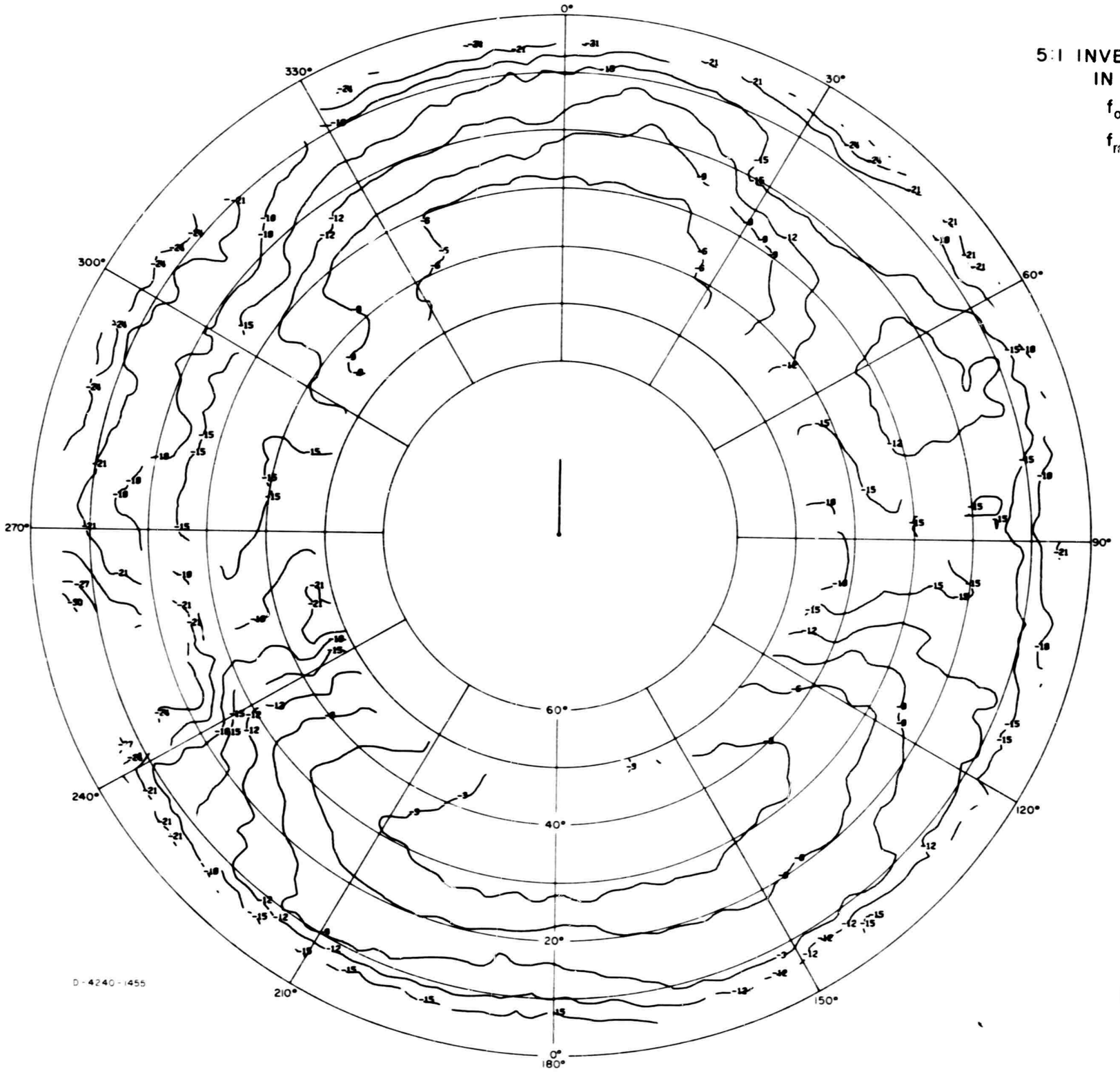

5:1 INVERTED-L
IN FOLIAGE
f_o 6 Mc/s
f_m = 8 Mc/s
E_θ

FIG. A-116

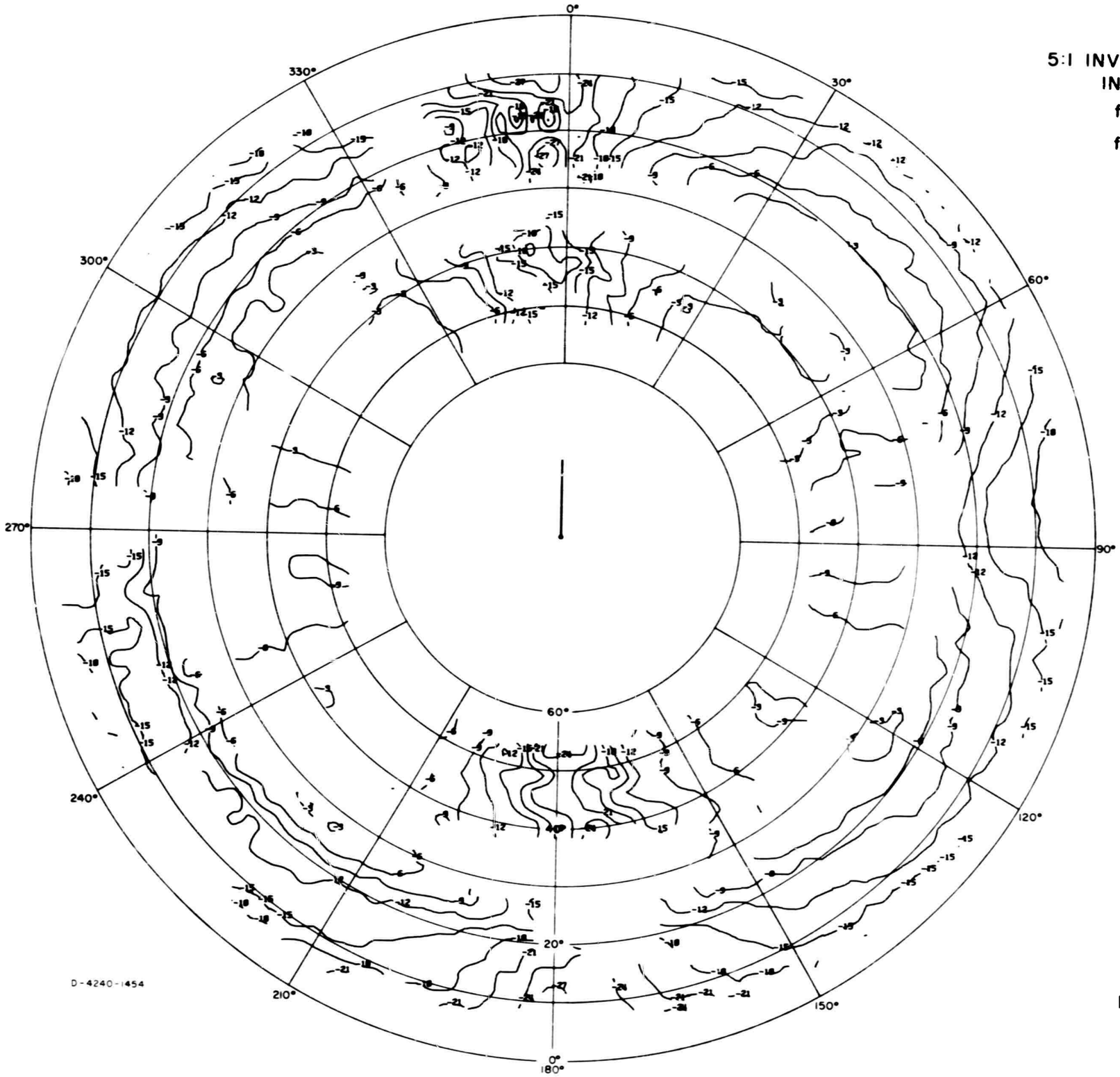

5:1 INVERTED-L
IN FOLIAGE
f_o = 6 Mc/s
f_m = 8 Mc/s
E_ϕ

D-4240-1454

FIG. A-117

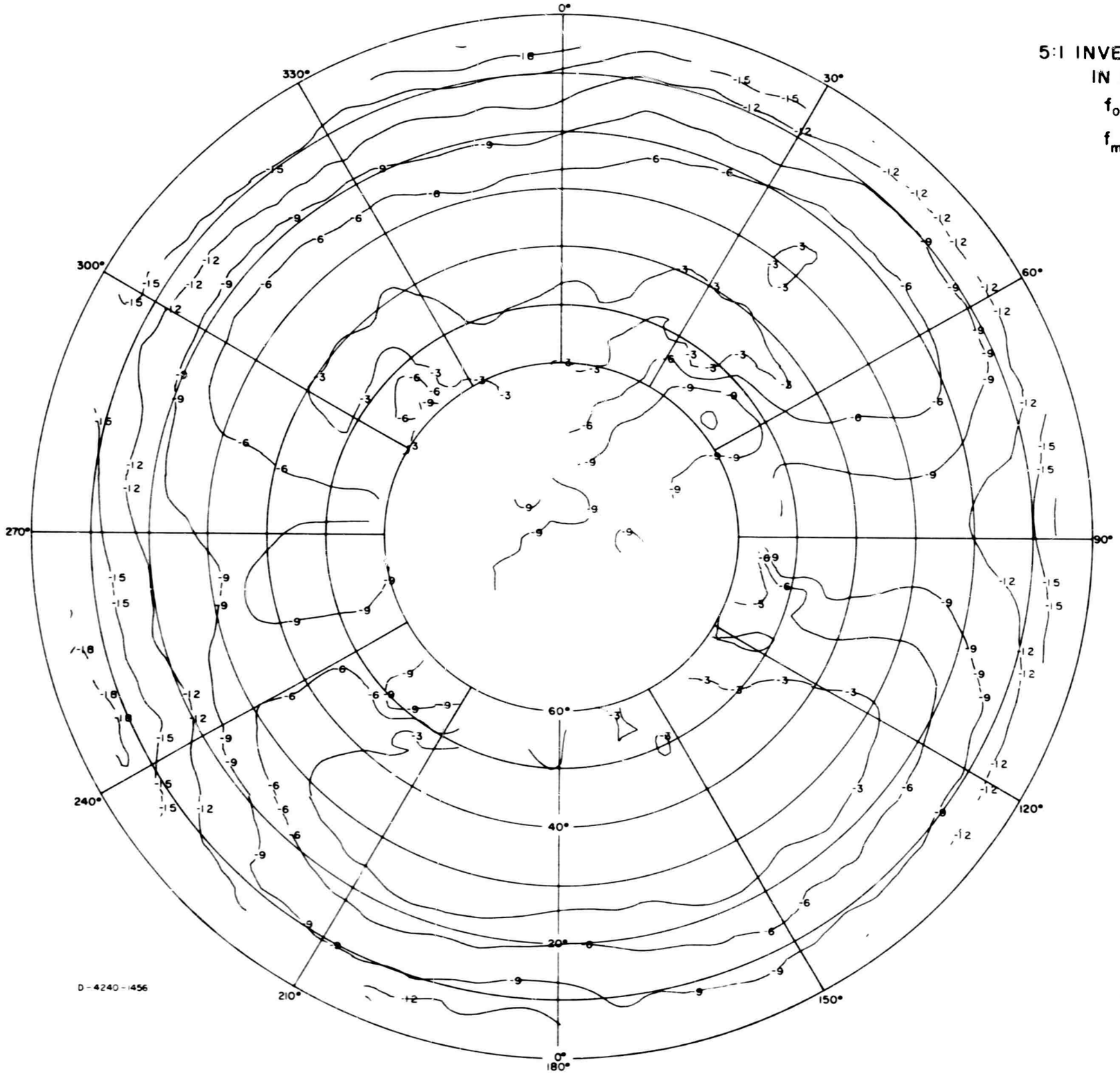

5:1 INVERTED-L
IN FOLIAGE
f_0 = 6 Mc/s
f_m = 8 Mc/s
POWER

FIG. A-118

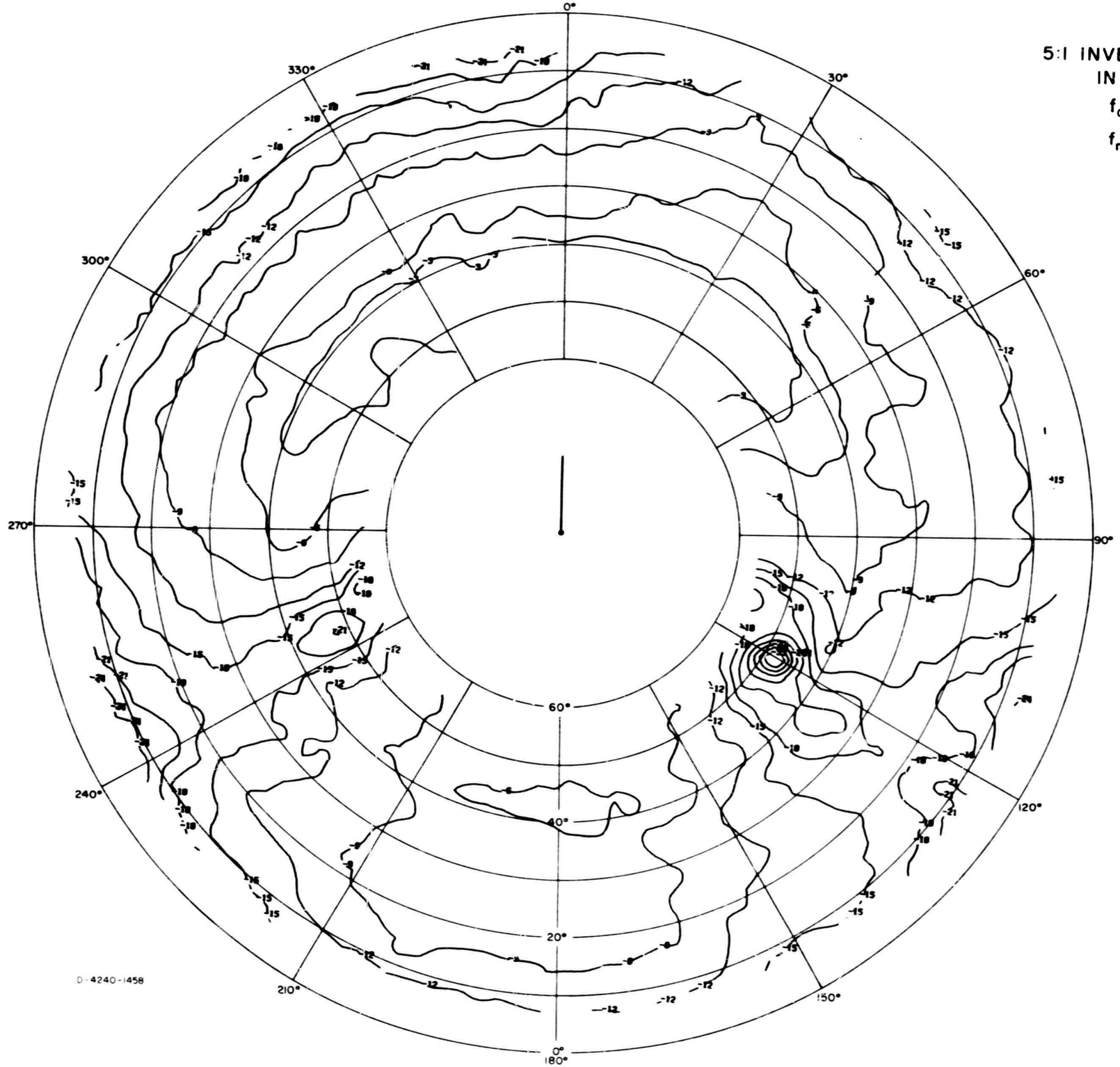

5:1 INVERTED-L
IN FOLIAGE
f_o = 10 Mc/s
f_m = 10 Mc/s
E_θ

FIG. A-119

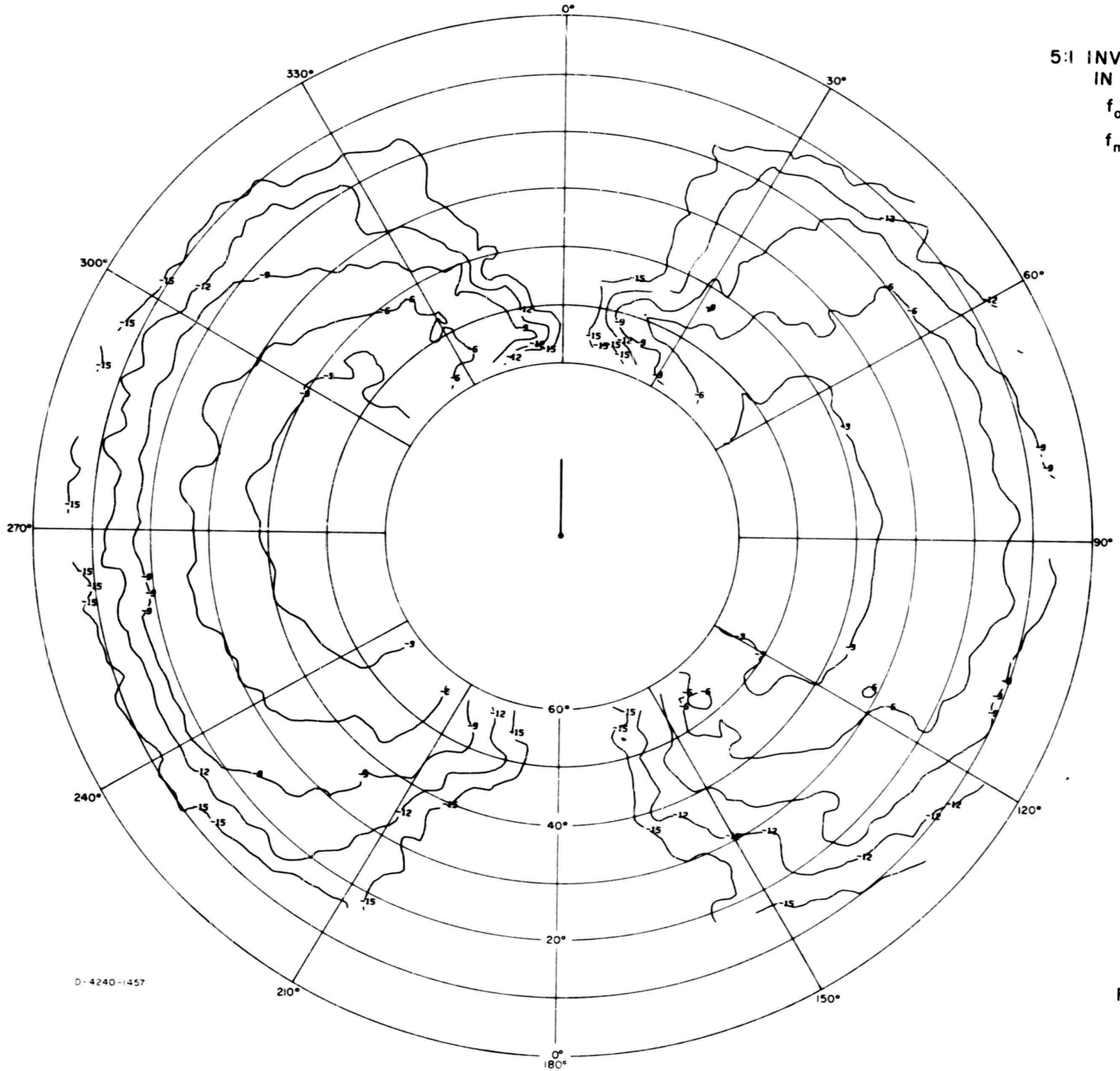

5:1 INVERTED-L
IN FOLIAGE
f_o = 10 Mc/s
f_m = 10 Mc/s
E_ϕ

FIG. A-120

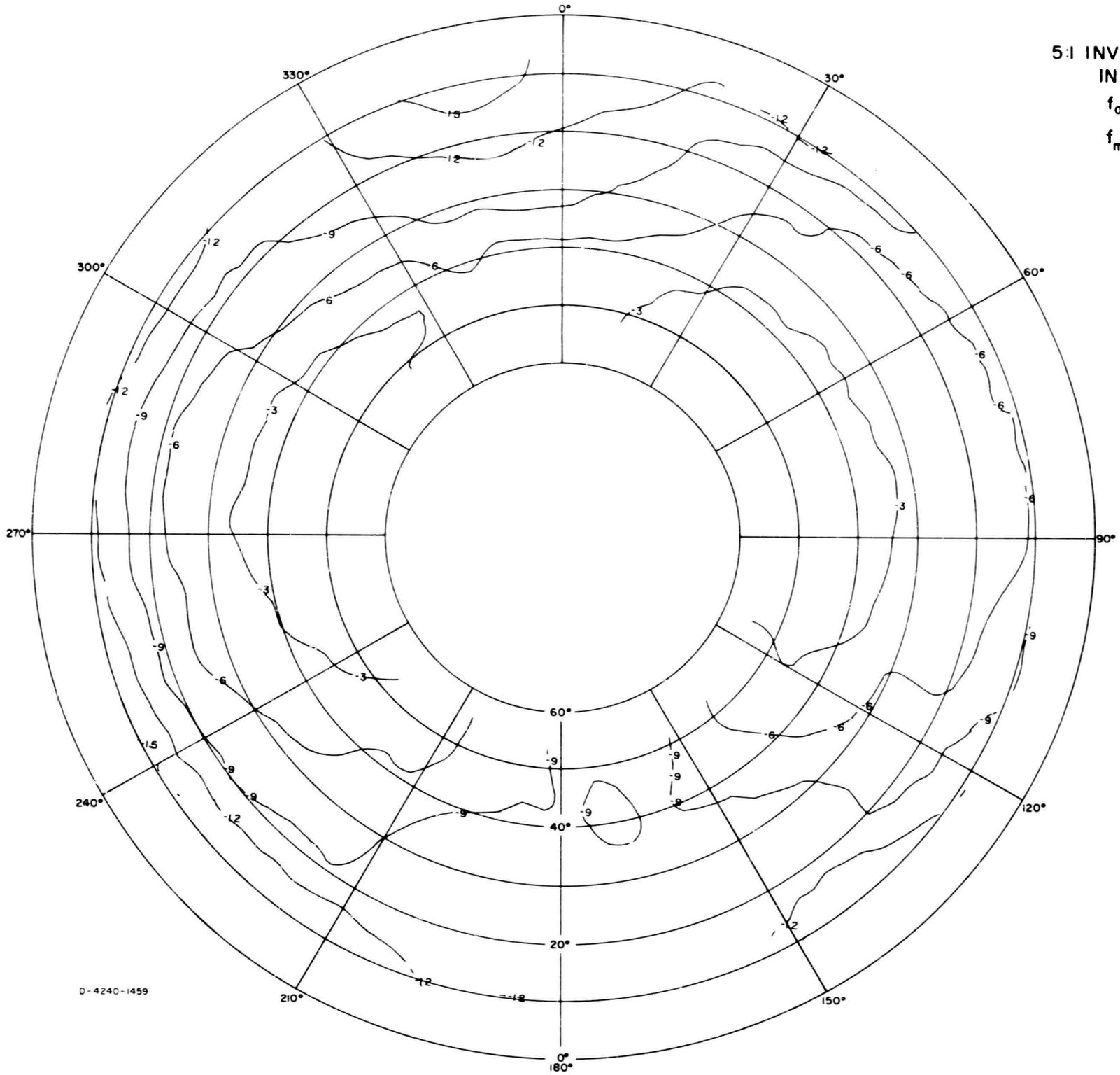

5:1 INVERTED-L
IN FOLIAGE
f_o = 10 Mc/s
f_m = 10 Mc/s
POWER

FIG. A-121

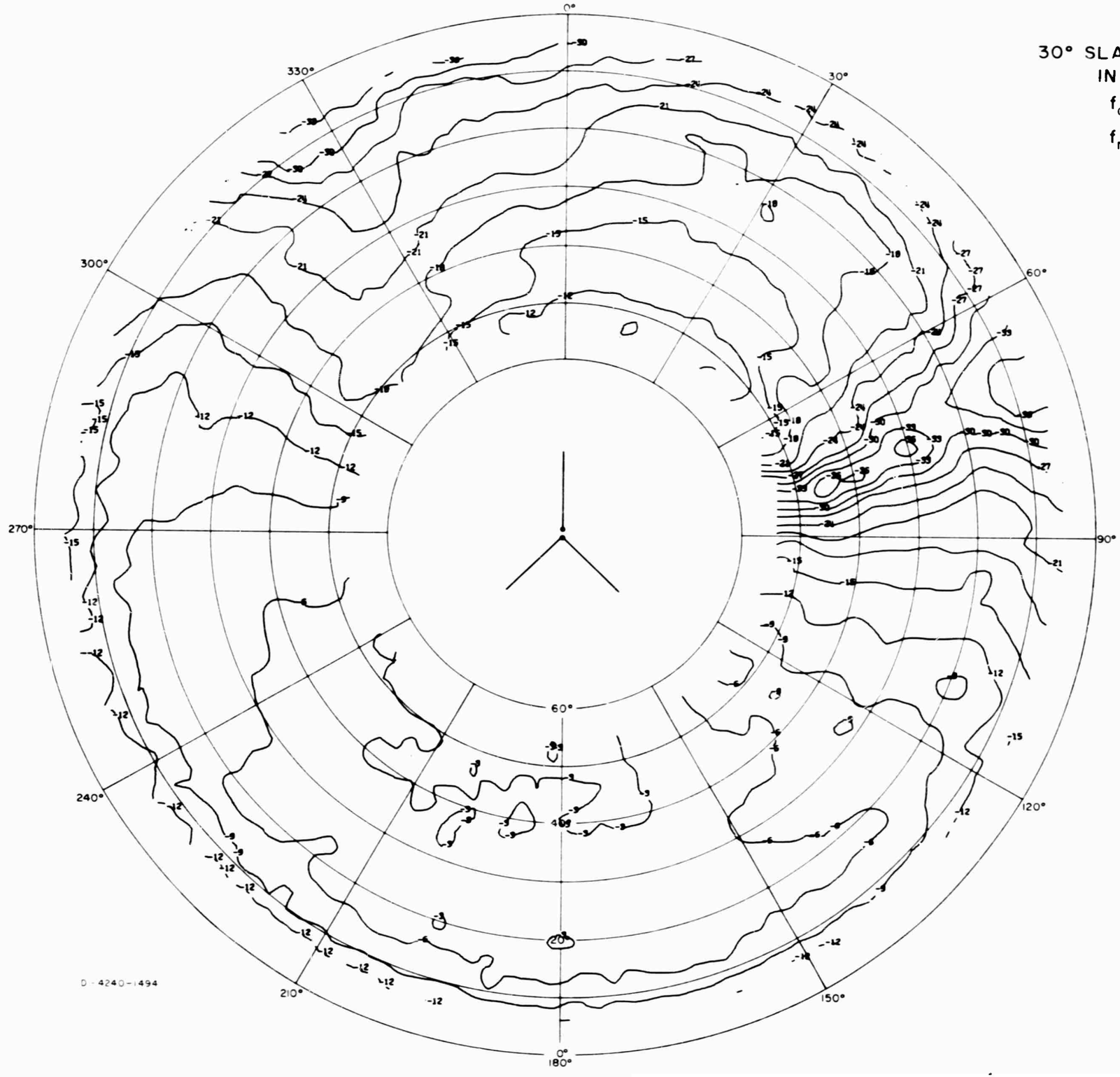

30° SLANT WIRE
IN FOLIAGE
f_o = 4 Mc/s
f_m = 4 Mc/s
E_θ

FIG. A-122

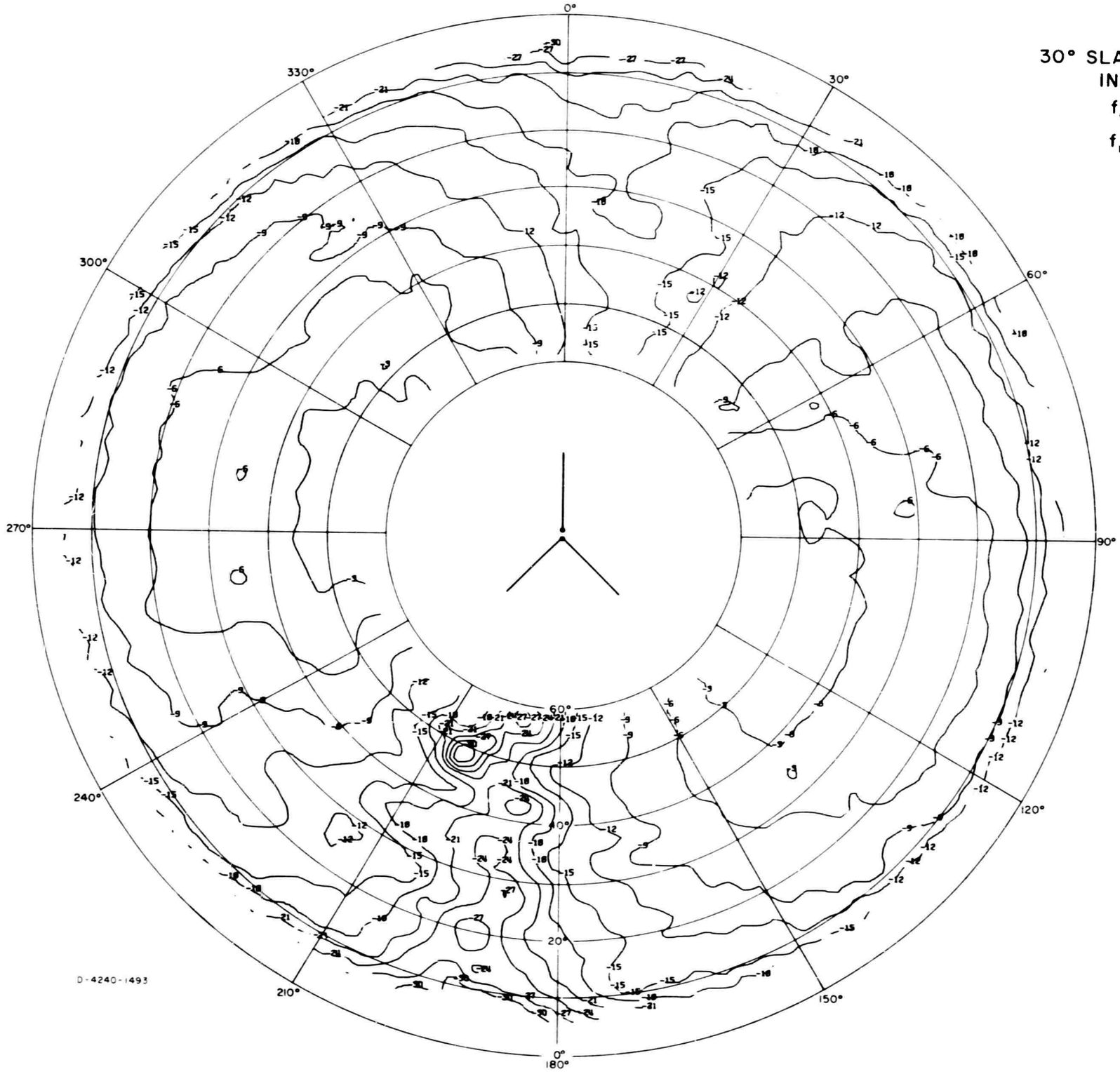

30° SLANT WIRE
IN FOLIAGE
f_o = 4 Mc/s
f_m = 4 Mc/s
E_ϕ

FIG. A-123

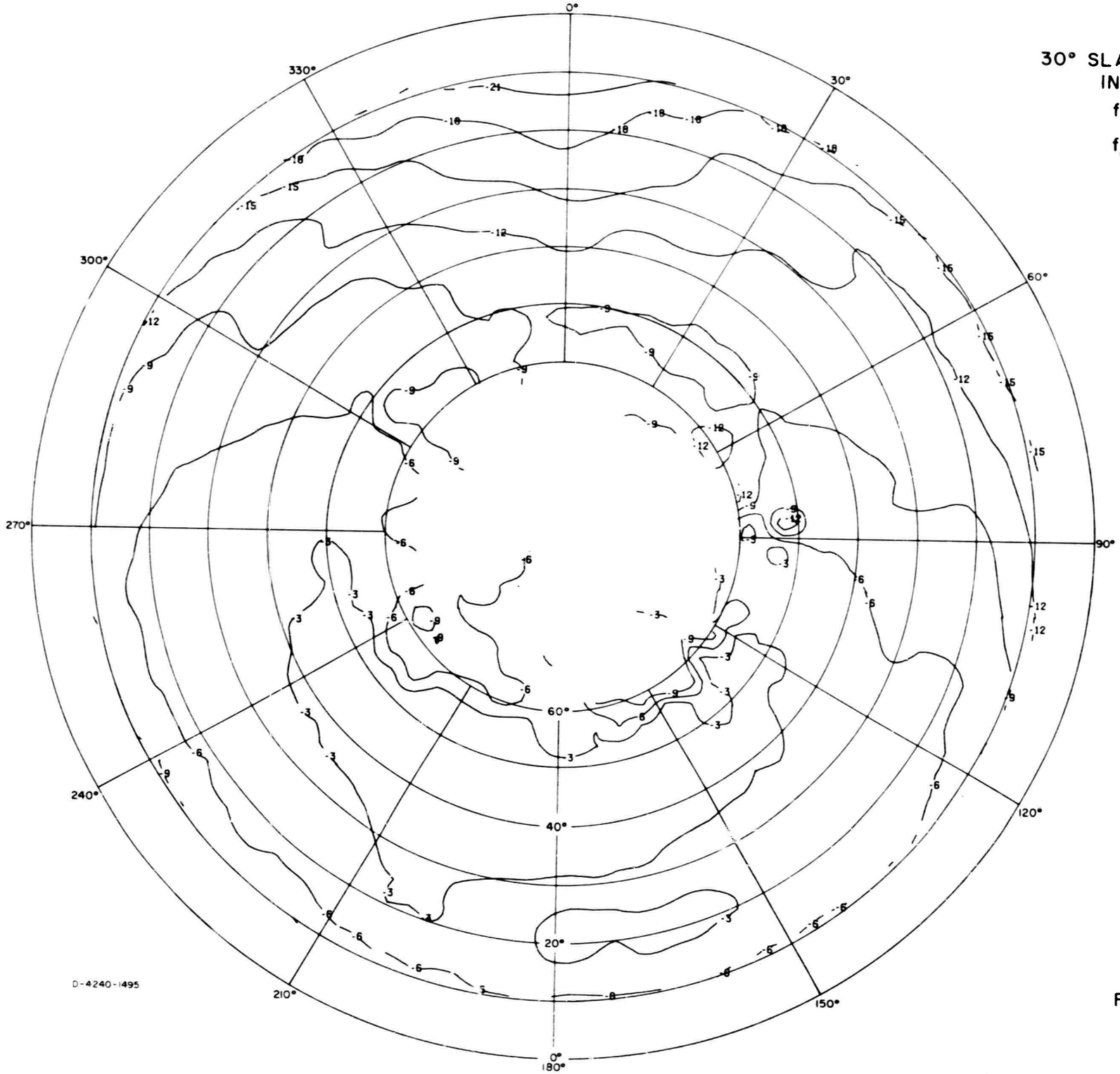

30° SLANT WIRE
IN FOLIAGE
f_o = 4 Mc/s
f_m = 4 Mc/s
POWER

FIG. A-124

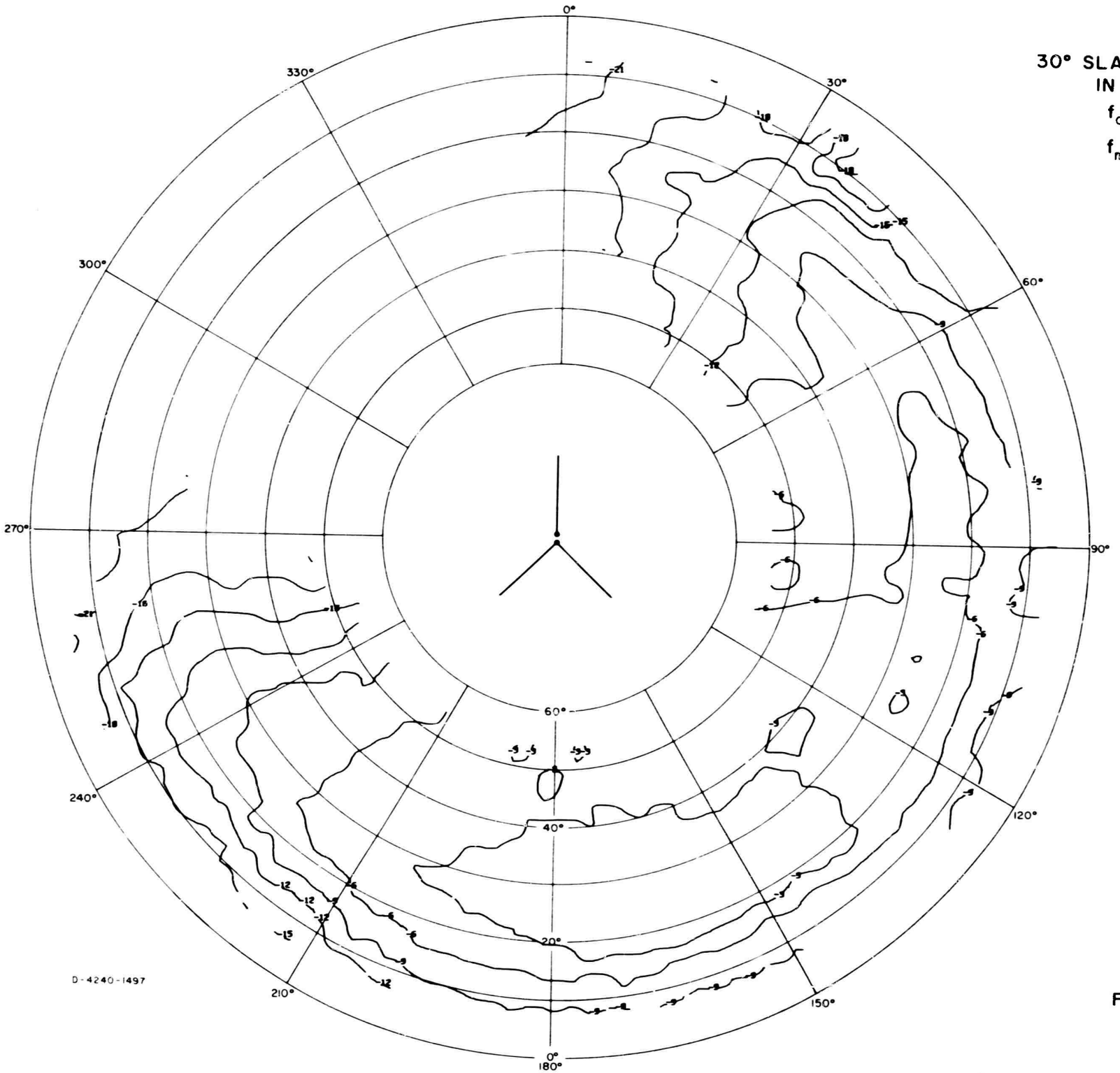

30° SLANT WIRE
IN FOLIAGE
f_0 = 6 Mc/s
f_m = 3 Mc/s
E_θ

FIG. A-125

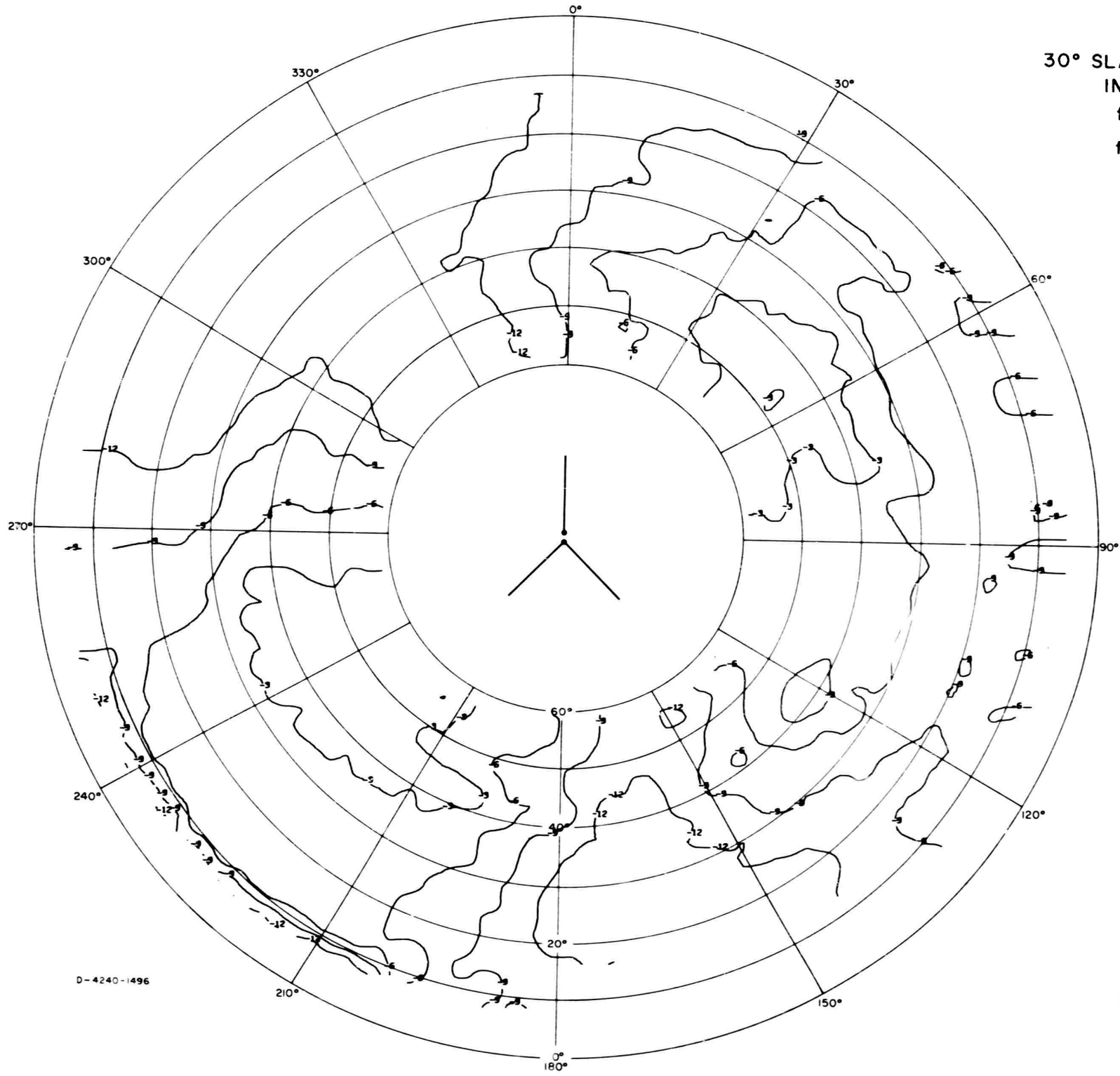

30° SLANT WIRE
IN FOLIAGE
f_o = 6 Mc/s
f_m = 3 Mc/s
E_ϕ

FIG. A-126

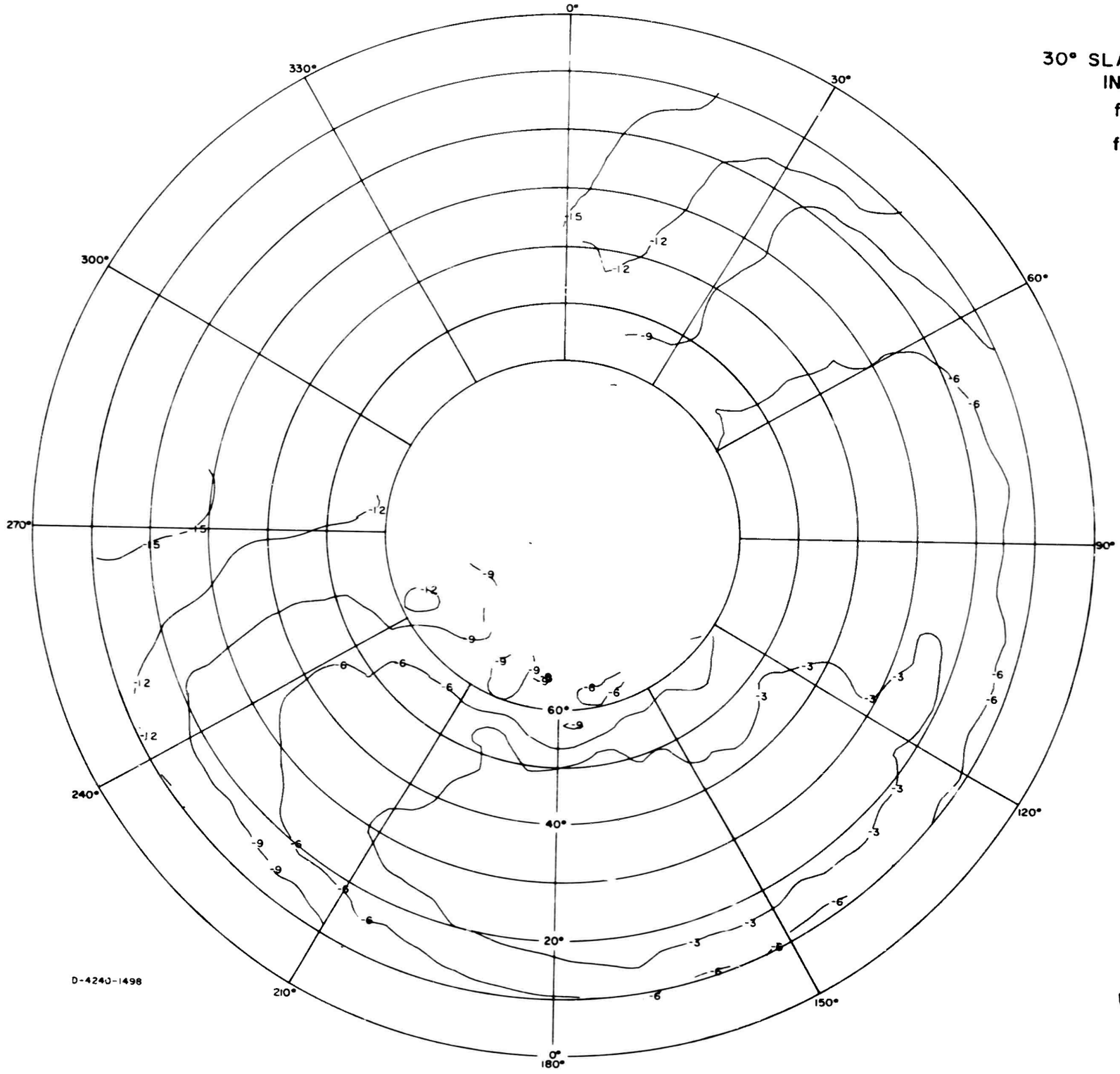

30° SLANT WIRE
IN FOLIAGE
f_o = 6 Mc/s
f_m = 3 Mc/s
POWER

FIG. A-127

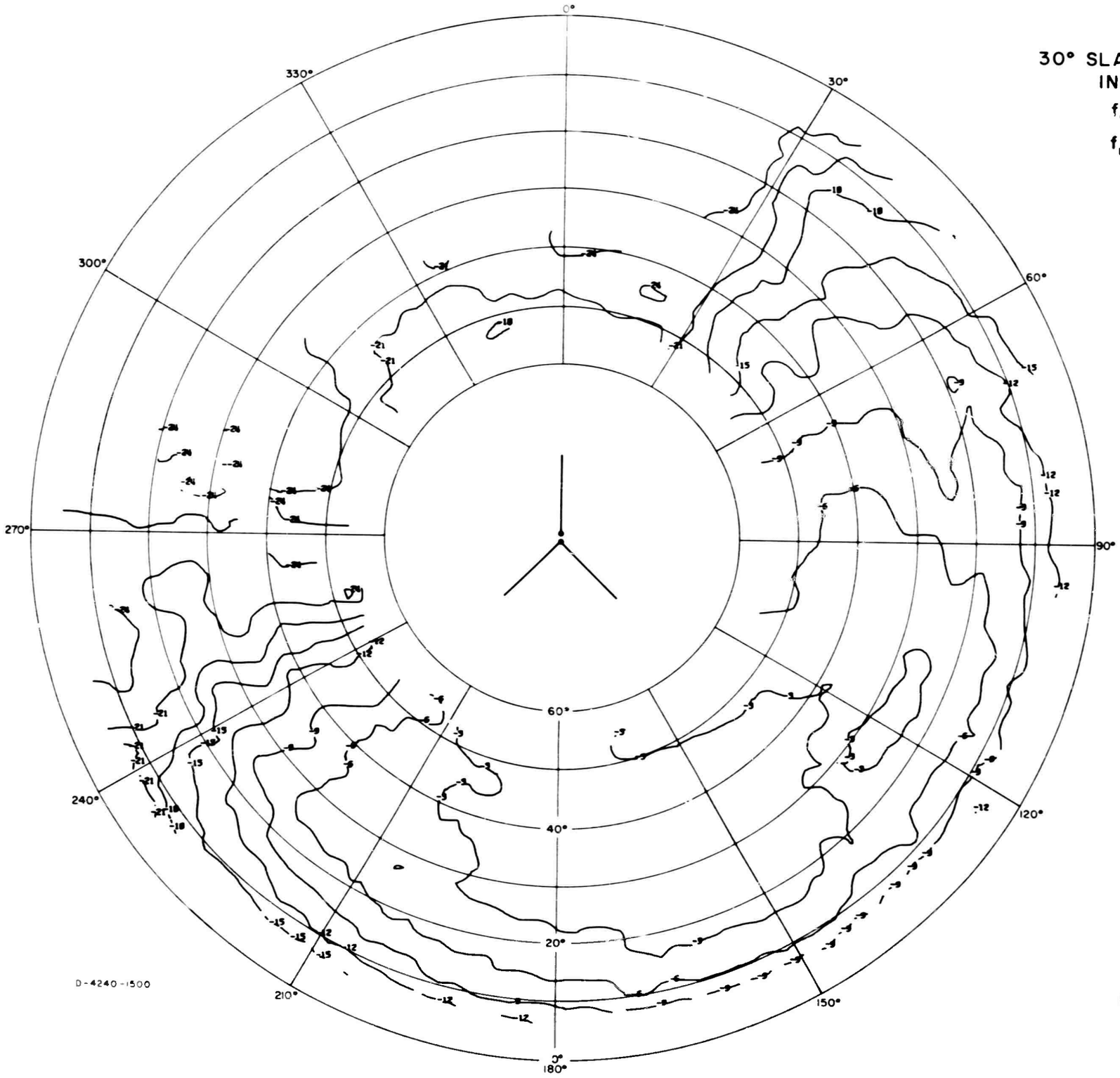

30° SLANT WIRE
IN FOLIAGE
f_o = 6 Mc/s
f_m = 4 Mc/s
E_θ

FIG. A-128

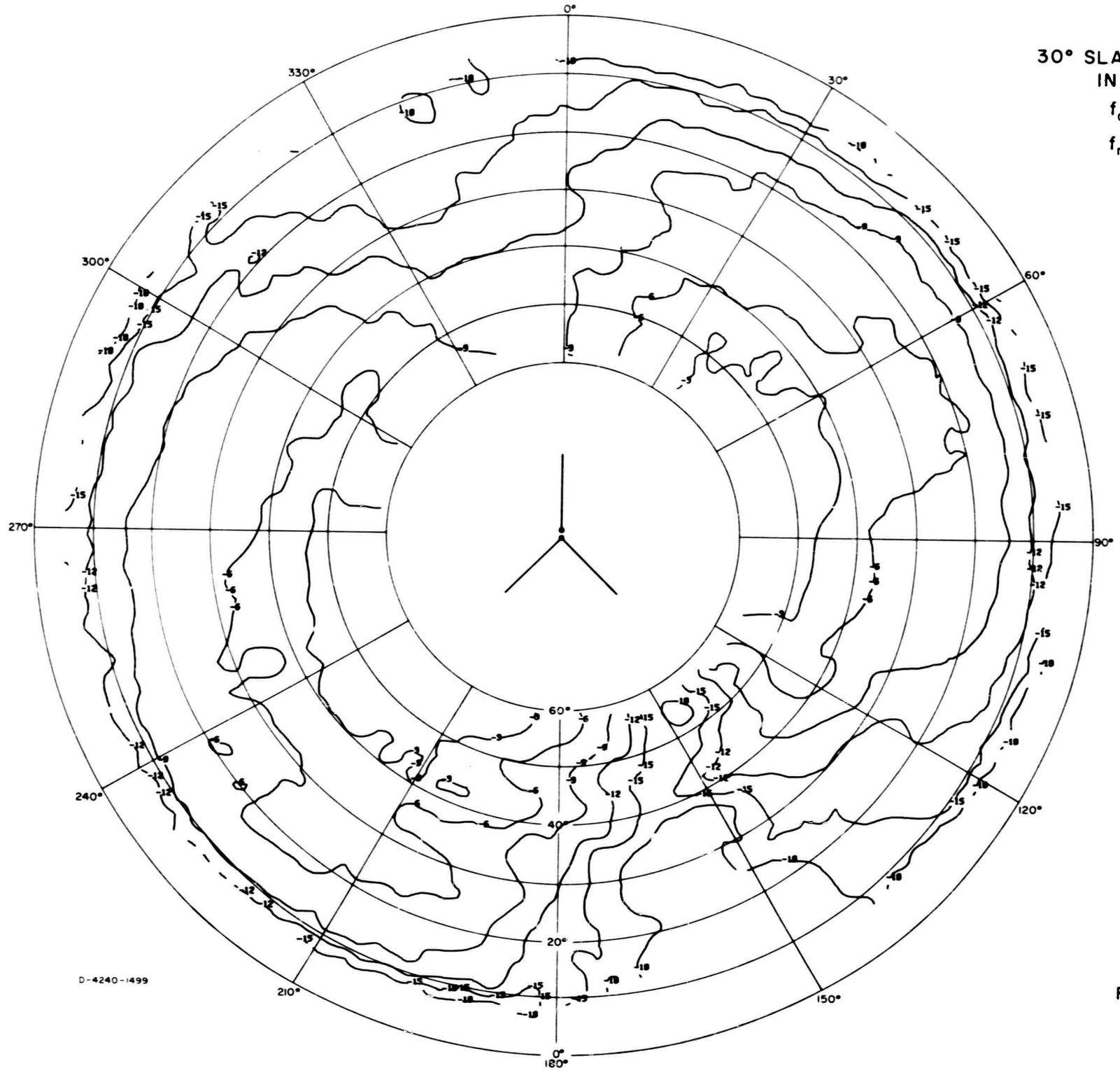

30° SLANT WIRE
IN FOLIAGE
f_o = 6 Mc/s
f_m = 4 Mc/s
E_ϕ

FIG. A-129

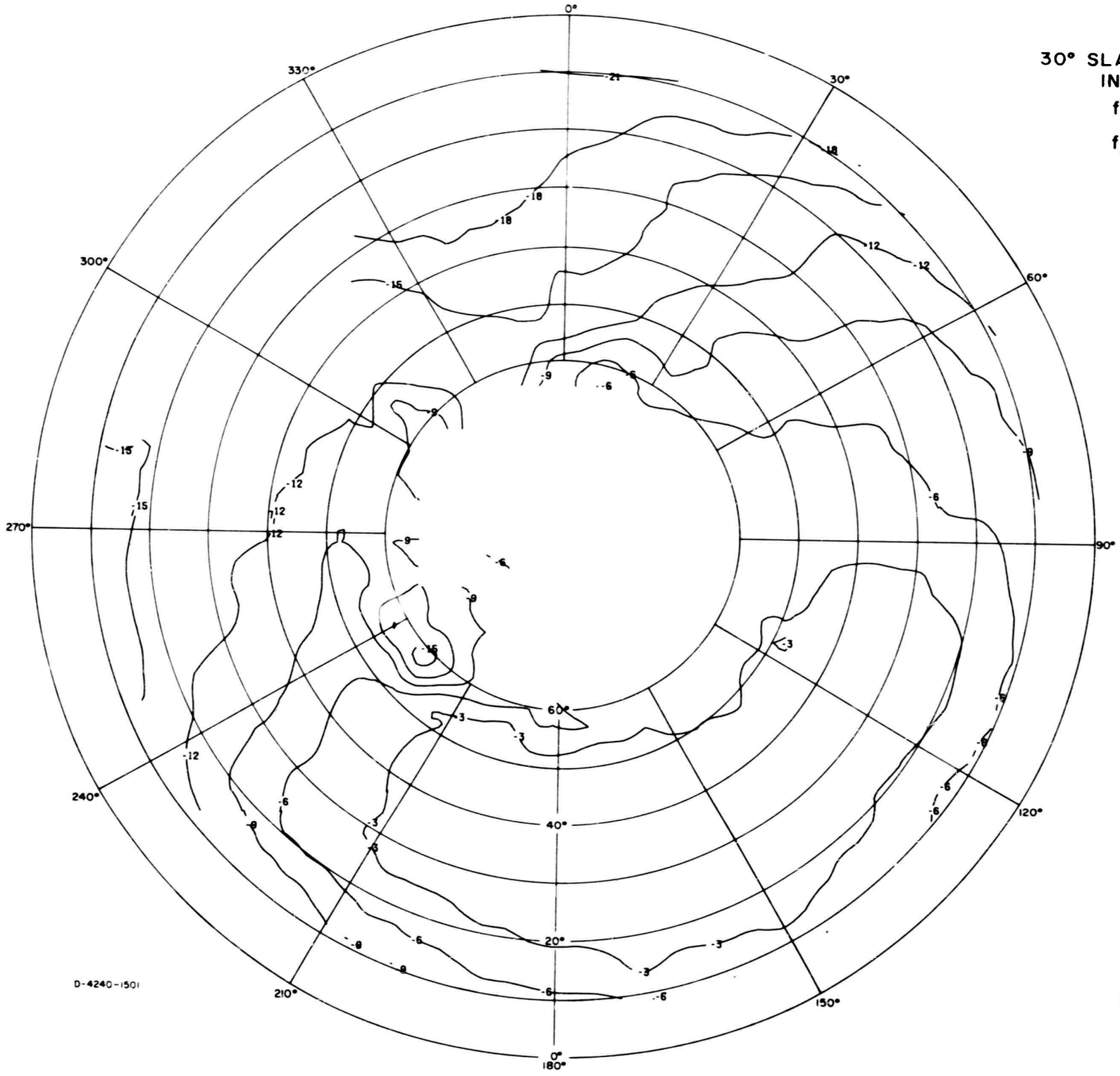

30° SLANT WIRE
IN FOLIAGE
f_o = 6 Mc/s
f_m = 4 Mc/s
POWER

FIG. A-130

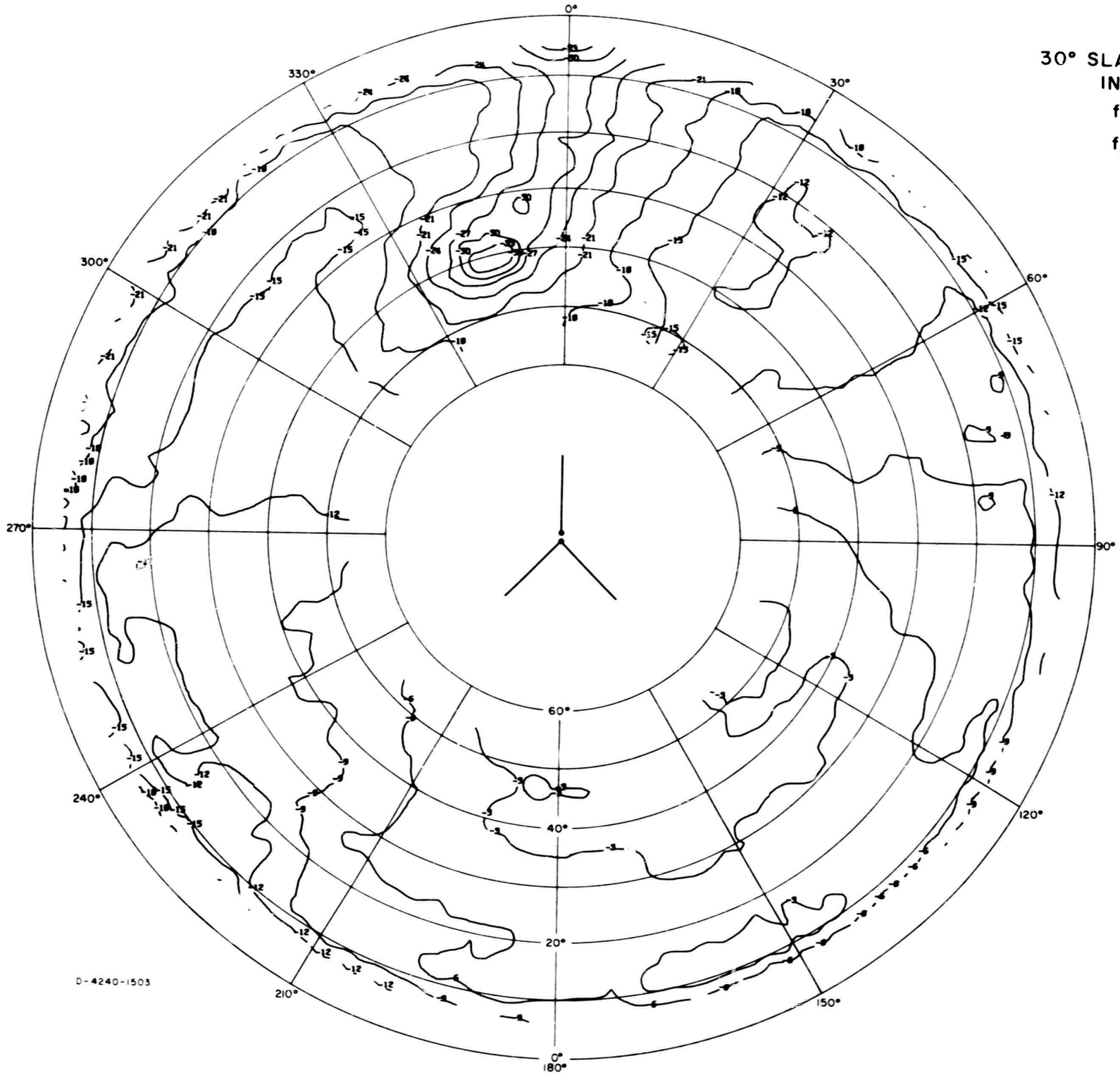

30° SLANT WIRE
IN FOLIAGE
f_o = 6 Mc/s
f_m = 6 Mc/s
E_θ

FIG. A-131

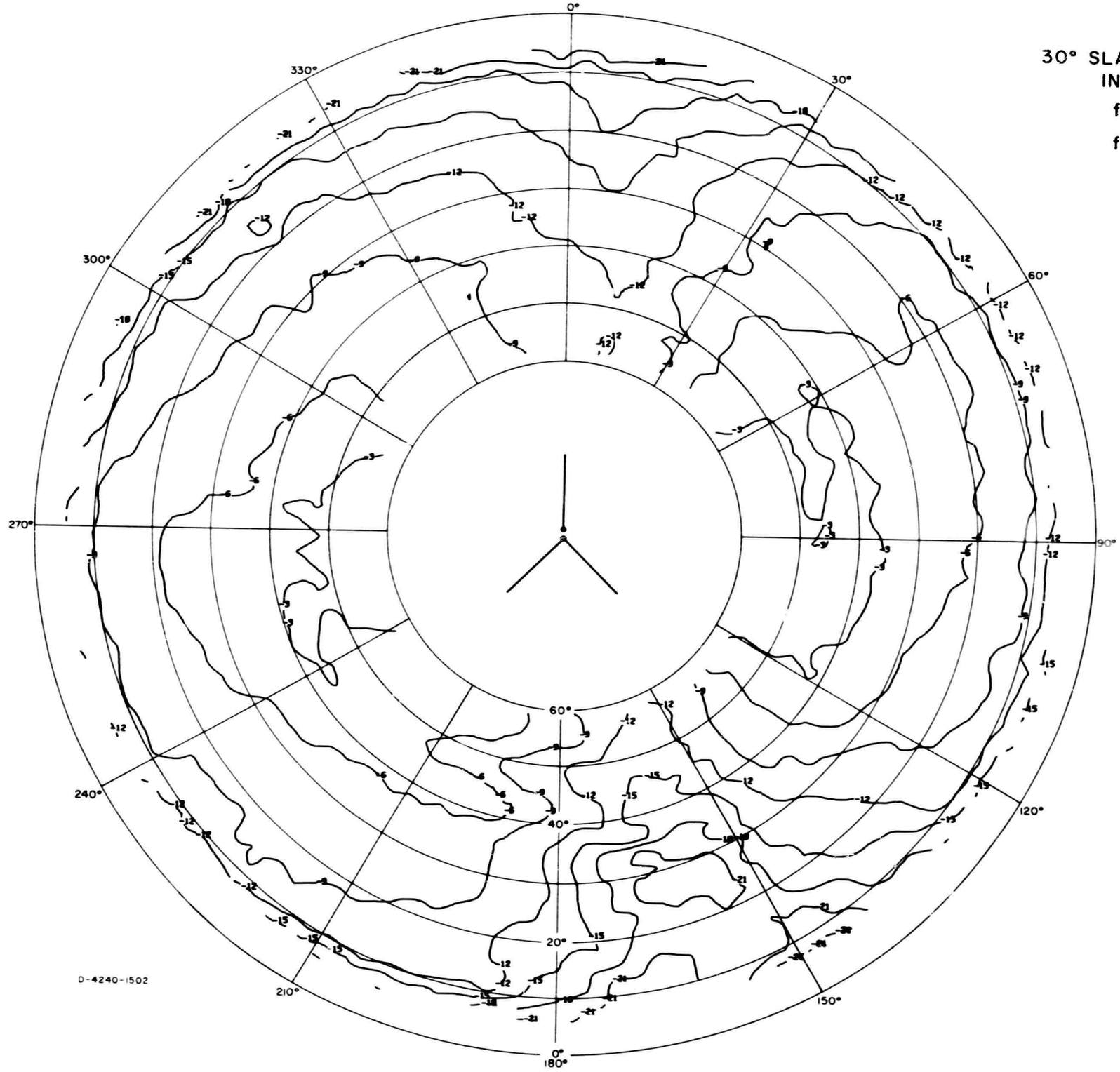

30° SLANT WIRE
IN FOLIAGE
f_0 = 6 Mc/s
f_m = 6 Mc/s
E_ϕ

FIG. A-132

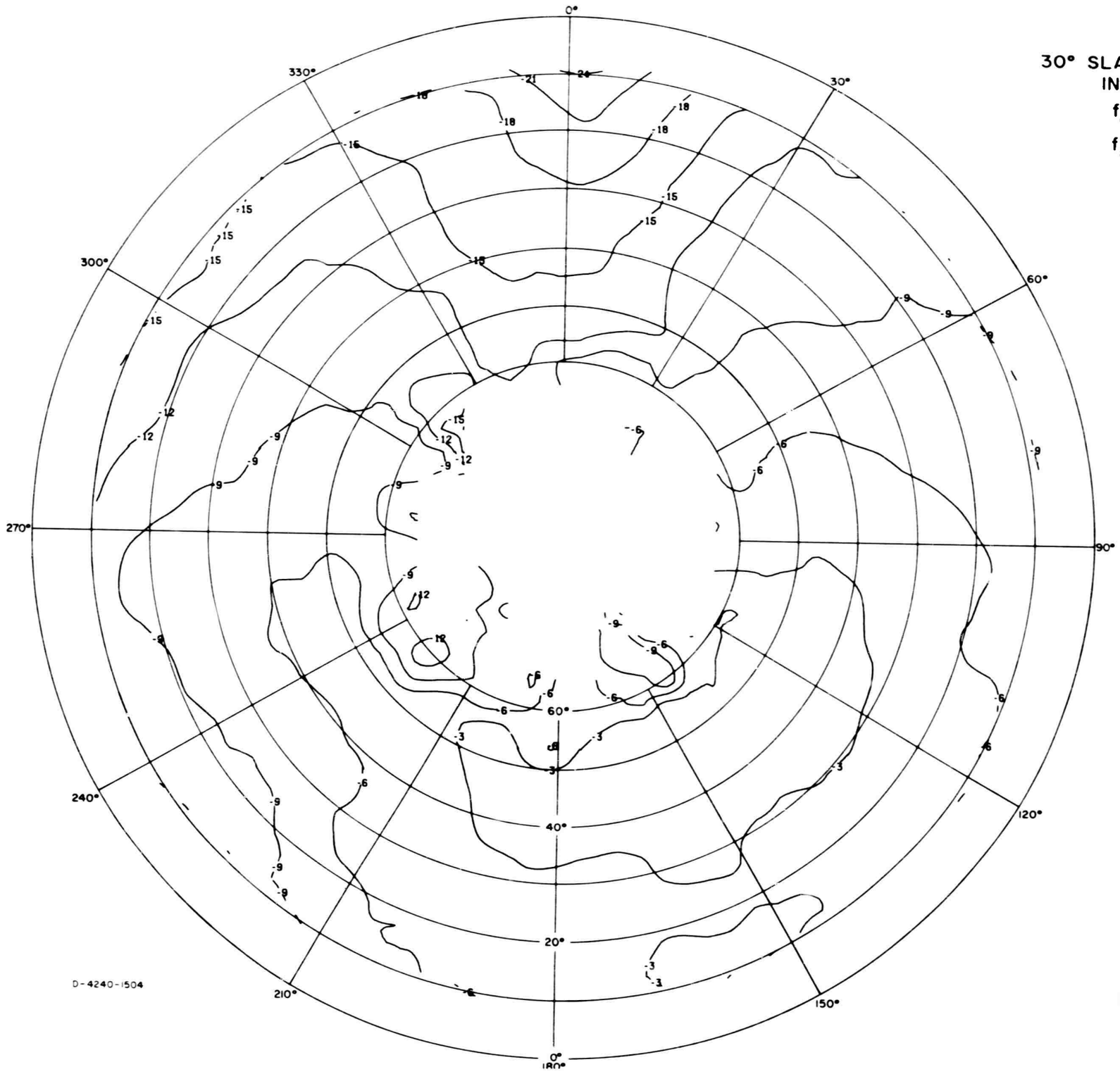

30° SLANT WIRE
IN FOLIAGE
f_o = 6 Mc/s
f_m = 6 Mc/s
POWER

FIG. A-133

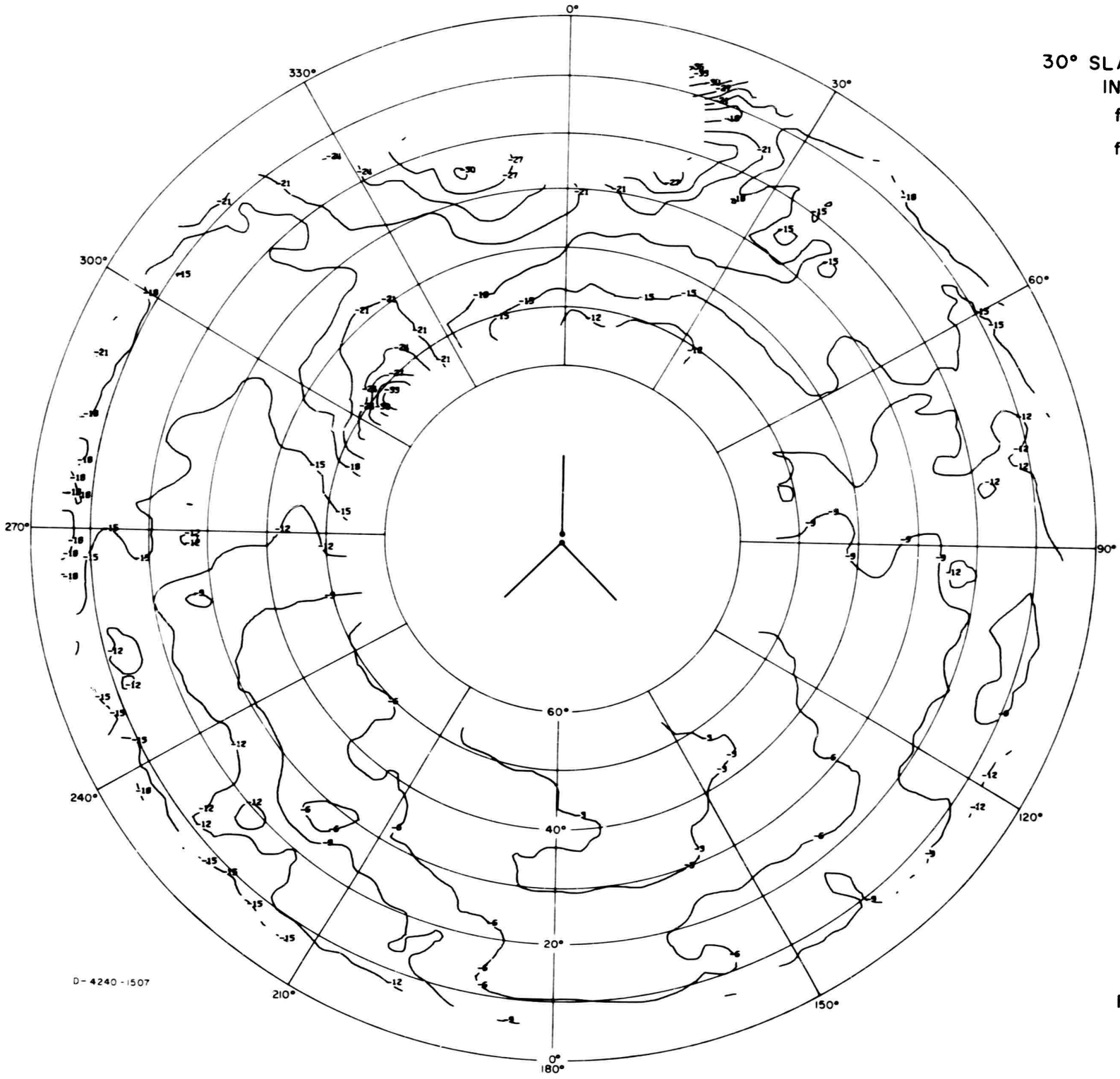

30° SLANT WIRE
IN FOLIAGE
f_o = 6 Mc/s
f_m = 8 Mc/s
E_θ

FIG. A-134

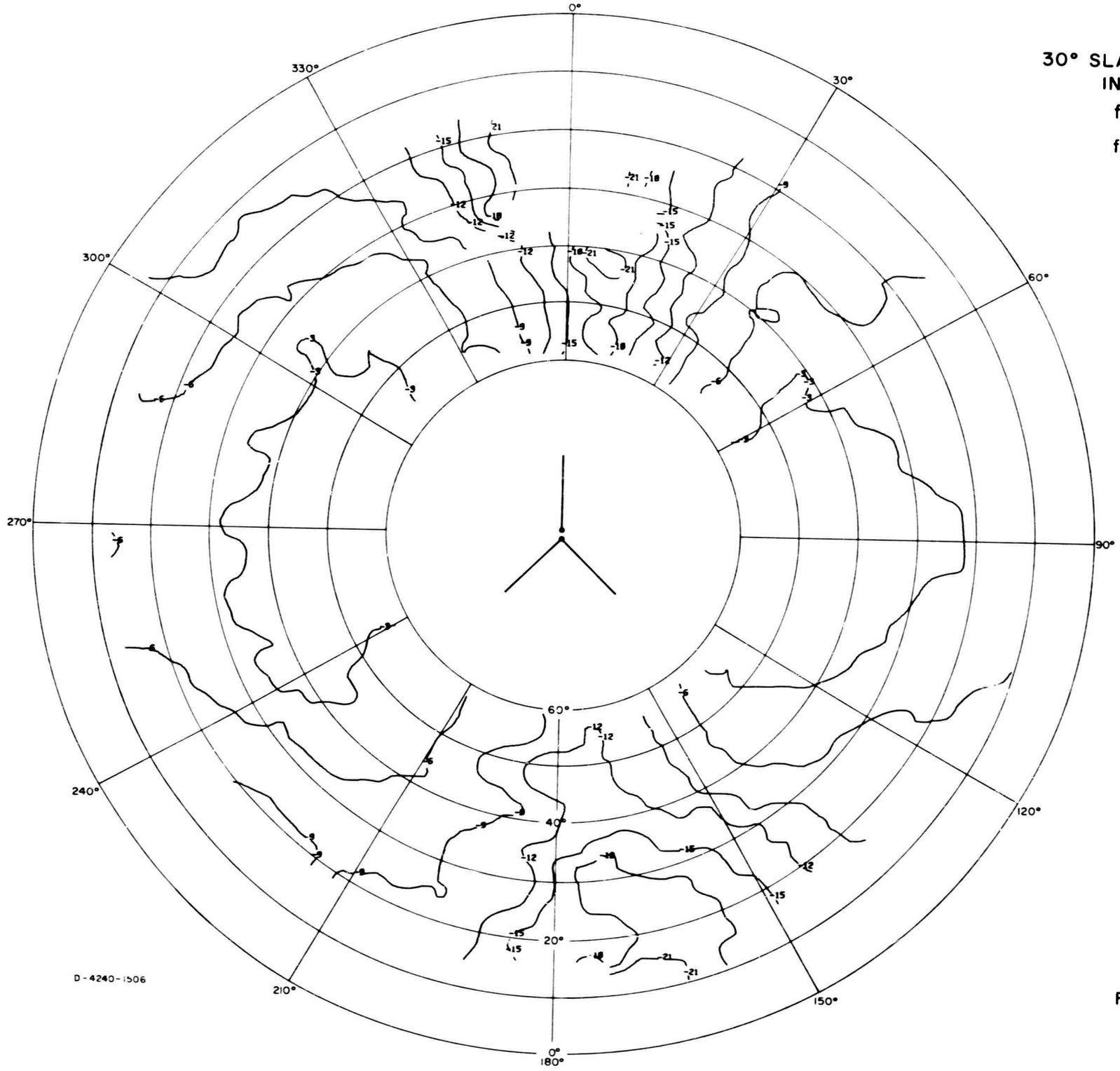

30° SLANT WIRE
IN FOLIAGE
f_o = 6 Mc/s
f_m = 8 Mc/s
E_ϕ

FIG. A-135

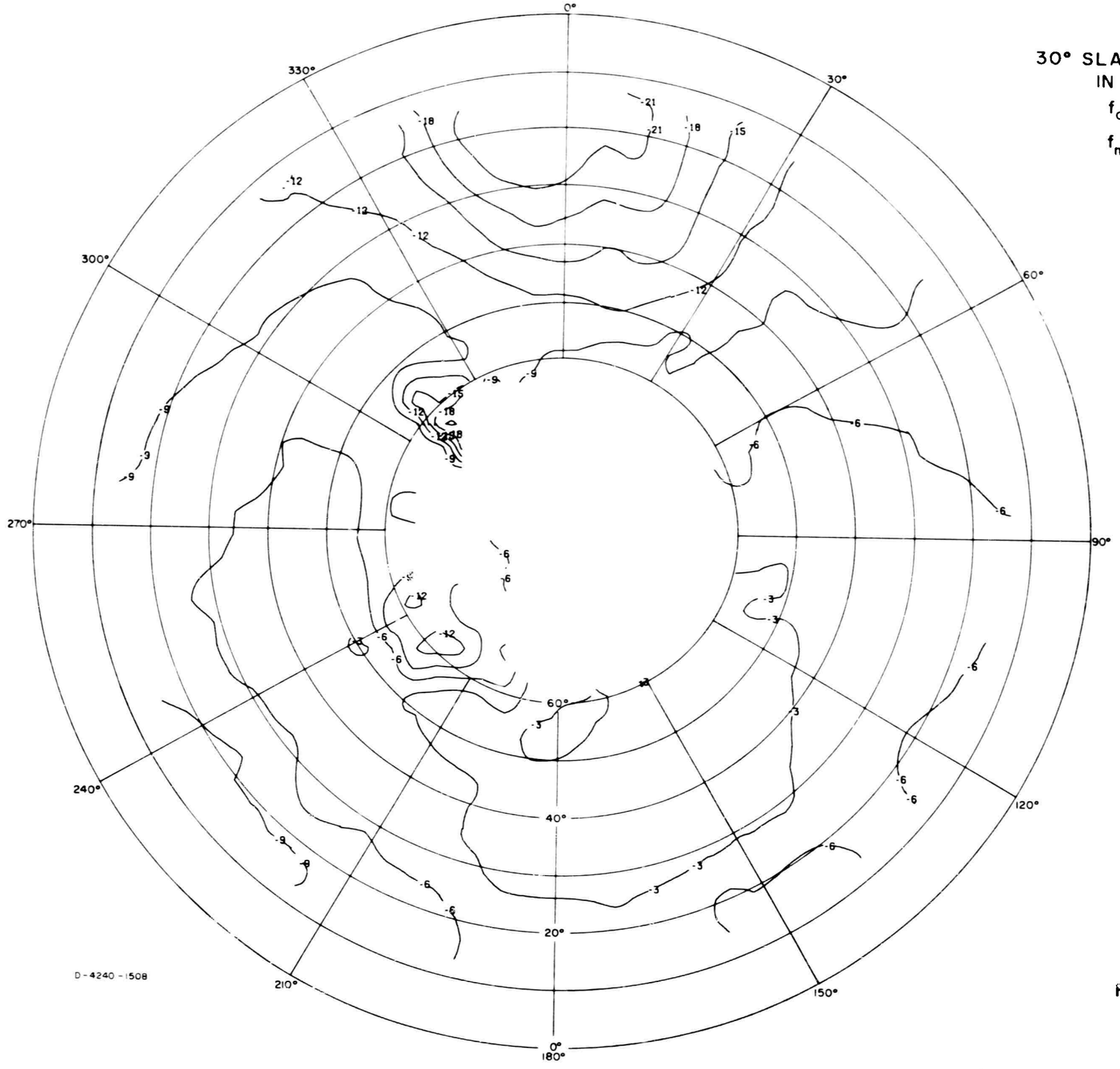

30° SLANT WIRE
IN FOLIAGE
f_o = 6 Mc/s
f_m = 8 Mc/s
POWER

FIG. A-136

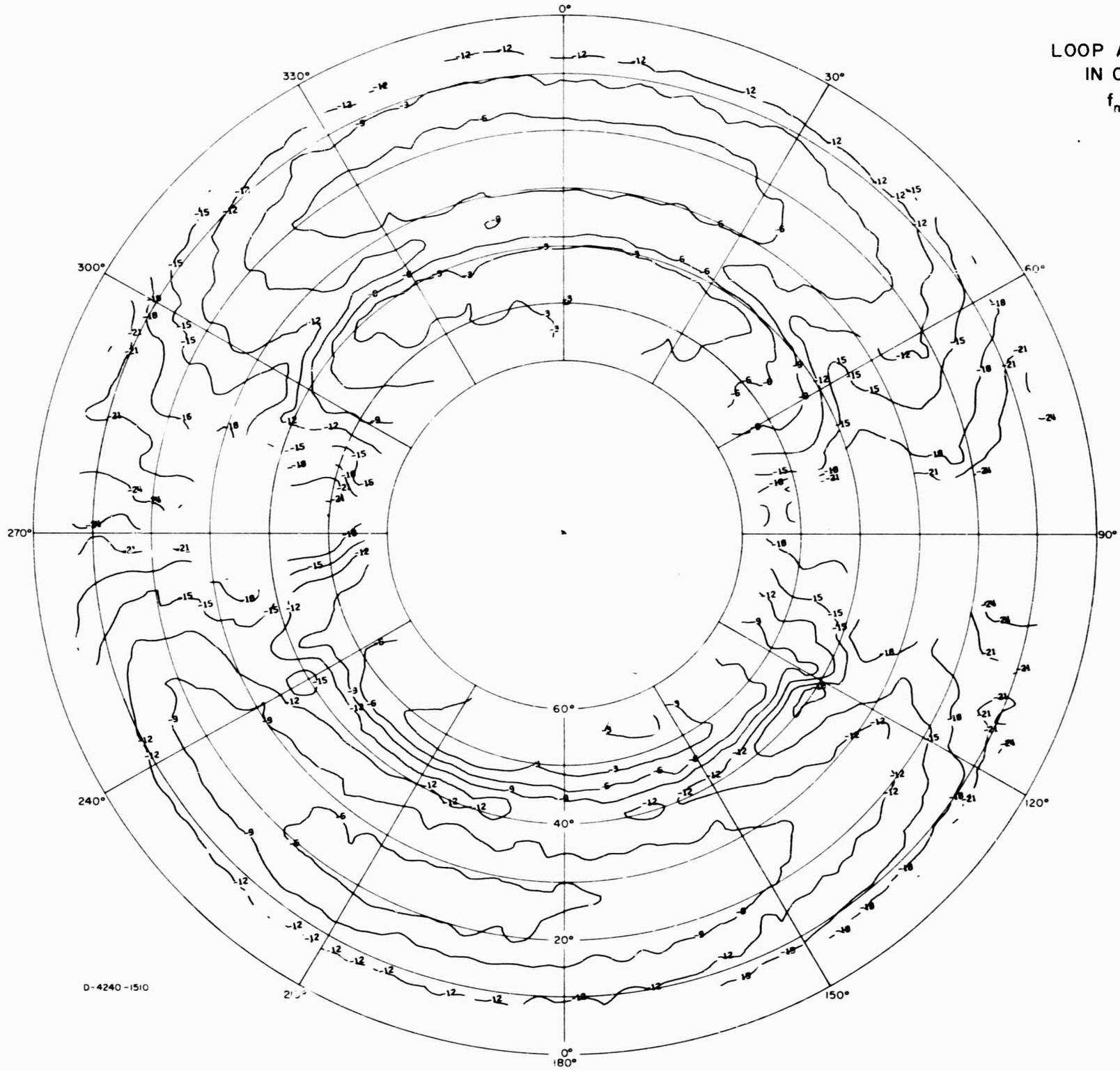

LOOP ANTENNA
IN CLEARING
f_m = 6 Mc/s
E_θ

FIG. A-137

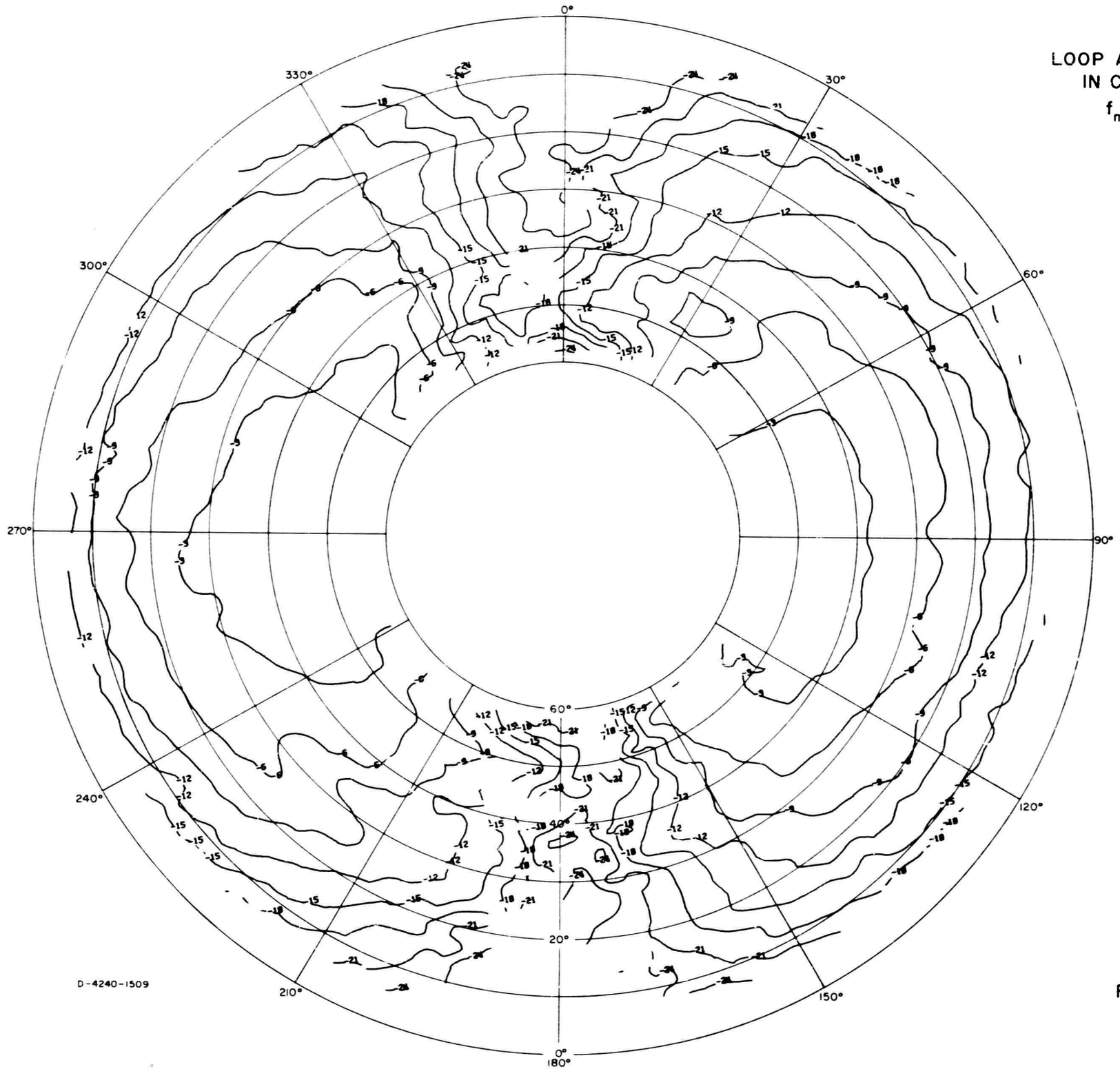

LOOP ANTENNA
IN CLEARING
f_m = 6 Mc/s
E_ϕ

D-4240-1509

FIG. A-138

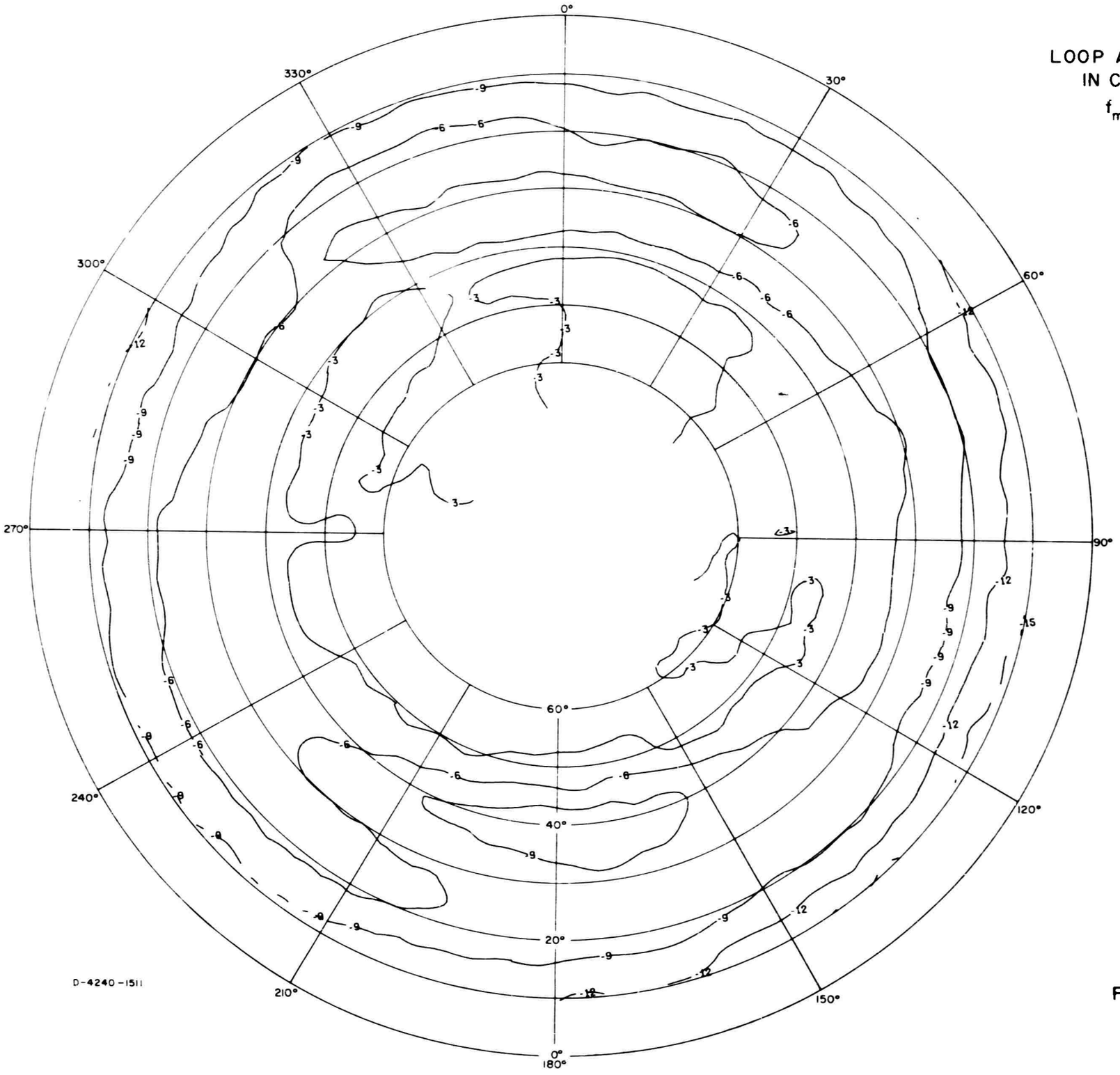

LOOP ANTENNA
IN CLEARING
f_m = 6 Mc/s
POWER

FIG. A-139

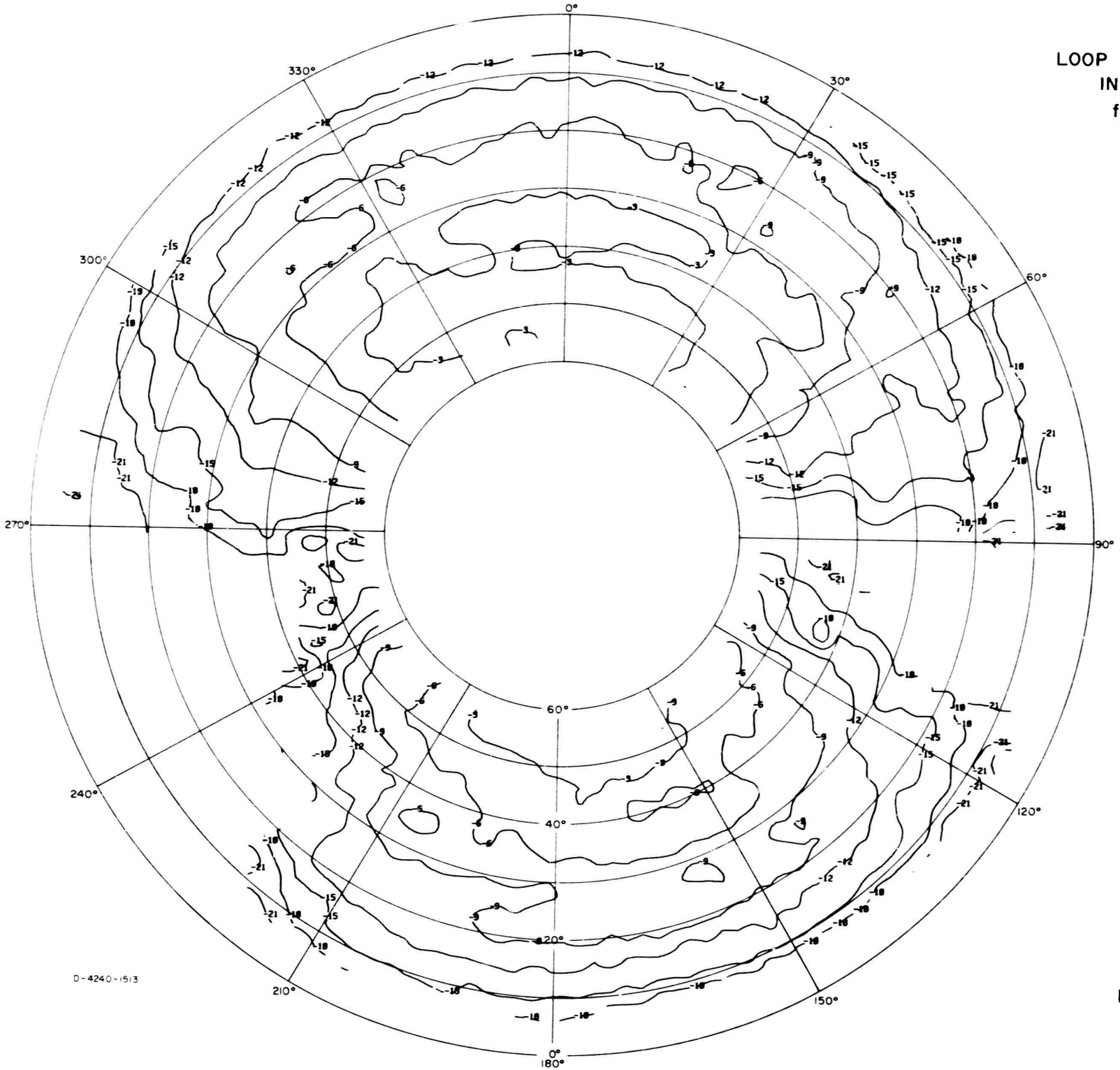

LOOP ANTENNA
IN FOLIAGE
$f_m = 6$ Mc/s
E_θ

FIG. A-140

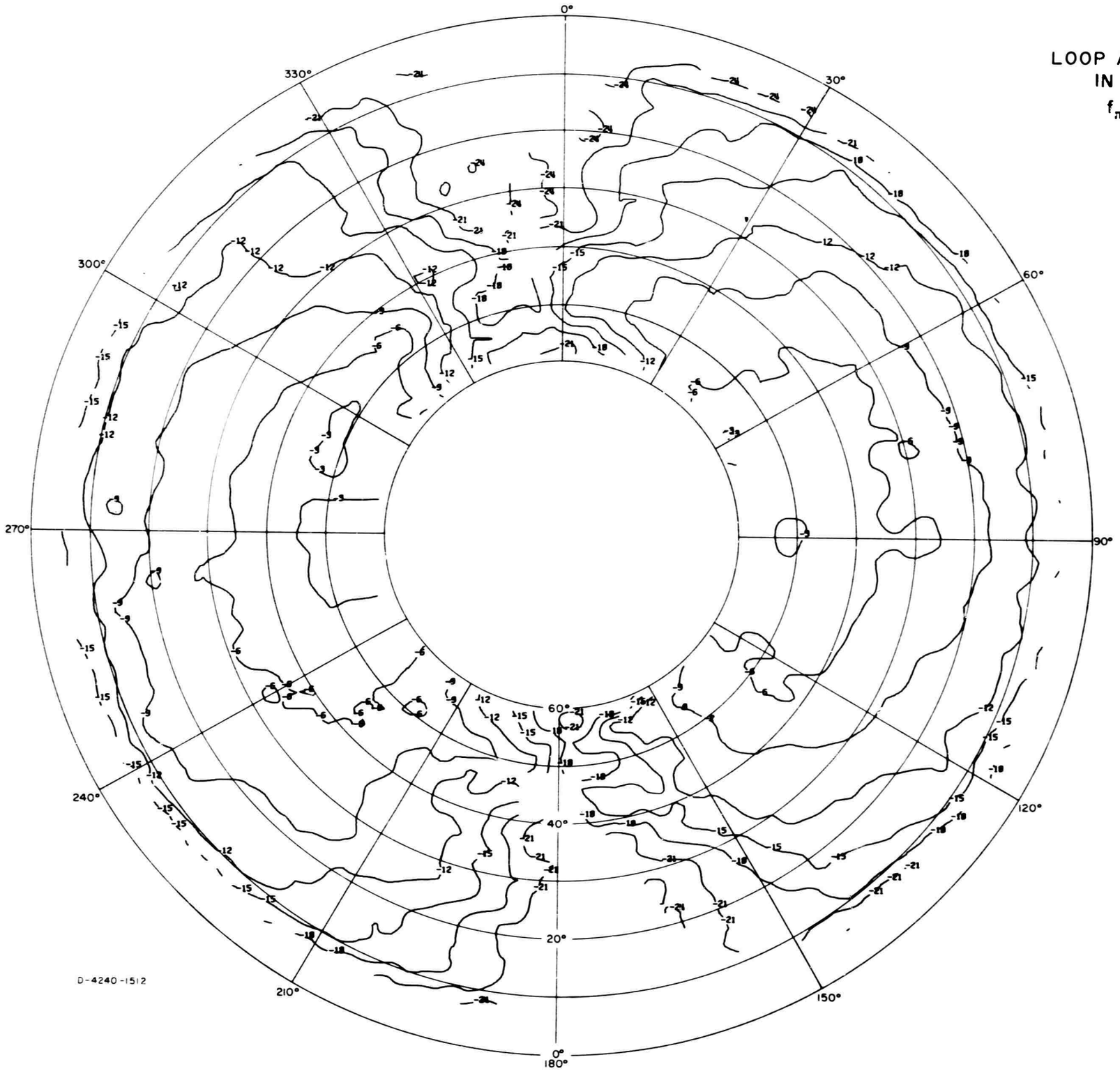

LOOP ANTENNA
IN FOLIAGE
$f_m = 6$ Mc/s
E_ϕ

FIG. A-141

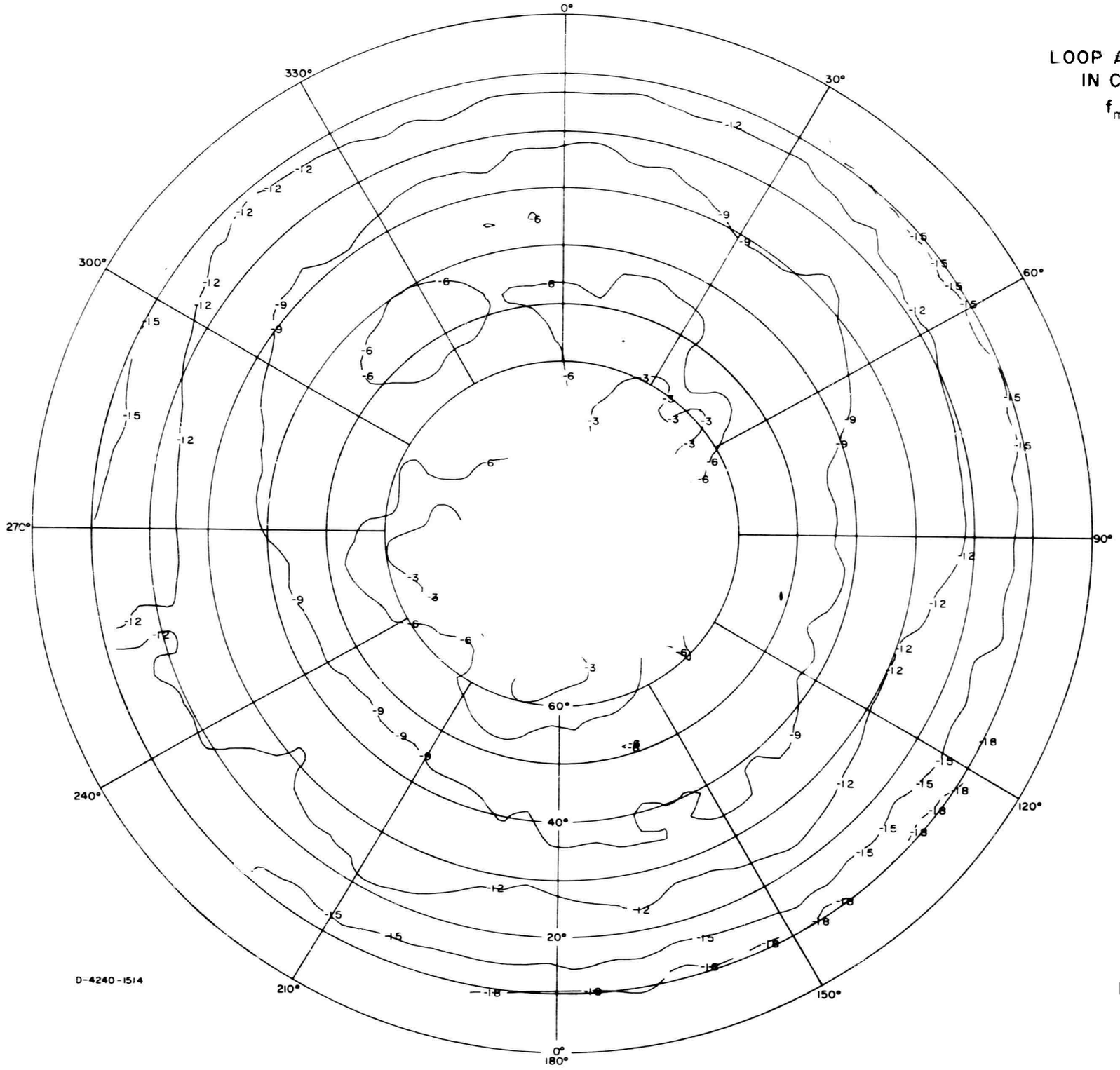

LOOP ANTENNA
IN CLEARING
f_m = 6 Mc/s
POWER

FIG. A-142

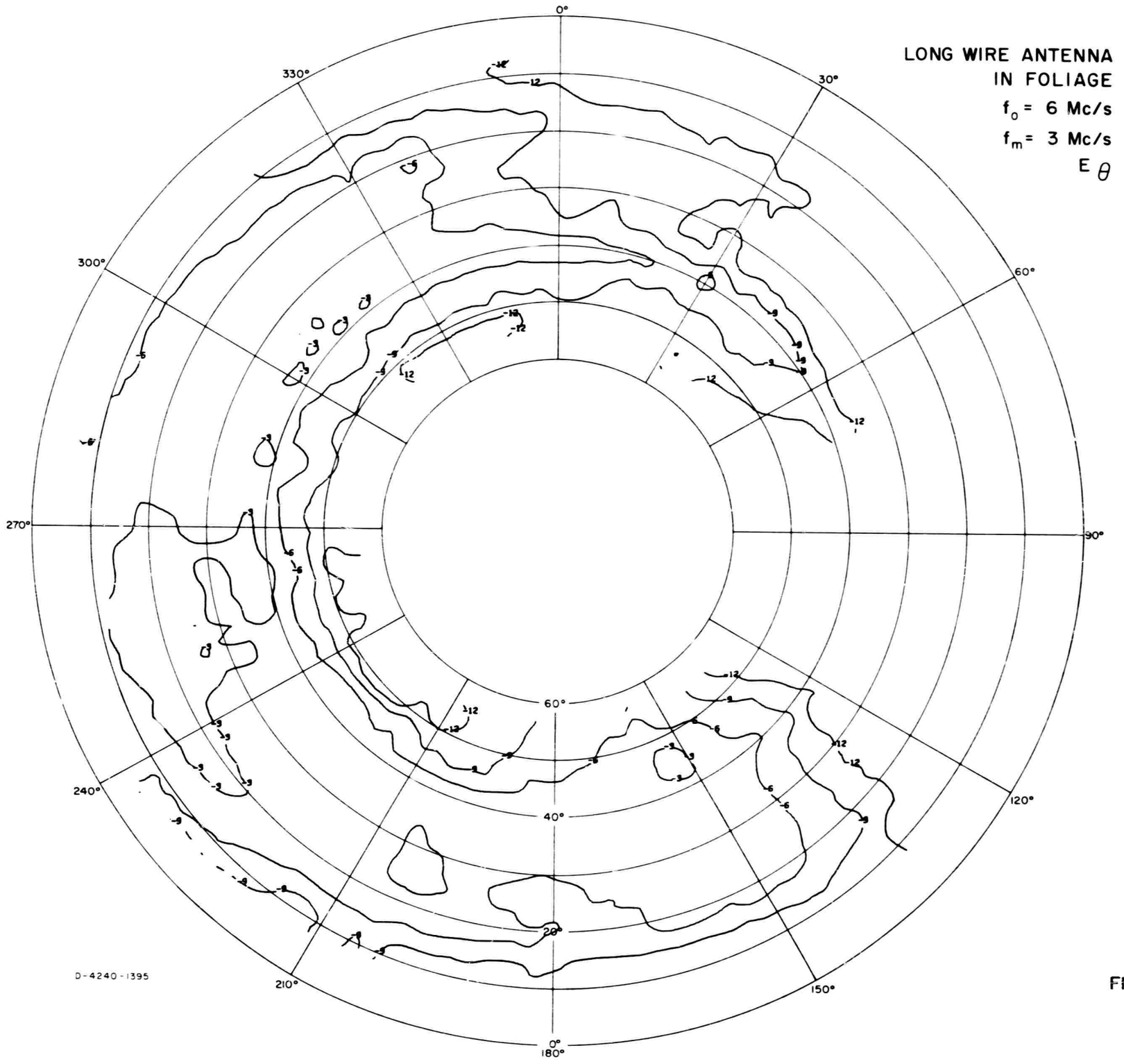
LONG WIRE ANTENNA
IN FOLIAGE
f_0 = 6 Mc/s
f_m = 3 Mc/s
E θ
0°
30°
60°
90°
120°
150°
180°
210°
240°
270°
300°
330°
60°
40°
20°
D-4240-1395

FIG. A-143

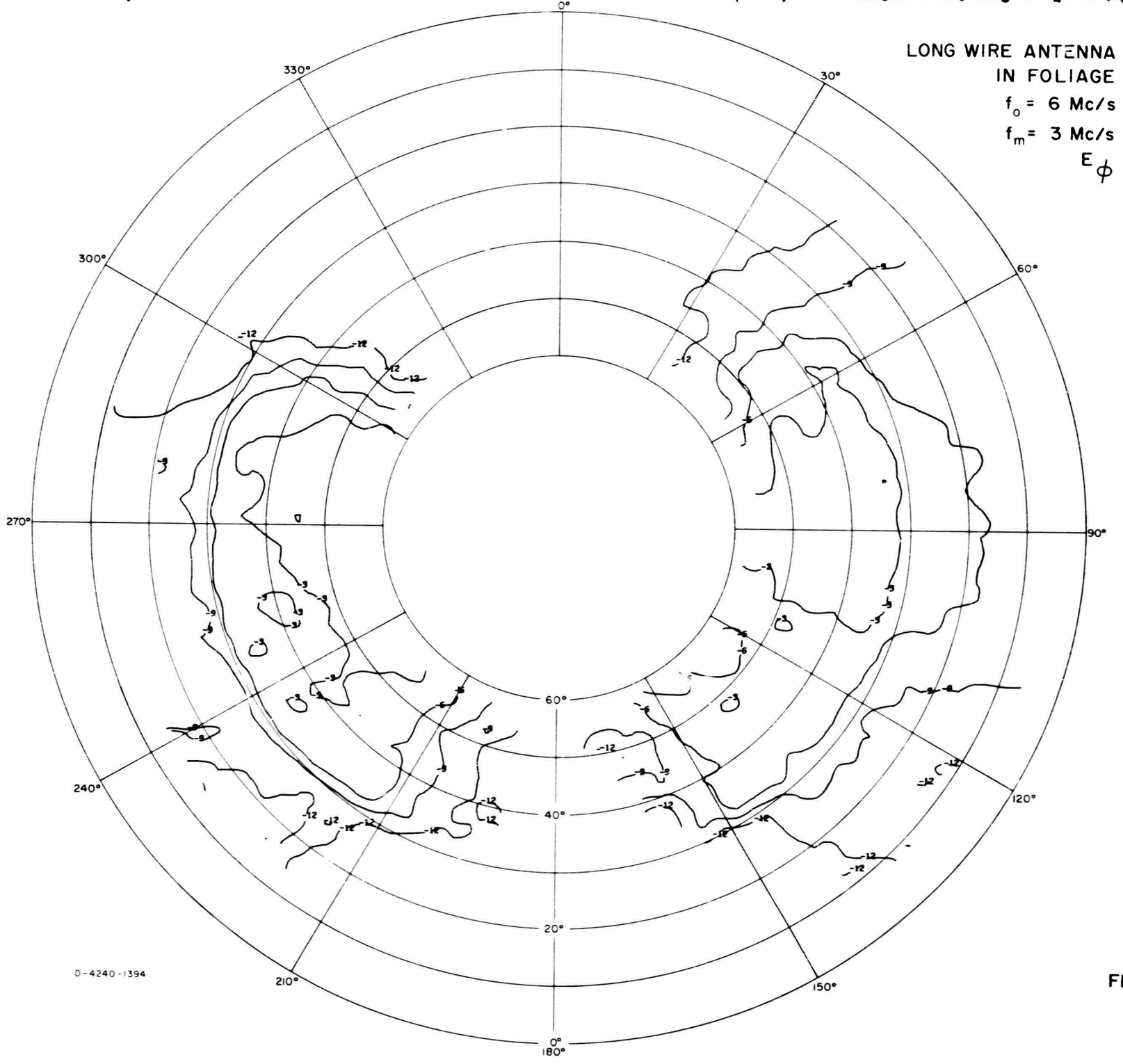
LONG WIRE ANTENNA
IN FOLIAGE
f_o = 6 Mc/s
f_m = 3 Mc/s
E_ϕ
0°
30°
60°
90°
120°
150°
180°
210°
240°
270°
300°
330°
20°
40°
60°
D-4240-1394

FIG. A-144

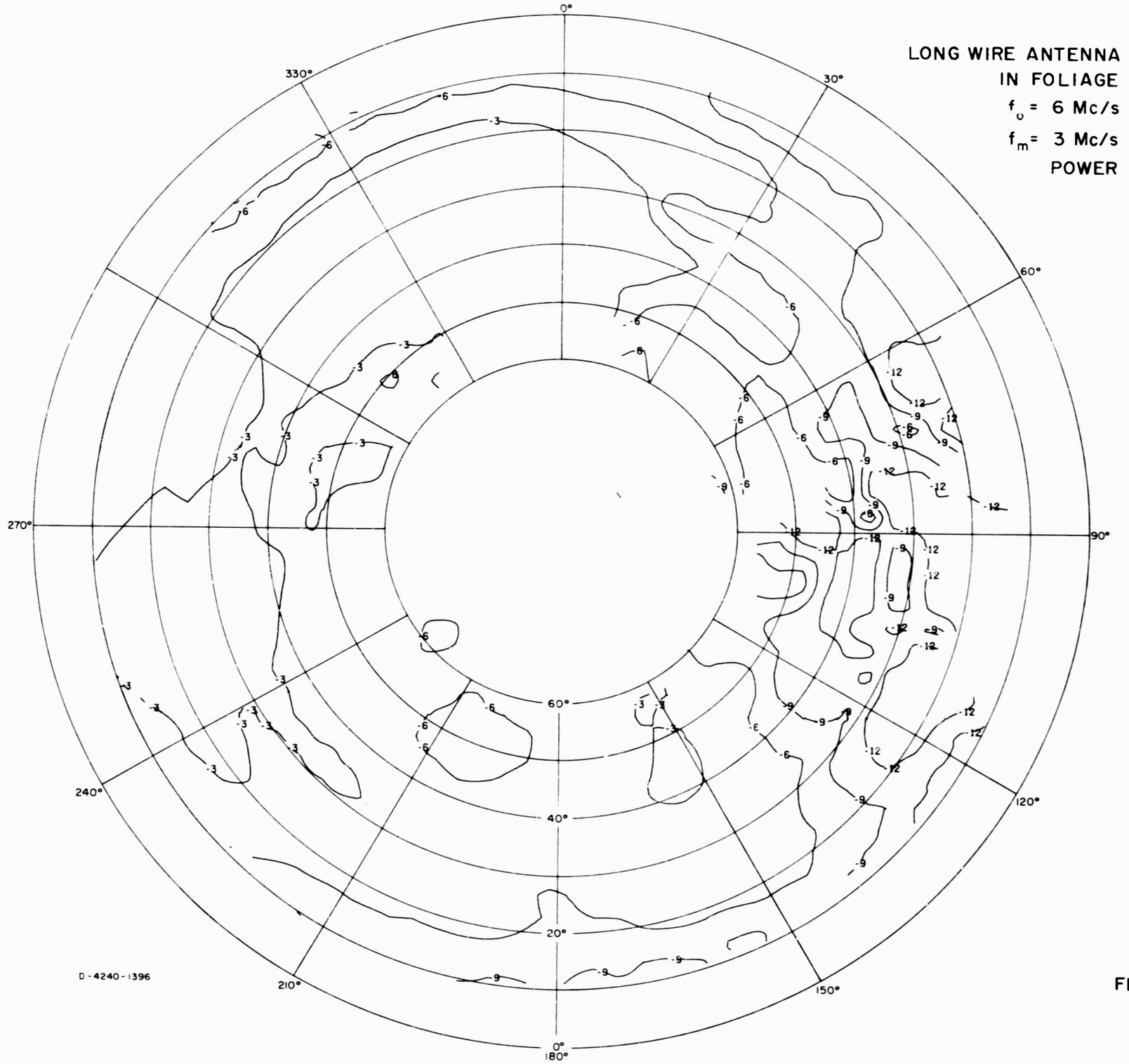
LONG WIRE ANTENNA
IN FOLIAGE
f_o = 6 Mc/s
f_m = 3 Mc/s
POWER
0°
30°
60°
90°
120°
150°
180°
210°
240°
270°
330°
60°
40°
20°
0°
D-4240-1396

FIG. A-145

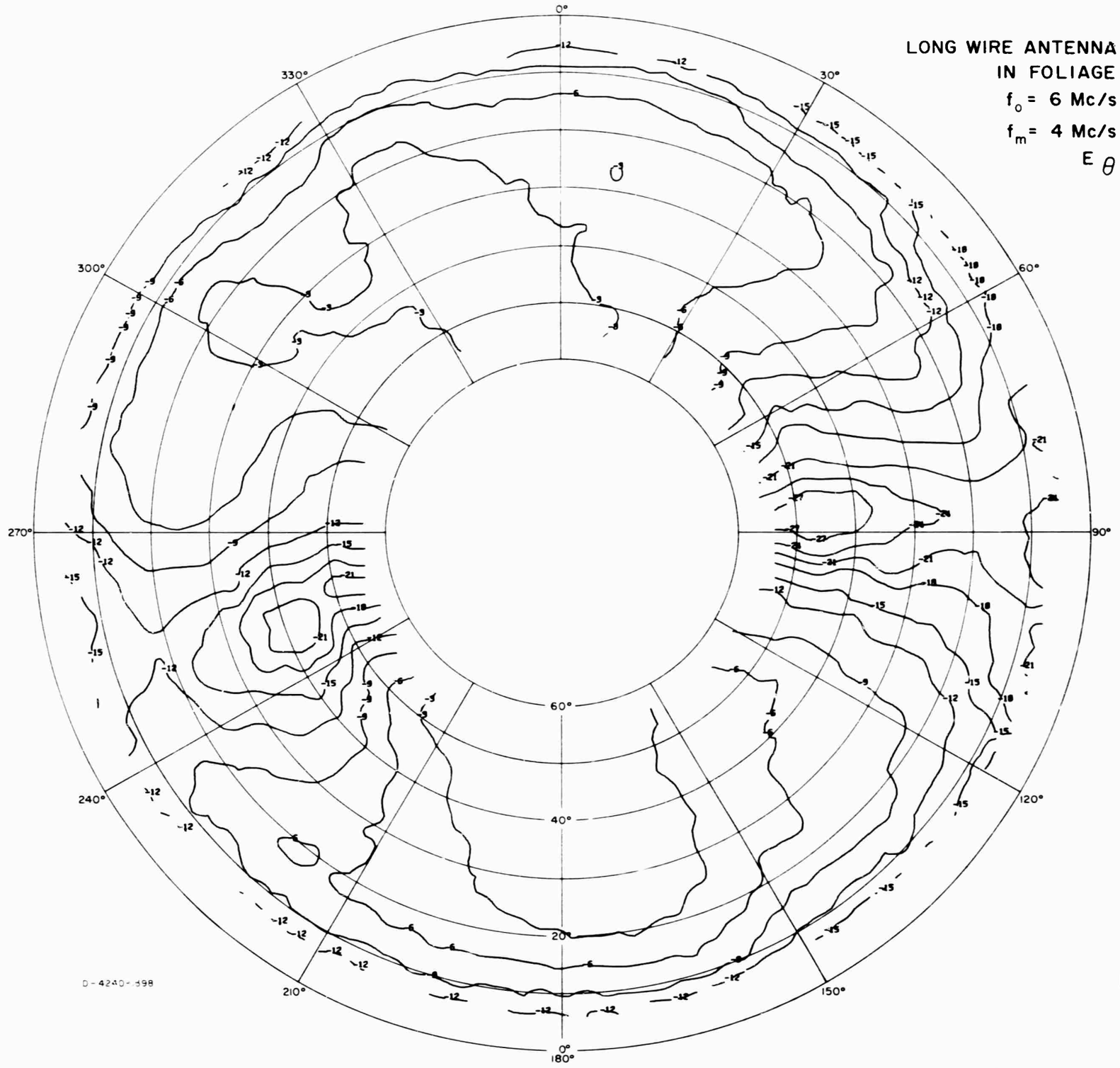
LONG WIRE ANTENNA
IN FOLIAGE
f_o = 6 Mc/s
f_m = 4 Mc/s
E θ
0°
30°
60°
90°
120°
150°
180°
210°
240°
270°
300°
330°
20°
40°
60°
D-42401-698

FIG. A-146

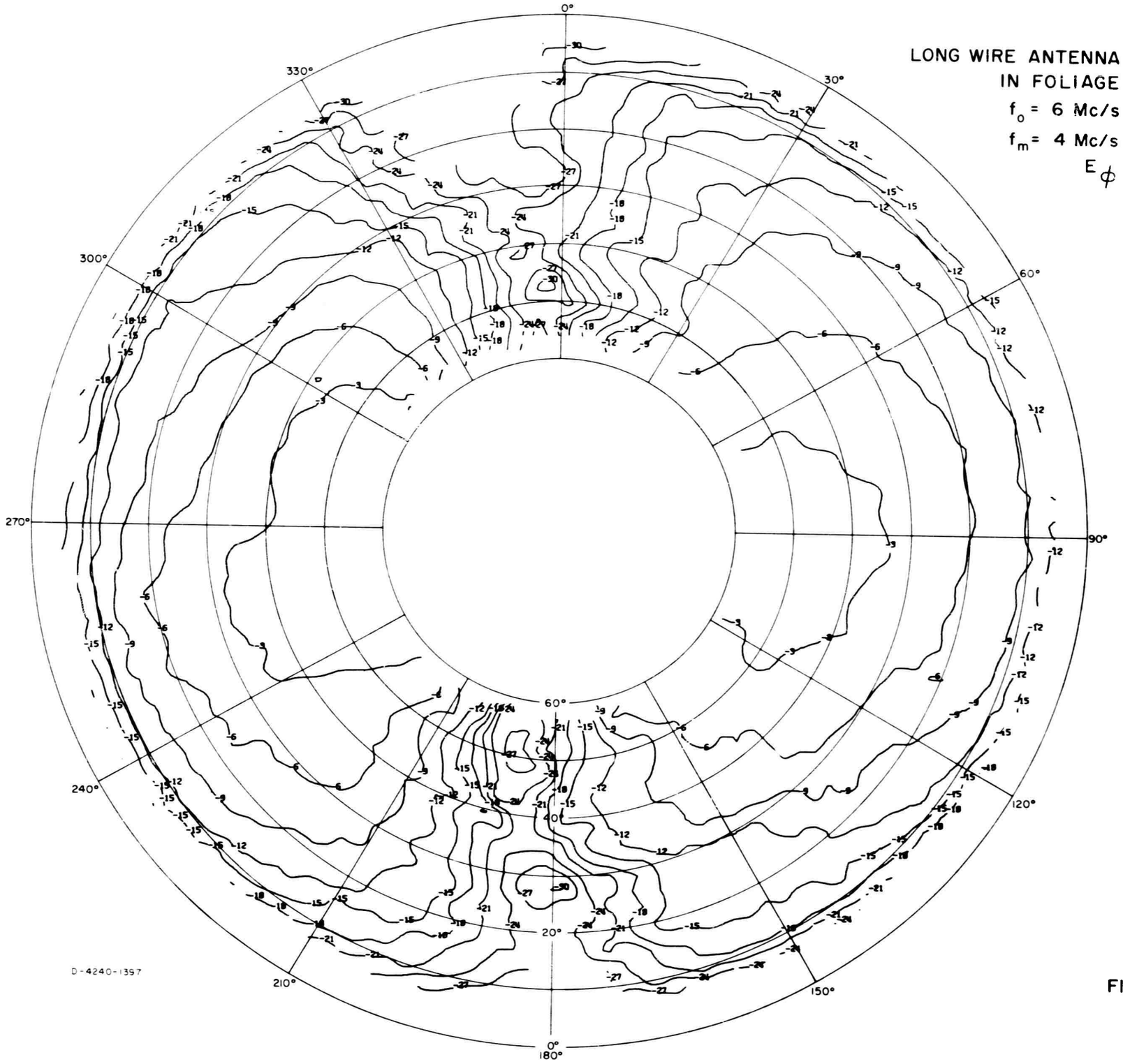
LONG WIRE ANTENNA
IN FOLIAGE
f_o = 6 Mc/s
f_m = 4 Mc/s
E_ϕ
0°
30°
60°
90°
120°
150°
180°
210°
240°
270°
300°
330°
20°
40°
60°
D-4240-1397

FIG. A-147

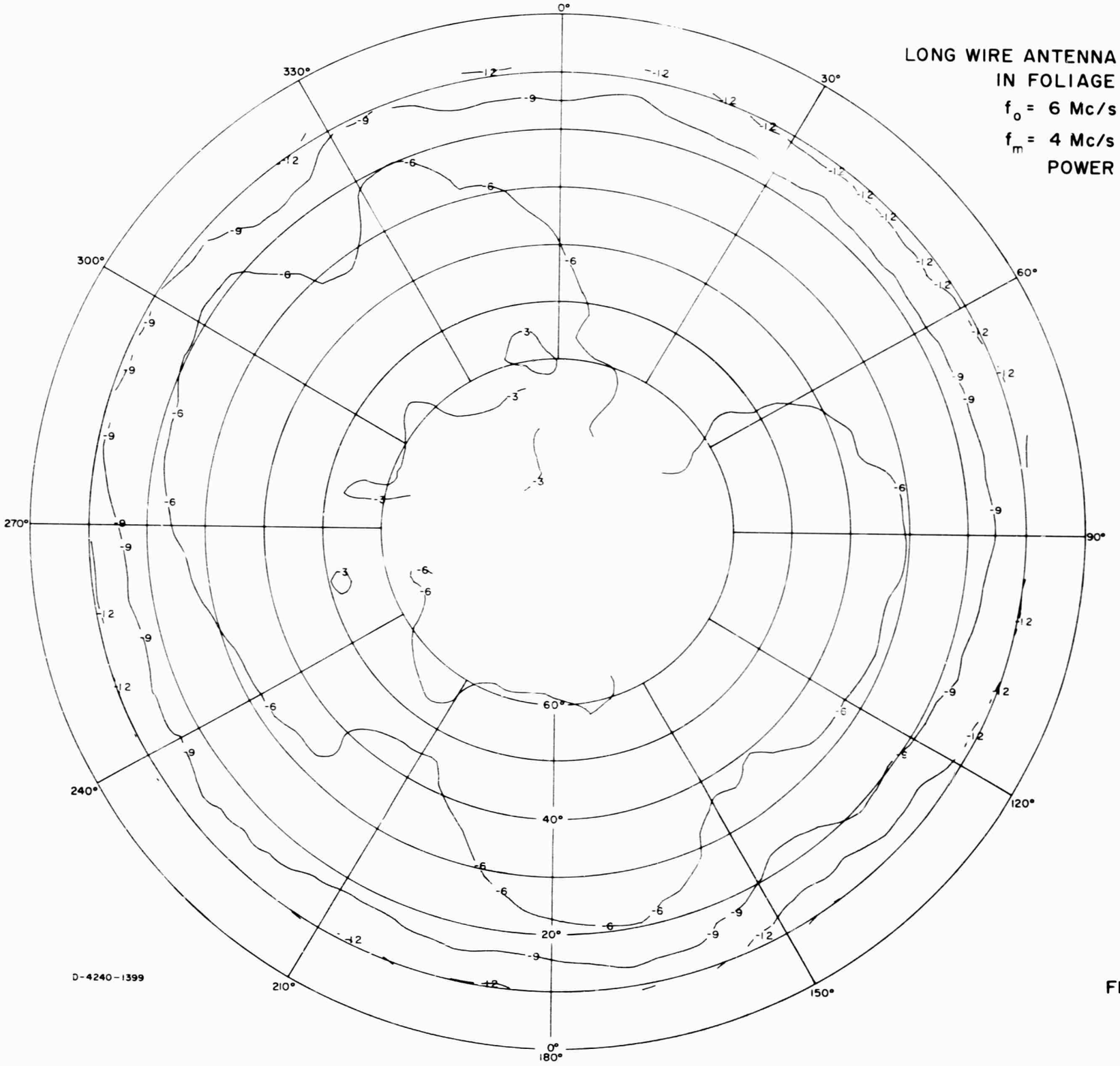
LONG WIRE ANTENNA
IN FOLIAGE
f_o = 6 Mc/s
f_m = 4 Mc/s
POWER
0°
30°
60°
90°
120°
150°
180°
210°
240°
270°
300°
330°
20°
40°
60°
-3
-6
-9
-12
D-4240-1399

FIG. A-148

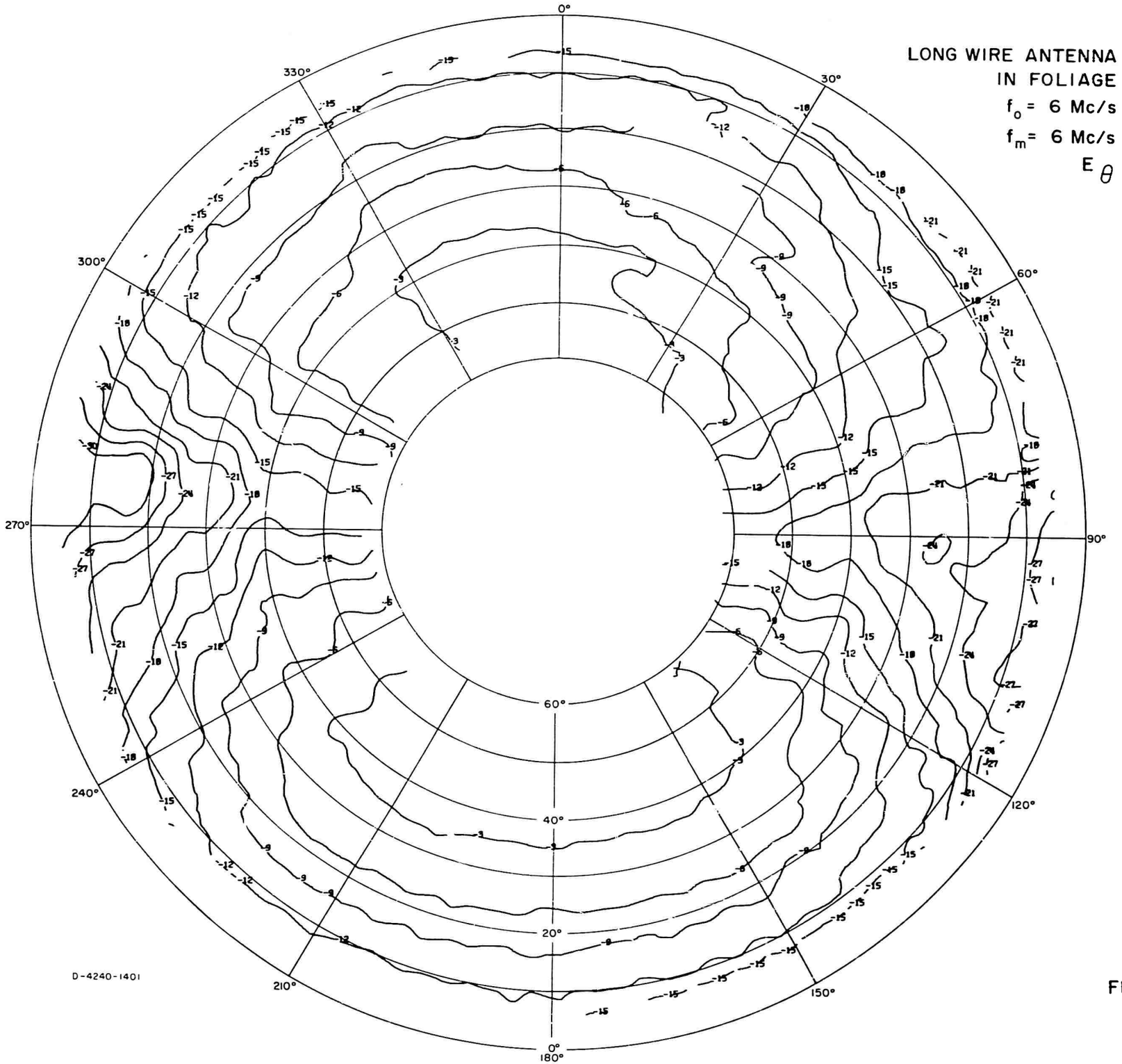
LONG WIRE ANTENNA
IN FOLIAGE
f_o = 6 Mc/s
f_m = 6 Mc/s
E_θ
0°
30°
60°
90°
120°
150°
180°
210°
240°
270°
300°
330°
20°
40°
60°
D-4240-1401

FIG. A-149

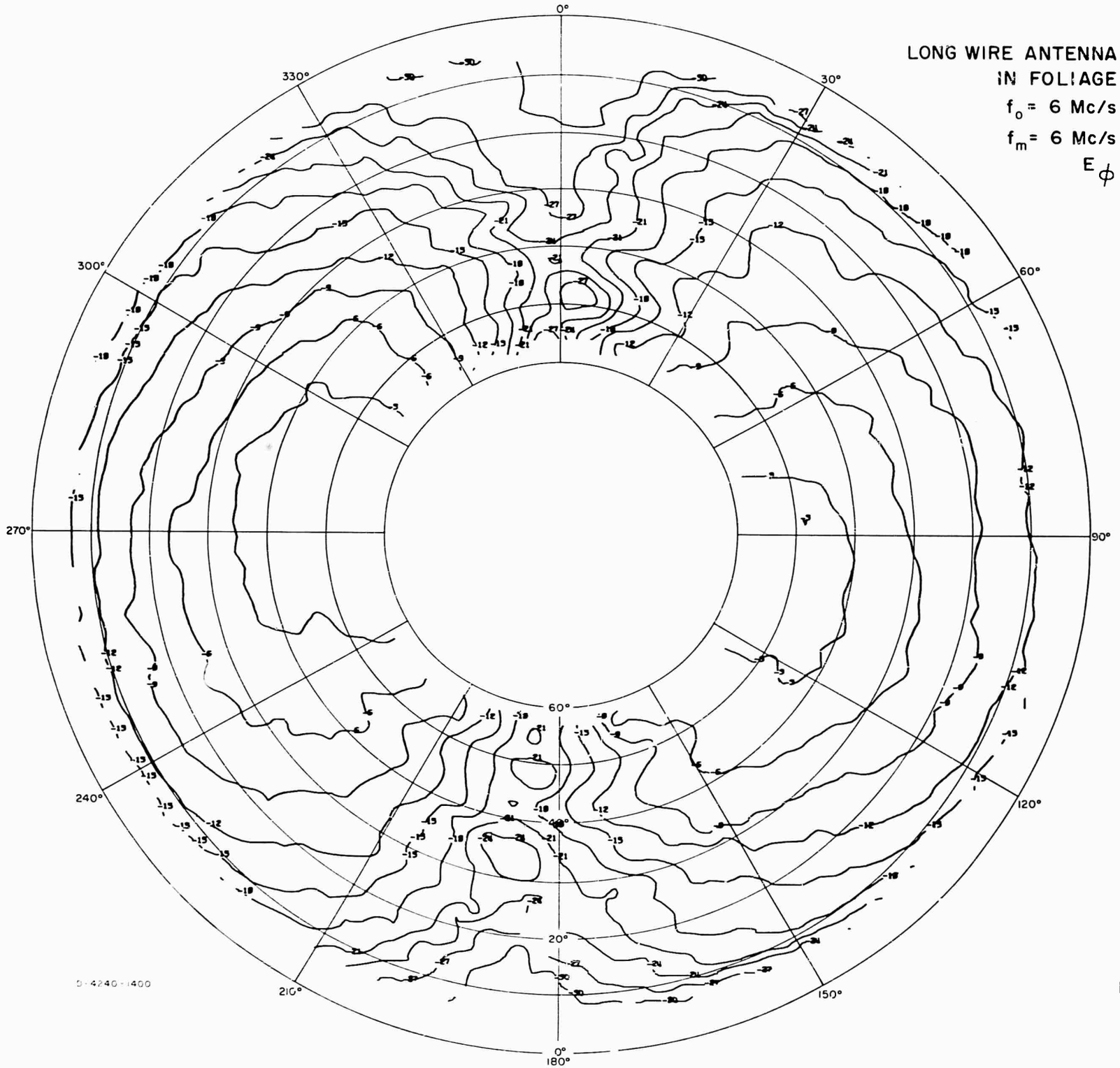
LONG WIRE ANTENNA
IN FOLIAGE
f_o = 6 Mc/s
f_m = 6 Mc/s
E_ϕ
0°
30°
60°
90°
120°
150°
180°
210°
240°
270°
300°
330°
20°
40°
60°
D-4240-1400

FIG. A-150

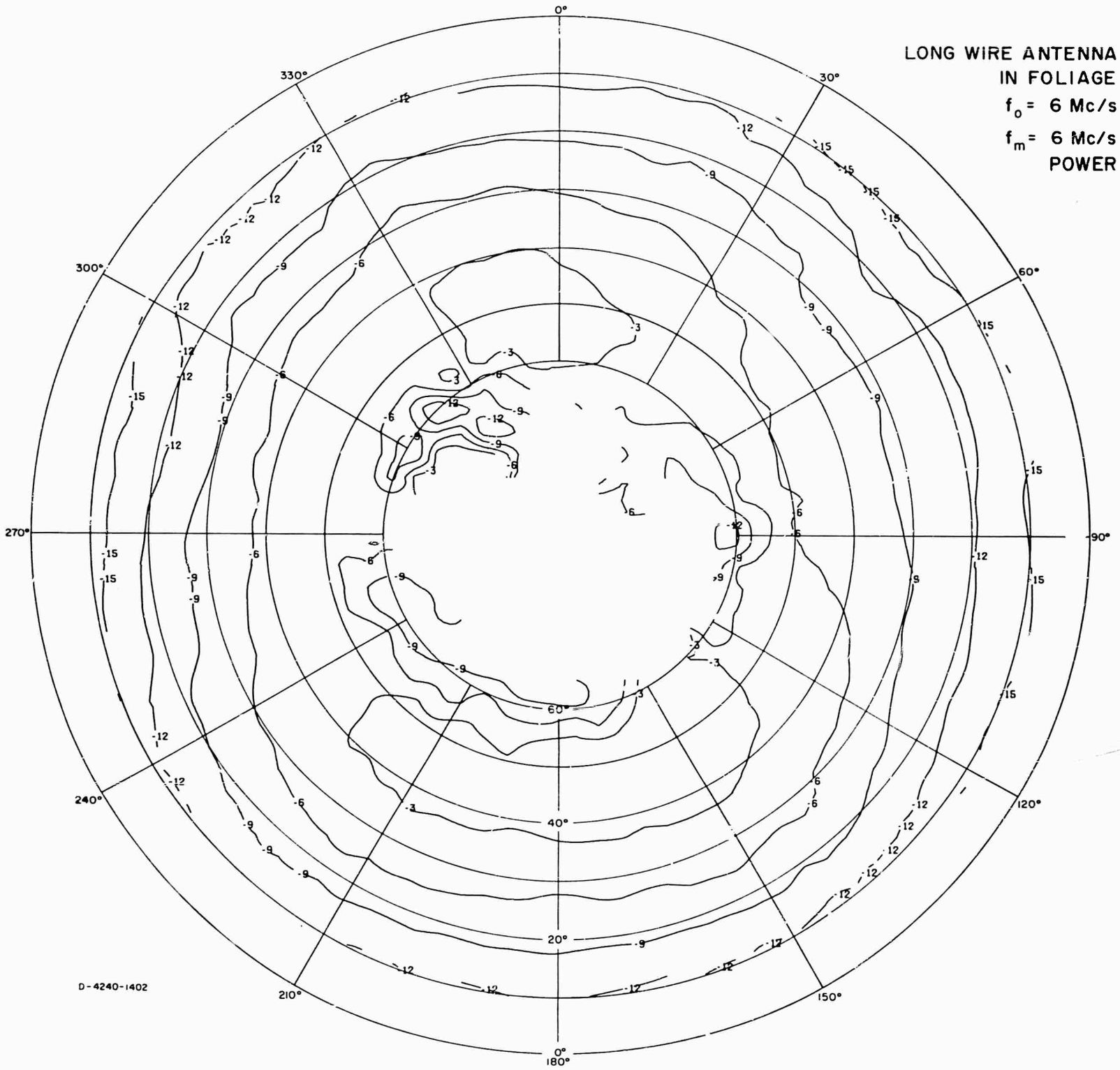
LONG WIRE ANTENNA
IN FOLIAGE
f_o = 6 Mc/s
f_m = 6 Mc/s
POWER
0°
30°
60°
90°
120°
150°
180°
210°
240°
270°
300°
330°
D-4240-1402

FIG. A-151

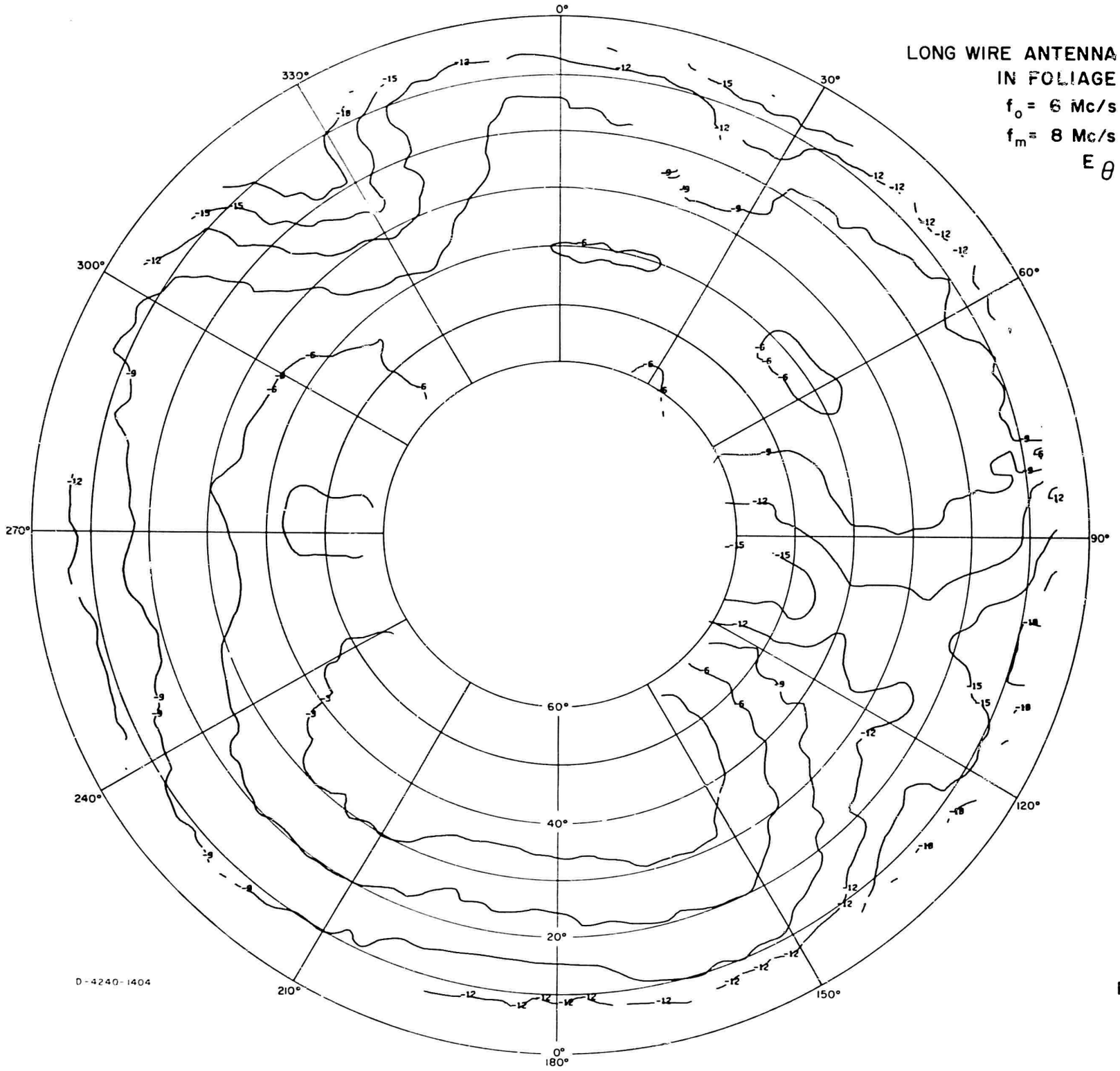
LONG WIRE ANTENNA
IN FOLIAGE
f_o = 6 Mc/s
f_m = 8 Mc/s
E_θ
0°
30°
60°
90°
120°
150°
180°
210°
240°
270°
300°
330°
20°
40°
60°
D-4240-1404

FIG. A-152

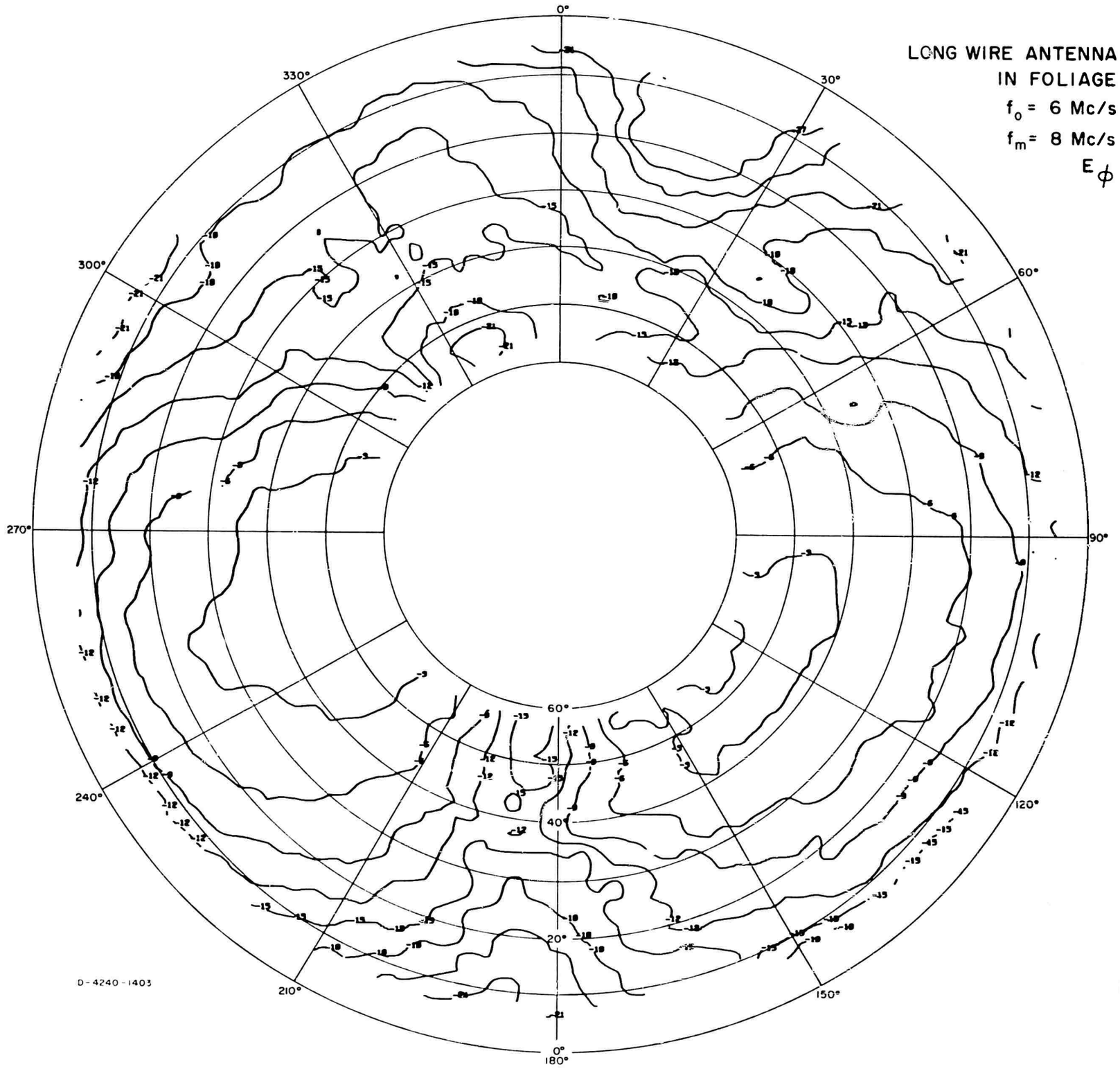
LONG WIRE ANTENNA
IN FOLIAGE
f_o = 6 Mc/s
f_m = 8 Mc/s
E_ϕ
0°
30°
60°
90°
120°
150°
180°
210°
240°
270°
300°
330°
60°
40°
20°
D-4240-1403

FIG. A-153

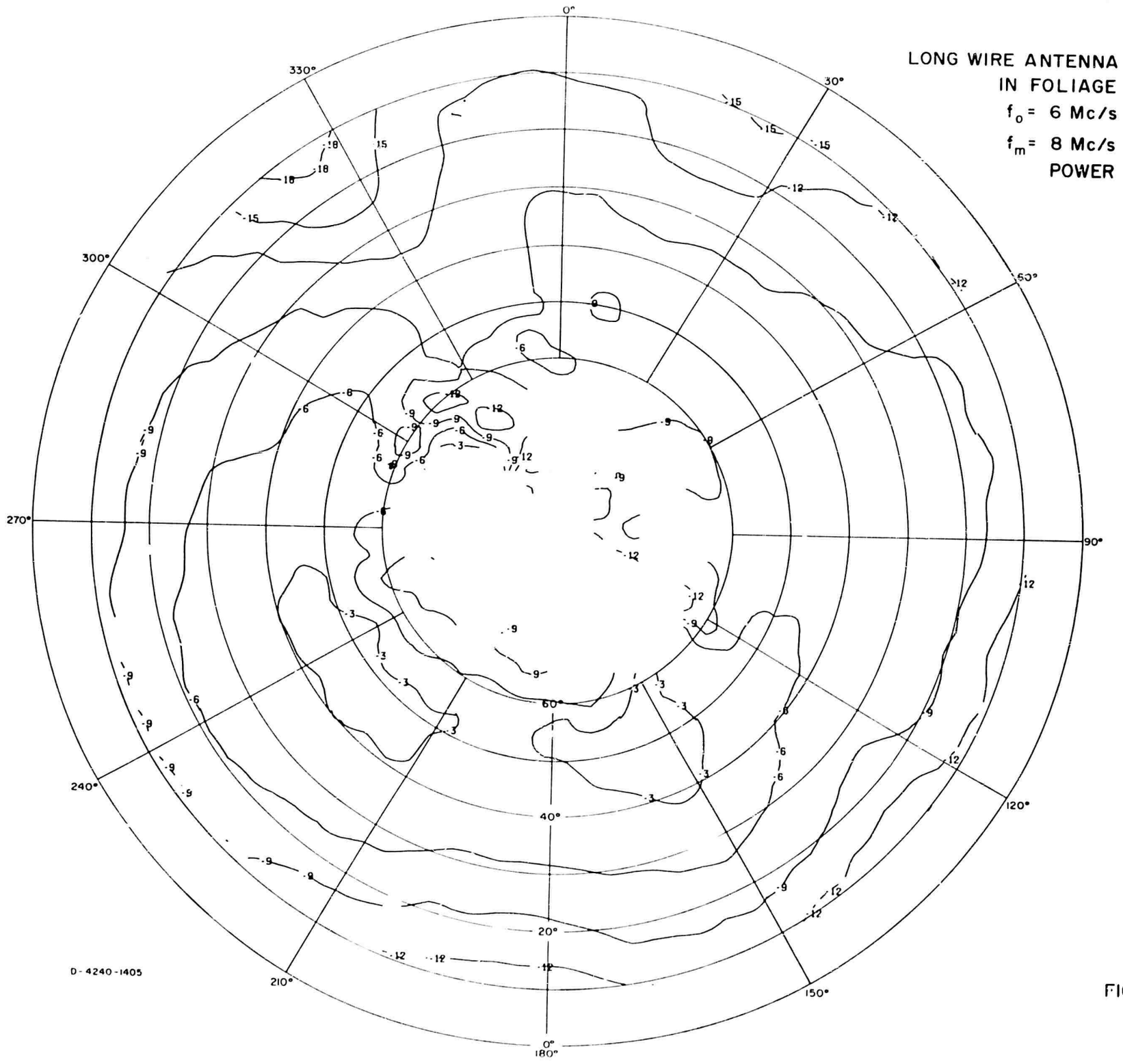
LONG WIRE ANTENNA
IN FOLIAGE
f_o = 6 Mc/s
f_m = 8 Mc/s
POWER
0°
30°
60°
90°
120°
150°
180°
210°
240°
270°
300°
330°
20°
40°
60°
D-4240-1405

FIG. A-154

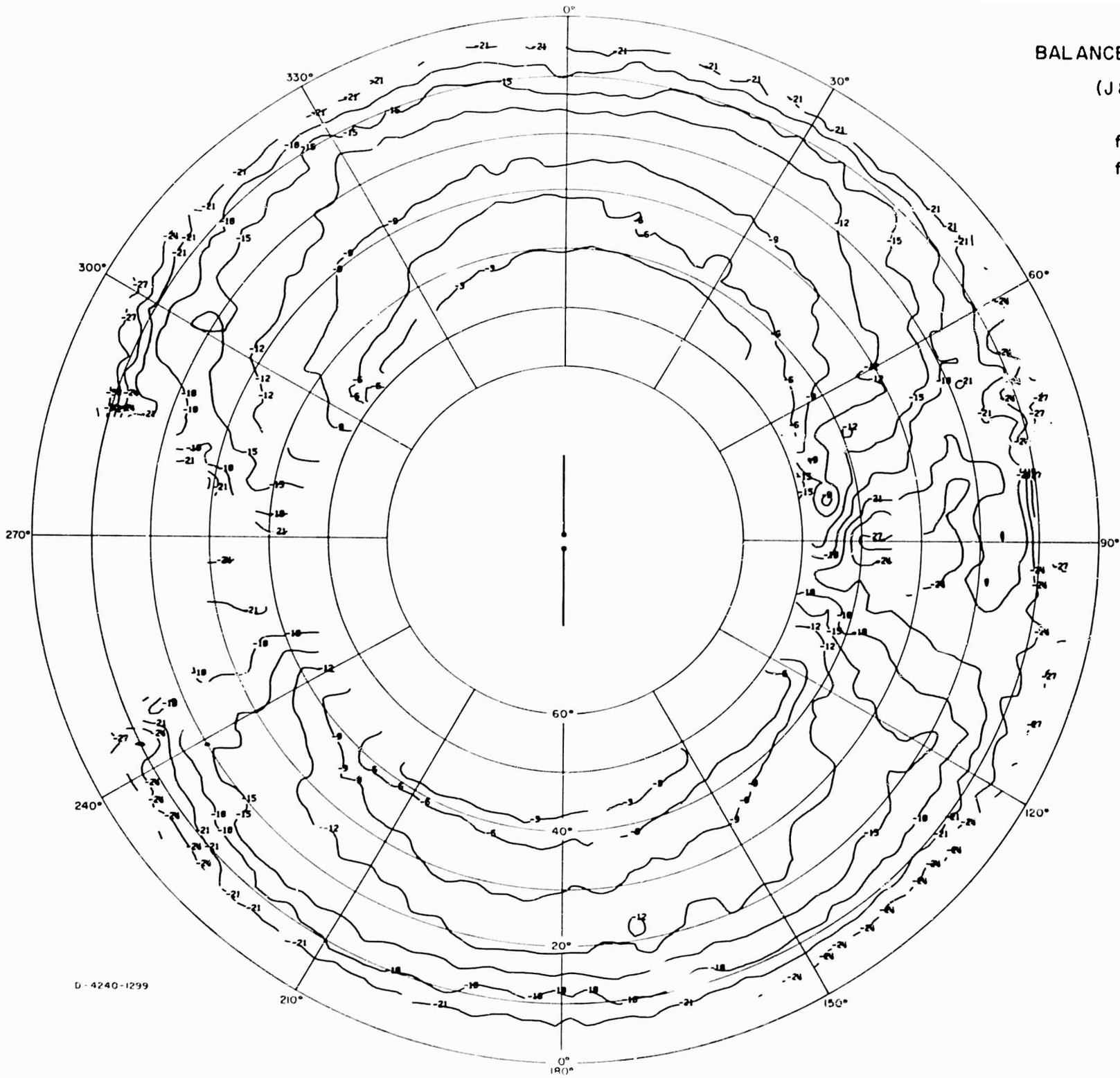

BALANCED DIPOLE

(J & B TYPE)

$h_a = 40'$

$f_o = 6$ Mc/s

$f_m = 6$ Mc/s

$E\theta$

FIG. A-155

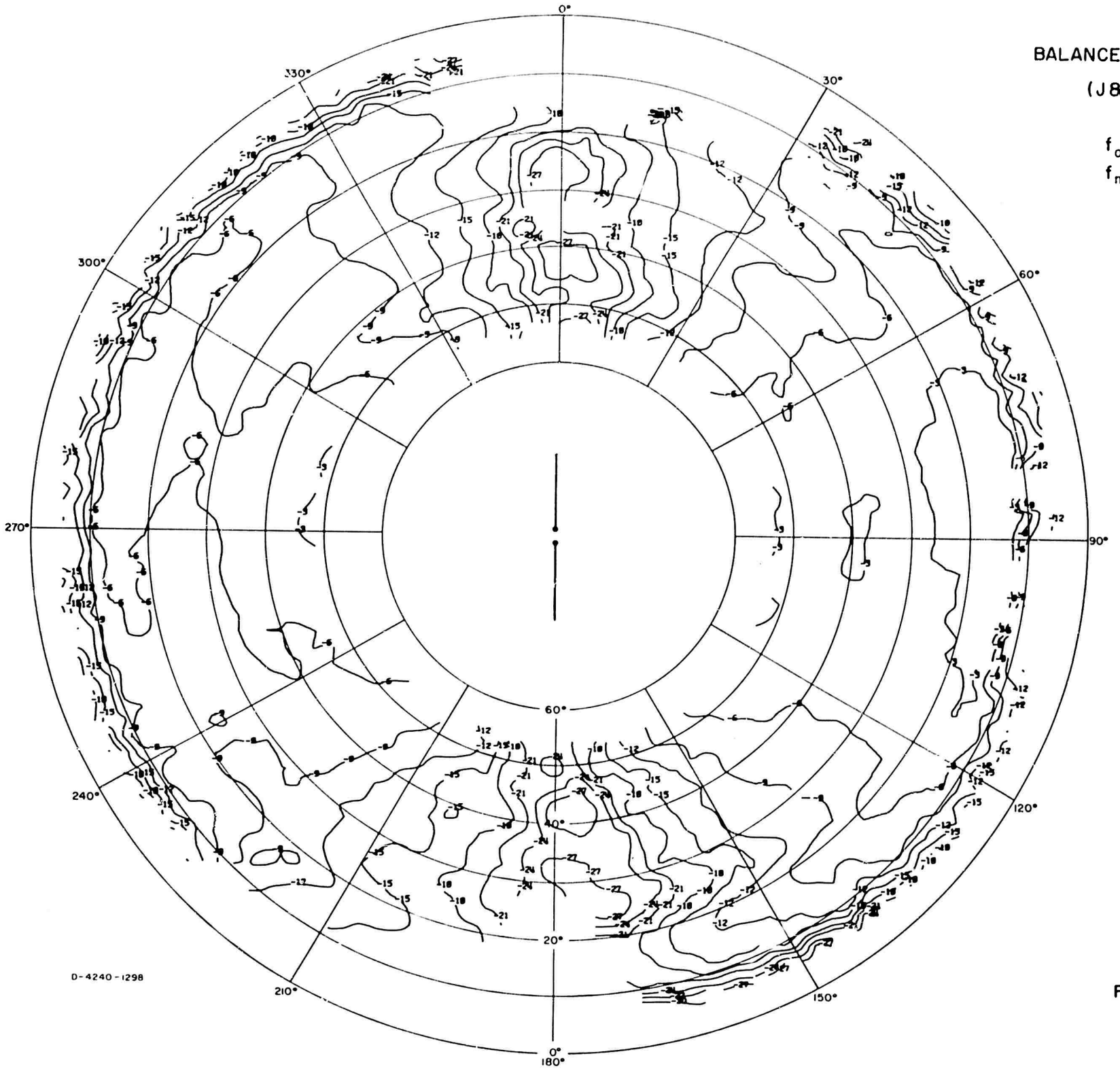

BALANCED DIPOLE

(J&B TYPE)

$h_a = 40'$

$f_o = 6$ Mc/s

$f_m = 6$ Mc/s

E_ϕ

FIG. A-156

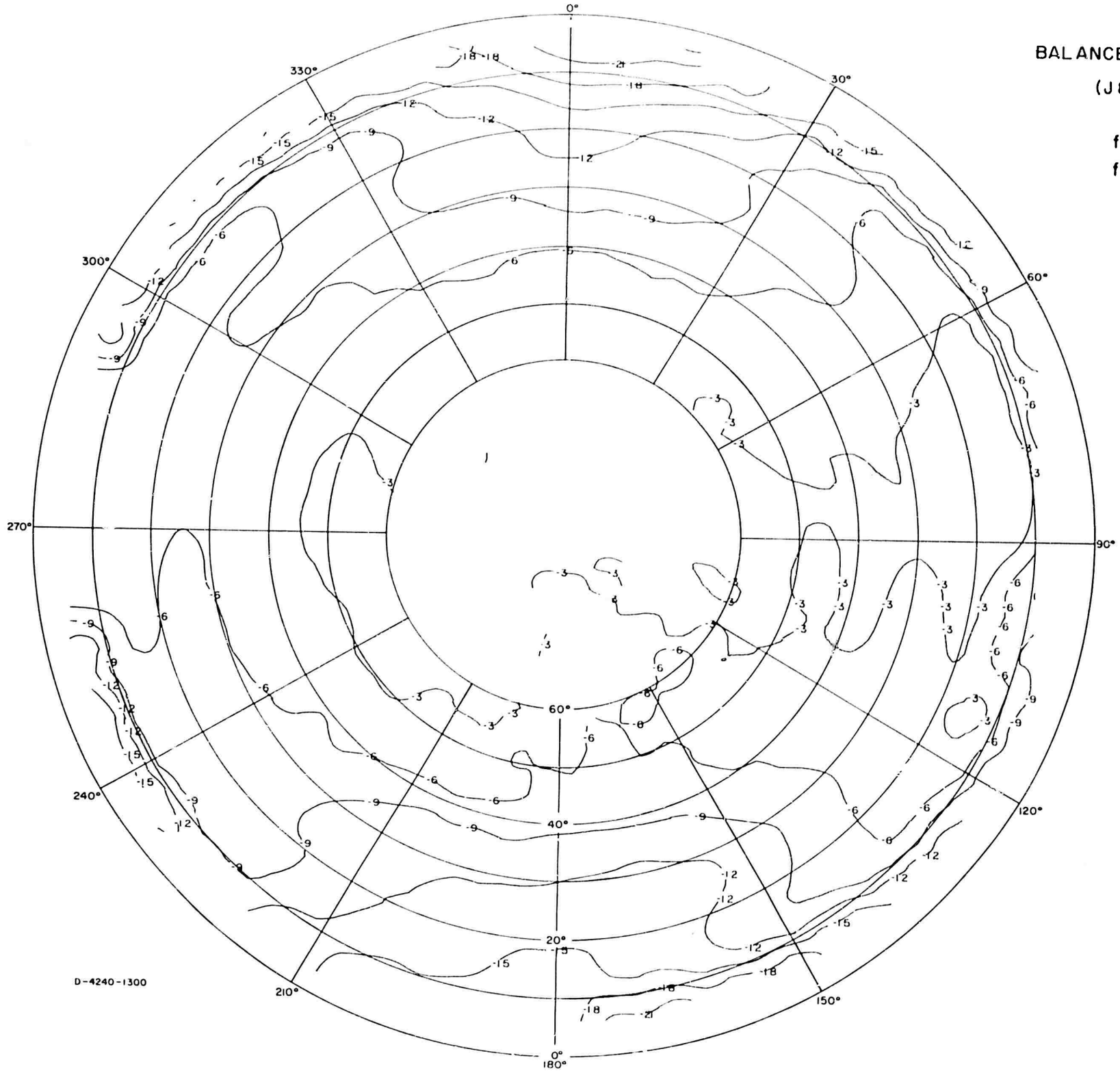

BALANCED DIPOLE

(J&B TYPE)

$h_a = 40'$

$f_o = 6$ Mc/s

$f_m = 6$ Mc/s

POWER

FIG. A-157

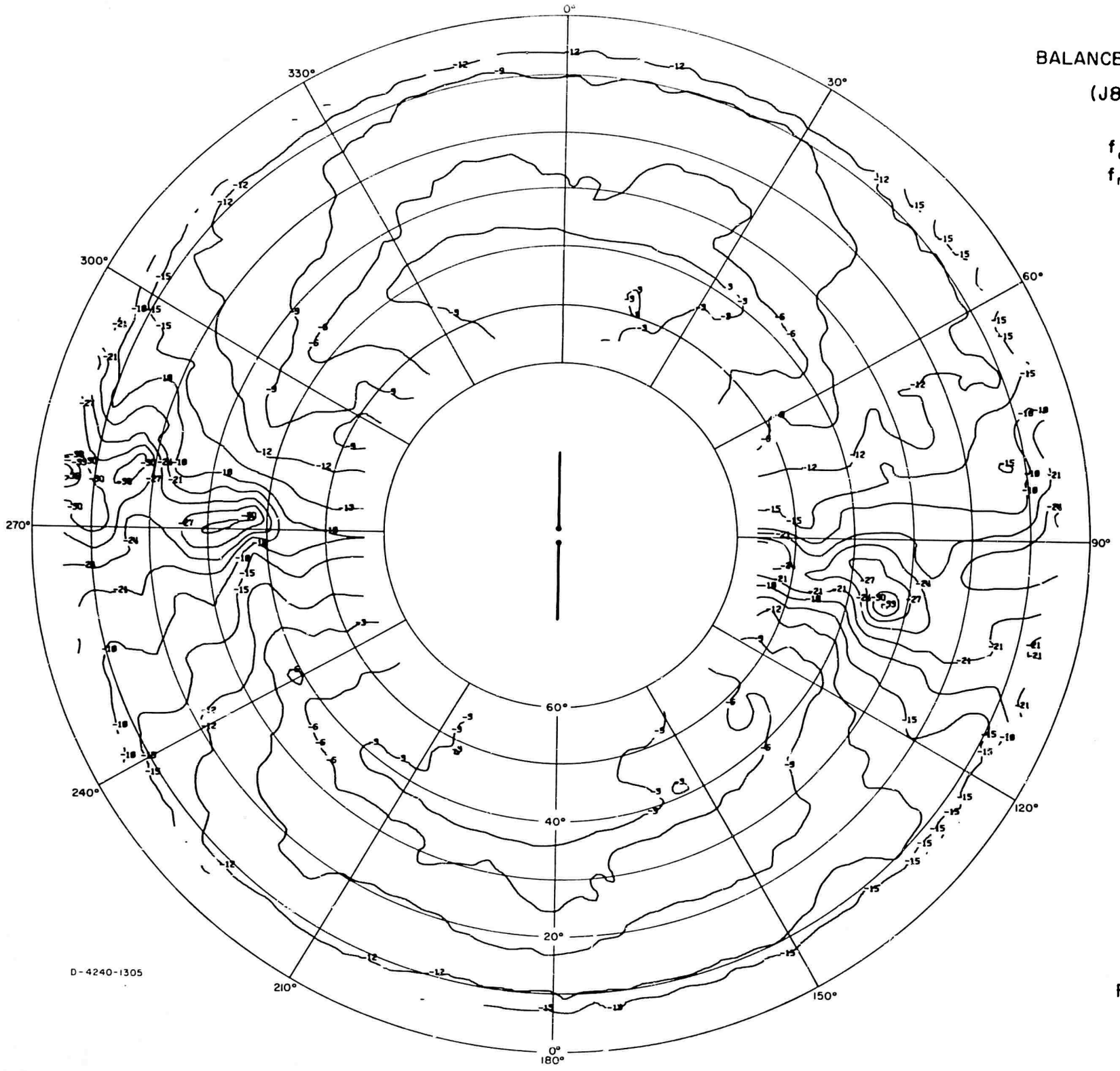

BALANCED DIPOLE

(J&B TYPE)

$h_a = 80'$

$f_o = 6$ Mc/s

$f_m = 6$ Mc/s

E_θ

FIG. A-158

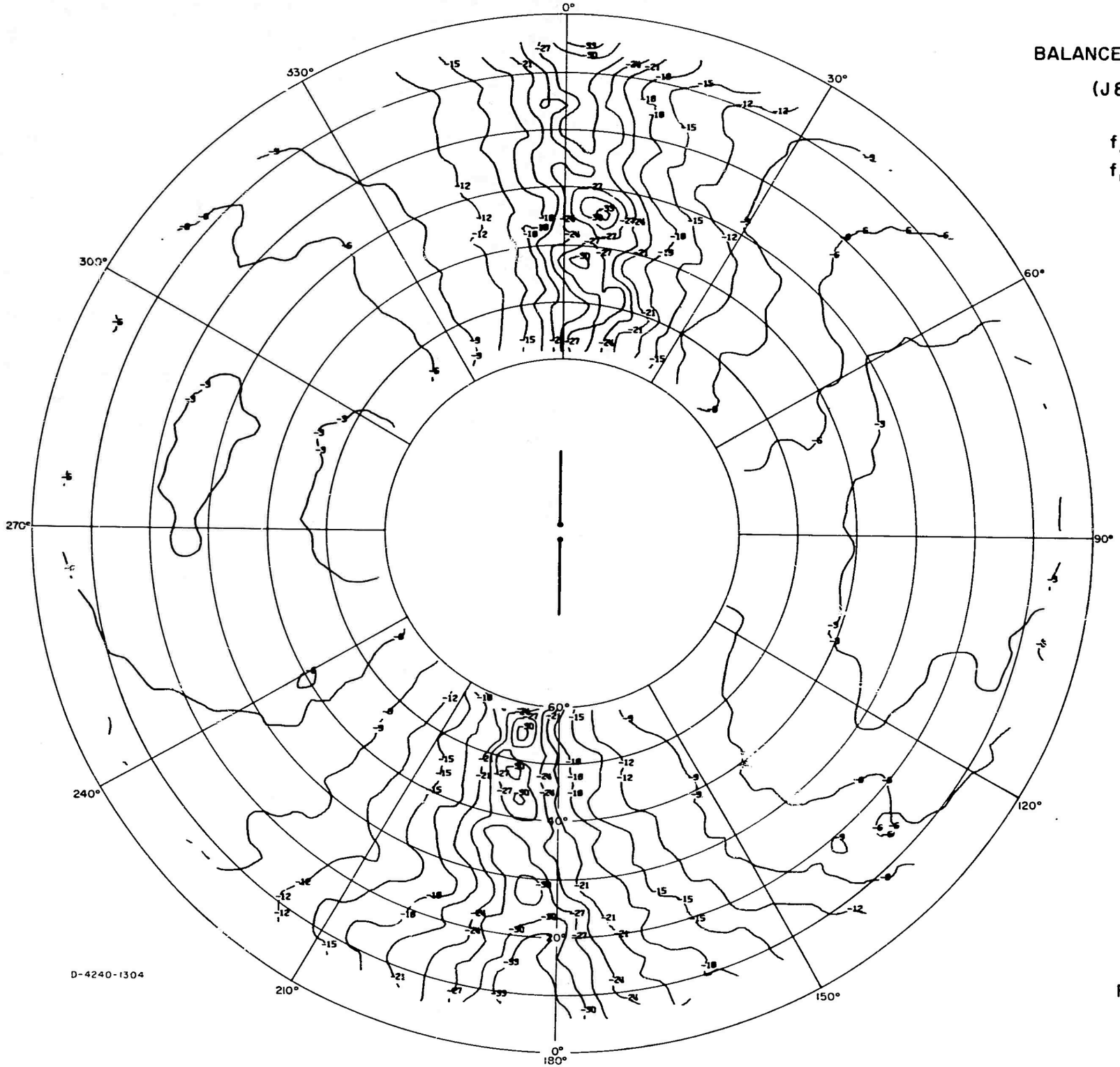

BALANCED DIPOLE

(J & B TYPE)

$h_a = 80'$

$f_o = 6$ Mc/s

$f_m = 6$ Mc/s

E_ϕ

FIG. A-159

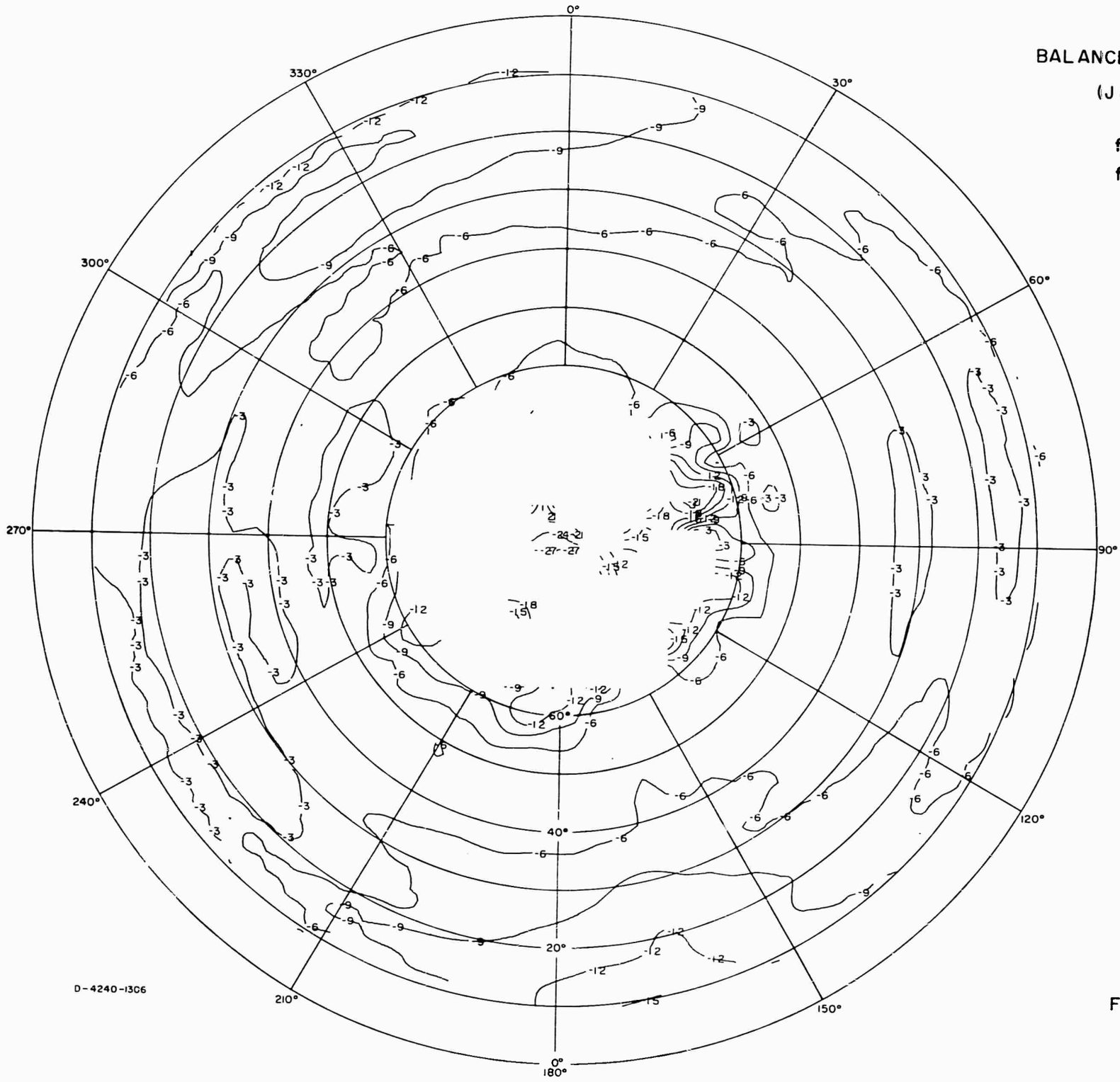

BALANCED DIPOLE

(J & B TYPE)

$h_a = 80'$

$f_o = 6$ Mc/s

$f_m = 6$ Mc/s

POWER

FIG. A-160

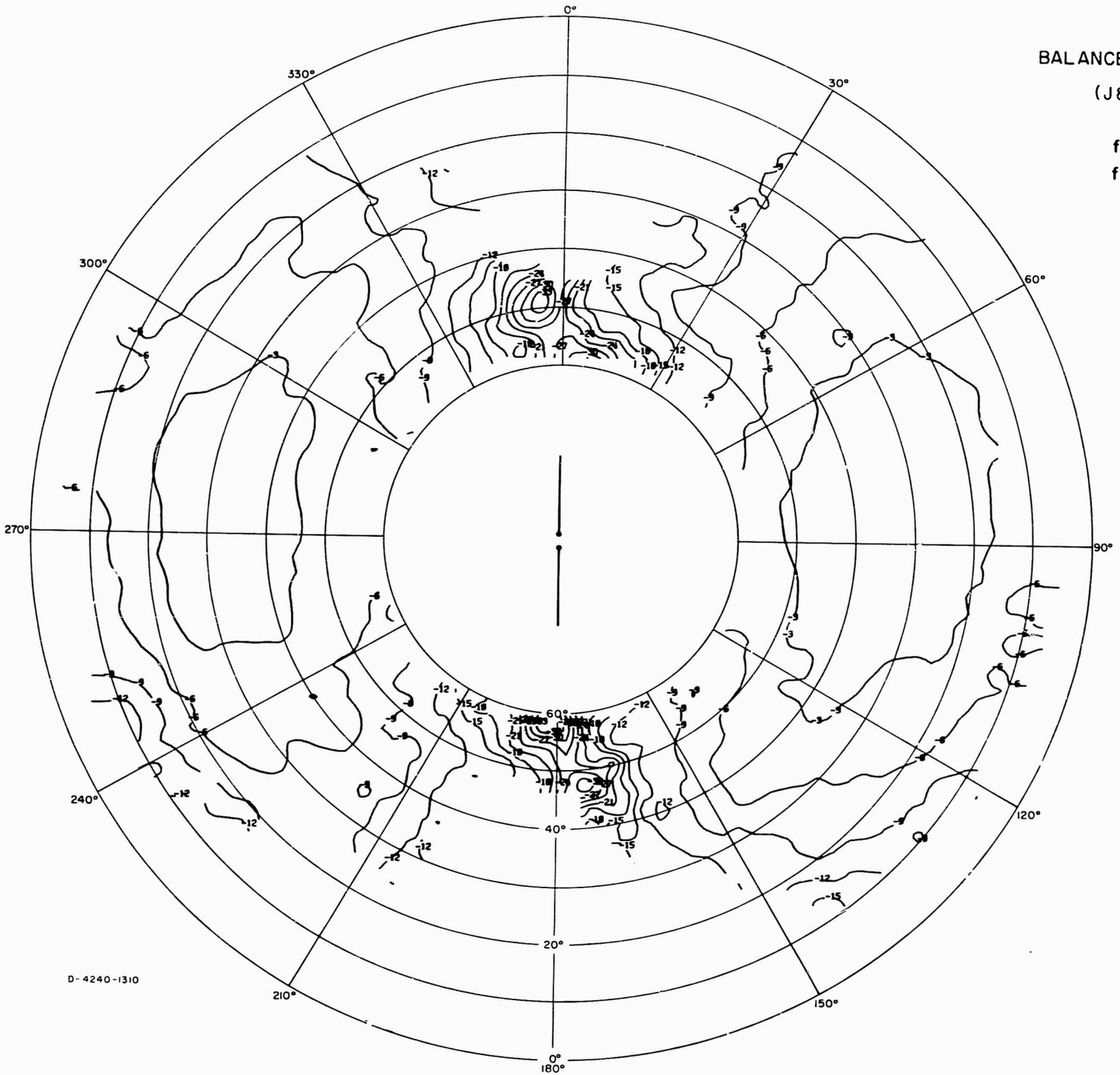

BALANCED DIPOLE

(J & B TYPE)

$h_a = 40'$

$f_o = 12$ Mc/s

$f_m = 12$ Mc/s

$E\phi$

D-4240-1310

FIG. A-161

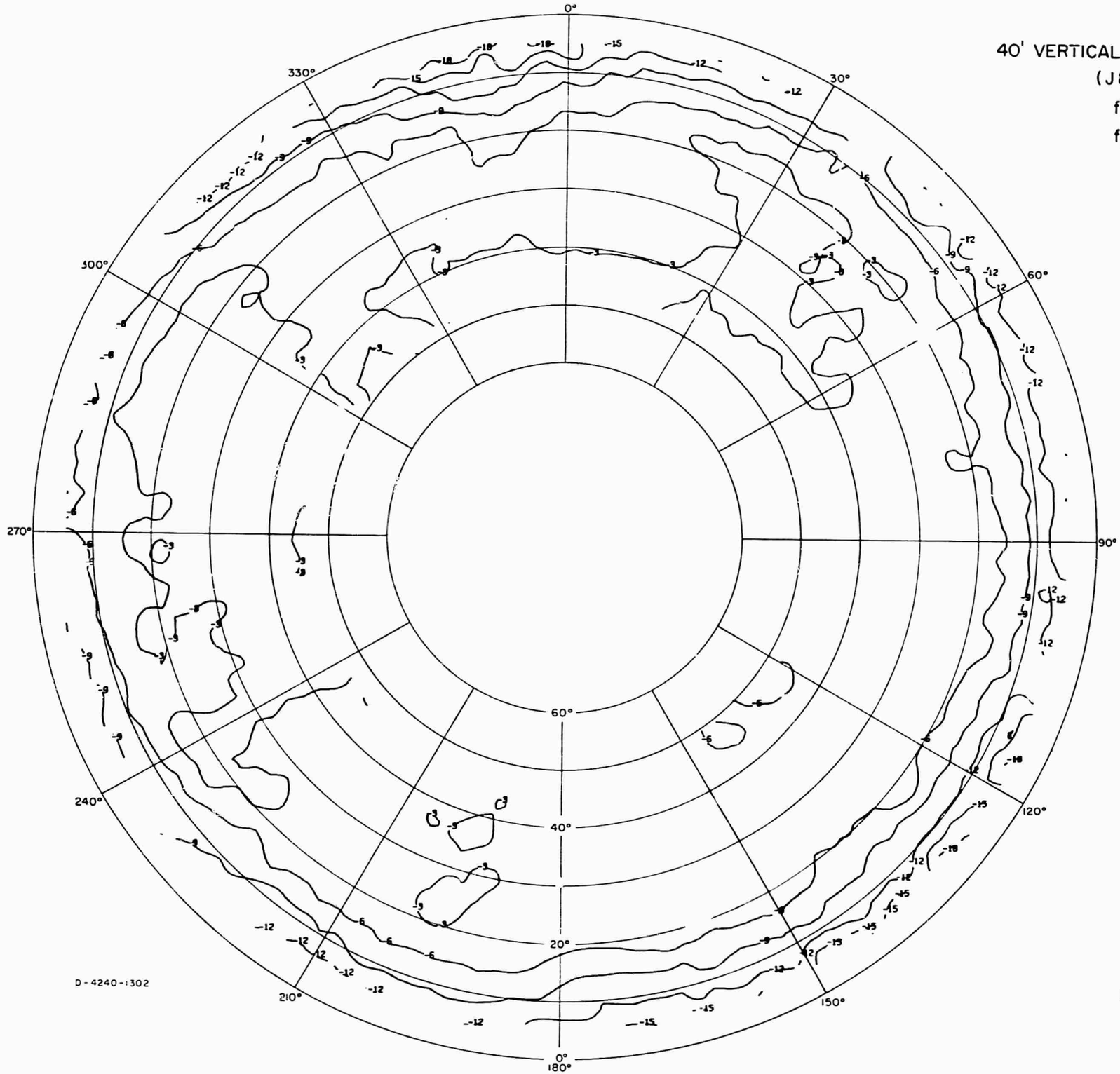

40' VERTICAL ANTENNA
(J & B TYPE)
f_o = 6 Mc/s
f_m = 6 Mc/s
$E\theta$

FIG. A-162

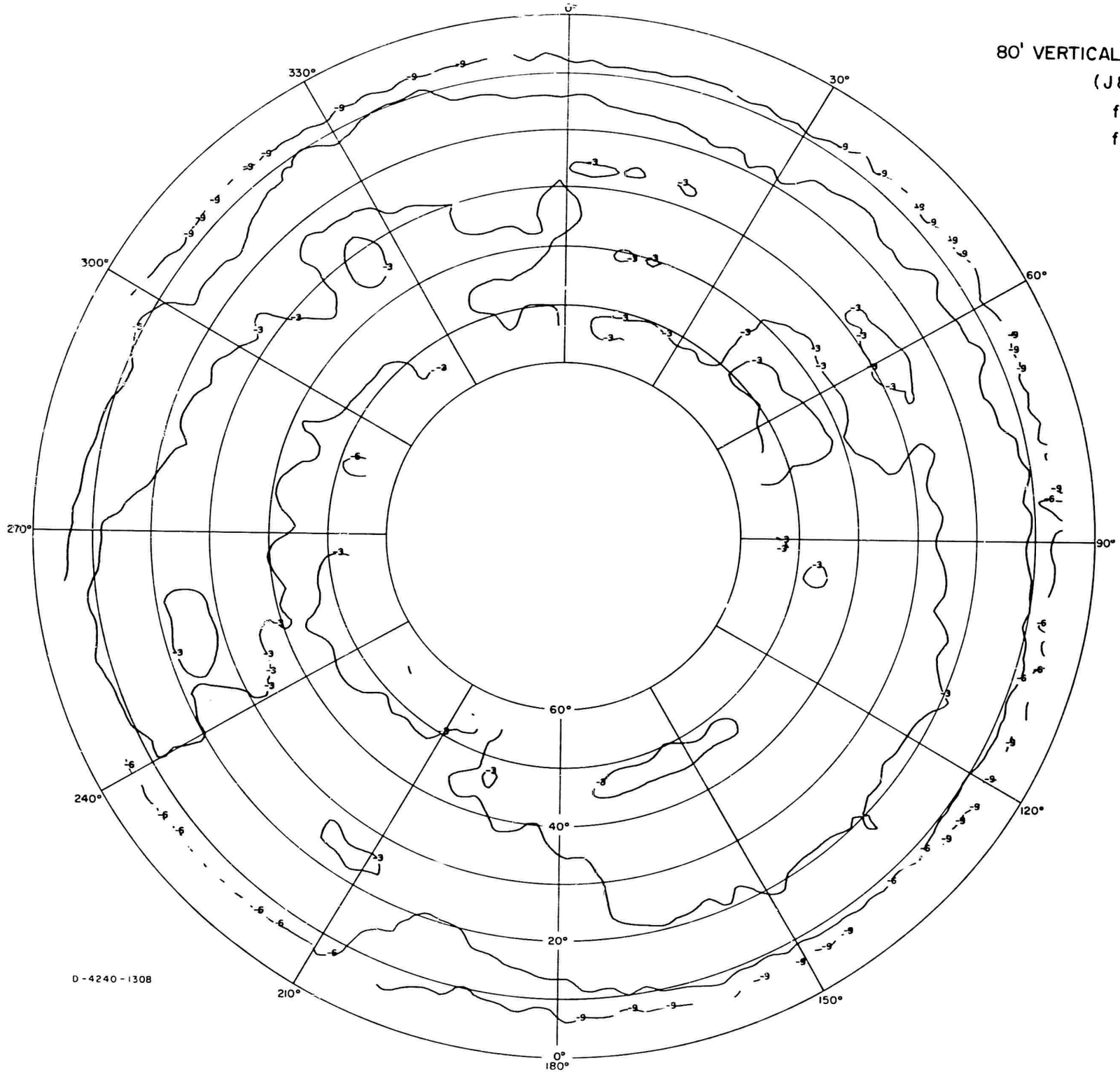

80' VERTICAL ANTENNA
(J & B TYPE)
f_o = 2 Mc/s
f_m = 2 Mc/s
E_θ

D-4240-1308

FIG. A-163

20' VERTICAL ANTENNA
(J&B TYPE)
f_c =12 Mc/s
f_{max} =12 Mc/s
Eφ

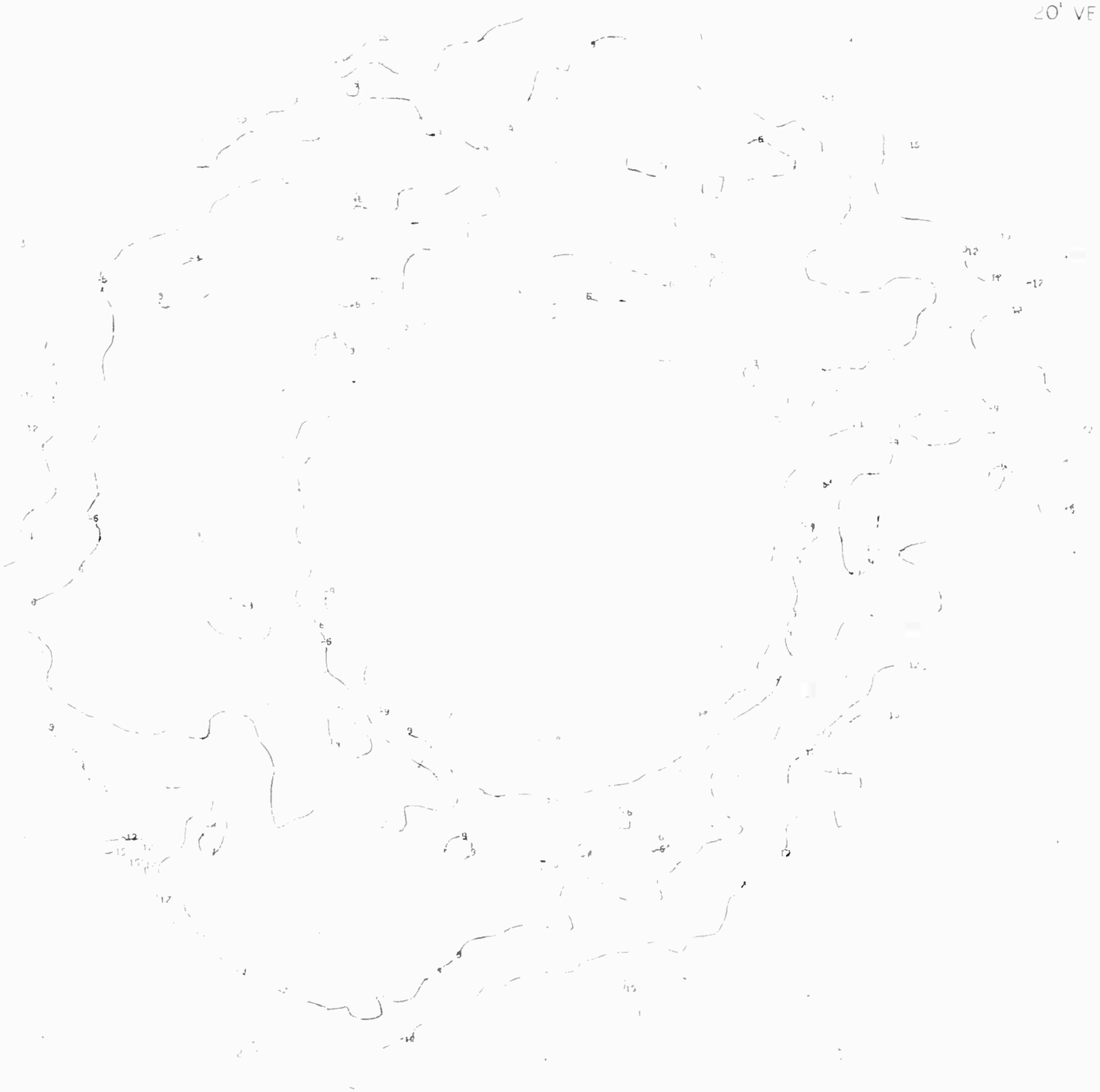

FIG A-164

DOCUMENT CONTROL DATA - R & D

Security classification of title, body of abstract and indexing annotation must be entered when the overall report is classified

1 ORIGINATING ACTIVITY (Corporate author)
Stanford Research Institute
333 Ravenswood Avenue
Menlo Park, California 94025

2a REPORT SECURITY CLASSIFICATION
Unclassified

2b GROUP
N/A

3 REPORT TITLE
FULL-SCALE PATTERN MEASUREMENTS OF SIMPLE HF FIELD ANTENNAS IN A TROPICAL FOREST IN THAILAND

4 DESCRIPTIVE NOTES (Type of report and inclusive dates)
Special Technical Report 35

5 AUTHOR(S) (First name, middle initial, last name)
Gary E. Barker Glenn D. Kochrsen

6 REPORT DATE	7a TOTAL NO OF PAGES	7b NO OF REFS
February 1968	219	10

8a CONTRACT OR GRANT NO	9a ORIGINATOR'S REPORT NUMBER(S)
DA 36-039 AMC-00010(E) b PROJECT NO Order No. 5384-PM-63-91 c ARPA Order No. 371 d	SRI Project 4240 9b OTHER REPORT NO(S) (Any other numbers that may be assigned this report)

10 DISTRIBUTION STATEMENT
Distribution of this document is unlimited.

11 SUPPLEMENTARY NOTES	12 SPONSORING MILITARY ACTIVITY
	Advanced Research Projects Agency Washington, D.C.

13 ABSTRACT
During June and July 1966, measurements of the radiation patterns and impedances of selected HF field-expedient antennas were made in a tropical forest in Thailand on frequencies in the range 2 to 15 Mc/s. These tests--part of the Advanced Research Projects Agency's SEACORE Program--completed a sequence of measurements on the same and similar antennas (including dipoles, inverted L's, slant wires, and monopoles) in an open, level field, in a U.S. conifer forest, and in a dry-evergreen forest in Southeast Asia.

The pattern measurements were made by towing a small, battery-powered transmitter driving a short Hertzian dipole on a long dielectric cable behind an aircraft whose position was electronically tracked. The results are presented as stereographic contour maps showing the response for orthogonal polarizations ("vertical," E_θ and "horizontal," E_φ) as functions of azimuth and elevation for the elevation range from about 5° to about 55° from the horizon. The power response (normalized Poynting vector) is presented in the same format for the elevation range from 5° to the zenith. Relative gain values are presented for the maximum observed response of the various antennas on a given frequency and for the polarization response E_θ/E_φ for a given antenna and frequency. The data indicate that vertical polarization is attenuated more than horizontal polarization, and that scattering of the vertically polarized signal begins at about 12 Mc/s.

Impedance data are presented on Smith charts for each antenna over the range of frequencies for which pattern data were obtained. They show that the environment tends to become part of the antenna.

DD FORM 1 NOV 1473 (PAGE 1)
S/N 0101-807-6801

KEY WORDS	LINK A		LINK B		LINK C	
	ROLE	WT	ROLE	WT	ROLE	WT
Field Expedient Antennas						
Dipole Antennas						
Monopole Antennas						
Inverted-L Antennas						
Slant Wire Antennas						
Loop Antennas						
Antenna Pattern Measurements						
SEACORE						
Southeast Asia						
Thailand						
Dry Evergreen Forest						
Jungle						
Tropical Forest						
Xeledop						
Antenna Impedance						
Antenna Directivity						
High Frequency (HF)						